Swash Plate Axial-Piston Hydraulic Motors: A Study of Surface Protective Treatments for the Piston/Cylinder Interface

Thawhid Ahmed Khan

Submitted in accordance with the requirements for the degree of
Doctor of Philosophy

The University of Leeds
School of Mechanical Engineering
Leeds, UK

March, 2017

The candidate confirms that the work submitted is his own, except where work which has formed part of jointly-authored publications has been included. The contribution of the candidate and the other co-authors in published work from this thesis has been clearly indicated. The candidate confirms that appropriate credit has been given within the thesis where reference has been made to the work of others.

In the papers contributing to this thesis, the candidate (first author) carried out all the experiments, analysis and preparation of the manuscripts. All other authors contributed by proof reading and providing insight on the discussions.

This copy has been supplied on the understanding that it is copyright material and that no quotation from this thesis may be published without proper acknowledgement.

Papers Contributing to this Thesis

- Khan, T.A., Tamura, Y., Yamamoto, H., Morina, A., Neville, A. Friction and Wear Mechanisms in Boundary Lubricated Oxy-Nitrided Treated Samples. Wear, Volumes 368-369, pp. 101-115, 2016. Featured in Chapter 6.

- Khan, T.A., Tamura, Y., Yamamoto, H., Morina, A., Neville, A Tribological Response of MoS_2 Coated and Oxy-Nitrided Samples with Alternative Extreme Pressure and Anti-Wear Additives. Under review at Tribology International. Featured in Chapter 9.

- Khan, T.A., Tamura, Y., Yamamoto, H., Koide, S., Morina, A., Neville, A. Effects of Using Alternative Extreme Pressure (EP) and Anti-Wear (AW) additives with Oxy-nitrided Samples. To be submitted to Tribology Letters. Featured in Chapter 8.

Conferences and Awards

Conferences presented:

- Khan T *et al.* Hydraulic motors: A tribological study, Tribo UK Conference, Loughborough 2015.

- Khan T *et al.* Friction and wear reduction mechanisms of oxy-nitrided treated samples, International Tribology Conference, Japan 2015.

- Khan T *et al.* Optimising friction and wear reduction with oxy-nitrided treated samples, Turkey Tribology, Turkey 2015.

- Khan T *et al.* Tribological performance of oxy-nitrided samples, Gordon Research Seminar, USA 2016.

- Khan T *et al.* A Tribological Response of MoS_2 Coated and Oxy-Nitrided Samples with Alternative Extreme Pressure and Anti-Wear Additives, 43rd Leeds-Lyon Symposium on Tribology, Leeds 2016.

Awards received:

- IOM^3 - Andrew Carnegie research grant, 2015.

- Armourers and Brasiers - Atomic Weapons Establishment (AWE) international travel grant, 2016.

- National Science Foundation award, 2016.

Acknowledgments

Abstract

Presently, there is a global push to improve the productivity of heavy duty machinery. With increasing demands to apply to stricter fuel and emission standards alongside increasing energy costs, it has become vital to maximise the energy efficiency of systems. Swash plate axial piston motors have inefficiencies up to 15% caused by fluid leakage and internal friction. Mechanical systems are being modified to reduce friction amongst components whilst allowing them to run at higher operating conditions and temperatures. This is where surface improvement technology plays a crucial role. By achieving compatibility between the modified surfaces and lubricant additives optimum efficient systems can be achieved. MoS_2 coatings and nitriding heat treatments are applied to sample surfaces to improve their tribological properties. There are however only a few studies that focus on the tribochemical interactions of nitrided samples with lubricant additives.

This study aims to investigate the impact of the properties of the modified surfaces on tribological and tribochemical interactions. The primary focus will be validating the application of the nitriding treatment to improve the durability of components and investigating the interactions with various lubricant additives in comparison to alternative treatments.

To achieve this, tribological performance of the various samples and oils has been evaluated using the Cameron Plint TE77 tribometer in the boundary lubrication regime. This was followed by using the MTM-SLIM testing rig to validate the trends observed with the TE77 and add another level of complexity to the testing conditions. The MTM SLIM would allow visualisation of the formation and development of a tribofilm on the sample variants whilst using testing conditions similar to that used within a hydraulic motor. A number of surface analysis techniques were employed in this study such as Scanning Electron Microscopy (SEM), Energy Dispersive X-ray (EDX), X-ray Photoelectron Spectroscopy (XPS) and Raman spectroscopy. They helped to characterise the tribofilms formed and understand the effect of the properties of treated surfaces.

The results of this study indicate that the mechanical properties of the compound layer formed during the nitriding process had a significant impact on the sample tribological properties, allowing it to perform better than the untreated and MoS_2 coated samples. However the inertness of this layer prevents the formation of a thick tribofilm which could further impact friction and wear. However the presence of additional layers upon the nitrided surface are shown to impact not only tribological behaviour but also tribochemical formation, due to the chemical compounds present.

Critically the results showed that not only did the type of treatment applied to the samples impact the tribological behaviour but also the chemical interactions with the compounds within the lubricant played a significant role. This was shown with the MoS_2 coated samples and sulphurised olefin additive, where the synergy between coating and FeS formed lead to the lowest friction system observed within this study.

This study has shown that the oxy-nitriding process is an effective treatment to improve the tribological performance of the samples, with lower friction and wear being achieved compared to alternative samples. The presence of an oxide layer led to the formation of FeS_2 within the tribofilm. However, due to the relative thinness of the tribofilm the impact on friction was minimal. The thickness of the tribofilm with the nitrided was influenced by the presence of nascent iron on the sample surface. The tribological influence of the oxide layer was minimal however with alternative layers such as FeS the friction and wear response the influence was significant. The project demonstrated that the various additive types could positively and negatively impact the friction and wear of the modified surfaces depending on its tribochemical interaction.

Table of Contents

List of Figures

List of Tables

Nomenclature

Term	Definition
AW	Anti-Wear
BL	Boundary Lubrication
BO	Base Oil
C_p	Specific Heat Capacity
E	Young's Modulus
E^*	Reduced Young's Modulus
EDX	Energy Dispersive X-ray
EHL	Elastohydrodynamic Lubrication
EP	Extreme Pressure
F	Friction Force
FIB	Focussed Ion Beam
H	Hardness
h_{min}	Minimum Film Thickness
K	Thermal Conductivity
L	Sliding Distance
m	Mass
ML	Mixed Lubrication
MTM	Mini Traction Machine
P	Pressure
PAO	Poly-Alpha-Olefin
Q	Volume Loss
R	Radius of Curvature
R_a	Surface Roughness
SEM	Scanning Electron Microscope
SO	Sulphurised Olefin
T	Temperature
TCP	Tricresyl Phosphate
U	Entrainment Speed
W	Normal Load
XPS	X-ray Photoelectron Spectroscopy
ZDDP	Zinc Dialkyldithiophosphate
α	Pressure Viscosity Coefficient
η	Viscosity
λ	Lambda Ratio
μ	Friction Coefficient
ρ	Density

Chapter 1 Introduction

Global competitiveness pushes manufacturers to receive the most from their equipment, and forces them to try and achieve small increases in machine productivity which could mean the difference between profit and loss. With increasing demands to apply to stricter fuel and emission standards alongside increasing energy costs, it has become vital to maximise the energy efficiency of systems, components and tribological contacts. Heavy duty mobile construction machineries are controlled using hydrostatic transmissions (Figure 1-1), where it is crucial that the efficient conversion of mechanical to hydraulic energy is carried out [1-3]. Industrial hydraulics is recognised as one of the most cost-effective methods of supplying power to a range of manufacturing processes. In the event of system failure, downtime can cost thousands of pounds per hour, which can lead to significant financial loss. Therefore it is crucial to ensure proper maintenance to prevent failure and high efficiency [4].
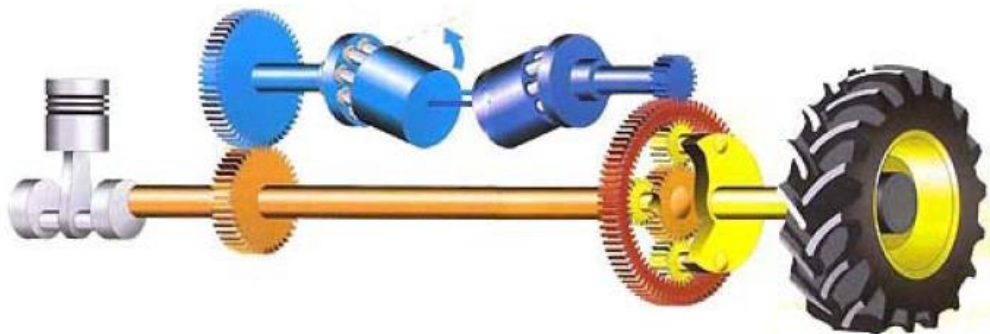
Figure 1-1. A hydrostatic transmission including the engine, transmission and wheel [2].

Over the years these hydrostatic systems have become smaller and lighter alongside utilizing higher pressures to achieve this goal of maximum system efficiency. Increasing the systems energy efficiency causes a fall in the use of energy by the hydrostatic drive lines and working kinematics [1-3].

Within hydrostatic systems, swash plate type axial-piston pumps and motors are used to transmit power hydraulically. The axial motor concept is focussed on a rotating barrel of spring-loaded pistons aligned against an angled swash plate in order to provide a pumping action; through the controlling of the plates angle the output displacement can be determined [5]. This mechanical output

is then used to perform useful work [6, 7]. It has been shown that swash plate axial piston motors are only 85 to 95% efficient with power transmission, due to volumetric & torques losses from leakage and internal friction [6].

This project aimed to define and understand the tribological behaviour of a swash plate type axial-piston hydraulic motor in terms of reducing wear and friction at the piston/cylinder component interface to improve the performance and efficiency of the hydrostatic system. The focus is on the effect of heat treatments or coatings applied to the piston surface on the tribology and tribochemistry processes happening between lubricants and interacting surfaces.

1.1 Aims and Objectives

There is strong need in today's market to push mechanical systems further alongside ensuring the durability of components. The overall aim of this project was to increase the system efficiency by primarily understanding the interface and lubricant interactions within a surface treated system. This study provides a novel insight into the selection of an ideal surface treatment to be applied to the piston/cylinder interface, which would deliver optimal wear and friction results whilst increasing the life and efficiency of the hydraulic motor or friction pairs within systems. Key objectives of this project are:

➢ To investigate the wear and friction results when different surface improvement techniques are applied during wear tests on a reciprocating tribometer.

➢ Assess the wear and friction effects of a range of lubricant additives applied alongside surface modification techniques.

➢ Conduct a series of surface analysis measurements in order to understand the tribochemistry behind the wear and friction mechanism occurring when using different surface improvement techniques and lubricant additives.

➢ Validate and investigate friction and wear trends using an alternative tribometer with contact conditions close to that observed within a hydraulic motor.

The results from this project will help to select and validate the application of a new surface protection treatment to pistons within a piston/cylinder friction pair.

1.2   Contribution of this Thesis

In this thesis the application of a variant of the nitriding heat treatment process will be investigated as a method to improve the tribological properties of a piston component. To understand the friction and wear behaviour, a number of questions need to be answered such as:

- What is the impact of the different layers formed after surface treatment on friction and wear?
- How do these layers influence the formation and properties of a tribofilm?
- Can the surface treatment processes be modified to improve tribological and tribochemical interactions?
- What additives can be used to further optimise the behaviour of the treatments?

Experimentation and surface analysis are combined to give an insight into the behaviour of the treatment variants.

The results from this study were presented at several national and international conferences highlighting the tribochemical interactions of the modified surfaces with lubricant additives. Publication in the peer-reviewed Wear Journal illustrated the key factors influencing the tribological and tribochemical behaviour of nitrided surfaces. Komatsu used the project as a basis to implement the application of the nitriding treatment to friction pairs within the hydraulic motors.

1.3 Thesis Outline

- Chapter Two: Fundamental theory relevant to this is presented.

- Chapter Three: Literature review of the hydraulic system and viable surface enhancement treatments and lubricants to be applied within a hydraulic motor.

- Chapter Four: Materials, equipment and experimental procedures used in this study are presented.

- Chapter Five: Surface characterisation of the treated samples used within this project. This will help to gain an understanding of the impact of each treatment on the material mechanical and tribological properties.

- Chapter Six: The friction and wear behaviour of treated sample variants with fully formulated oil is investigated. This will help to gain an understanding on how the layers formed after treatment impact the behaviour observed.

- Chapter Seven: Expands on exploring the tribological and tribochemical influence of the layer variants applied upon the nitrided layer.

- Chapter Eight: The friction and wear effect of using alternative extreme pressure and anti-wear additives with the sample variants.

- Chapter Nine: Validation of the behaviour of the nitrided (QPQ) and MoS_2 coated samples with various additives using an alternative to the reciprocating tribometer was carried out.

- Chapter Ten: Discussion on results obtained from Chapter Six to Chapter Nine is presented.

- Chapter Eleven: Main conclusions from this study are detailed and recommendations for future studies are outlined.

Chapter 2 Fundamental Theory

2.1 Tribology

William's [8] states tribology is "the science and technology of interacting surfaces in relative motion and of related subjects and practices" which takes into consideration every aspect of lubrication, friction and wear. Hydraulic systems efficiency can significantly be affected by tribological factors, where friction losses are blamed for a third of the energy waste of global energy consumption.

In the 1960's the failure and breakdown of machines in plants was a frequent occurrence, due to poor lubrication which was causing high friction and wear. It was determined that tribology had great potential in contributing towards the reduction in energy and material loss. Through the reduction of friction and wear, a reduction in energy loss and an increase of the lifetime of components can be achieved respectively. To achieve this lubrication plays a crucial role in the ability to reduce friction between interacting surfaces and protecting them against wear through the formation of a lubricating film [9].

2.2 Friction

Friction is the mechanical force which hinders or resists movement between two surfaces and can lead to wear, deformation and heat loss [10].

The ratio between the tangential force (F) and the normal applied load (W) is known as the coefficient of friction (µ), is a widely used function in engineering (Equation 2-1), depicting the friction resistance of interacting surfaces. Its behaviour is influenced by the Amonton-Coulomb friction laws; independence from the load, the contact area and the sliding speed [11].

$$\mu = \frac{F}{W} \qquad\qquad (2\text{-}1)$$

Guillaume Amontons [12] two-first friction laws stated that "the resistance due to friction rises or falls proportionately with the amount of normal load whatever plane size or shape." His work concluded that resistance due to friction was the same whatever the materials when the interacting surfaces were covered in lubricant (rendered pork fat in this case). He proposed that friction resistance is roughly equivalent to a third of normal load. His definition of friction was "anything else than the action by which a part pressed on the other is moving on the surface to that which it touches." He believed friction was the force needed to overcome surface inequalities, therefore in the case of rigid surfaces the theory of the proportionality of the friction force with load was applied. Compared to non-rigid surface inequalities he compared the proportionality of friction with load to the linearity of the load-displacement replacement seen with springs.

In the latter half of the 18th century, Coulomb was commissioned to investigate friction. He believed Amontons' experiments were carried out in a set environment/laboratory and were on a smaller scale than expected in actual situations in machines and therefore could not accurately portray friction conditions occurring. Coulomb's study aimed to study precisely under numerous conditions the reliance of friction on the nature of materials interacting, the extent of the surfaces, the load that surfaces bear. His key general findings were [13]:

- Dry friction of woods and metals appeared to be propositional to the normal load.
- Friction is lower when sliding than after a standstill time, especially in case of woods.
- Speed has low effect on dry friction of wood or on friction of metals.

Coulomb also documented varieties of friction behaviour besides his general findings:

- When interacting surfaces are reduced to the minimum size and the sliding direction is with the wood grains, friction decreases when the normal load or sliding speed increases.

- With the application of a low normal load related to the extent of surface, friction is high and increases with the sliding speed.
- Heterogeneous material contacts showed to produce different results than with interacting homogeneous contacts. Friction is very dependent on the sliding speed, and static friction intensity increases slowly relatively to waiting time.
- Applying lubricant (fat or suet) to surfaces showed very different friction behaviours depending on the contact conditions.

Coulomb's explanation to these varieties in friction focussed on various physical causes such as gearing of surface asperities, deformation of interacting surfaces due to high pressure, entanglement of wood fibres, and surface coherence due to nearness of surfaces. Regarding the influence of other factors, he concluded that friction is proportional to load, independently of the extent of surface [11].

For several machine and system components such as hydrodynamic bearings and gears low friction coefficients are desirable. This can be achieved through several methods such as the use of low-friction material or the lubrication of surfaces or application of heat treatments and coatings to the material surface. The opposite effect can be seen when using a selection of materials or using rough and aggressive surfaces that still interact with the opposing surface even with lubrication, this effect would be needed for other machine elements such as brakes and clutches [10]. For the piston/cylinder interface within a swash plate axial piston motor, low friction coefficients would need to be achieved to help improve the motors efficiency.

2.3 Lubrication

Friction and lubrication are intertwined and intimately connected. Lubrication is simply described as a lubricant which is used between two sliding surfaces with the aim to reduce friction and limit damage to the surfaces. It aims to help two contacting bodies to behave in the most efficient and favourable way in a desired and set state. Blau [14] states that for lubrication to work effectively, interfacial geometry must be properly designed alongside the selection of

appropriate running conditions (speed, temperature, load and environment), which in turn should complement the selected lubricant composition.

The ultimate purpose of lubrication is to separate two moving surfaces which are relative to each other using a film. Four different lubrication modes can be identified depending on the thickness of the film and the geometric conformity of the surfaces [15]. These regimes allow the performance analysis of a system in relation to friction and wear. The four regimes are described below [10]:

- **Boundary Lubrication (BL):** There is high asperity interaction between the two surfaces even though there is a fluid present (Figure 2-1). The lubrication characteristics are controlled by the surface films chemical and physical properties that are of molecular proportion. The properties of the lubricant film at the contacting surfaces determine the frictional mechanisms.
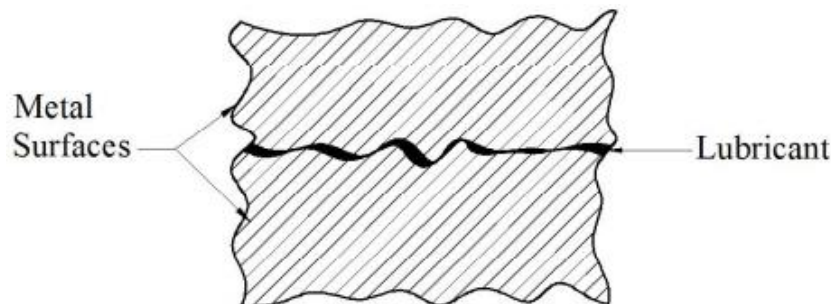
Figure 2-1. Boundary lubrication between two interacting surfaces

- **Mixed Lubrication (ML):** The two surfaces are partially separated and partly in contact (Figure 2-2). The separation is created due to the lubricating film and the regime is influenced by a mixture of boundary and fluid film characteristics.
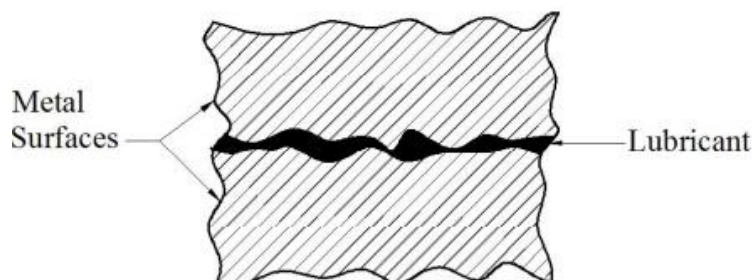
Figure 2-2. Mixed lubrication between two interacting surfaces.

- **Elastohydrodynamic Lubrication (EHL):** A hydrodynamic fluid film is present and prevents any asperity contact between the two surfaces, which are usually characterised as being non-conformal (Figure 2-3). Due to high pressures being developed, the lubricants pressure and temperature viscosity characteristics and also the elastic deformation of solid surfaces are deemed important. Friction is present in this mode due to the shearing of the viscous lubricant. The applied load to the system does not really affect the minimum film thickness, as the contact area increases with the load creating a larger lubricated area to support the load.
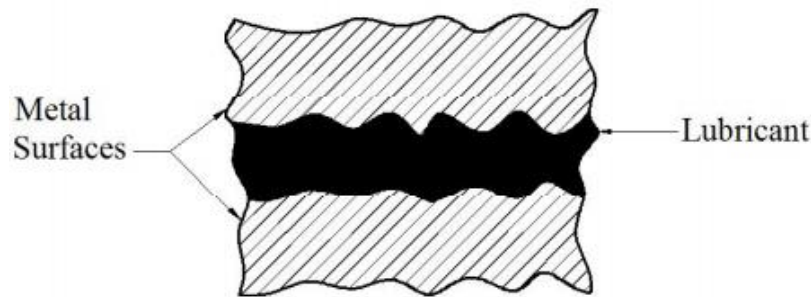
Figure 2-3. Hydrodynamic lubrication between two interacting surfaces.

- **Hydrodynamic Lubrication (HL):** A thick lubricating film prevents any contact between the two surfaces, which are characterised as being conformal. As with EHL friction is present due shearing of the viscous lubricant. Due to sliding motion applied load affects the minimum film thickness.

The lubrication state between the piston and cylinder interface can be determined by a range of parameters such as surface roughness, sliding velocity to the hardness of the material. By calculating the minimum film thickness, the lambda ratio (Equation 2-2) can be determined which would allow the identification of the lubrication mode [14]. The lambda ratio is classified as the ratio of film thickness to the composite surface roughness.

$$\lambda = \frac{h_{min}}{\sqrt{R_{q1}^2} + \sqrt{R_{q2}^2}} \qquad (2\text{-}2)$$

Where λ is the lubrication regime, h_{min} and R_q is the surface roughness of the two interacting surfaces.

For modelling the wear of the piston/cylinder interface the following definition of the lubricating regimes can be used [14]:

Boundary lubrication - **$\lambda < 1$**

Mixed lubrication - **$1 < \lambda < 3$**

Full lubrication - **$\lambda > 3$**

Using the Dowson-Hamrock equation (Equation 2-3) the minimum film thickness can be calculated based on point contact, as the piston/cylinder interface can be modelled as this.

$$\frac{h_{min}}{R'} = 3.63 \left(\frac{U\eta}{E'R'}\right)^{0.68} (\alpha E)^{0.49} \left(\frac{F}{ER'^2}\right)^{-0.073} \left(1 - e^{-0.68k}\right) \tag{2-3}$$

Where h_{min} is the minimum film thickness (m), R' is the reduced radius (mm), E' is the reduced contact modulus (GPa) (Equation 2-4), U is the mean sliding speed (m/s), η is the dynamic viscosity at atmosphere pressure (Pa.s), α is the pressure viscosity coefficient of the lubricant (1/Pa) and k is the elliptical parameter (1.0339 for pin).

$$E' = 2\left[\frac{1-\upsilon_1^2}{E_1} + \frac{1-\upsilon_2^2}{E_2}\right]^{-1} \tag{2-4}$$

E_1, E_2 and υ_1, υ_2 are the elastic moduli and Poisson's ratios for each of the interacting bodies.

The Stribeck curve relates friction coefficient or film thickness against viscosity, load and speed, and also identifies the position of the lubrication regimes in relation to these parameters (Figure 2-4). Boundary lubrication is shown to occur at low viscosity and speed but at a high applied load. With little

lubrication between the two surfaces and high surface contact, high friction results are observed [16].

With an increase in speed and viscosity or a decrease in applied load, fluid film forms allowing the two interacting surfaces to separate. This stage is acknowledged as mixed lubrication as the formed film supports more and more of the load. With the separation of the surfaces and increase in lubrication fluid, a drop in friction coefficient is observed. Hydrodynamic lubrication occurs when a full fluid film is developed due to the speed or viscosity increasing and there is no surface contact with the load being fully supported by the film. At this point friction coefficient is at a minimum and no wear occurs due to there being no solid-solid contact [14].

There is a noticeable rise in friction in the hydrodynamic lubrication region; this is related to fluid drag, where the drag on surfaces from the fluid increases with higher speeds. The same effect is observed with increasing the viscosity of the lubricant [17].
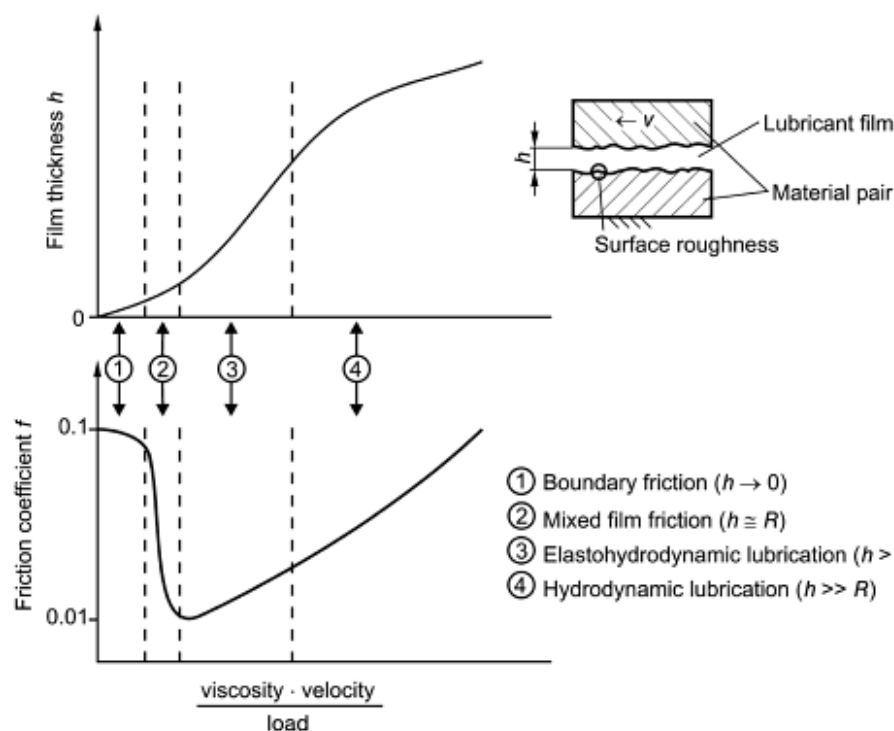
Figure 2-4. The Stribeck curve according to Czichos and Habig [16].

Figure 2-5 is a Stribeck curve of friction coefficient against film thickness, which demonstrates the behaviour of a hydraulic motor (bold section of curve). The first bold section up 0.6λ represents the sliding motion in the stroke, and the second portion up to 2λ is the squeeze motion experienced at the end of the stroke [14]. The cylinder/piston interface within a swash plate type axial piston motor is reported to run in boundary lubrication.
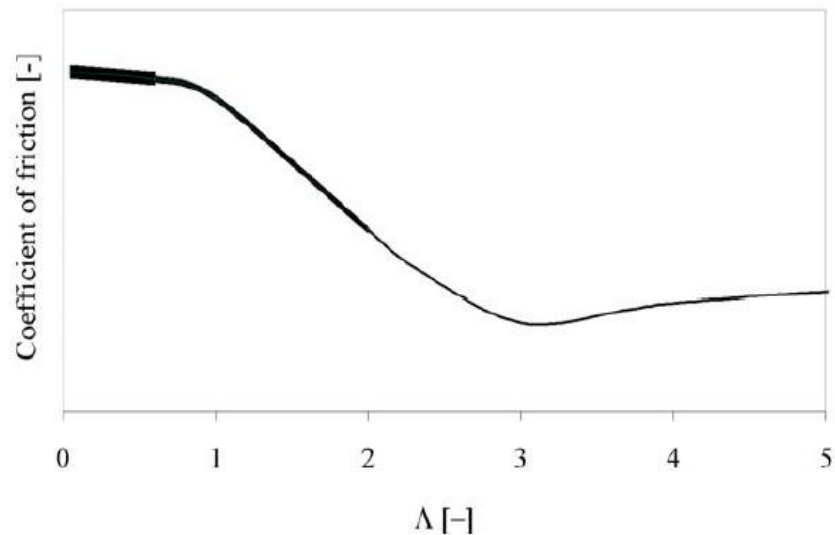
Figure 2-5. A Stribeck curve comparing coefficient of friction versus film thickness, with hydraulic motor operation indicated by the boldface portion of the line [14].

2.4 Wear

Wear is acknowledged as one of the most damaging processes in machine components, as it can cause surface damage or during the interaction of two moving surfaces it can cause material removal, which can lead to changes to surface topography and surface properties. To maximise component efficiency the ultimate goal is to minimise wear for a number of reasons such as with a rapid increase of wear, seizure can occur causing the component to be completely destroyed. Another reason is that wear particles released could ultimately damage other machine elements in the hydraulic motor [10, 14, 18].

In boundary lubrication the wear process of the piston/cylinder interface interaction, can be influenced by factors such as surface coatings and treatments alongside lubricant additives [14].

The most common types of wear are described below and highlighted in Figure 2-6 [14]:

- **Adhesive wear:** Debris is formed or joins on to a surface when the junction between two materials is damaged/broken. This type of wear mainly occurs in boundary and mixed lubrication regime.

- **Abrasive wear:** Material is removed from the softer surface of two materials. This usually occurs in boundary lubrication regimes.

- **Fatigue wear:** When materials are subjected to cyclic loading damage occurs progressively and locally. The main cause of fatigue wear is high local stresses between surface contacts.

- **Chemical wear:** Loss of material from surfaces due to chemical reactions causing oxidation or corrosion of them, which can be due to contaminants and high levels of chemical active additives.

- **Polishing wear:** Wear generated as a result of mechanical-chemical interaction between the surfaces. This type of wear leads to a very smooth surface texture. This can lead to failure in lubricated components since the polished surface is unable to preserve enough oil on the surface.
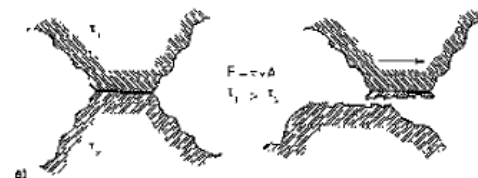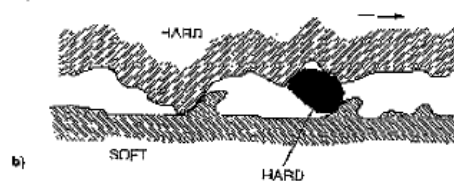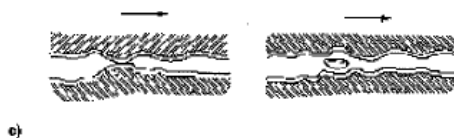
Figure 2-6. Schematic diagram of four different types of wear mechanisms [18].

Wear rate incorporates the effect of time to allow the assessment of the evolution of the system. In the majority of cases wear begins at a high level, termed as the running-in period after which wear reduces to a steady state. This can be due to the presence of anti-wear additives which form a protective tribofilm [19].

The wear rate of a material can be defined as:

$$W = \frac{\text{Volume of material removed}}{\text{Sliding Distance}} \tag{2-5}$$

The Archard equation (Equation 2-6) directly relates wear volume loss to applied load, stating that they are directly proportional but the wear is inversely proportional to the surface hardness [8].

$$Q = \frac{KWL}{H} \tag{2-6}$$

Where Q is the volume loss due to wear, K is a dimensionless constant, W is the applied load, L is the sliding distance and H is the hardness of the softest contacting surface.

2.5 Interacting Surfaces

Two non-conforming solids initially contact at a single point or along a line. These initial contact points and the area close to their vicinities are deformed under the application of a load, and touch over an area which is smaller when comparing against the dimensions of the two bodies. Hertzian contact theory can be applied to systems where there is contact between two surfaces of low conformity and high curvature. This theory allows the determination and prediction of the shape of the area of contact and its evolution as the applied load is changed. This understanding allows the calculation of the deformation and stresses acting on both bodies within the area of contact [20]. Depending on the shape of the rubbing surfaces, there are different type's contacts. Within this study the contact can be defined either as a ball-on-ball or ball-on-flat contact, with both being considered to be a point contact.

Figure 2-7 presents a schematic representation of a point contact [21], with Table 2-1 highlighting the equations used to calculate the contact areas and pressures.
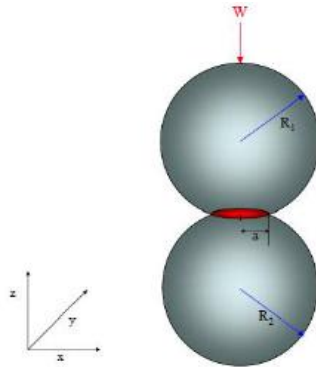
Figure 2-7. Schematic diagram showing two bodies in a point contact [21].

Table 2-1. Equations for calculating Hertzian contact pressure for point contacts. [8]

Radius of contact area, a	$a = (\frac{3WR^*}{4E^*})^{1/3}$
Relative radius of curvature, R^*	$R^* = \frac{1}{R_1} + \frac{1}{R_2}$
Reduced Young's modulus, E^*	$E^* = \frac{2\,E_1 E_2}{(1-v_1^2)E_2 + (1-v_2^2)E_1}$
Maximum contact pressure, P_{max}	$P_{max} = \frac{1}{2\pi}(\frac{3WE^{*2}}{R^{*2}})^{1/3}$
Mean contact pressure, P_{mean}	$P_{mean} = \frac{2}{3}P_{max}$

2.6 Flash Temperature

Frictional heat is generated with the interaction of two surfaces which causes an increase in temperature. This is generally referred to as flash temperature. Due to the difficulty of measuring the temperature rise within a contact, several numerical models are used to provide an estimate of the temperature rise [22-25].

Equation 2-7 can be used to calculate the maximum temperature rise at high sliding speeds within a point contact. Equation 2-8 is used to estimate

temperatures at slow speeds, whereas Equation 2-9 is used to estimate maximum temperature at all sliding velocities.

$$T_{max} = \frac{qa}{K\sqrt{\pi Pe}} \ (Pe > 10)$$ (2-7)

$$T_{max} = \frac{qa}{K} \ (Pe < 0.2)$$ (2-8)

$$T_{max} = \frac{qa}{K\sqrt{\pi(1.2373 + Pe)}}$$ (2-9)

Pe is the Peclet number and is given by $Pe = U_s a/2k$. U_s is the relative sliding velocity $|U_2 - U_1|$, a the radius of the contact area and k the thermal diffusivity ($k = K/\rho C_p$). K is the thermal conductivity, ρ the density and C_p the specific heat capacity of the material. q is the heat supply rate given by $q = \mu P U_s$ where μ is the friction coefficient and P the contact pressure.

2.7 Tribochemistry

The chemical reactions that occur under boundary lubrication conditions between lubricant molecules and a material's surface are defined as tribochemistry. Tribochemistry is the investigation into the changes of matter in chemical and physiochemical terms due to the influence of mechanical energy. These reactions are crucial to mechanical systems as they can determine the reliability and lifespan of machine components through influencing the lubrication processes occurring [26, 27].

Two key mechanisms have been suggested as the catalysts for tribochemical reactions resulting in the formation of a protective layer [28]:

- Thermal induced reactions caused by high temperatures at asperities
- Mechanical induced reactions caused by shear stress at the tribocontact.

This investigation will focus on the interactions of different surfaces and treatments with a range of lubricants and additives.

Chapter 3 Literature Review

3.1 Introduction

The literature review in this chapter aims to explore key work that help give an understanding of the interaction of components within a hydraulic system. There is a review on the application of surface treatments to improve the durability of friction pairs, with a strong focus on the variants of nitriding. This will help to explain the tribological behaviour of a nitride layer under a range of testing parameters. It will also closely examine the interactions of the surface with a range of extreme pressure lubricant additives. Structurally, the review will be split so as to deal with many aspects of the hydraulic system and the application of surface modification techniques to components.

Firstly a brief overview of the workings and key components within a hydraulic system are discussed. This is followed with a review on the causes of inefficiencies and failures of hydraulic motors, with a particular focus on friction pair components.

Following this an overview on the possible surface protection treatments which can be applied to the surface of the pistons within a piston/cylinder interface is presented. Different variants of the nitriding process are highlighted and discussed in depth.

The final section of the literature review then focusses on the mechanical properties of the nitrided layers formed and the influence of lubricant additives on the tribological behaviour. The tribochemistry of the tribofilm when using common lubricant additives with the nitrided layer is compared to the well document behaviour with untreated steel systems. Finally, a summary is presented to bring together the most defining points reviewed.

3.2 Analysis of Hydraulic Systems

Hydraulic systems take mechanical energy provided from an electric motor or an internal combustion engine which is then converted into pressure and fluid flow used to carryout useful work. They can be made up of a hydrostatic transmission (Figure 3-1) which consists of two main components: a hydraulic pump and motor, with the possibility of adding a gear box between the IC engine and the pump. Mechanical energy from the IC motor is transformed into hydraulic energy by the pump which is then transferred to the motor which then reconverts this energy to a mechanical one, which can be used in the case of mobile equipment, to drive the wheels [1, 2, 29].
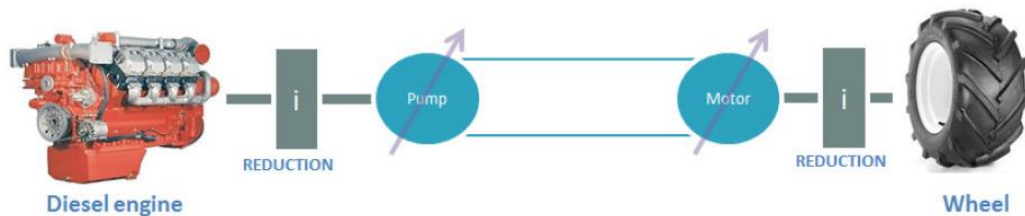
Figure 3-1. The key components powering a hydrostatic drive [3].

Compared to other transmissions such as a discrete gear transmission, the hydrostatic drive has several advantages such as:

- ➢ The ability to operate over a wide range of torque/speed ratios
- ➢ Transfer high power with low inertia
- ➢ There is dynamic braking

A common problem associated with hydrostatic transmissions is the increase in leakage from the pump & motor as the applied load increases, which leads to a reduction in the motors output [30]. This will be discussed in greater detail further on in the chapter.

3.3 Hydraulic Pumps

In a hydraulic transmission the pump aims to provide flow within the system. It converts the mechanical energy from an IC engine in to hydraulic energy. Hydraulic power is the product of pressure and flow. At the inlet of the pump a partial vacuum is created, which leads to fluid being forced in by atmosphere

pressure created by this restriction. This fluid is then transferred into a hydraulic transmission system by the pump [7].

3.4 Hydraulic Motors

Hydraulic motors essentially do the opposite function of a pump; energy is extracted from the fluid pushed to the motor from the pump and converted to a mechanical form to perform work such as rotating a wheel [7].

3.4.1 Piston Motors

This study focuses on one type of continuous rotation hydraulic piston motor. Compared to pumps rather than pushing the fluid, the fluid acts on the motor causing its continuous rotation. The two types of piston motors are fixed or variable displacement units. When fluid pressure is applied to the end of pistons reciprocating inside a cylinder block a torque is generated. The fluid pushed from the hydraulic pump acts on the motors' pistons. This pressure causes them to extend and when they retract the fluid is ejected. In hydraulic motors containing either a bent-axis, eccentric ring or swash plate the piston motion is represented as a circular shaft motion. Piston motors are recognised as one of the most efficient of hydraulic motors with the capability of operating at high pressures and speeds [7].

3.4.2 Swash Plate Axial-Piston Motor

Axial piston motors are surpassing vane and gear hydraulic motors as the popular alternative for developing hydraulic power. Its design simplicity and variable output displacement, allows it to offer versatility within hydraulic systems [31]. With fixed displacement swash plate axial-piston motors (Figure 3-2) the cylinder block and drive shaft are positioned on the same axis. The motor is composed of a group of key components such as a cylinder block, pistons, swash plate, valve plate and drive shaft as shown in Figure 3-2. Fluid is pushed through the valve plate into the cylinder plate, forcing the pistons out of the cylinder block and to slide against the angled swash plate. This causes the cylinder block and pistons to rotate causing the drive shaft to

revolve. The set swash plate angle forces the pistons back into the cylinder block, forcing fluid out through the valve plate and returning to the reservoir [7].

Figure 3-3 illustrates the operational cycle of the motor, which shows that flow enters at a high pressure at point D. The displacement chamber volume is increased up to point C, but due to the expansion of the fluid a drop in pressure is observed to point B. Fluid flows out until point A as the displacement chamber opens to the low pressure line at the outlet. The fluid is compressed when the displacement chamber closes to the outlet due to its reduction in volume up to point D. The cycle then repeats continously [32].

The force of the piston, the radius of the piston circle and the angle of the swash plate determine the torque delivered by the motor. By increasing the swash plate angle, the greater the torque output will be for any given pressure [31].
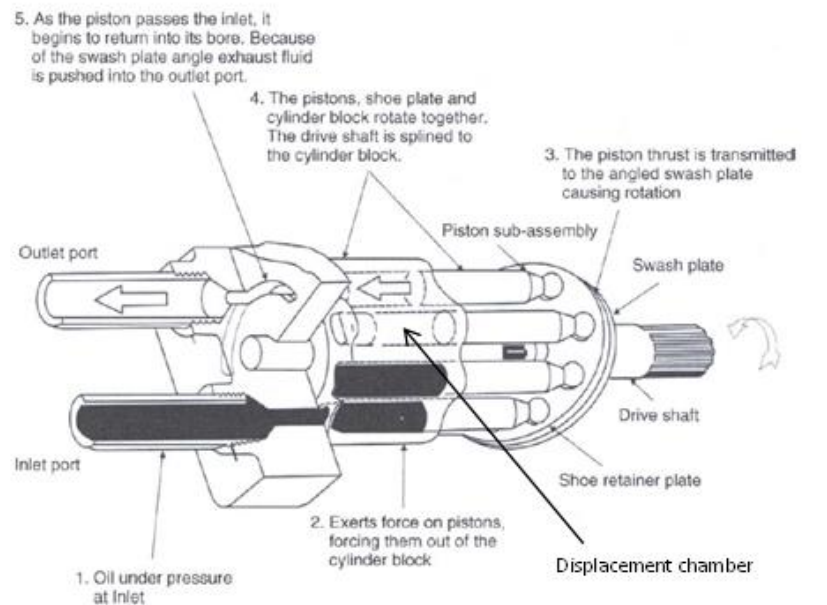
Figure 3-2. An in-line swash plate axial-piston motor [7].
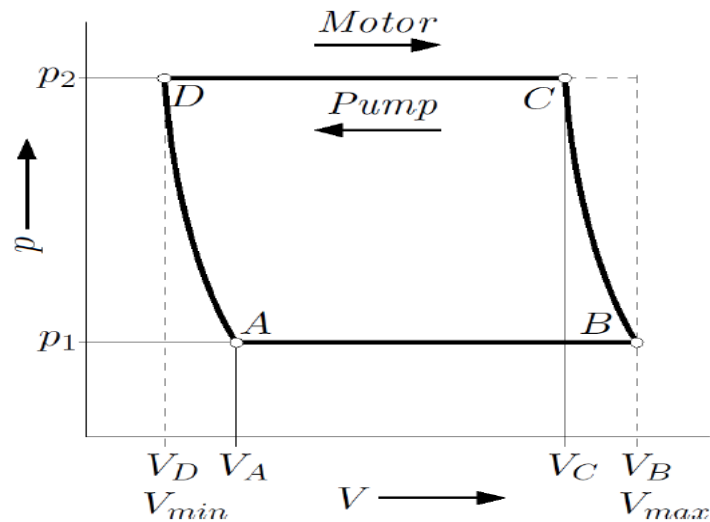
Figure 3-3. Ideal operational cycle of a swash plate motor [32].

Hydraulic motors and pumps are used within systems containing highly – pressurized liquid and are responsible for the efficient conversion of energy, hence tribology plays a significant role in the performance of the components. Figure 3-4 highlights the factors limiting the efficiency and capability of hydraulic motors. The influence of tribology within hydraulic equipment can be related to the following areas [33]:

(1) Operating fluids also being used as lubricants.
(2) Operating conditions are varied over a wide range hence there is widely varying contact pressures on the sliding members [33, 34].
(3) The sliding parts are also in charge of seals.
(4) Sliding parts within the motor/pump.
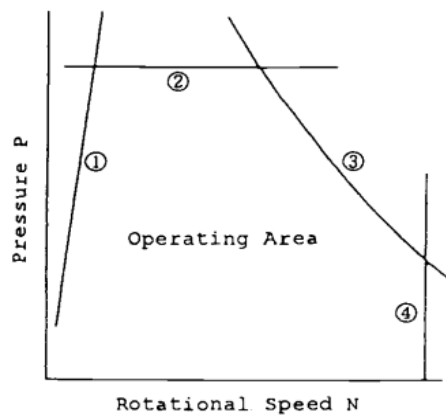
Limits of Operation of hydraulic pumps and motors
(1: Fluid film formation, 2: Mechanical strength,
3: Heat balance or life of rolling bearing, 4: Cavitation)

Figure 3-4. Limits of operation of hydraulic systems [33].

Volumetric efficiency of the motor is influenced by the internal leakage between the motor inlet and outlet, whereas mechanical efficiency is affected by the friction between mated surfaces and also fluid turbulence [7].

3.4.3 Efficiency Loss of Piston Motors

As stated previously swash plate axial-piston motors are only 85% to 95% efficient, with losses occurring due a range of factors such as internal friction and leakage [6]. Several sliding/friction pairs such as the following can be identified within a hydraulic motor (Figure 3-5) for being responsible for the loss efficiency [33]:

> ➢ Interaction between the swash plate and piston slipper.
> ➢ Interaction between the valve plate and cylinder block.
> ➢ Interaction between the piston and cylinder wall.
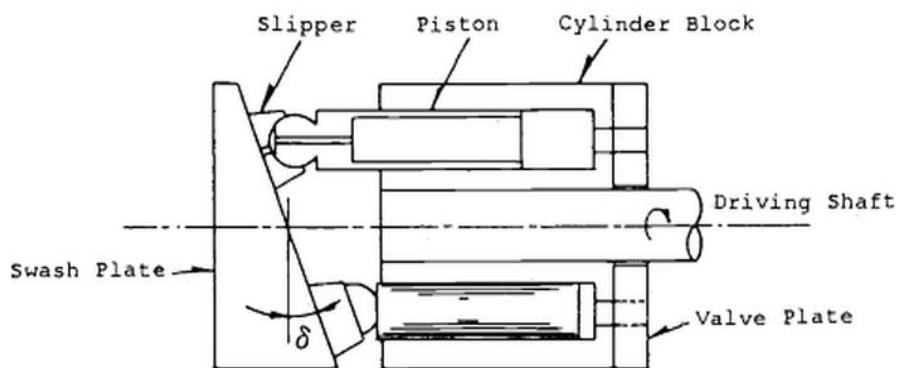
Figure 3-5. Typical sliding parts of swash plate type piston pump [33].

> i)   Interaction between the swash plate and piston slipper

A bronze slipper is commonly positioned between the swash plate and piston head, with hydraulic fluid being fed through the internal passages to the piston/slipper and slipper/swash plate interfaces, providing lubrication to these surfaces. Axial motors are commonly used with mining equipment and industrial applications involving environments where it is very difficult to keep foreign particulate matter out of the working fluid. Eventually these particles can block the small lubricating passages or become embedded between interacting surfaces causing severe wear [5].

During cold start-up, there is minimal lubrication at the slipper which causes rapid acceleration of wear [5]. Heavy scoring of the piston slipper surface (Figure 3-6) which acts as a seal for hydrostatic balance pressure, can cause fluid leakage. This leakage can cause a pressure drop between the piston area and slipper's balancing area, reducing the hydrostatic balancing force which increases the load on the lubricated surfaces of the slipper and swashplate. The eventual loss of hydrostatic balance causes slipper failure [35].
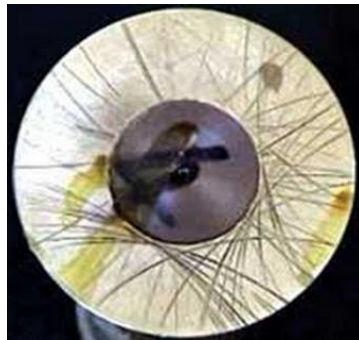
Figure 3-6. Heavily scored piston slipper by third party particles within the hydraulic motor [35].

ii)   Interaction between the valve plate and cylinder block

The valve plate and cylinder block interface is deemed to be a crucial sliding component. With the rotation of the cylinder block, the pistons within the cylinders perform a suction and discharge action of the oil within the system. At this point, momentarily the pressure distribution on the valve plate varies requiring an optimal force balance to reduce the leakage flow rates and friction [36].

There are two key axial forces acting on the surface between the valve plate and cylinder block: a pushing and separating force. A pushing force is generated by highly pressured pistons pushing the cylinder block to the valve plate. If this force is too large, the faces will be subjected to high friction and wear which will reduce the overall mechanical efficiency. Alternatively the separating force due to the pressure distribution on the seal lands is too big, the cylinder blocked is pushed way from the valve plate causing excessive leakage losses [36].

iii)   Interaction between the piston and cylinder wall

This study will primarily be focussing on the piston/cylinder wall interface and its effect on the performance of the hydraulic motor.

When low shaft speeds are used during working, the pistons operate in boundary lubrication conditions and experience large side loads caused by the eccentric nature of the drive and the inability to produce a significant centring force [37]. With the increasing of the sliding speed of the piston there is a reduction in the frictional forces present within the cylinder block. This reduction is due to an increase in fluid film build-up which in turn prevents direct contact between the piston and cylinder. But with the continuous increase of the piston's sliding speed an increase in friction of the cylinder bore is observed. This phenomenon can be explained by the increase in viscous shear of the lubricating fluid when a fully hydrodynamic lubrication regime is achieved. Hydraulic motors are seen to be affected with the increase of sliding speed which impacts the friction force observed within the cylinder bore [6]. Due to the lateral forces acting on the pistons being so large, it is very difficult to avoid metal contact between the cylinder wall and piston especially at large swash plate angles. In this circumstance it is effective to reduce the friction acting on pistons by inducing the hydrostatic effect to the sliding components [33].

The manufacturing tolerances of the piston and cylinder bore can determine the clearance between the two components which can influence factors such as the load bearing ability of the lubricating film and leakage of the system. Smaller clearances are preferable to improve the carrying ability and reduce the leakage from the interacting components, but too low clearances can cause metal on metal contact of the piston and cylinder (Figure 3-7) which can severely affect the mechanical efficiency and reliability of the motor. The disadvantage associated with smaller clearances is the significant increase in manufacturing costs required to improve assembly error and surface roughness, factors which play a crucial role in determining leakage loss and carrying ability of the components at reduced clearances [38].

Figure 3-7. Metal-on-metal contact between the piston and cylinder components within the hydraulic motor causing eventual seizure.

A key source of energy dissipation at the piston/cylinder interface during the operation of the motor is fluid viscous shear. This release of energy causes an increase in temperature of the rotating cylinder which leads to uneven temperature distributions across the systems mechanical components. An increase in temperature of solid components leads to internal thermal stress causing its deformation and change in the thickness of the fluid film acting and also its load carrying ability. These changes can cause catastrophic failure of the system through "piston stick" [39].

3.4.4 Causes of Failure

Hydraulic motors can be completely destroyed by a process commonly known as seizure, which is caused by catastrophic wear. Several causes of seizure initiation have been identified [18]:

1. Entrapment of particles between sliding surfaces
2. Lubricant film breakdown
3. Loss of running clearances between components due to thermal expansion.

3.4.4.1   Entrapment of Wear Particles

Wear particles created due to the interaction of sliding surfaces can cause significant problems if they are entrapped between the piston/cylinder interface as they may become embedded into the softer surface and initiate scratching of the harder one. The wear particles themselves may initiate

seizure or cause the breakdown of the lubricating film through their abrading action. The build-up of a significant amount of wear particles between the cylinder and piston will propagate wear and scuffing of the interface [18].

3.4.4.2   Lubricant Film Breakdown

The primary cause of seizure is said to be the breakdown of the lubricant film at interacting surfaces. The lubricant film can be of several types produced due to different conditions such as a films produced under boundary lubrication through the interaction of lubricant additives with the contacting surfaces or a thick hydrodynamic film which allows the separation of the two mating surfaces. Under low-speed, high torque conditions when starting-up the hydraulic motor operates in boundary condition. When the speed of the system and/or the viscosity of the oil decreases, the lubricant film becomes very thin where it can reach a point where the entire load is supported by the interacting asperities of the contacting surfaces. This process can eventually initiate seizure [18, 40].

3.4.4.3   Thermal Expansion

Energy losses due to viscous shear can cause the thermal expansion of solid components causing a situation where the piston is stuck in the cylinder bore causing seizure [18, 39].

3.4.5 Current Research Focus

Current research has highlighted the significance of the friction acting at the cylinder/piston interface and its influence on the failure of the axial-piston motor. There is a movement away from traditional materials and treatments which are deemed inadequate to resolve issues involving the motors reliability, efficiency and performance. Yamaguchi states that to solve the tribological problems associated with hydraulic systems; three key areas need to be improved [41]:

   I.   Hydraulic fluids
  II.   Materials and surface treatments

III.   Mechanisms and designs of the system

Traditional techniques used to reduce friction at interacting surfaces include the optimisation of the surface topography of the piston and cylinder and also the application of coatings to the piston. Wear resistant and low friction coatings would act as prevention against the embedding and abrasion of wear particles in to the surfaces of interacting components during operation, whilst reducing the clearance between them which would minimise lubricant leakage and acting friction.

3.5 Surface Improvement Techniques

With an increasing demand for high quality and performance from ferrous materials, there is a constant need to modify and improve components protection against wear and corrosion. Developing industrial applicable surface modification and coating processes within the stringent environmental regulations, is becoming a leading challenge in surface improvement technology [42].

Wear is deemed to be one of the key processes reducing the life expectancies of engineering components. Increases in wear will eventually reduce the operating efficiency of the system through the power losses, leakage and rate of component replacement. One of the most common problems observed in industrial applications is sliding wear which can eventually lead to scuffing or galling [43].

Engine designs and mechanical systems are being modified to reduce friction amongst components whilst allowing them to run at higher operating temperatures. Czichos [44] stated that friction and wear cannot only be determined by the properties of the material but also the characteristics of the engineering system. Reducing wear can be achieved through modifying operating parameters, lubricant and optimising the wear counterface combination [43]. This is where surface improvement technology plays a crucial role. The final aim is to produce durable and optimum efficient systems. This can be achieved by ensuring compatibility between surfaces and

lubricants within tribological environments, as it is not sufficient enough to just introduce new or modified materials to achieve desired results [26,27].

Surface improvement treatments can be divided in to two broad categories:

1) Surface coatings
2) Surface treatment

The former involves treatments where a layer of hard material is deposited or formed on the surface, whereas the latter involves the production of a hardened surface by surface treatment, usually achieved by the diffusion of elements such as nitrogen or carbon into the surface. Coatings can be deposited through a range of methods such as chemical deposition, physical vapour deposition, spraying and electro-deposition, whereas surface treatments usually involve carburizing, nitriding and metallizing [45].

However there are a number of different variations of for the classification of surface treatments. Bell's [46] classification is described as:

1) Coating and plating
2) Thermochemical treatment
3) Thermal treatment
4) Implantation

According to Bell's [46] classification coating and plating refers to the addition of material to the surface, whereas thermochemical and thermal treatment corresponds to treatments that change the surface chemistry and those which change the surface microstructure respectively. Implantation involves ion implantation processes.

In comparison Wilson [47] has categorised surface treatments from a tribological point of view:

1) Short-life surface treatments
2) Long-life surface treatments

Short-life treatments refer to the application of thin, relatively ductile and soft layers to a surface. The aim of these layers is to behave as running-in coatings in the initial stages of operation, as they are usually worn away rapidly and have a shorter life than the component.

On the other hand, long life surface treatments increase the hardness of the material surface and are expected to survive the life of the component.

A number of surface improvement technique options can be suggested to be used to improve the wear resistance of the piston and cylinder surfaces within axial piston motors:

   I.   Diamond Like Carbon (DLC) coating
   II.   Molybdenum disulphide (MoS_2) coating
   III.   Nitriding/Nitrocarburising Variants
       a. Salt bath oxy-nitriding heat treatment
       b. Plasma oxy-nitriding heat treatment
       c. Gas nitriding heat treatment
       d. Sursulf

Techniques II-III will be the primary focuses of this project and will be applied to samples used during experimental analysis. Currently treatment II is used on the piston surfaces of a swash plate axial-piston motor. This study will investigate the option of substituting this treatment for a variant of treatment III, by analysing and comparing the wear and friction effects on the motor when both treatments have been applied separately.

3.5.1 DLC Coating

DLC coatings are of carbon nature composed from graphite and diamond like bonds which essentially determine their physical and chemical properties. The coating is well known for its excellent tribological properties, due to its high hardness and chemical stability. With its low friction and ideal running-in properties, DLC is becoming a popular choice in the automotive industry helping to meet the stringent demands for fuel efficiency and component

durability. Figures show an annual increase of 50% in automotive application, but one of the problems faced in the industry is application of the coating to friction pairs where there are high temperatures and loads acting, factors which greatly impact the tribological characteristics of the coating. The components at the piston/cylinder interface are known to operate at high temperatures (80-120°C), pressures and sliding velocities. Previous research has shown that at temperatures above 100°C the coatings tribological behaviour is affected and it begins to lose its effectiveness above 300°C, increasing wear and friction. Komatsu's findings have shown that during metal on metal interaction of the piston and cylinder bore flash temperatures above 500°C were recorded. Due to this behaviour at high temperatures and the difficulty to mass produce the coating because of economic viability, it is challenging to apply the coating to friction pairs within a hydraulic system [48].

3.5.2 MoS_2 and Manganese Phosphate Coatings (Defric Process)

MoS_2 is one the most common solid lubricants used within industry today, with a range of techniques such as plasma spraying or sputtering methods being used to apply the suspensions of MoS_2 particles on to the friction surface to either form a dry or thin film. Solid lubricants are defined as solid materials that reduce friction and mechanical interactions of surfaces in relative motion. They are seen as alternatives in situations where traditional lubricants are deemed ineffective such as at high temperatures where the lubricant is oxidised or decomposed rendering it ineffective. Also the application of high loads and contact stresses on bearing points of interacting surfaces, can cause the squeezing out of liquid lubricants causing lubricant starvation [49]. This project applies a sprayed-on solid film lubricant (MoS_2) coating paint to a manganese phosphated layer (Figure 3-8).
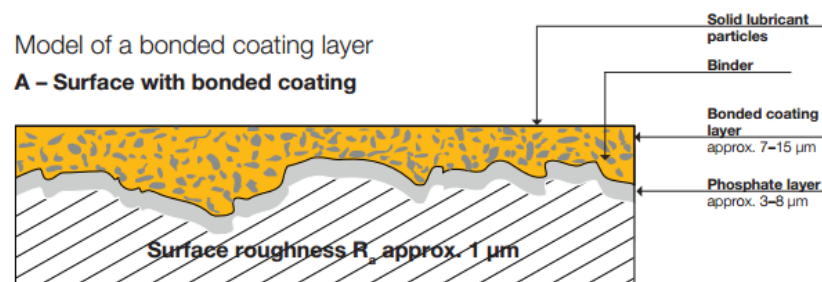
Figure 3-8. Schematic of bonded coating layer after the defric process [50].

The MoS_2 compound has a hexagonal layered structure, with the crystal constituted by unit layers composed of three planes S-Mo-S. The layers are connected by weak molecular forces and MoS_2 is easy to slip between the layers; giving the formed layer excellent solid lubricating properties. In vacuum conditions MoS_2 coatings present excellent friction and wear resistance but when there is oxygen or humidity present these properties degrade [50-52].

Bonded solid lubricating films have excellent solid lubricating characteristics as they can strongly adhere to the substrate material to prevent adhesion of the metal friction pair effectively. In environments where lubricating oils or grease are unsuitable to use, MoS_2 coatings can be used instead making it an ideal option for use as lubrication material for machinery working in starvation [51]. The main constituents of a bonded coating are [50]:

- Solid lubricant – molybdenum disulphide (MoS_2), graphite, polytetrafluoroethylene (PTFE) or a combination of solid lubricants.
- Binder – organic or inorganic, composed of one or two components
- Solvent – organic or water

Manganese phosphate coatings are heavily used in the automotive industry as a running-in coating between interacting surfaces, with the aim to reduce the wear rate experienced. Due to the porosity of the surface layer after treatment a large amount of lubricant can be absorbed allowing the creation on a non-metallic barrier between two contacting surfaces, which prevents seizure occurring and adds protection against corrosion [53]. However within this project phosphating is used to roughen up the material to encourage the bonded coating is firmly rooted on the surface [50]. After the application of the coatings the sample is oven baked from 160-250°C.

A schematic diagram of the complete Defric process is highlighted below (Figure 3-9) [50]:
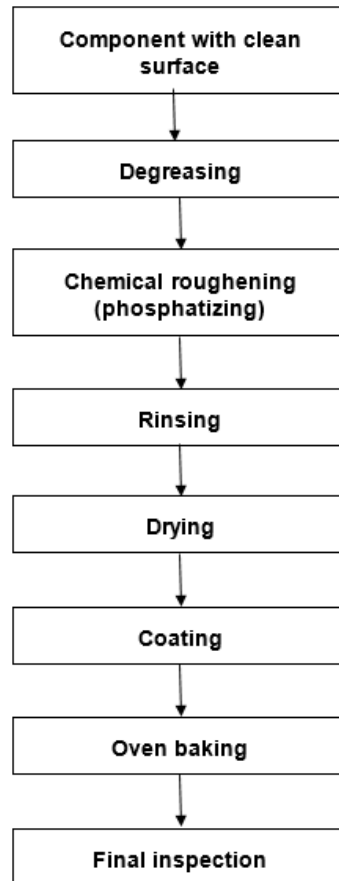
Figure 3-9. Schematic of complete Defric process [50].

3.5.2.1 Summary

The core benefits of a combination of an MoS_2 and manganese phosphate coating is its capability in producing low friction motion between surfaces and the ability to prevent galling and scuffing. This can be partly put down to the easy shear between the layers and the oil retaining capability of the coatings In many industries such as automotive and heavy equipment, the MoS_2 coating is used as a running-in coat to facilitate the breaking in of new interacting components such as gears, pistons and cylinder liners. The key disadvantages of the coating are the deterioration of its chemical stability and its dehydration behaviour when exposed to high temperatures as expected between the piston/cylinder interface. The coatings primary aim is to act as a running-in coating, but with the application of high load conditions as expected at friction pairs, the coating can easily be removed exposing the substrate material below which may significantly increase the wear rate and cause the

seizure of the component [54]. In the presence of moisture the lubricating properties of MoS_2 deteriorates due to the oxidation of the MoS_2 to MoO_3, which does not have the lubrication properties of the former compound. With the increase of MoO_3 content, abrasive wear behaviour increases leading to the increase of friction coefficient for the surfaces being lubricated [49].

3.5.3 Principles of Heat Treatment of Steels

The mechanical properties of steel are greatly influenced by its microstructure, which can be modified through heat treatment to achieve desired mechanical properties.

Many steels owe their durability to the presence of certain alloying elements. Carbon is deemed to be a key element controlling the properties of all steels. With iron alloyed with carbon, the carbon content influences the transformation over a temperature range. When an iron-carbon alloy is formed, carbon is present either in solution or in the elementary form of graphite, or in a combination as iron carbide (Fe_3C). The iron-carbon phase diagram (Figure 3-10) shows the phase changes occurring during very slow cooling or heating in relation to temperature and carbon content [55].

Steels are iron alloys with relatively low carbon weight content (<2%). Alloys with carbon above 2% are generally classified as cast irons. Carbon is one the elements which is known to stabilize austenite by increasing the range of austenite formation in steel, facilitating heat-treatment of low carbon steel. As shown in phase diagram (Figure 3-10) as carbon content increases the formation of ferrite from austenite decreases, this point is commonly known as the eutectoid point [55, 56].

Steels with less than 0.8% carbon are known as hypoeutectoid steels. These are relevant for the steels used within this study. The microstructure of slowly cooled hypoeutectoid steel is shown below (Figure 3-10) [55]:
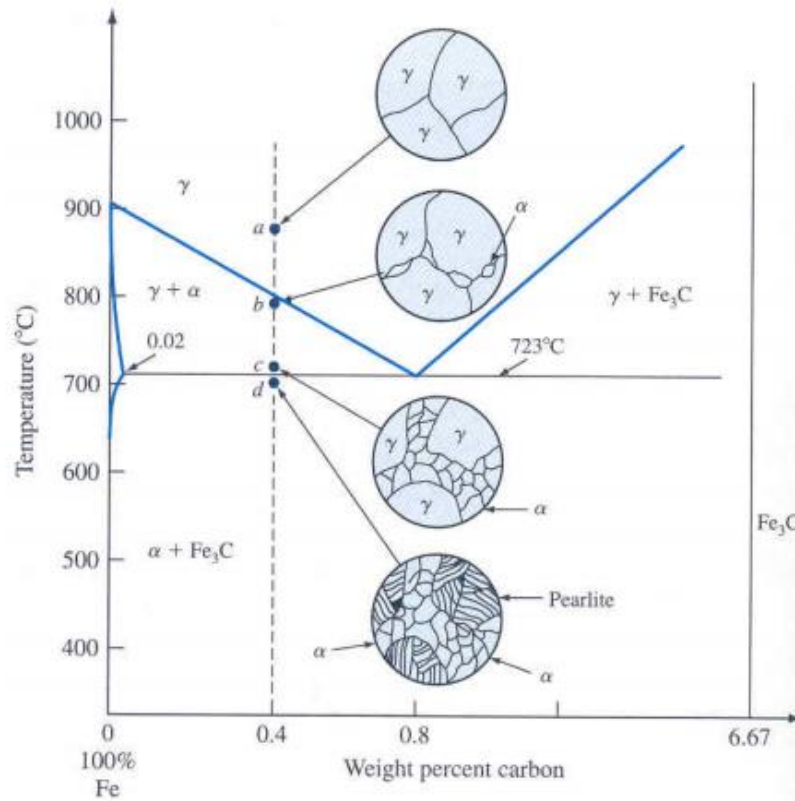
Figure 3-10. Schematic representation of the microstructural changes occurring during slow cooling of 0.4% C steel. a) Formation of austenite (gamma – γ), b) Formation of a grain at γ grain boundaries, c) Growth of ferrite α at grain boundaries [55].

It can be surmised that depending on carbon content, the structure of the slowly cooled (annealed) carbon steels at room temperature will be [56]:

1. 0.007-0.025% carbon – ferrite.
2. 0.025-0.8% carbon – ferrite and pearlite.
3. 0.80-2.06% carbon – pearlite and carbides precipitated from austenite.
4. 2.06-4.2% carbon – pearlite and graphite.

The iron-carbon phase diagram allows the selection of the temperature for annealing, normalising and hardening.

3.5.4 Metallographic Structure and Associated Properties

The common types of microstructure that can be formed during heat treatment are [55]:

Ferrite: Solid solution of carbon and other alloying elements in body-centered cubic (α-Fe). Known for its soft and ductile properties, with a hardness of 70-100 BHN.

Cementite: Compound composed of iron and carbon. It has an orthorhombic crystal structure, known for its brittle and hard properties with a hardness of 65-85 HRC.

Pearlite: Is a eutectoid mixture of cementite and ferrite possessing a hardness of RC 10-30.

Martensite: Is the supersaturated solid solution of carbon and other elements in alpha iron with a distorted lattice.

3.5.5 Nitriding and Nitrocarburizing Fundamentals

The nitriding process is a ferritic thermochemical case hardening process where the surface of a component is enriched with atomic nitrogen allowing it to dissolve interstitially into the iron matrix after diffusing into the surface zone. The treatment is usually carried out within the temperature range of 400-590°C and if the nitrogen concentration is greater than 2.5 wt% a single or multi-phase nitride layer is created, which can improve the wear resistance of the component alongside other dynamic characteristics of the ferrous material. One of the advantages of nitriding or nitrocarburizing is the low temperature the process is carried out at, which prevents phase transformation to austenite which prevents the physical distortion of the component which would essentially reduce its service life [42, 56, 57].

Nitriding refers to the process where only nitrogen is introduced to the surface, but if carbon is also diffused in simultaneously this treatment is referred to as nitrocarburizing. Post nitriding/nitrocarburizing, oxidation can be carried out producing a layer of magnetite on top of the nitrided zone. This layer acts as a running-in coat and can further improve the treated components friction and wear properties [42].

The key properties produced by nitriding can be summarized as follows [55]:

1. High fatigue strength.
2. High surface hardness and wear resistance alongside reduced risk of scuffing and galling.
3. Improved corrosion resistance,

3.5.5.1   Microstructure of Nitrided Zone

The nitriding/nitrocarburizing treatment usually produces two distinct layers at the surface of the component, the first layer is commonly known as the compound layer, with a diffusion zone directly below (Figure 3-11) [42]. Most of the Nitrogen diffuses in to the metal forming a deep diffusion zone, only 10% of the nitrogen remains at the surface which combines with carbon and iron to create the tough compound layer [55].
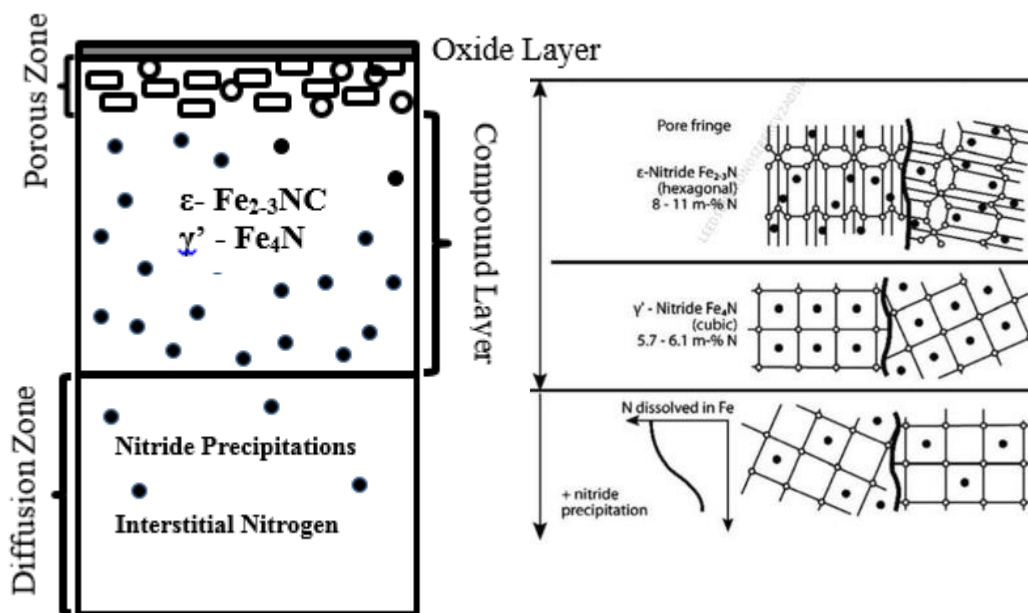
Figure 3-11. Schematic diagram of the structure through the cross-section of an oxy-nitrided sample [16].

Using the iron-nitrogen phase diagram Figure 3-12, due to nitriding being carried out at temperatures within the ferrite phase field, the process has to occur below eutectoid temperature (590°C). When nitrogen content exceeds 0.1 wt%, γ'-nitride (Fe₄N) phase is formed, consisting of an fcc arrangement of Fe atoms with ordered occupation of the N atoms at the octahedral interstitial sites. With nitrogen content over 6 wt%, γ' phase begins to form in

to ε-nitride ($Fe_{2-3}N$) phase, which in contrast has hcp arrangement of Fe atoms with ordered occupation of the N atoms at the octahedral interstitial sites. Below 500°C as the nitrogen content increases ζ-nitride (Fe_2N) phase begins to form [58].
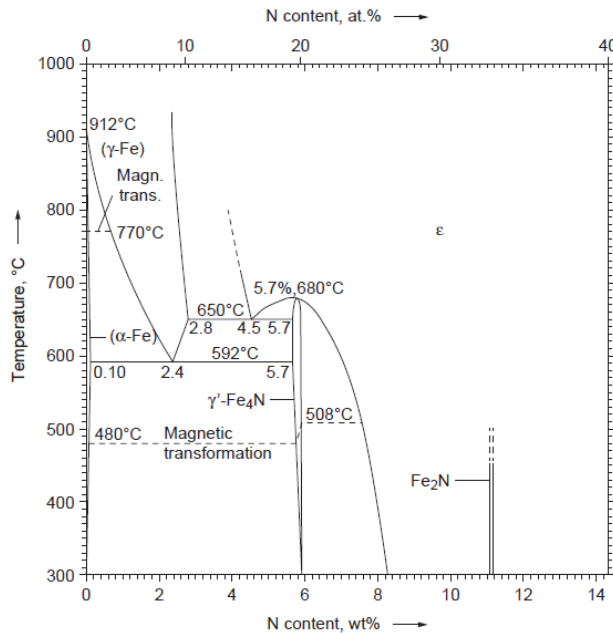
Figure 3-12. Iron-Nitrogen phase diagram [56].

As nitrogen diffuses into the surface of the steel during the nitriding process, these iron nitrides begin to form as solubility wt% limits are reached. The compound layer usually composed of γ' & ε- nitride phases is commonly referred to as the white layer [43]. The layer can be composed of iron nitrides either as a single layer of γ'-Fe_4N or ε –$Fe_{2-3}N$ or as a mixed-phase compound layer composed of both types of nitrides. γ-phases are seen to dominate the compound zone after nitriding, whereas ε-phases are almost solely seen after nitrocarburizing [58]. Compared to the nitriding process, nitrocarburising has a greater effect on the composition of the compound layer and of the wear properties of the component [42, 56, 57, 59].

Both phases have different crystalline phases with the ε-phase having a hexagonal closely packed (HCP) structure while the γ-phase has a face centred cubic (FCC) arrangement [60]. A nitride layer purely composed of γ-phase is of higher hardness than that of one composed of ε-single phase. The single γ-phase also increases the wear resistance and fatigue strength of the

parts compared to ε-phase, whereas the latter phase improves the scuffing wear resistance under high loading conditions. However a higher percentile of the ε-phase is desired in the nitride layer due to its toughness and ductility and limited brittleness [61]. The two crystalline structures with the application of shear stresses responded differently. Ease of plastic deformation with materials is determined by the number of available slip planes, and for successive plastic deformation to occur it is necessary for at least five independent slip systems to be present. The limitations of slip planes within the HCP structure reduces the probability of plastic deformation occurring, and improves its ductility [60].

However with a nitride layer composed of a mixture of ε and γ' phases it is prone to spalling due to its brittleness caused by the presence of two phases and sliding bands. With the application of high stresses the compound layer is fractured alongside the formation of hard abrasive particles [62, 63].

The impact of both phases on the properties of compound layer are summarised in Figure 3-13 [64].

γ' – phase: Fe_4N_{1-x}	Two sandwiched layers or mixture of γ' – phase and ε-phase	ε-phase: $Fe_3(N,C)_{1+x}$
Monophasic less brittle	Biphasic Very brittle	Monophasic more ductile

Gas Nitriding | Nitrocarburizing

Figure 3-13. Different types of compound layers formed with nitriding variants [64].

The presence of carbon during the nitrocarburizing process stabilises the ε – $Fe_{2-3}(N,C)$ phase allowing it to form at much lower nitrogen levels than in the absence of carbon. This results in faster growth of the compound layer due to the much wider solubility range of carbon and nitrogen in the ε-phase enabling a steeper concentration gradient than in the γ'-phase as shown by the Fe-N-C phase diagram (Figure 3-14) [43, 65]. Figure 3-15 is a schematic diagram of the formation and evolution of the compound layer upon nitriding α-Fe.
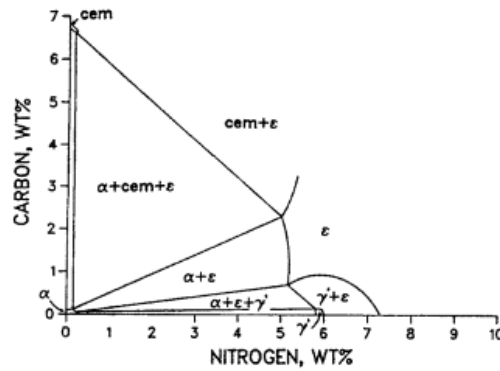
Figure 3-14. Fe-N-C phase diagram at 570-580°C [65].
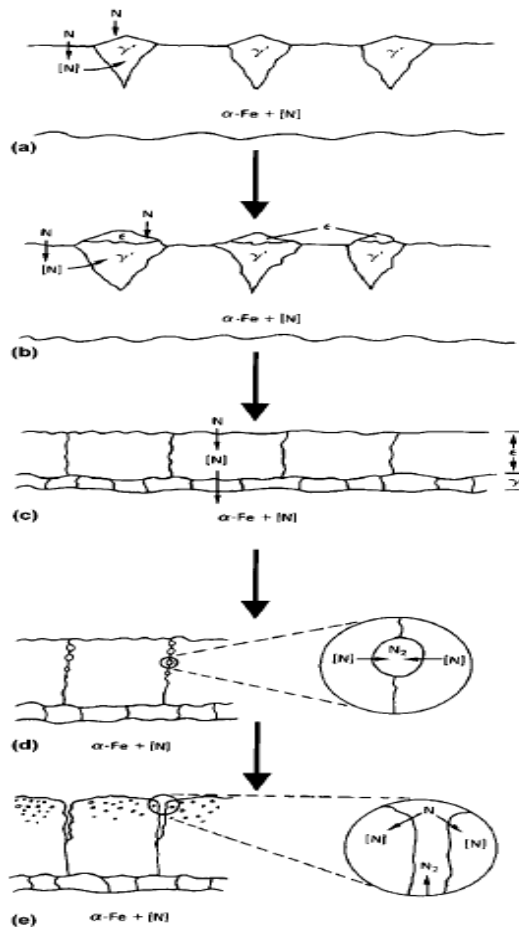
Figure 3-15. Schematic illustration of the microstructural stages of compound-layer formation and evolution upon nitriding α-Fe. a)Nucleation of γ' nitride at the surface followed by its growth with Nitrogen presence b) ε phase can grow on top of the γ' particles c) As a result a double ε/γ' layer has formed, and further growth can only be established by nitrogen transport through both sublayers. d) Decomposition of iron nitride underneath the surface of the compound layer occurs for extended stages of nitriding, leading to development of pores filled with N2 gas at grain boundaries and within the grains. e) Pores at grain boundaries leads to channels at grain boundaries in contact with the outer nitriding atmosphere [56].

The nitrogen rich compound layer contains porosity caused by the association of dissolved nitrogen as gas molecules (N_2) at grain boundaries and within grains. At the surface-adjacent part of the layer, porosity is most distinguishable due to this layer having the largest dissolved nitrogen content [56, 57, 66]. The advantage of this porosity is that they behave as small

reservoirs of lubricants forming a self-lubricating surface improving wear resistance [64].

Binder et al [58] found that ε-phase compound layers showed superior performance in sliding wear tests, with wear volume loss being approximately twice less than that of the γ' phase. They proposed that the model of the wear process (Figure 3-16) consisted of the wear of the compound layer until the occurrence of micro-cracks, which had the ability to propagate and reach the interface of the compound/diffusion layers. Hard particles are formed by the fracturing of the compound layer due to repeated loading, these particles can induce plastic deformation and the creation of other wear particles.
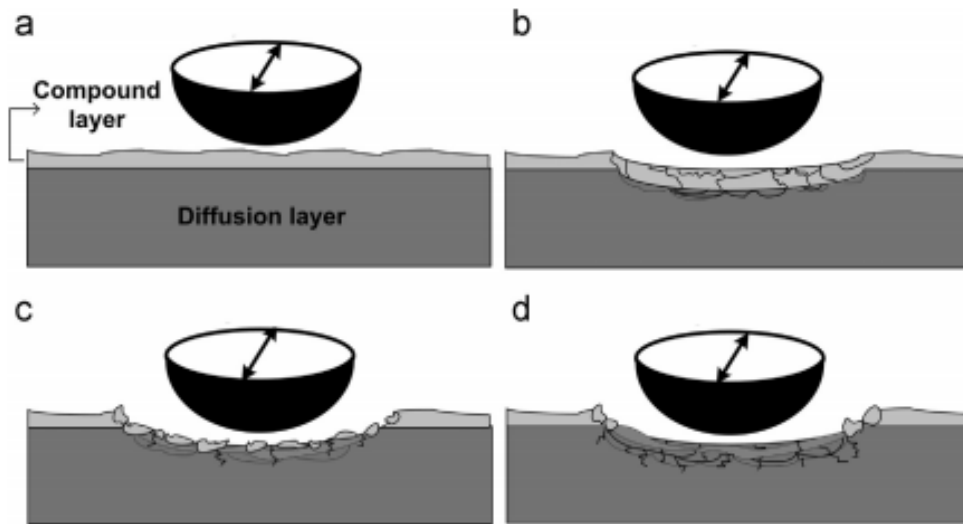
Figure 3-16. Proposed wear mechanisms for the compound layer after nitriding [58].

Wear resistance is influenced by the hardness of the compound layer, where harder surfaces generally produce more wear resistant surfaces. This provides effective resistance against abrasive particles and nitrocarburising especially improves protection against adhesive wear [64].

With the additional presence of a shallow porous layer at the surface of the compound layer the scuffing and seizure resistance properties of the samples are improved. The compound layer's ability to reduce the tendency to cold weld against interacting surfaces and provide low friction combined with the lubricant reservoirs due to the porosity present on the outer layer of the

compound layer act to give significant protection against adhesive wear and scuffing [64].

The diffusion layer lies beneath the compound layer with a thickness ranging from 0.1-0.8mm, due to the decrease of nitrogen content from the edge to the core of treated components iron nitrides are not formed in this zone. With unalloyed steels the crystalline phases produced in the diffusion layer are influenced by the cooling rate after treatment. At a faster cooling rate e.g. using water, a higher hardness is achieved in the zone compared to slow cooling which allows greater ductility [59]. Binder et al [58] demonstrated that the nature of the compound layer had no influence of the frictional behaviour however this behaviour was instead governed by the properties of the two different layers present after nitriding.

With alloyed steels the diffusion zone is mostly composed of solid solution (α-Fe,N), and due to alloying elements nitrides and carbonitrides such as γ' - Fe_4N and ζ-Fe_2N are formed in the diffusion layer formed by precipitation [56, 66]. This is due to the diffused nitrogen interacting alloying elements such as aluminium, chromium and vanadium. The nitrides created such as aluminium nitrides are shown to exhibit very high hardness values and also influence the depth of the diffusion zone [42].

The diffusion zone hardness is influenced by either the presence of interstitial solution of nitrogen or the formation of nitrides. In the first case small amounts of nitrogen increase the hardness of steel drastically this is effective with low alloy steels. Whereas in the second situation with the formation of nitrides of iron nitrides or alloying elements cause precipitation hardening, making this the predominate hardening mechanism with alloyed steels [64].

Enhancement of a component surface with nitrogen or nitrogen and carbon can be achieved using three techniques [42]:

- Use of a molten salt (salt bath oxy-nitriding)
- Using a gas mixture (gas nitriding)
- Using energy plasma (plasma oxy-nitriding)

3.5.5.2   Salt Bath Oxy-Nitriding Heat Treatment

Salt bath nitriding is a well-established thermochemical process used widely in a range of industries from automotive to oil. The process significantly improves wear and corrosion resistance alongside fatigue strength, and is considered as an alternative to other processes such as case hardening and galvanic techniques. Since the 1970's there has been environmental concerns about treatments employing toxic cyanide-based baths. With the implementation of stringent anti-pollution measures there has been the development of alternative treatments. The Tufftride process by Degussa in Germany, uses a cyanide free salt bath process, with as little as three to four percent cyanide being present in the bath [55].

The process consists of five stages [42, 67, 68]–

I.   Degreasing – Removal of dirt from surface.
II.   Preheating – Removes any water on the components alongside producing a thin oxide layer on surface on the components which benefits the nitriding process.
III. Nitriding – Surface of ferrous material enriched with nitrogen.
IV.   Oxidising – Nitrided layer covered by an oxide film.
V.   Mechanical Processing – Oxide layer moderately polished and oxidised again – due to rough surface.

When the process is carried out from steps I-III, it is referred to as an Isonite (Iso) process and when done using steps I-V it is known as QPQ (Figure 3-17) [69].
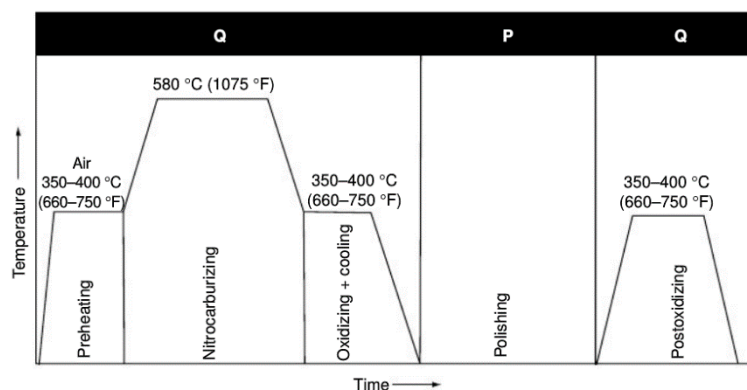
Figure 3-17. Salt bath nitriding heat treatment process [69].

The samples are nitrided in a molten salt bath of cyanate at 400-600°C which causes its catalytic decomposition to form cyanate, carbonate and adsorbed nitrogen. Due to the formation of carbonate, both nitrogen and carbon diffuse in to the surface of the steel to form a nitrate layer consisting of carbon, hence this process is recognised as nitrocarburising (Equation 3-1) [42, 67, 70].

$$4CNO \rightarrow CO_3^{2} + 2CNO + CO + 2N \tag{3-1}$$

Nitrocarburizing creates a layer consisting of an outer compound layer and an underlying diffusion layer. The samples are then oxidised in a specialised cooling bath at 370-430°C, which produces an oxide layer on the surface of the treated component [59].

Post oxidation of the nitrided layer forms a compound layer composed of ε-carbonitride and magnetite, this is due to free iron & iron nitrides from the compound layer combining with oxygen molecules to form a stable oxide layer. Magnetite (Fe_3O_4) is known to improve the wear and corrosion resistance of a surface due to its low friction properties and chemical stability, and acts as some sorts as a running-in protective layer. The magnetite phase growth is enhanced with the presence of ε-carbonitrides in the compound layer due to more oxygen being present in this phase [56, 71, 72].

3.5.5.3   Plasma Oxy-Nitriding Heat Treatment

Plasma nitriding commonly known as ion nitriding uses low energy plasma to introduce nitrogen and in some cases carbon into the surface of ferrous components, within a vacuum environment filled with gas mixture of nitrogen, hydrogen and an additive gas containing carbon [42, 73]. Typically a gas mixture of 25% nitrogen with 75% hydrogen is used, with the nitrogen concentration being increased to 50% during processing to increase the rate of case development. Using a higher range of nitrogen concentration (above 50%) will lead to the formation of an excessive white layer. If too low a percentage of nitrogen is used, the formation of the case is reduced [55]. The ionised gas serves as a medium for both heating and nitriding [43]. The component to be treated is made the cathode of an electrical circuit whilst the

chamber is used as the anode (Figure 3-18). Using a voltage of 300-800V between the two electrodes within a pressure range of 1-8 mbar a glow discharge is created. This discharge covers the component at the cathode and the component becomes heated by the transfer of energy due to ionic bombardment. This energy transfer allows the diffusion of nitrogen in to the components surface where it interacts with existing elements to form the nitrided structure described previously [73].

Post-oxidation of the nitrided component is carried out by exchanging the gas mixture used for nitriding to a gas composition of hydrogen and oxygen. The process is usually carried out at a lower temperature than nitriding, allowing the formation of a stable iron oxide layer. The process has to be controlled to prevent the formation of hematite instead of magnetite in the oxide layer [73, 74].
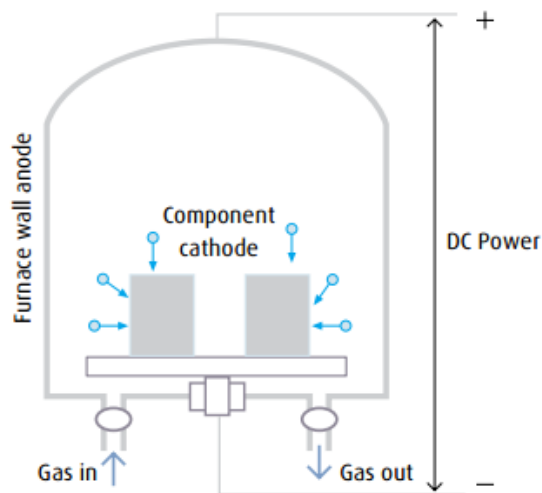
Figure 3-18. Cross section of a plasma nitriding furnace [74].

3.5.5.4   Gas Nitriding Heat Treatment

The gas nitriding process (Figure 3-19) is carried out using a convection furnace in an ammonia atmosphere at temperatures ranging from 490-530°C. The ammonia can be mixed with nitrogen or hydrogen. The furnace is heated up to the chosen nitriding temperature in the presence of nitrogen before ammonia is added; this is done to minimise the risk of explosion by the mixing of ammonia and oxygen [57]. Only part of the ammonia dissociates catalytically at the surface of the hot steel sample, and some of the nascent

nitrogen is absorbed [43]. Initially there is a rapid transfer of nitrogen to the components surface as a high flow rate is used, but once the compound layer is produced the process is then controlled and carried on until the desired nitriding depth is reached. Cooling of the sample is carried out in nitrogen to prevent oxidation [57].
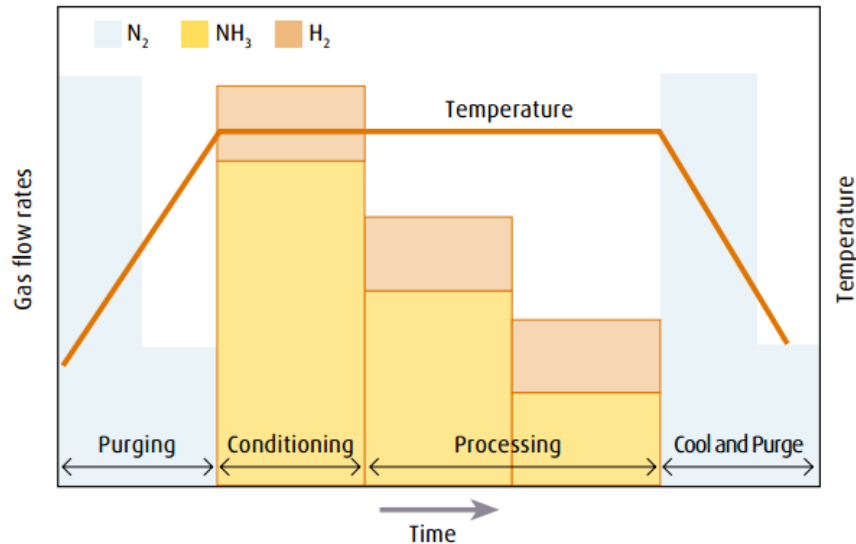
Figure 3-19. Gas nitriding process [74].

3.5.5.5   Sursulf

The Sursulf (SN) process is a low polluting, cyanide free nitriding salt bath treatment which uses sulphur as accelerant. The bath is composed of a mixture of cyanates and carbonates of lithium, sodium and potassium along with small amounts of potassium sulphide (K_2S). The cyanate is used as the source for nitrogen and sulphide (K_2S) is the source for sulphur. At the surface the cyanate catalytically decomposes at the surface of the steel components being treated, to liberate carbon monoxide and nascent nitrogen diffuses in to the material of the sample being treated to form a compound layer. The sulphides in the bath also react with components being treated to form iron sulphide on the outer surface layer and filling the porosity present on this surface of the treated component. The presence of a sulphide layer acts as solid lubricant due to its close packed hexagonal crystalline structure allowing easy slip along the close-packed plane [51, 55].

The presence of sulphur within the treatment bath stabilises the formation of primarily ε-phase within the compound layer and a very shallow finely porous zone.

With only the presence of ε-phase, there is a reduction in the loss of particles from the surface as compared with the amount of lost from biphasic compound layers containing both γ'-phase and ε-phase [64].

3.5.5.6 Case Depth Modification

The case depth obtained by nitriding can be influenced by a range of factors such as nitriding temperature, duration, steel composition, microstructure and availability of nitrogen [55].

For all variants of the nitriding technique the compound layer thickness is shown to be influenced by the alloy content in the steel (Figure 3-20). The thickness is seen to decrease with the increasing of alloy content for all variants of the technique. For the salt bath nitriding technique with the decreasing of carbon content of the steel a reduction of the compound layer thickness is also observed [57].

The compound layer thickness is also influenced by the nitriding temperature where at the higher temperatures between 400-580°C, a thicker layer is formed due to the increase in nitrogen diffusivity [75].

With the increase of nitriding time the diffusion layers thickness is also seen to increase, but with steels of a higher alloy content a lower depth is observed when compared over the same times and nitriding temperatures. This may be due to alloying elements absorbing nitrogen to form nitrides, thus a greater concentration of nitrogen atoms will be needed to reach a set depth when compared to steels where there are no elements to trap any nitrogen [57].
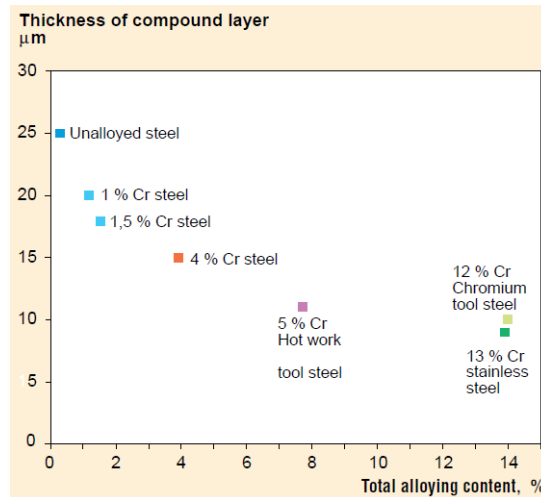
Figure 3-20. The effect of the alloying contents of the treated steel on the hardness of the compound layer [57].

3.5.6 Environmental and Technical Difficulties

Salt bath nitriding is a popular choice due to a range of factors such as its ability to produce tough and wear resistant nitride layers in fairly short process times and it is conceptually simpler and cheaper when compared to its counterparts - plasma and gas nitriding [59].

The key problem with using salt baths is that it presents some serious environmental concerns. One of these problems is with the post processing cleaning steps of the salts used, which contain high percentages of toxic potassium and sodium cyanide. Compared to plasma oxy-nitriding, the latter seems to present fewer environmental problems and is seen as a greener process where virtually no toxic products or waste are created. Plasma oxy-nitriding is not only considered to be the more environmental friendly option but also the better choice to produce superior results in terms of surface improvement. Salt bath and gas nitriding can produce surfaces which are brittle and spalled which requires grinding or cleaning to remove but this is not a problem associated with the plasma process. Plasma techniques help to achieve higher surface hardness whilst maintaining the core properties of the material due to lower processing temperatures (Figure 3-21) [66, 76, 77]. One of the advantages of salt bath nitriding over the other variants is the production of a single phase compound layer; a mixed structure formed by gas and plasma nitriding causes high internal stresses and the interface between the

two crystalline phases is weak. This is due to the volume growth difference with the formation of the two phases. The high stresses also cause an increase in friction and the samples wear rate [78].
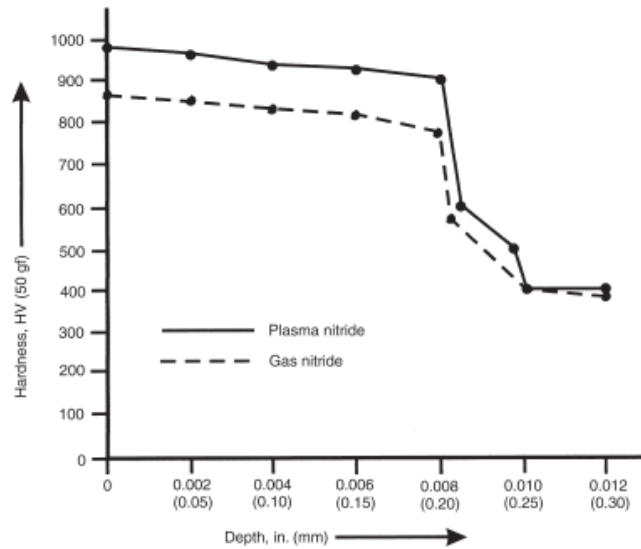
Figure 3-21. Comparative hardness of plasma nitriding versus gas nitrided steel [77].

When comparing gas nitriding to plasma nitriding, the former is less harmful to the environment compared to salt bath nitriding but it still produces significant amounts of exhaust fumes and gases which are still detrimental to the environment. A significant risk associated with gas nitriding is possibility of explosions due to the use of a combustible atmosphere during the application of the treatment. Plasma nitriding does not have the same problems associated with gas nitriding and has actually shown to have reduced processing times and energy consumption as shown in Figure 3-22 [63, 76].

	PNC	GNC	GNC/PNC
Amount of gas used, $m^3 h^{-1}$	0·6	6·0	10
Total carbon emission via CO and CO_2, $mg\, m^{-3}$	504	137253	272
Total amount of NO_x gas, $mg\, m^{-3}$	1·2	664	553
Output rate of residual carbon beaming gas, $mg\, h^{-1}$	302	823518	2726
Output rate of residual NO_2 gas, $mg\, h^{-1}$	0·72	3984	5533

Figure 3-22. Comparisons of emissions for plasma (PNC) and gas nitrocarburizing (GNC) [76].

3.5.7 Material Optimisation

The difficult task faced with producing optimal results through the use of surface treatments is the selection of the base material. This factor is most critical with the nitriding process, where it is important to select a type of steel which will not only be appropriate for the operating environment of the component but will also produce good nitriding results whilst being cost effective and easy to mechanically process [77].

3.5.7.1   Alloying Elements for Nitriding Steel

Certain types of alloyed steels have been shown to respond better to nitriding in terms of surface hardness, distortion, core hardness and formation of stable nitrides. The most common elements found in nitriding steels are aluminium, chromium, molybdenum, tungsten and vanadium. The effects of each of the elements are described below and highlighted in Figure 3-23 [77]:

> **Aluminium**: forms extremely tough and hard nitrides during the nitriding process at the materials surface, but wt% content over 1% will cause the surface to crack under extreme loading conditions. This will occur due to the core of the material being ductile compared to the surface which may cause crack propagation to occur during heavy loading.

> **Chromium**: are known to form stable nitrides and a tough casing, but a high content such as those found in stainless steels make it difficult to nitride. This is due to the chromium elements reacting with oxygen to create a chromium oxide barrier on the surface of which depasivation must occur before the nitriding treatment is effective.

> **Molybdenum**: allows the formation of stable nitrides and prevents the surface of the steel becoming brittle during nitriding.

> **Tungsten**: allows the steel to retain its hardness at high operating temperatures.

> **Vanadium**: forms stable nitrides alongside tough grains in the case.

It is very difficult to nitride stainless steels using conventional methods such as salt bath and gas nitriding due to the surfaces passivation caused by the high content of chromium [77]. It can be achieved using the plasma nitriding process which allows the surface to be highly activated [57].
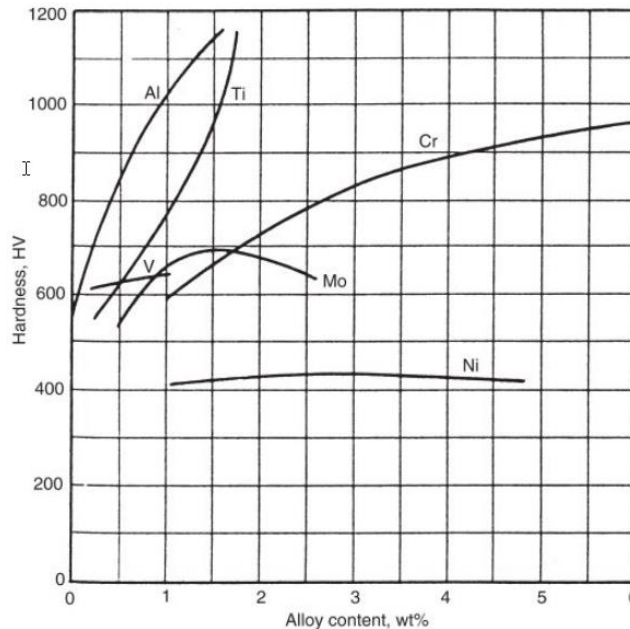
Figure 3-23. Effect of alloying elements on hardness after nitriding [77].

This study will use a low carbon alloy steel (31CrMoV9) for samples that will be nitrided, this material will replicate the one used for pistons in a hydraulic motor by Komatsu Global, the sponsors of the project [79].

3.6 Lubricants

The function of a lubricant is to essentially control the friction and wear in the system it is applied to. It is important to access the performance of the lubricant in relation to its influence on the friction, wear and degradation prevention behaviour of a system. Oils can be of different origins mineral or synthetic which provides a vast array of hydrocarbon compounds. These substances are not only used for their lubrication properties but to help control other factors such as wear and friction. Lubricants made from mineral oils are partly refined and impure, the balance of this impurity and purity is crucial to the oxidation stability of the oil. Additives are added to the lubricant to change its properties and modify its overall performance. The additives can dictate

specific characteristics such as wear, friction, corrosion tendency and oxidation amongst others [80].

Lubrication oils typically used are composed of 95% base stock and 5% additives. Two main sources of base stock are mineral or synthetic, each type of oil exhibit different properties and are suitable for different applications [80].

Mineral oils: Are the most commonly used lubricants. Manufactured from crude oil, there are certain advantages and disadvantages to the usage of mineral oil to lubricate specific machinery and components, which must be considered before it is used within lubricating systems. The low cost of mineral oils ensures its continued use in many industries even with the rapid development of synthetic oils.

Synthetic oils: They were originally developed as a replacement for mineral oils for countries which lacked a reliable supply of it. Even with the high costs of manufacturing, in some cases three times higher than mineral oils, synthetic alternatives are increasingly being used especially in specialised applications where the lubricating properties of mineral oils are deemed inadequate. Mineral oils have serious disadvantages such as oxidation and viscosity loss at high temperatures and solidification at low temperatures. With the increasing demand of high performance lubricants to increase the durability and performance of machinery, the development of synthetic oils without the flaws of mineral oils has rapidly progressed.

The base stock/oil of lubricants whether mineral or synthetically derived can be categorised in to five categories highlighted below (Figure 3-24) [81].

API BASE OIL CATEGORIES				
Base Oil Category	Sulfur (%)		Saturates (%)	Viscosity Index
Group I (solvent refined)	>0.03	and/or	<90	80 to 120
Group II (hydrotreated)	<0.03	and	>90	80 to 120
Group III (hydrocracked)	<0.03	and	>90	>120
Group IV	PAO Synthetic Lubricants			
Group V	All other base oils not included in Groups I, II, III or IV			

Figure 3-24. Base oil categories and properties [81].

Properties of an ideal base oil are for it to be moderately viscous, inert towards surface, thermally stable, less volatile, provide wear and friction reduction and have good additive solubility [82].

3.7 Hydraulic Fluids

Hydraulic fluids are considered to be an integral component of a hydraulic system. Its main purpose is to act as a lubricant, sealant and a medium to transfer heat and energy. One of the key advantages of hydraulic fluids is its ability to take the shape of any container, which allows the efficient transfer of force across the hydraulic system. It is crucial that a clean, high quality fluid is used to optimise the operation of the motor [7].

With the expectation of hydraulic systems to run under high pressures and loads, closer component fits are necessary which in-turn can cause acute lubrication problems. Eighty percent of hydraulic system break-downs are connected to fluid failure. This why hydraulic fluids with adequate lubricating properties are needed to provide sufficient lubrication between interacting components through the formation of continuous films, adaptable over a range of temperatures and pressures. They also need to have high chemical stability and wear resistant properties to allow the application of high loads. The tribological properties of the motor can be significantly affected by other properties of the fluid such as viscosity, concentration of contamination and additives [30, 83].

3.7.1 Lubricant Viscosity

Using a fluid of too low viscosity prevents the sealing of clearances in the system which results in a loss of motor efficiency due to the increase of internal leakage. Low fluid viscosity leads to the system operating in boundary condition and the failure of the lubricating film, which increases wear until failure due to seizure occurring. Fluids with higher viscosities create better lubrication regimes due to the formation of a thicker lubricating film, hence a reduction in wear and friction can be observed. Using a fluid of too high viscosity also has significant consequences such as the oil being too thick

preventing it from flowing easily through the motor, requiring it to work harder which in-turn reduces the motors efficiency. It can also cause the overheating of the motor which may lead to cavitation [30].

Running temperature and pressure has an important role on influencing the viscosity of the fluid, a decrease is observed with the increasing of both factors. Fluids with a high viscosity index are less affected by temperature, than those with a low V.I. With the high temperatures experienced at the piston/cylinder interface of the hydraulic motor, it can be expected to run in boundary condition with metal-on-metal occurring increasing wear and friction. Due to the inability of the fluid to protect the interacting surfaces additives are added to form a solid-like protective film [83].

3.7.2 Lubricant Contamination

As stated earlier it is crucial to use clean, high quality lubricant as it greatly influences the performance of the system. There are a range of common sources of contamination [30]:

➢ **Contaminated new oil**: The oil is contaminated during manufacture and handling and is then used in the system.

➢ **Internally produced contaminants**: Particles produced from the rubbing of surfaces will remain in the system until the fluid is cleaned or removed. As explained previously the interaction of these particles with surfaces can lead to the seizure of the entire motor.

With swash plate axial-piston motors as particles of material are removed from the component surfaces, there is an increase in fluid leakage caused by enlargement of clearances, alongside an increase in operating temperature. The removal of particles allows the exposure of surface material to the lubricating fluid which increases the loss of material and the degradation of the motors performance. The most common areas of contamination in a hydraulic axial-piston motor are highlighted in Figure 3-25 [30].
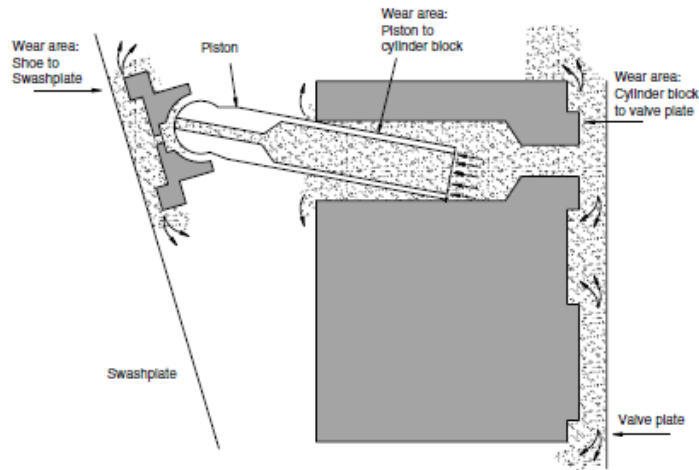
Figure 3-25. Critical areas in an axial piston pump where contamination produces excessive wear [30].

3.7.3 Lubricant Additives

The performance of lubricants can be enhanced through the use of a combination of additives. These additives allow the improvement of performance properties of the base oil, which is essentially responsible for giving the lubricant its inherent properties such as lubricity, viscosity etc. It is critical to have a balance of concentration of the additives mixed with the base oil, as an additive can enhance aspects of the system behaviour alongside also negatively impacting its chemistry [83, 84]. Ninety five to ninety eight percent of hydraulic fluids are composed from base oils, whilst the rest is from additives. The most important additives are surface active modifiers such as friction modifiers, dispersants/detergents and wear inhibitors shown in Figure 3-26 [16].

Type	Chemistry
Antioxidants (AO)	Phenolic and aminic AO, zinc dialkyldithiophosphate (ZnDTP)
Steel/iron corrosion inhibitors	Carboxylic acid derivatives, sulfonates, succinic acid compounds
Antiwear (AW) additives	Esters, ZnDTP
Extreme pressure (EP) additives	Phosphorous and sulphurous compounds, thiophosphates, sulphurised hydrocarbons (active and inactive)
Friction modifiers	Fatty acids, polar compounds, esters
Detergents/dispersants	Ca and Mg phosphates, sulfonates, phenates
Viscosity index improvers (VIIs)	Polymethacrylates
Pour point depressants (PPs)	Polymethacrylates

Figure 3-26. Most common additives in hydraulic fluids [16].

The lubricating mechanism of additives on worn surfaces is known as adsorption lubrication. The formation of a low shear strength interface between interacting surfaces helps to achieve a lubricating or friction reduction effect. The two types of adsorption are physisorption and chemisorption, with the latter occurring at higher temperatures and being more effective within practical applications [80].

➤ Physisorption

Physical adsorption is when the molecules of the adsorbate can attach or detach from a surface without any irreversible changes to the surface or the adsorbate. Although most liquids and gases physisorb to most solid surfaces, this process is limited by a temperature threshold. The bonding between the substrate and the adsorbate is provided by dispersion forces (Figure 3-27). The process is effective in reducing friction as long as temperatures do not excessively exceed ambient temperature.
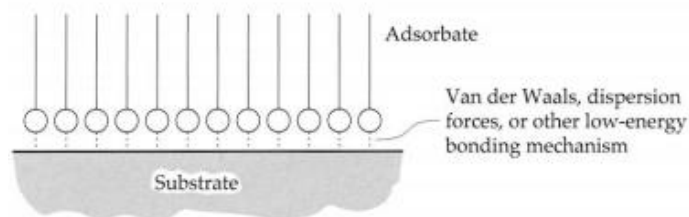
Figure 3-27. Schematic illustration of physisorption [80].

➤ Chemisorption

Chemical adsorption is an irreversible or partially irreversible form of adsorption partially due to chemical bonding between the substrate and the adsorbate (Figure 3-28). The strength of the chemical bonding between the adsorbate and the substrate depends on the reactivity of the substrate material.
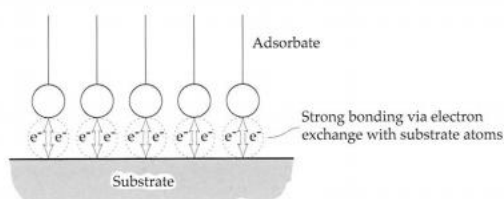
Figure 3-28. Schematic illustration of chemisorption [80].

3.7.3.1   Extreme Pressure (EP) Additives

EP additives are used to reduce wear and prevent seizure occurring due to the interaction of surfaces. EP additives act with surfaces under severe distress and aim to prevent failure from scuffing or seizure. They inhibit metal on metal adhesion when the natural protective oxide layer is removed due to surface contact in high load, temperature and speed conditions [49]. Generally most EP additives contain at least one aggressive non-metal such as sulphur, which can react with the exposed metallic surface to create a protective surface film which can improve friction and wear behaviour [80]. The additives are activated at certain temperatures and pressures, in the case of sulphur based EP additives high pressures and temperatures are needed to produce a tribofilm [49].

3.7.3.2   Anti-Wear (AW) Additives

Anti-wear additives differ from extreme pressure types as they are designed to operate and produce protective surface films to reduce wear rates, under normal operating conditions. Whereas EP additives are applied to situations of severe environments as they have the ability to react swiftly with the surface under distress.

AW additives are able to reduce the wear rates of interacting materials by either forming a thick protective film, which can prevent contact between the two surfaces and is removed in place of the surface material or by modifying the geometry of the surface asperity through chemical bonding to allow the formation of a hydrodynamic film [49].

3.7.3.3   Zinc Dithiophosphates (ZDDP)

ZDDP is the most common additive used in hydraulic fluids, as it is well known for its excellent antiwear and extreme pressure properties. Additives determine the wear and friction behaviour of the system through the formation of tribofilms on running tracks due to sliding contacts. These tribofilms are formed through thermochemical reactions of additive molecules with the metallic surface. The molecular structure of ZDDP is shown in Figure 3-29.

The advantages gained though additives can either be further improved or eliminated depending on the surface treatment or coating applied [48, 85]. The effectiveness of ZDDP and its wear properties are said to be improved when using harder surfaces where there is only a small difference between the hardness of the two interacting surfaces [86, 87].
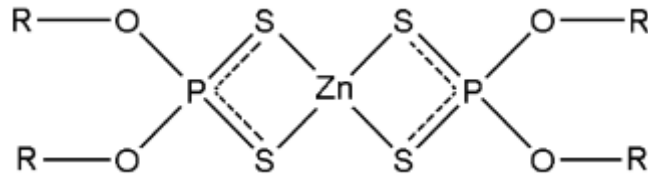
Figure 3-29. Simple structural formula of ZDDP [88].

The structure of the tribofilm is influenced by several factors such as the composition of the lubricant and the interaction of the two surfaces. Under moderate contact conditions, the ZDDP reacts with iron in the surface material and a thick inorganic amorphous phosphate film is formed. The film consists of glass containing zinc, phosphorous, oxygen and iron sulphide. The production of long chain polyphosphates has been shown experimental to provide better wear resistance compared to a layer composed of short chains [88, 89].

It is believed that ZDDP can reduce wear in boundary lubrication through a number of mechanisms: (i) by the formation of a protective film, which acts as a viscous lubricant and separates interacting surfaces, (ii) the digestion of hard and abrasive oxide particles helping to reduce third body abrasion [89, 90]. The most accepted mechanism is that the ZDDP tribofilm acts as a mechanically protective barrier, preventing direct contact between surfaces. This helps to reduce stresses at asperity contacts. Williams *et al* [91] suggested that the ZDDP tribofilm is softer than the substrate and could reduce the asperities in contact. The thickness of the tribofilm is dependent on a number of factors highlighted in the following section.

There have been contradictory reports on the effect of ZDDP of friction behaviour of contacts. It has been reported that the formation of a ZDDP

tribofilm increases friction due to the roughness of the pads present, which promotes boundary lubrication and higher friction [92, 93].

Taylor *et al* [94] found that an increase in friction was due the tribofilm preventing lubricant being entrained into the rolling/sliding contact. It is believed that the formation of a ZDDP tribofilm would prevent the flow of lubricant in to the contact area causing lubrication starvation. In contrast, other studies have reported studies have reported that the presence of ZDDP had either a neutral [95] or helped to decrease friction. The difference in the reported results can be attributed to the differences in testing conditions and parameters used in each study [96].

The mechanism of tribofilm formation with ZDDP on steel surfaces can be summed up as follows [97]:

1. ZDDP is physisorbed onto the steel surface
2. With the rubbing of the interacting surfaces, ZDDP decomposes and reacts in the rubbing contact due to high local temperatures at the interacting asperities. Spikes and Fujita [90] suggest that catalytic and triboelectronic processes alongside thermal interactions maybe responsible for the decomposition of ZDDP.
3. Initially the phosphorous and sulphur from the ZDDP additive react with the steel surface to form iron sulphide and phosphate. On the rubbing surface zinc sulphide and long chained phosphates form from the decomposition of ZDDP. As rubbing continues a mixture of iron suphides/phosphate and zinc sulphide/phosphate begins to cover the surface.
4. On the rubbed surface the decomposed products of ZDDP continue to react within the rubbing contact, Fe diffuses from the steel surface and reacts with the long chain Zn phosphate to create shorter chain phosphates.
5. Within the tribofilm a constant ratio of Zn/P phosphate cannot be maintained causing the polymerisation of zinc phosphate to form longer chain length zinc phosphate. This process is enhanced with longer rubbing times.

6. This process results in the formation of a multi-layer tribofilm, as shown in Figure 3-30 [98].
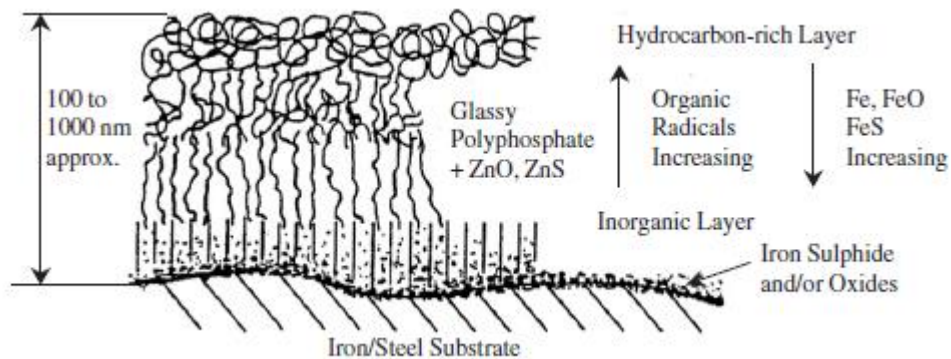
Figure 3-30. ZDDP film structure [98].

It is deemed important to characterise the chain length of the phosphates formed to understand the tribochemical reaction of ZDDP. The chain length of the phosphates can determine the mechanical and rheological properties. Important parameters used to characterise the phosphate glass are the P/O atomic ratio and the ratio of bridging oxygens (P-O-P) to non-bridging oxygens (-P=O and P-O-Zn). The disadvantage of using this method of characterisation is the presence of sulphur in the contact could partially substitution oxygen in the polymer chain backbone (O-P-S instead of O-P-O). The quantification is also easily affected by the presence of contaminants. The use of ΔBE (Zn 3 s – P 2$p_{3/2}$) has the advantage of being independent of static-induced uncertainties, and combined with the BO/NBO intensity ratio it can used as an effective analytical tool [99].

3.7.3.4 ZDDP Film Formation and Thickness

The thickness and formation of the tribo film produced by ZDDP is influenced by a number of physical parameters:

➢ **ZDDP Concentration**: Willermet *et al* [100] showed that at higher concentrations the decomposition rate of ZDDP increased producing a thicker tribofilm and a greater surface area is covered. This demonstrates that the antiwear performance is greatly influenced by this factor.

➢ **Lubricant Temperature**: Palacios [101] work showed that with the increasing of temperature of the lubricant, the decomposition of ZDDP increases producing a thicker tribofilm which would in turn reduce the frictional force. But thicker films are reported to produce worse anti-wear results due to a reduction in their durability and lubricant viscosity. A reduction in mechanical strength and the formation of short chain polyphosphates is also observed [88]. Lin *et al* [86] report that with lubricants containing ZDDP, at temperatures below 50°C a physisorbed film is formed but at 80°C and above a combined chemisorbed and chemically reacting film is created.

➢ **Applied Load**: Nicholls *et al.'s* [88] study showed that with an increase in load and applied pressure ZDDP decomposition increased and a thicker tribofilm was formed. The increase in decomposition was suggested to be initiated by an increase of pressure at areas of asperities contacts.

➢ **Sliding Frequency**: So *et al* [87] reported, with the presence of ZDDP additives in lubricants at higher sliding frequencies, the tribofilm is formed faster hence a decrease in friction coefficient was observed.

➢ **Surface Roughness:** Yin *et al* [90] states that the interaction against a rougher counter face would provide greater opportunity for ZDDP to become trapped between the two surfaces, which would encourage the formation of thicker tribofilms.

3.7.3.5 Interaction of ZDDP with Oxide and Nitrided Layers

At room temperature the ZDDP molecules physically adsorb to the iron oxide layer. Lubricant temperatures above 60°C cause the decomposition of ZDDP molecules, releasing zinc ions which then adsorb on the iron oxide layer. This causes the formation of an enriched zinc adsorption layer on the iron oxide. During mechanical sliding, free iron ions interact with the tribofilm, where some interact with the sulphur from the DDP-, creating iron sulphides such as FeS_2. Zinc sulphide is also created by the interaction of free Zinc (Zn) and Sulphur ions. This increases the thickness of the layer containing Zn. This mechanical mixing also enhances the formation of polyphosphates alongside

some Zn ions becoming oxidised [102]. This process is highlighted in Figure 3-31.

Xia *et al* [103] found that ZDDP additive reacted with nitride layer present to form a tribochemical film with low shear strength. The film has a good synergistic effect with the hard nitride surface because of the interplay between of the phase composition of the layer and tribochemical reactions under lubrication conditions. The combination of the oxide and tribochemical film together with the nitride layer contributes to a reduction in friction and wear.
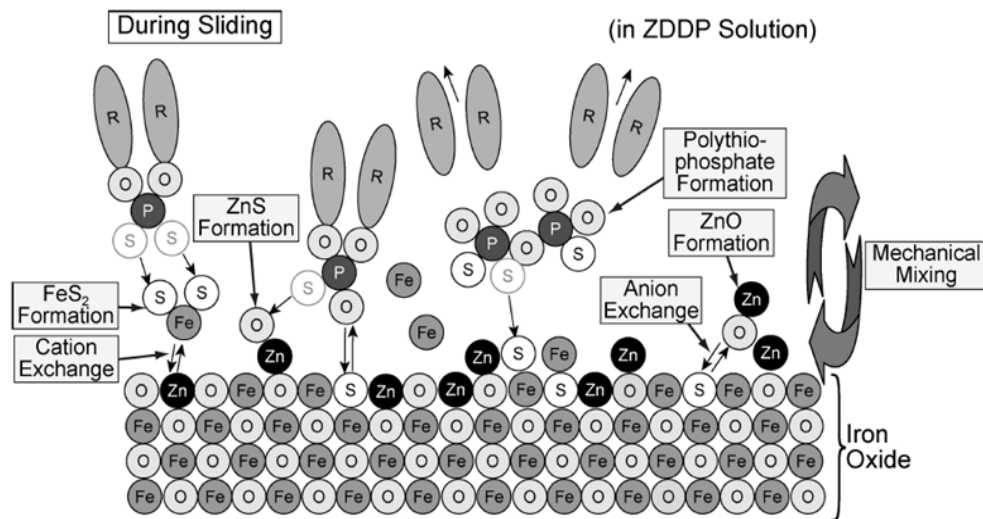
Figure 3-31. Proposed model of tribofilm formation on the iron oxide in ZDDP containing a lubricant [102].

The interaction of ZDDP with worn nitrided surfaces has shown to produce shorter chains of polyphosphates, which are known to provide better tribological properties. The presence of iron oxides on the surface react with the polyphosphates, which can cause a shortening of chains and the formation of shorter chain length iron/zinc phosphates [102]. Worn nitrided surfaces are expected to contain higher amounts of Phosphorous & Carbon elements compared to non-treated surfaces, as the phosphates and carbon chains can be easily adsorbed on to the nitrided layer. A tribofilm would prevent the direct contact and adhesion of two interaction surfaces helping to reduce friction and wear [104].

3.7.3.6 Lubricant Additives for Oxy-Nitrided Steel Surfaces

This project will have a strong focus on improving the friction coefficient and wear rates of samples which have been oxy-nitrided, so it is important to identify the additives which interact most effectively with this heat treatment. Sulphurized olefin (extreme pressure additive) and Tricresyl phosphate (anti-wear additive) are commonly used additives which have shown to have excellent synergistic effects to reduce friction and wear of oxy-nitrided steels [105].

> **TCP:** Shown to have strong antiwear properties in boundary lubrication conditions due to it reacting with iron present to form a thick iron phosphate lubricating film and iron oxide. The effectiveness of the TCP tribofilm formed is determined by the presence of oxygen in the reacting environment. TCP significantly increases the load carrying ability of the treated samples, alongside reducing friction and anti-wear behaviour [106].

> **SO:** SO is widely used as an EP additive, usually found in two types, one based on a long chain olefin with 10-20% sulphur, and the other based on a shorter olefin and higher sulphur content. The higher the sulphur content the higher the expected incidence of S-S bonds in the molecule and the higher therefore its reactivity and EP potency [107]. Under boundary conditions the additive reacts with the oxy-nitrided surface to form a film composed of iron oxide and iron sulphide (FeS). The film has a thick lubricating continuous structure which provides it with good anti-wear properties [108].

When using both additives the synergistic effects for increasing load-carrying ability of the produced tribofilms is greater than just using a single additive. With the increasing of the applied load the friction coefficients of the samples decreases [105].

3.7.3.7 Detergent & Dispersant Additives

Lubricants need to have the ability to prevent unwanted products from causing thermal and oxidative degradation. It is crucial to have additives in the lubricant that are able to suspend insoluble contaminates and keep surfaces clean; this can be achieved by the combined action of detergents and dispersants. Detergents are classed as a stabilizer and deposit control agent additive, with the aim to prevent the formation of harmful products in bulk lubricants and therefore essentially control the build-up of rust and corrosion in hydraulic motor components. They neutralize any acid present in the fluid by chemically reacting with it [49].

Dispersants differ from detergents in three significant ways; they do not contain any metals unlike dispersants. They virtually have no acid neutralizing ability, as they rapidly deplete when they react. Finally dispersants are of a higher molecular weight than detergents, this allows them to be more effective with the suspending of contaminates and cleaning. Dispersants play a significant role with the dispersing of soot particles and sludge to prevent it's settling and deposits [49].

3.7.3.8 Effect of Detergent on ZDDP Tribofilms

Detergents are a common additive to hydraulic lubricants so it is important to understand and analyse the possible effects it may have on the formation of ZDDP tribofilms. Recent studies have shown that detergents are responsible for the deterioration of the effective anti-wear tribofilms formed by ZDDP; this is caused by the competition of surface sites between ZDDP and the detergent which could essentially reduce ZDDP's surface concentration. Using over based calcium detergents reduces the rate of decomposition of ZDDP, and leads to the formation of short chained polyphosphates and calcium phosphate in the tribofilm which effectively reduces its anti-wear properties [109].

3.8 Summary of Literature Review

The literature provides an insight in to the role of hydraulic axial piston motors in a hydrostatic transmission system. The problems relating to the piston/cylinder friction pair component was highlighted, and the factors which influence its failure were investigated. Based on this literature review, there seems to be a lack of understanding regarding the best choice of coating that could be applied to the piston which would help reduce the friction and wear of the component. There are limited studies focussing on the tribo-interactions between nitrided surfaces and lubricant additives. With the ever growing demand to extend the durability of heavy equipment, surface improvement techniques such as nitriding combined with lubricant additives can be applied friction pairs within the system to improve their tribological properties. Therefore, the first objective of this project will be to investigate the most suitable heat treatment to be applied to piston in terms of reducing friction and wear. This stage will involve understanding why the chosen treatment provides the best results. Another key stage will to be gain an understanding how different lubricant additives interact with the chosen surface treatments to determine the best choice to give optimum wear and friction results. These stages will aim to provide a solution which will not only prevent the failure of the hydraulic motor but also improve its performance and efficiency. The final stage of the study would involve simulating a contact replicating the piston/cylinder interaction to investigate the tribological response of the chosen treatments if used in application.

Chapter 4 Materials and Methods

4.1 Introduction

This chapter outlines the main experimental procedures applied within this study. This includes both mechanical and chemical analysis techniques used to assess wear and changes to surface properties.

4.2 Surface Treatment

4.2.1 Treatment Specifications

The different nitriding treatments applied were commercial samples produced by HEF Durferrit using salt bath or gas furnace techniques. The procedure for salt bath nitriding is highlighted in Table 4-1 and the samples produced are characterised in Chapter 5.

The salt bath nitriding variant is the chosen technique to be applied to the piston component within the hydraulic motor to replace the existing Defric treatment currently used. The Defric coating treatment is produced by Parker Trutec, consisting of the application of a manganese phosphate coating followed by a MoS_2 layer. The treatment process is highlighted in Table 4-2.

4.2.2 Salt Bath Oxy-Nitriding

The pin/ball samples are nitrided for the QPQ and Isonite treatments in a molten salt bath of cyanate at 400-600°C forming a nitride/compound layer. With the Sursulf treatment the salt bath is sulphur activated. For the QPQ treatment this process is followed by post oxidation in a specialised cooling bath at 370-430°C, which produces an oxide layer on the surface of the treated component. The nitriding procedure forms a layer ranging in thickness from 10-15 μm with oxidation creating a 0.5 μm oxide on top. Table 4-1 highlights the procedure used for the QPQ treatment.

Table 4-1. QPQ treatment process breakdown.

Process	Temperature °C	Time (min)
Cleaning	40~60	<5
Pre-heat	250±30	<30
Nitriding	580±10	<120±10
Oxidizing	400±10	<20±10
Cooling	In water	<2
Polishing	-	-
Post-oxidizing	400±10	-

4.2.3 Gas Nitriding

The gas nitriding process is carried out on the plate samples using a convection furnace in an ammonia atmosphere at temperatures ranging from 490-530°C. Only part of the ammonia dissociates catalytically at the surface of the hot steel sample, and some of the nascent nitrogen is absorbed [43]. Cooling of the sample is carried out in nitrogen to prevent oxidation [57]. This nitriding variant produces a layer 10 µm thick.

4.2.4 Defric Coating

The pins/balls are initially hardened using the gas nitriding process described in section 4.2.4, however the nitrided layers formed are removed through polishing leaving the hardened substrate. The surface is then phosphate before the spray-on application of a molybdenum disulphide (MoS_2) running-in paint coating (28µm) on top. After the application of the coatings the sample is oven baked from 160-250°C. The procedures form a 5 µm thick manganese phosphate layer followed by a 28 µm MoS_2 coating. Table 4-2 highlights the procedures used.

Table 4-2. Defric treatment process breakdown.

Process	Temperature °C	Time (min)
Cleaning with Absorbent	60±10	10±5
Water Rinsing	R.T.	1±0.5
Surface Regulation (Refining)	R.T.	1±0.5
Coating Chemical Thynthesis (Phosphating)	95±5	12.5±2.5
Water Rinsing	R.T.	1±0.5
Hot Water Rinsing	90±10	1±0.5
Dry (Stoving)	120±20	-
Defric Coating	-	-
Baking	180	60
Inspection	-	-

4.3 Pin/ball Substrates and Counter Bodies

For the pin on plate tribotesting, the pins were used to represent the piston components of the piston/cylinder contact within the hydraulic motor whereas the plates represented the latter. The characteristics of the pins and plates used are highlighted below:

- EN 10085 steel pin with semi spherical end with a radius of 10mm, with a substrate hardness 300 HV_1 and a roughness (R_a) of 0.08 μm. Different nitriding variants and the Defric coating treatment were applied to the pins. The surface finish achieved with each treatment is highlighted in Table 4-3.

Table 4-3. Surface finish of pin samples after various surface treatments.

Treatment	Surface Finish (R_a - µm)
Plain	0.08
QPQ	0.05
Defric	0.30
SN	0.15

- FCD 600 cast iron plate of dimensions 7×7×3 mm. The treatment applied to the plates is kept constant – gas nitriding, which leaves a surface finish - 0.6 µm.

For the Mini Traction Machine (MTM) tribometer tests (section 4.6), a ball on disc configuration was used. The characteristics of the components are highlighted below.

- EN 10085 ¾ inch ball, with a substrate hardness 300 HV_1 and a roughness (R_a) of 0.02 µm. The QPQ heat treatment and Defric coating was applied to the balls. The surface finish achieved with each treatment is highlighted in Table 4-4.

Table 4-4. Surface finish of MTM ball samples after various surface treatments.

Treatment	Surface Finish (R_a - µm)
Plain	0.03
QPQ	0.03
Defric (MoS_2)	0.68

- FCD 600 cast iron disc – 46 mm diameter. The treatment applied to the plates is kept constant – gas nitriding, which leaves a surface finish - 0.5 µm.

4.4 Test Lubricants

Within this study four lubricants were used, they are summarised in Table 4-5. A group I mineral oil (Oil A) is used to create a fully formulated hydraulic oil (Oil B) containing Ca, P, S and Zn elements. ZDDP is blended in to the oil alongside anti-oxidants, detergents and dispersants.

Oil's C and D use a blend of the base oil (Oil A) with alternative EP additives SO (1.5%) and TCP (0.25%) individually.

Table 4-5. Oils used within this study.

Oil	Type
Oil A	Mineral oil (Group I)
Oil B	Fully –formulated
Oil C	Oil A + SO
Oil D	Oil A + TCP

4.5 Pin-on-plate Tribotests

4.5.1 Large TE77

The large Cameron Plint TE77 reciprocating tribometer allows the tribological investigation when simulating the interaction of various contacts with varying conditions such as applied load and temperature. In this study the piston/cylinder contact is characterised to interact within boundary lubrication which is simulated using the TE77. Using a simple pin-on-plate configuration allows the opportunity to gain a basic understanding of the tribological behaviour of the different materials and lubricants being used within this study. Before testing all mechanical components are sonically cleaned in acetone for fifteen minutes and dried thoroughly. Heating of the lubricant present within the sample holder is controlled by a thermo couple which regulates the oil temperature to that set by the user. The heater plate is positioned below the sample holder. A load is used to measure the frictional force and using an analogue to digital convertor a digital signal is produced. A schematic of the TE77 tribometer is highlighted in Figure 4-1 [110]. A data file of the friction force every 300 seconds for the duration the length of the test is produced

using Labview software. Each data file is composed of 1000 measurements taken every 0.3 seconds. After completion of the test the pin and plate components are rinsed with heptane to remove excess oil and then stored in aluminium foil to avoid contamination.
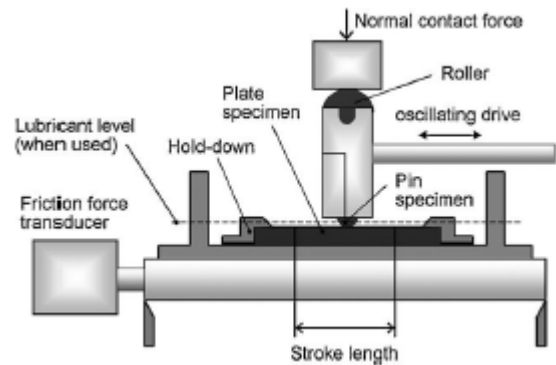
(a)   (b)

Figure 4-1. (a) Images of large TE77 tribometer (b) Schematic of a TE77 tribometer [110].

4.5.2 Test Conditions for TE77 Tribotests

Through the application of a load an initial maximum Hertzian contact pressure (using Equation 2-1) is given to emulate the conditions between a piston/cylinder friction pair. The experimental set up conditions detailed in Table 4-7 are derived from testing conditions used by Komatsu to match those observed between components with the running of a hydraulic motor. For calculations the material properties used are summarised in Table 4-6. Oils A-D (Table 4-5) were used for this section of testing.

Table 4-6. Properties of substrates used for pin and plate samples.

	Pin	Plate
Material	EN 10085	FCD 600
Radius	Radius 10 mm	-
Young's modulus	190-210 GPa	190-210 GPa
Poisson's ratio	0.27	0.27

Table 4-7. Test conditions for TE77 tribotests.

Set up	Conditions
Stroke length	7 mm
Sliding speed	0.17 (12Hz) & 0.35 m/s (25Hz)
Hertzian contact pressure	0.92-1.90 GPa
Lubricant temperature	80 °C
Volume of oil	10 ml
Testing duration	2 h
Lambda ratio, λ	0.009 -0.02

Figure 4-2 shows images of the tribopair after the TE77 tribotests. The wear scars generated on both samples were further analysed to determine chemical composition and morphology.

Figure 4-2. Images of a TE77 worn pin and plate samples.

4.6 Mini Traction Machine with Space Layer Imaging Method (MTM -SLIM) Tribotests

4.6.1 MTM SLIM

Figure 4-3 shows images of the MTM SLIM equipment from PCS instruments that was used within this study. The ball sample is fitted to a mechanical shaft whereas the disc is fixed to the bottom of the lubricant bath. The MTM allows the simulation of a sliding/rolling condition with both the ball and disc rotating

during tests (Figure 4-4) [111]. This tribometer allows the extension of the tests and analysis carried out when using the TE77 tribometer, whilst replicating contact conditions similar to that observed within the hydraulic motor. The MTM allows testing using pre-programmed test profiles highlighting the temperature, speeds, load, test sequence and the rate of data acquisition.
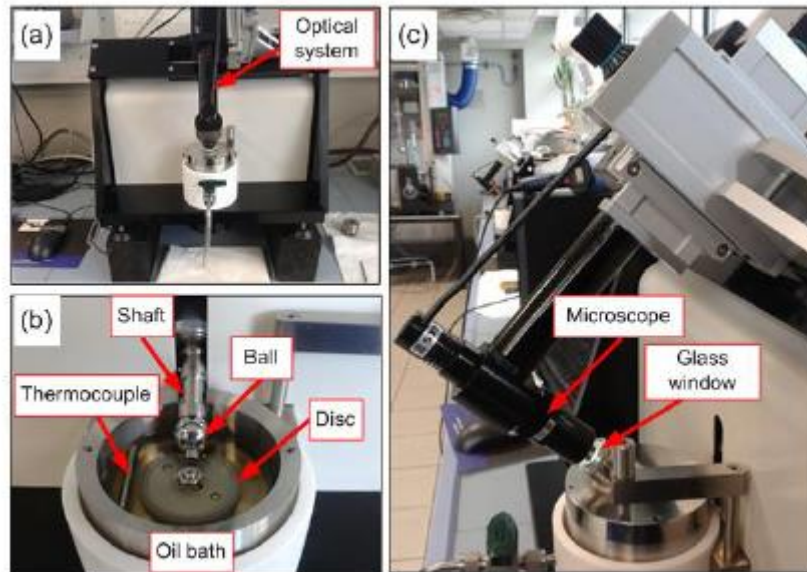
Figure 4-3. Images of the Mini Traction Machine.

Using the space layer interferometry method images of the ball during testing could be obtained and analysed. This technique uses a glass disc coated with a semi-reflective chromium layer which is attached to the glass window. An interference image is formed when light passes through the disc and is partially reflected from the chromium layer and steel ball. By recombining these beams which have travelled various distances an interference image is formed. Using proper calibration the thickness of the tribofilm between the glass disc and steel ball can be calculated. However due to the high roughness of the treated balls used within this study, it is difficult to accurately determine the thickness of tribofilm formed on the surface. The interference images obtained during tests were only used to monitor changes on the ball wear track with rubbing time.
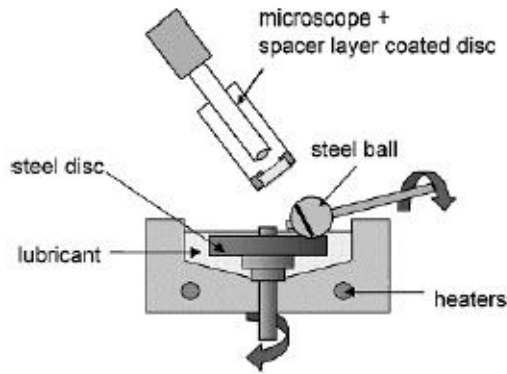
Figure 4-4. Schematic of MTM SLIM tribometer [111].

4.6.2 Test conditions for MTM Tribotests

Tests with the MTM were conducted using treated ¾ inch EN 10085 steel balls and 46 mm FCD 600 diameter discs.

During testing, the temperature was kept constant at 80°C and a load of 36N was applied corresponding to an initial Hertzian contact pressure of 1 GPa. The sliding-rolling ratio (SRR), defined as the ratio of the sliding speed (U_b-U_d) to the entrainment speed (U_b+U_d)/2 (where U_b and U_d are the speed of the ball and the disc, with respect to the contact) was 150% [111]. Yamaguchi [41] states the piston and cylinder component within the piston pump is a pure sliding contact, but for this study a percentage of rolling contact will be applied to replicate the rotation of the pistons within the cylinder block.

The tribological tests were split into three alternative stages which were carried out at fixed time intervals, with an overall two hour testing period. The first stage, known as the conditioning phase, included rubbing the ball and disc together at a fixed slow entrainment speed in the mixed lubrication regime to encourage the formation of tribofilm on the ball and disc wear track. This was then followed by applying the Stribeck curve parameters, starting at a high speed - 2 m/s (mixed regime) and continued towards the lowest speed value - 0.01 m/s (boundary regime) to protect the formed tribofilm by preventing damage at low speeds when in boundary lubrication regime. The final stage involved halting the test and the ball sample was loaded against the spacer layer-coated window, where an image was captured which would allow the measurement of the tribofilm. Table 4-8 summarises the conditions

used with the tribometer within this study. Lubricants B-D (Table 4-5) were used within this section of testing.

Table 4-8. Testing conditions for MTM - SLIM.

Conditioning Phase	
Temperature	80°C
Load / Hertzian Contact Pressure	36 N / 1 GPa
Entrainment Speed	0.1 m/s
Sliding-rolling Ratio	150%
Stribeck Curve Phase	
Temperature	80°C
Load / Hertzian Contact Pressure	36 N / 1 GPa
Entrainment Speed	2 to 0.01 m/s
Sliding-rolling Ratio	150%

Figure 4-5 shows an example of the tribopair immediately after the completion of a test. Circular wear tracks are present on both the disc and ball, which can be further analysed for chemical composition and morphology.
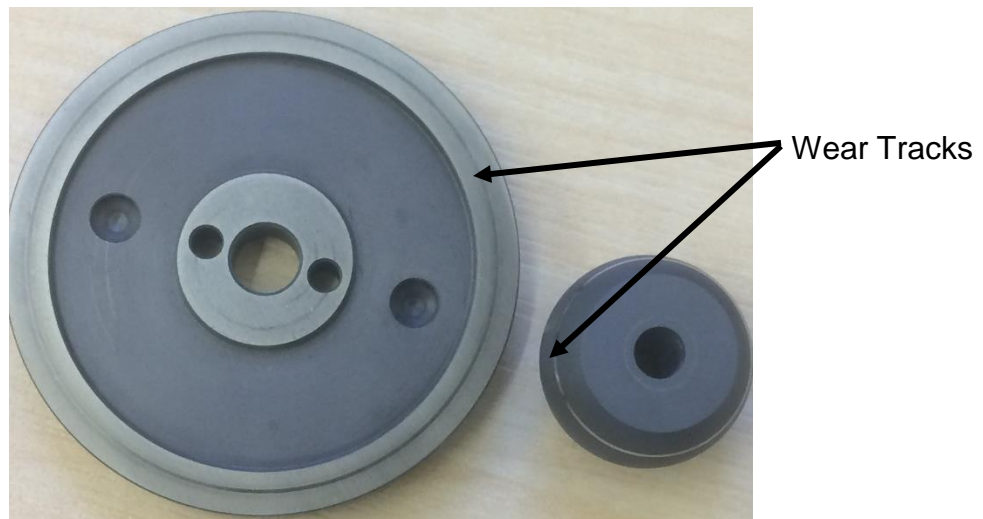
Figure 4-5. Images of the worn MTM plate and ball tribopair.

4.7 Sample Preparation Techniques

For the samples to be analysed using a range of surface analysis techniques a number of preparation processes were carried out. Initially the pin samples were cut in half across their lengths using a Accutom cutter and a diamond cut-off wheel. The cut samples were then mounted into a resin case, allowing the pins cross-section be polished using polishing paper and 3-0.1 µm diamond paste. The samples were then etched in 3% nital solution to reveal the microstructure of the treated steel. If the samples were to be analysed using SEM, the resin case in which the samples were mounted was coated in carbon to prevent charging.

4.8 Analytical Techniques

Certain analytical techniques were applied to characterise the modified surface prior to and post testing. SEM, EDX and XRD were amongst the techniques used to characterise the modified surfaces prior to testing. Post testing FIB-SEM was used to determine the presence and thickness of a tribofilm formed followed by XPS and Raman spectroscopy to determine its chemical properties. To analyse wear results and changes to surface topography interferometry and contact profilometry were employed.

4.8.1 Micro Hardness Measurements

The mechanical property hardness can be measured through a number of techniques such as using a micro-indenter. A Mitutoyo micro-hardness testing machine was used to measure the micro - hardness of the specimens. A chosen load is applied for duration of time, with this procedure being repeated a minimum of ten times around each area of interest. This technique was used to analyse the hardness of the different layers formed after the application of different coatings and heat treatments to the specimens.

It was difficult to take microhardness readings close to the edge of the top of the surface, where it was required that each corner of the indentations were

made at least half the length of a diagonal from the surface edge to prevent the sample edging effect.

4.8.2 Scanning Electron Microscope (SEM)

SEM analysis was carried out using a Carl Zeiss EVO (Figure 4-6) [112]. Under vacuum conditions high resolution images are produced to nano-meter scales (nm) using electrons to produce images instead of conventional light, which has the advantage of having longer wave lengths. This allows the observation and characterisation of metallic materials prior and post experiments. All images were recorded at an accelerating voltage of 20 keV corresponding to a volume fraction analysis depth around 2-3 µm.
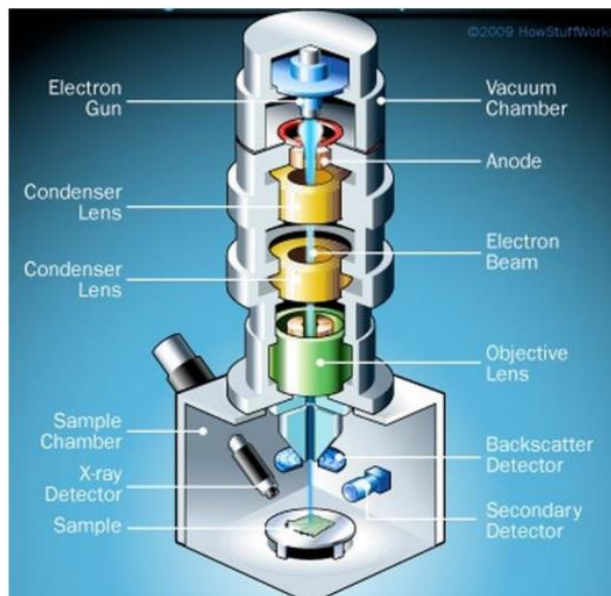
Figure 4-6. Schematic representation of a SEM [112].

Scanning electron microscopes use a focused beam of high-energy electrons to bombard the samples surface producing a range of signals of the material such as secondary electrons, backscattered electrons and X-rays are produced. When the electron beam interacts with the atoms in the specimen surface there is an emission of secondary electrons (SE). Due to the kinetic energy of the supplied electrons, the electrons in the sample are knocked out of their orbiting shell. To keep the atom in a state of equilibrium, an electron from a higher energy shell will jump to the inner shell. This results in an emission of an X-ray with a characteristic wavelength of the given element. Back-scattered electrons (BSE) are electrons supplied by the beam that are

reflected from the sample by elastic scattering. These signals allow the identification of surface features and small particles present [112].

4.8.3 Energy Dispersive X-ray Analysis (EDX)

EDX was the technique used to identify the elemental and chemical composition of the different treated samples or an area of interest. The EDX system is integrated within SEM, and when the specimen surface is being bombarded with electrons, the energy of the X-ray signal released is measured which is then used to identify the atom which released it. This analysis technique was used to determine the chemical composition through the cross-section of different treated specimens, alongside analysing the surface chemistry after testing allowing the characterisation of any tribofilms formed.

4.8.4 Electron Probe Micro Analysis (EPMA)

EPMA was used to establish the composition of small areas on the specimens. A beam of accelerated electrons is focussed on the surface of a specimen using a series of electromagnetic lenses, and these energetic electrons produce characteristic x-rays within a small volume (1-9 μm^3) of the specimen. The x-rays are analysed by energy dispersive detectors, where the resulting energy spectra allows the identification of the qualitative elemental composition of the sample. The characteristic x-rays are detected at particular wavelengths, with quantitative analysis being carried out using their intensity. Locally resolved analysis becomes possible due to the ability of the diameter of the exciting electron beam spot to be focussed below 1 μm [113].

The advantages of this technique are its high spatial resolution and sensitivity, where in some cases individual analysis can be extremely short.

4.8.5 Focused Ion Beam (FIB)

FIB sample preparations and subsequent SEM were utilised as a technique to quantify the exact thickness, composition and morphology of any tribofilm formed on the specimens tested. The sample was prepared using an FEI

Nova200 dual beam SEM/FIB fitted with a Kleindiek micromanipulator for in situ lift-out. A 1 µm carbon film was deposited on to the centre of the wear scar area of 20 µm × 30 µm at 320 pA. Using a Ga^+ ion beam FIB milling was carried out to create an initial volume of 20 µm × 20 µm × 10 µm at 30,000 pA. Then a cleaning cross section was done at 1000 pA. Further cleaning cross sections were carried out at 320 pA with a volume of 25 µm × 1.5 µm × 8 µm. The milled area was then imaged and analysed using SEM-EDX (Figure 4-7).
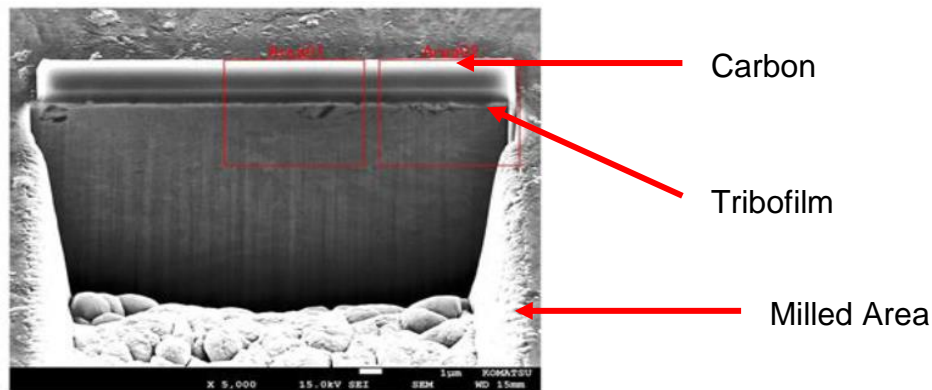
Figure 4-7. FIB section of Plain pin sample.

4.8.6 X-ray Diffraction (XRD)

XRD measurements are taken using X'PERT and is known to be a non-destructive technique used to analyse and determine the phase structure of the layers present in the specimen. Radiation is reflected off the specimen's surface, from which the appropriate crystal structure can be identified from its unique reflection with Bragg's law (Figure 4-8).

Crystal structures are composed of layers, which act as a mirror. When there are X-rays with wavelengths similar to the distances between each of the planes, they can be reflected with the angle of reflection being equal to the angle of incidence. Bragg's diffraction law (Equation 4-1) highlights this phenomenon [114]:

$$2d\sin\theta = n\lambda \tag{4-1}$$

Where d is the spacing between the diffracting planes or lattice, θ is the incident angle, n is any integer and λ is the wavelength of the beam.
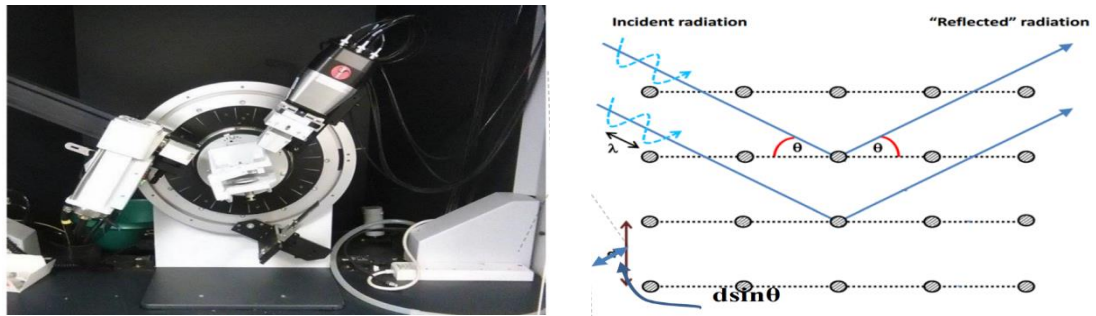
Figure 4-8. a) Shows the setup of the X'PERT XRD rig. b) Schematic representation of Bragg diffraction [114].

When this law is achieved, there is constructive interference produced by the diffracted X-rays and this can be detected by sensors scanning at set angles. 2θ scans between $0°$ and $80°$ were carried out using Cu Kα radiation, and through the analysis of diffraction patterns it was possible identify and validate the crystal phases present.

4.8.7 White Light Interferometry

3D images of wear tracks generated on the plate samples after tribotests were obtained using white light interferometry using NPFLEX from Bruker, UK. The equipment is able to move in 3-dimensions to accurately use non-contact methods to produce an image of the surface examined. The 'Vision64' software suite allows the analysis and interpretation of data produced giving information such as volume lost, roughness and other useful surface parameters. The technique works by emitting white light which is split in two using a beam splitter. The first beam is directed towards an internal reference mirror while the second is directed towards the surface of the sample being analysed. Both of these beams are reflected back to a detector where waves of the same frequency undergo constructive interference and waves of different frequencies destructively interfere. These interference images are used to provide information on the topography of the samples being analysed.

Analysis of the plates used within this project showed no measurable wear occurring with all testing conditions, so these results will not be presented in this study.

4.8.8 Contact Profilometry

Contact profilometry can be used to provide data of higher accuracy than that received using non-contact interferometry, and was applied to the pin/ball
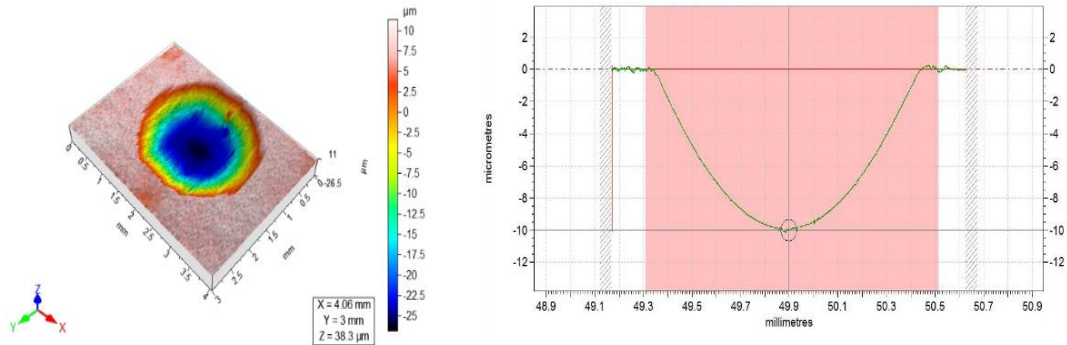
Figure 4-9. Wear measurements of the pin samples after TE77 tests.

samples used within this study. A Taylor Hobson Form TalySurf was used to carryout contact profilometry measurements. It is important to calibrate the stylus using a standard to ensure accuracy of measurements taken. Measurements were processed using the Ultra software suite which was used to produce visual images and numerical data. Profilometry data yields wear scar width and depth measurements, alongside surface topography readings such as roughness and other useful parameters.

4.8.9 X-ray Photoelectron Spectroscopy (XPS)

XPS is a surface sensitive analytical technique that uses X-rays to excite the surface of interest. Under high vacuum the X-rays cause the ejection of electrons which are characterised in terms of their kinetic energy, in electron volts (eV) using an electron detector (Figure 4-10) [115].

Within this study XPS were primarily employed to investigate any tribochemical interactions that may have occurred between the modified surfaces and lubricants used. XPS uses monochromatic X-rays from aluminium K alpha source. An approximate area of 500 μm^2 was analysed in the centre of the worn areas of the pin samples.
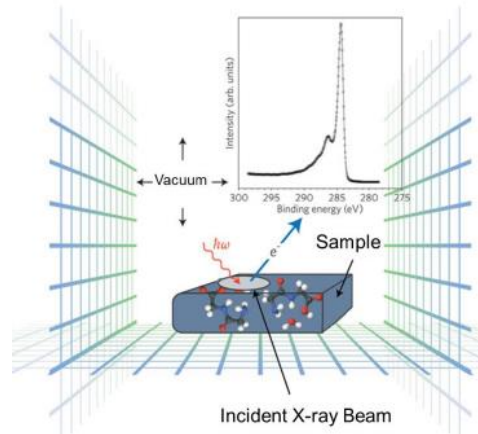
Figure 4-10. Schematic diagram how XPS analysis is conducted [115].

XPS is surface specific as it can only penetrate the upper few nanometres (5-10 nm) of the sample [116, 117]. Short survey scans were carried out to initially determine which elements were present. This was achieved using setting of 0.8 eV energy step size and 20 ms dwell time. High resolution scans of selected element peak regions were carried out to allow for full resolution of the peak components present. The settings for high-resolution scans were: 0.1 eV for energy step size and 100 ms for dwell time. In order to assess the variation in composition and to mitigate any contamination effects each sample was subjected to etching using a 3 kV, 10 mA argon-ion gun.

The data was analysed using Casa XPS software where the positions, areas and height of element peaks can be determined. Using C-1s known electron energy value of 284.8eV, the binding energy scale can be calibrated. Values of binding energies, full width at half maxima (FWHM) and relative sensitivity were taken and found from literature and then applied to the data received. There are certain instance where using XPS cannot definitively identify how the element is incorporated into a film. Two examples of this are calcium carbonate versus calcium phosphate which are detected at very similar eV values (347 eV for both compounds) and zinc oxide versus zinc sulphide (1021-1022 eV) [118-120]. In these cases a secondary analytical technique can be employed to fully attribute species present.

For this study the results for an etching depth of 1.34 nm are presented and focussed on in this study as it was believed due to the relative thinness of the tribofilms formed with the QPQ samples as shown by FIB-SEM, etching too

deep may change the chemical species present within the tribofilm. Using a low etching time would allow the analysis of the tribofilm close to its top surface avoiding any possible contaminants which may be present.

4.8.10 Raman Spectroscopy

Raman spectroscopy was the secondary analysis technique used to support the identification of key chemical species detected when using XPS. In this study a commercial Raman microscope (inVia Raman microscope, Renishaw plc.) was used. A light source is directed on to the sample and the scattered light is collected from the sample by the same lenses used to radiate the samples. A 488 nm wavelength (30 mW) Modu-laser Steller REN Argon laser and 785 nm (300 mW) diode laser are used as the exciting light source. The Raman spectrometer provided a maximum depth and lateral resolution of 2 µm.

There is a 180° backscattering of the scattered light from the specimen surface and it passes through a notched filter that removes Rayleigh scattering and then a lens through a slit is used to focus and direct them onto a diffraction grating. This scattered light is then split into component wavelengths or spectrum and detected on a charged-couple device (CCD) detector (Figure 4-11).
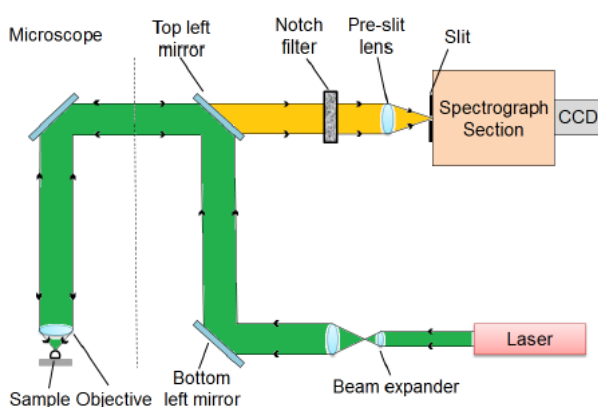
Figure 4-11. Schematic diagram of the Raman spectrometer.

With the Renishaw Raman spectrometer spectra can be obtained using two methods:

1. Single spot analysis: With this analysis option, a single spectrum is obtained from a single spot on the sample.

2. Spot-to-spot mapping: Several spectra are obtained from different spots on the samples in a single analysis, allowing the mapping of larger areas. However this technique is heavily time-consuming.

Using Renishaw's analysis software suite – WiRE program where Raman peaks were fitted with mixed Gaussian/Lorentzian curves to determine the peak frequency, FWHM and peak intensity.

4.9 Summary

The experimental techniques and analysis methods highlighted in this chapter allow the investigation of the impact of surface modification and lubricant additives have on the tribological behaviour of steel. Surface analysis makes it possible allows the ability to observe and characterise changes to the surface of a metal pre and post testing, whereas surface chemistry analysis allows the quantification and characterisation of any layers formed posting experiments. Combinations of the techniques listed above were used to complete a full and comprehensive investigation in to interaction of modified surface with various lubricant additives.

Chapter 5 Surface Characterisation

5.1 Introduction

The various surface treatments applied to the test samples have an impact on the mechanical properties and microstructure of the untreated base steel and play an important role on its friction and wear behaviour. In order to understand the effect of these surface protective treatments, characterisation of the samples treated layers are necessary. This is achieved through using SEM and EDX to characterise the changes in morphology and confirm the nature of the chemical composition of the layer.

From a tribological point of view it is also important to characterise the change of hardness through the different layers of a treated sample. The information gathered in this chapter will allow the correlation of the samples behaviour to the characteristics and properties of the layers present.

5.2 Pin Substrate Material

The base material used for the samples, on which the different surface improvement techniques were applied to, was low alloy/nitriding steel (EN 10085). The substrate contained key elements such as Mo, Cr & V, which enhanced the properties of the nitride layer formed. The elemental composition of the material is highlighted below (Table 5-1) combined with an SEM image of the microstructure of an untreated plain sample (Figure 5-1) [79]. The base material microstructure showed the presence of ferrite and pearlite phases as expected of an untreated sample with a carbon content 0.26-0.34% according to the iron-carbon phase diagram (Figure 3-10).

Table 5-1. Elemental composition of 31CrMoV9 Steel [79]

%C	%Si	%Mn	%P	%S	%Cr	%Mo	%V
0.26-0.34	≤0.40	0.40-0.70	≤0.025	≤0.030	2.30-2.70	0.15-0.25	0.10-0.20
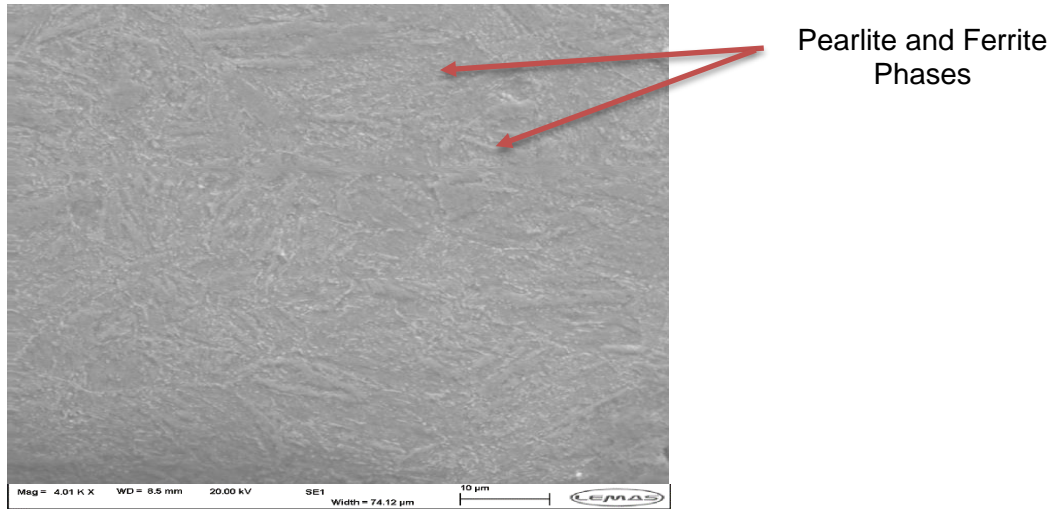
Figure 5-1. SEM image profile through the cross-section of a plain untreated sample.

5.2.1 Nitriding (QPQ) Treatment

5.2.1.1 Microstructure and Elemental Analysis

Figure 5-2 shows the SEM microstructure of the cross-section of a salt bath nitrided (QPQ) pin sample. The salt bath nitriding process was carried out at 580±10°C for 2 hours within a cyanate salt bath. This was followed by using a specialised cooling bath to form an oxide layer. This process was done at 400±10°C for 20 minutes. A very thin oxide layer (0.5 µm) is formed at the top surface, followed by a porous compound layer (white layer) with a thickness of 13-15 µm below. The porosity (~ 5-7 µm) formed on the compound layer is filled with the iron oxide (Fe_3O_4). Under this layer a thick diffusion zone of about 250 µm is formed. The Isonite process is identical to the QPQ treatment with the absence of an oxide layer.
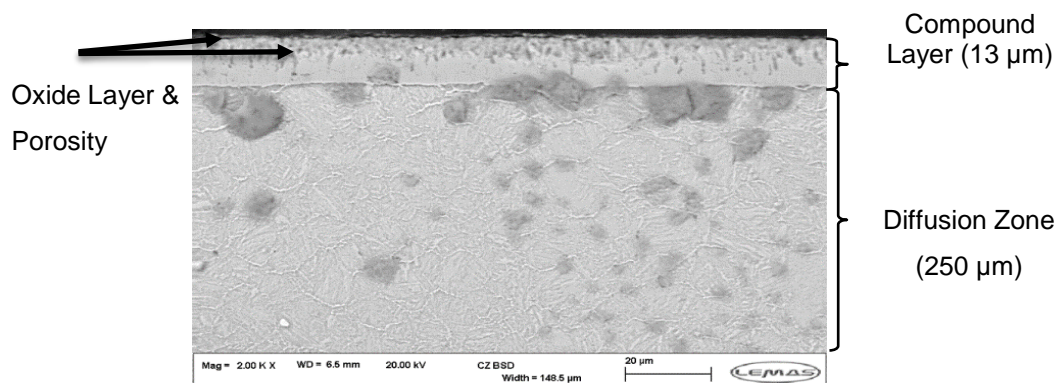
Figure 5-2. SEM image profile through the cross-section of a QPQ sample.
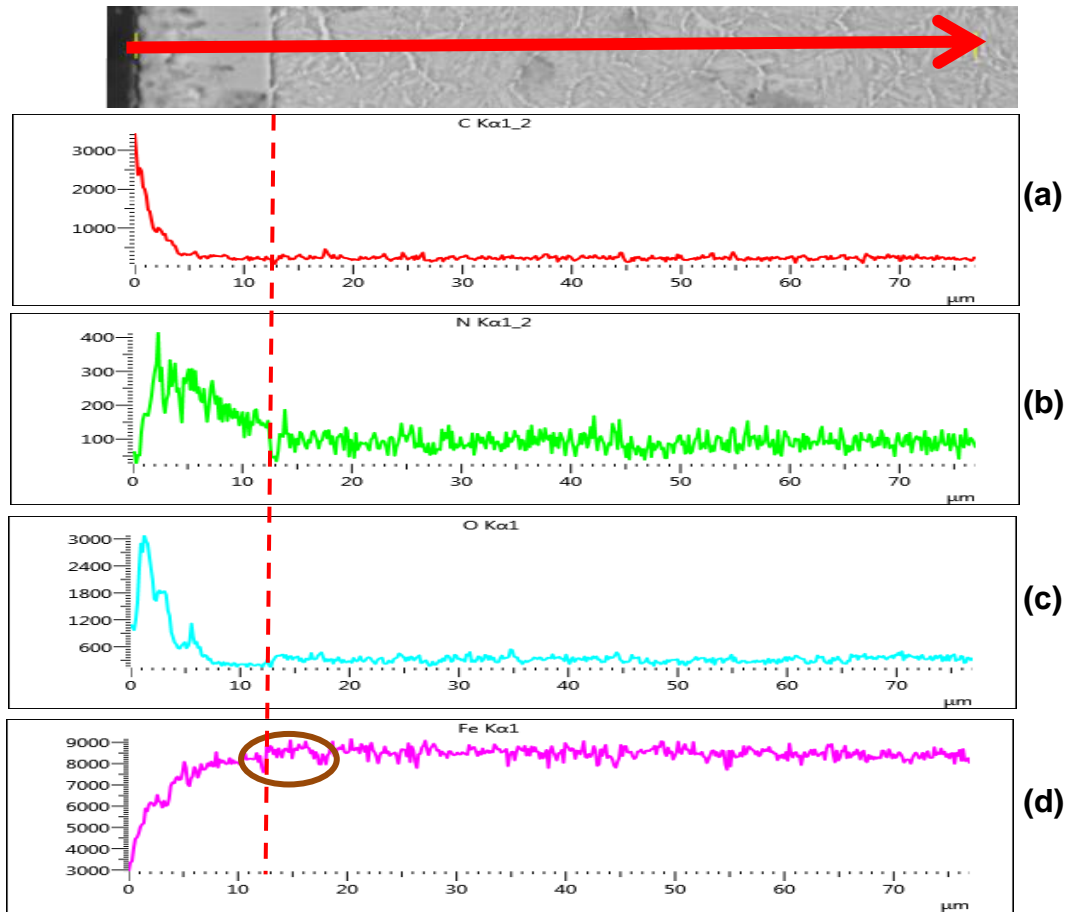
Figure 5-3. The elemental line profiles created using EDX through the cross-section of a QPQ sample: (a) C Profile (b) N Profile (c) O Profile (d) Fe Profile.

Using energy dispersive X-ray analysis (EDX) the C, Fe, N, O profiles through the QPQ samples can be line scanned from the surface to the core (shown in Figure 5-3). The distribution of C through the cross-section shows a high content at the surface, due to the presence of a carbon coating around sample, followed by a quick decline. With the O profile there is a presence through 6 μm of the cross section from the top surface, before there is a steep decline. The presence of O correlates to the depth of the porosity present on the surface of the compound layer. The porosity is formed after the nitriding process and is subsequently packed with Fe_3O_4 after the sample is oxidised, hence oxygen is detected below the top surface.

Using the nitrogen profile the compound layer thickness can be verified (13 μm – highlighted with dashed line) as the nitrogen peak begins to decline through the compound layer, and then levels off. The nitrogen profile is seen to have the lowest intensity compared to the others, which relates to the

gradual diffusion of nitrogen from the surface to the core during the oxy-nitriding process. At a 6 µm depth from the surface, an interesting phenomenon is observed where an increase of nitrogen content is measured. This is due to iron atoms diffusing from the nitrided layer to surface which is being oxidised, which leads to a redistribution of nitrogen atoms in the compound layer and nitrogen atoms become abundant [70]. The nitrogen rich compound layer contains porosity caused by the association of dissolved nitrogen as gas molecules (N_2) at grain boundaries and within grains. At the surface-adjacent part of the layer, porosity is most distinguishable due to this layer having the largest dissolved nitrogen content [56, 57, 66].

From the iron profile it is possible to see that its intensity becomes stronger after a depth of 13 µm (circled in Fe profile – Figure 5-3), where the compound layer ends. The compound layer has intermetallic/inert properties [121, 122] and the substrate has no real influence here. This changes at a greater depth where an increase in iron influence is observed.

5.2.1.2　　Hardness Profile

Figure 5-4 shows the microhardness curve for an applied load (9.81 N) against the distance from the surface for the oxy-nitrided samples. The peak hardness of the surface layer was 830 HV_1 at 0.05 mm from the surface, with the hardness of the diffusion layer gradually decreased with an increase in distance from the surface. The gradual decrease of nitrogen through the specimen would hinder the formation of iron nitrides and fine nitrides which would account for the decrease in hardness through the specimen's depth. The surface hardened layer depth at which the hardness reaches the value of the core substrate hardness (370 HV_1) was about 0.35 mm.

The case hardened depth is deemed to be lower than when using alternative nitriding processes due to the shorter treatment time of the salt bath nitriding treatment. The higher treatment temperature of the salt bath process compared to other variants leads to the production of coarse nitride precipitates resulting in lower surface hardness [123].
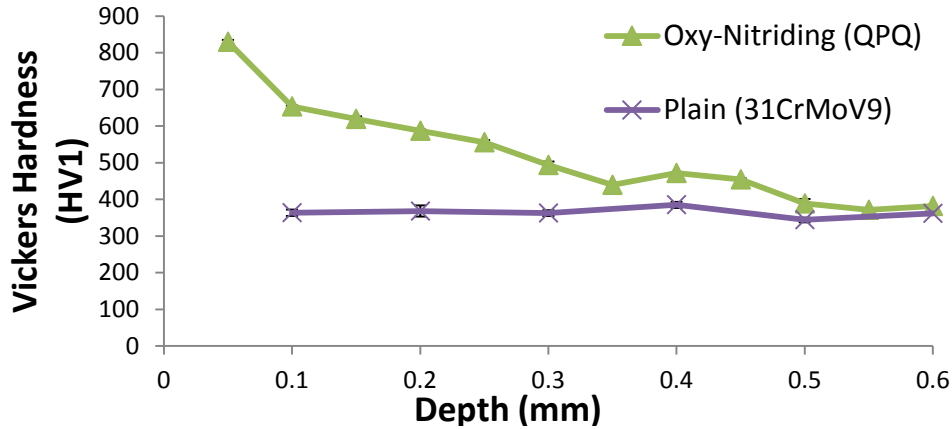
Figure 5-4. Comparison of the hardness through the treated (QPQ) sample's cross-section compared to the untreated Plain sample.

5.2.1.3 Phase Identification

Figure 5-5 shows the X-ray diffraction spectrum of the salt bath nitrided samples, through which the formation of magnetite (Fe_3O_4) and hematite (Fe_2O_3) phases were identified within the oxide layer. With the nitrided layers ε-$Fe_{2-3}N$ and γ'-Fe_4N phases were detected. The trends matched other similar studies who used nitrided samples [70]. With the nitrocarburising process the surface is treated in the presence of nitrogen and carbon, which enhances the formation of ε-nitride phases (Figure 3-14), as shown in Figure 5-5. The formation of ε-carbonitride phases are preferred over γ'-Fe_4N as they are more ductile and provide higher hardness and wear resistance alongside having a wider N and C solubility range in comparison [57, 65].
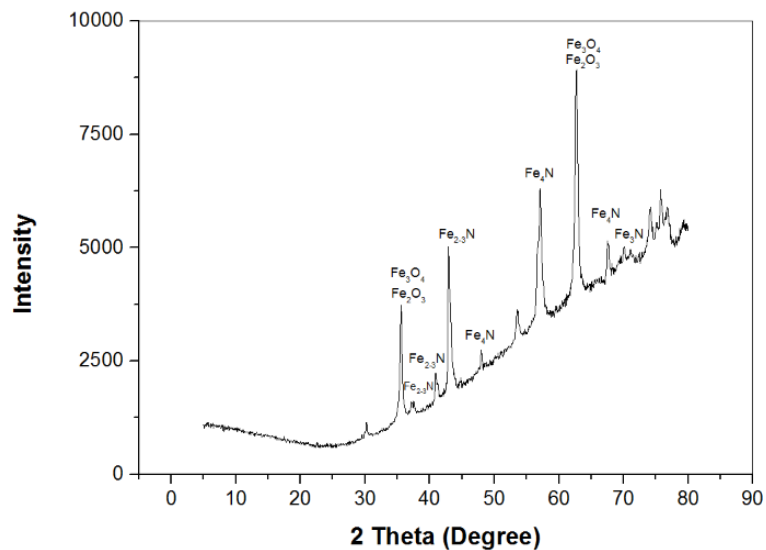
Figure 5-5. X-ray diffraction pattern of a QPQ sample.

5.2.2 MoS$_2$ Coated Sample

5.2.2.1 Microstructure and Elemental Analysis

Figure 5-6 shows the SEM microstructure of the cross-section of a MoS$_2$ coated pin sample, which possesses a thick granular layer followed by a thin coating underneath. The thick granular layer is the bonded coating (MoS$_2$) composed of a solid lubricant and binder.

Initially the thin 5 μm manganese phosphate coating is formed using a chemical thynthesis process at 95$\pm$5°C for 15 minutes. This was followed by the application of a 28 μm thick Defric coating consisting of MoS$_2$ particles which were sprayed on.

MoS$_2$ Coating (~28 μm)

MnP Layer (~4 μm)

Mag = 1.50 K X   WD = 10.0 mm   20.00 kV   CZ BSD   10 μm   LEMAS
Width = 198.2 μm
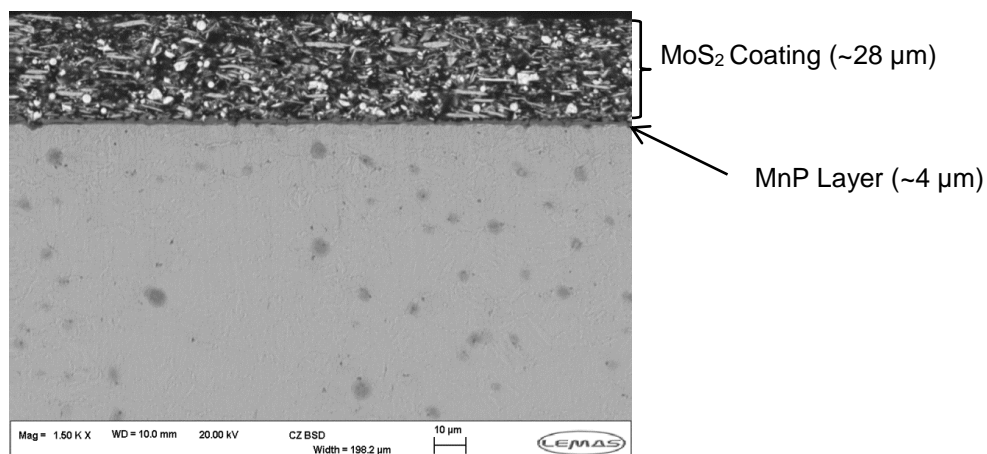
Figure 5-6. SEM image profile through the cross-section of a MoS2 coated sample.

Using EDX the Mo, S, C, Fe, N, Mn, P, O profiles through the MoS$_2$ samples can be mapped from the surface to the core (shown in Figure 5-8). The line scan showed that the first ~10 μm of the MoS$_2$ coating was shown to be composed of C & O due to the sprayed on application of an MoS$_2$ paint coating and then as expected mainly consisted of Mo & S, as it is composed of molybdenum di-sulphide. However using a Mo & S profile map scan (Figure 5-7) of the entire layer showed that MoS$_2$ was distributed through the entire coating from the top surface. The profiles show that the coating is ~28 μm thick, stopping where the manganese phosphate coating begins at a depth of ~28 μm. The Mo & S peaks overlap in EDX, but this indicates both elements

are present, but it is not possible to quantify the intensity of each individual element. There is a high distribution of C through MoS_2 and there is a steep decline at the point where the manganese phosphate layer begins and remains at a very low level through the diffusion layer. An opposite trend is observed with Fe, where a very low presence is observed through the MoS_2 and manganese coating, but there is a quick increase at the boundary and through the substrate. At a depth of 28 µm from the surface after the MoS_2 coating there is a peak of manganese and phosphorous of about 4 µm thickness, which validates the thickness and position of the manganese phosphate coating.

There is an overall increase of nitrogen presence at the end of the MoS_2 and MnP coating, and through the substrate. This increase is due to the original application of a gas nitriding treatment to the substrate, before the nitride layers were removed. Another significant peak appearing in the O profile when the manganese phosphate coating begins. This indicates the presence of oxygen in the layer supporting the results shown from using XRD.

(a) Molybdenum   (b) Sulphur
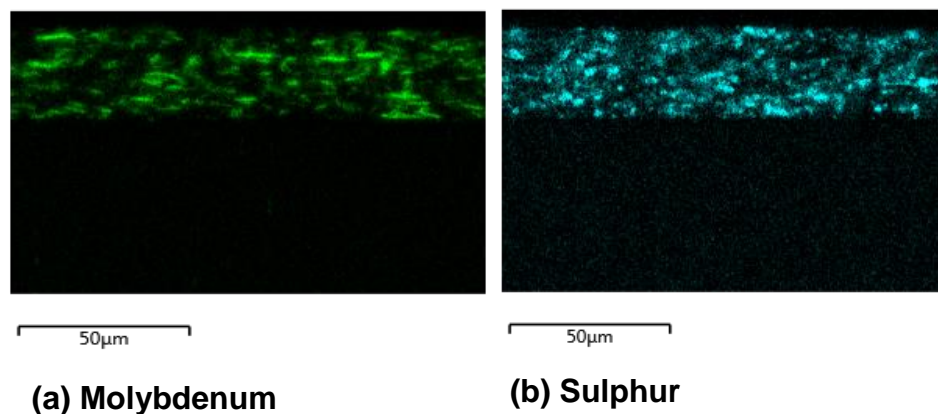
Figure 5-7. EDX mapping of (a) Mo & (b) S through the cross-section of the MoS$_2$ coated sample.
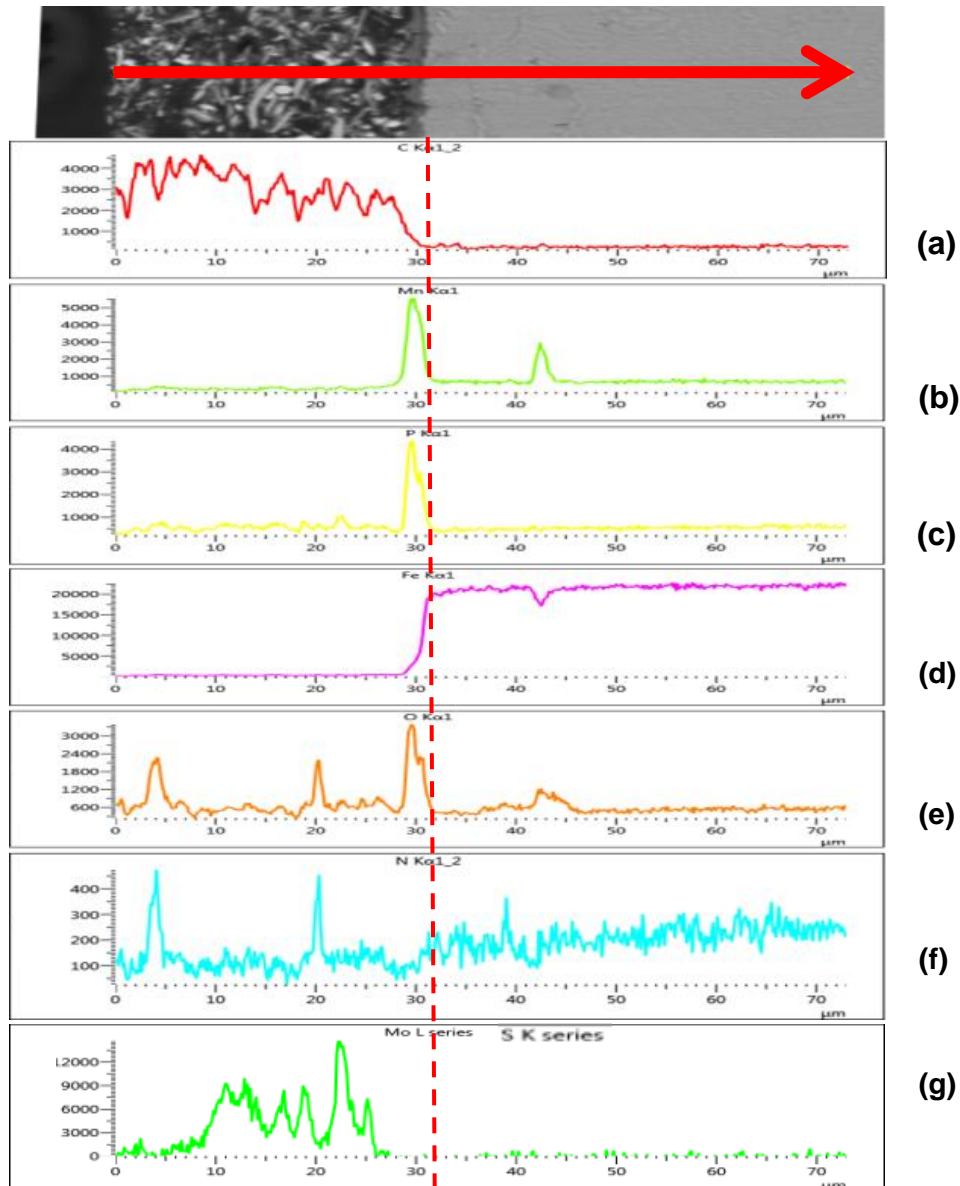
Figure 5-8. The elemental line profiles created using EDX through the cross-section of a MoS$_2$ coated sample: (a) C Profile (b) Mn Profile (c) P Profile (d) Fe Profile (e) O Profile (f) N Profile (g) Mo & S Profiles.

5.2.2.2 Hardness Profile

Figure 5-9 shows the microhardness curve for an applied load (9.81N) against the distance from the surface for the MoS$_2$ coated pin. The peak hardness of the surface layer was 763 HV$_1$ at 0.05mm from the surface, with the hardness of the diffusion layer gradually decreased with an increase in distance from the surface. The surface hardened layer depth at which the hardness reaches the value of the core substrate hardness (370 HV$_1$) was about 0.35mm.

Due to the relative softness of the MoS_2 layer it was applied on to a hardened substrate, which was achieved using gas nitriding after which the nitride layers were removed leaving just a diffusion zone. Using a material of high hardness would ensure contact loads are essentially supported by the contact material instead of the formed film. The hardening of the sample is also most likely responsible for the similarity of hardness through the cross-section of the QPQ samples.
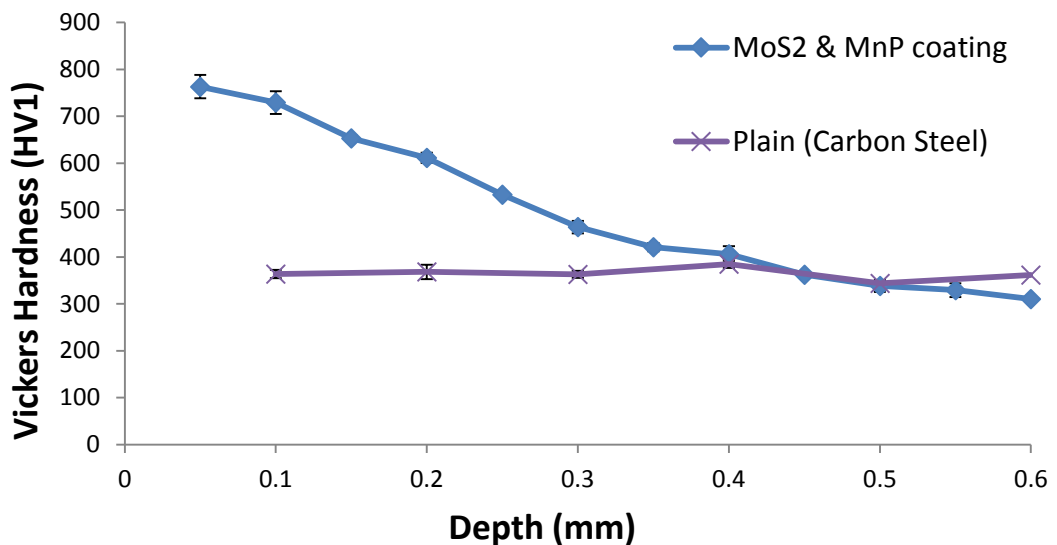
Figure 5-9. Comparison of the hardness through the treated (MoS_2 coated) sample's cross-section compared to the untreated Plain sample.

5.2.2.3   Phase Identification

Figure 5-10 shows the X-ray diffraction spectra of the MoS_2 coated samples through which the presence of MoS_2 is detected alongside MnP and $Fe_{2-4}N$ nitrided phases. γ-Fe_4N is most likely to be present within the diffusion layer formed by the gas nitriding process used to harden the substrate. Figure 3-13 highlights that a bi-phasic nitride layer is formed composed of ε & γ nitride phases when the gas nitriding process is used, and this is supported by the results gained from XRD (Figure 5-10).
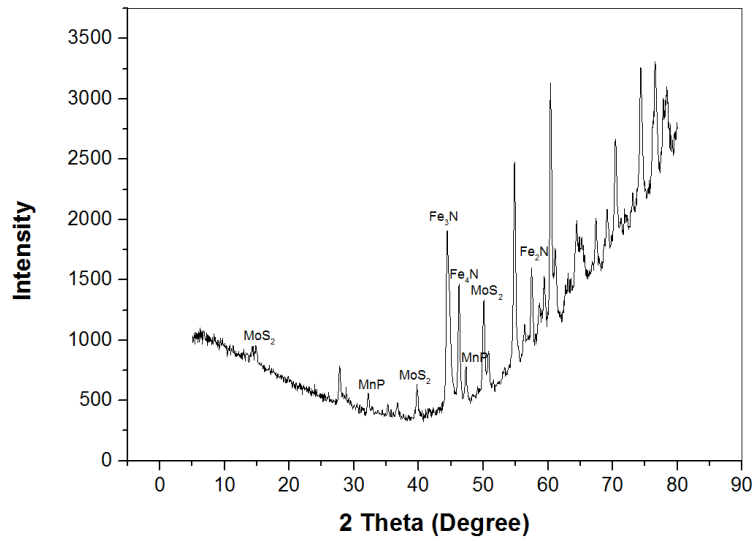
Figure 5-10. X- ray diffraction pattern of a MoS$_2$ sample.

5.2.3 Sursulf (SN)

5.2.3.1   Microstructure and Elemental Analysis

Figure 5-11 shows the SEM microstructure of the cross-section of a sulphur salt bath nitrided (Sursulf) pin sample. The salt bath nitriding process was carried out at 580$\pm$10°C for 2 hours within a sulphur activated cyanate salt bath. On the top surface a thin iron sulphide layer is formed (0.5 µm) which also fills in the porosity present on the compound layer. Like the QPQ treatment an 8 µm thick compound layer is created followed by a thick diffusion zone of about 200 µm.
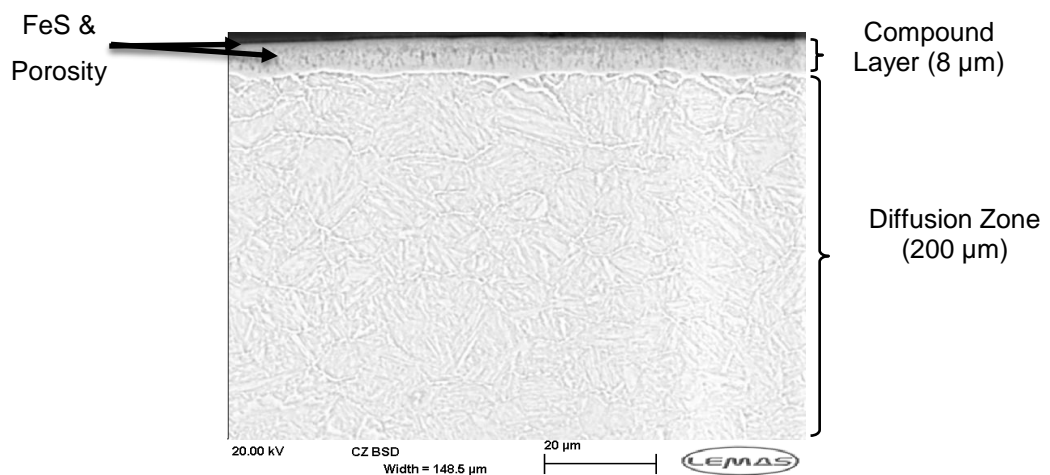
Figure 5-11. SEM image profile through the cross-section of a Sursulf sample.
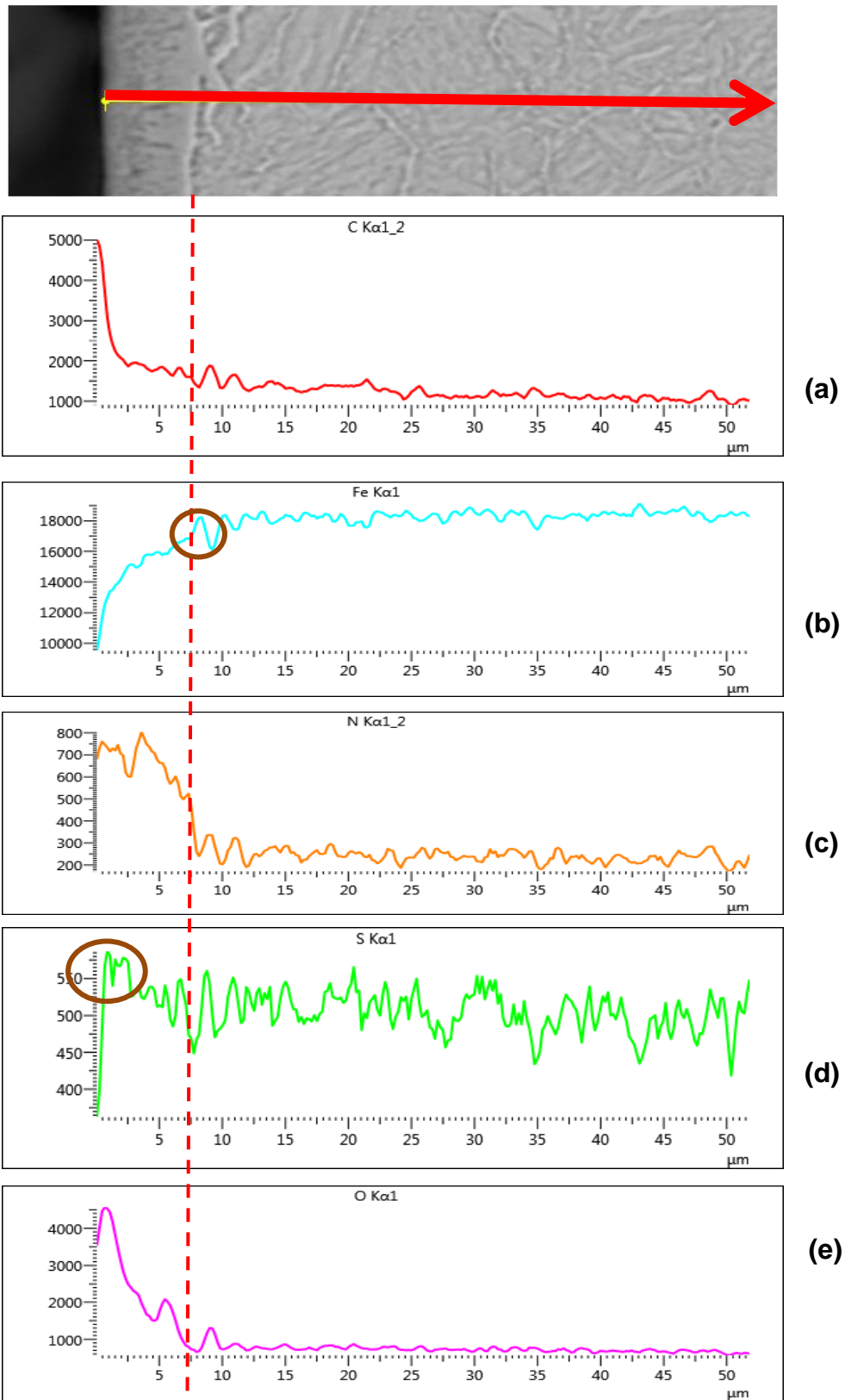
Figure 5-12. The elemental line profiles created using EDX through the cross-section of a Sursulf sample: (a) C Profile (b) Fe Profile (c) N Profile (d) S Profile (e) O Profile.

Using energy dispersive X-ray analysis (EDX) the C, Fe, N, O, S profiles through the Sursulf samples can be mapped using a line scan from the surface to the core (shown in Figure 5-12). The distribution of C through the cross-section shows a high content at the surface then a quick decline. Using the nitrogen profile the compound layer thickness can be verified (8 μm – highlighted with dashed line) as the nitrogen peak begins to decline through the compound layer, and then levels off. With the EDX scans carbon and nitrogen peaks are known to overlap, however due to the presence of the nitrided layer the nitrogen peaks can be clearly identified.

From the iron profile it is possible to see that its intensity becomes stronger after a depth of 8 μm (circled in Fe profile – Figure 5-12), where the compound layer ends. The compound layer has intermetallic/inert properties and the substrate has no real influence here. This changes at a greater depth where an increase in iron influence is observed.

The sulphur profile follows a similar trend observed with the oxygen profile with the QPQ samples. The presence of sulphur is detected for the depth of the porosity (4 μm) – circled in S profile, present on the compound layer. During the Sursulf process the porosity is packed with FeS instead of Fe_3O_4 as seen with the QPQ samples, hence sulphur is detected.

5.2.3.2 Hardness Profile

Figure 5-13 shows the microhardness curve for an applied load (9.81 N) against the distance from the surface for the Sursulf samples. The peak hardness of the surface layer was 756 HV_1 at 0.05 mm from the surface, with the hardness of the diffusion layer gradually decreased with an increase in distance from the surface. The gradual decrease of nitrogen through the specimen would hinder the formation of iron nitrides and fine nitrides which would account for the decrease in hardness through the specimen's depth. The surface hardened layer depth at which the hardness reaches the value of the core substrate hardness (370 HV_1) was about 0.20 mm.
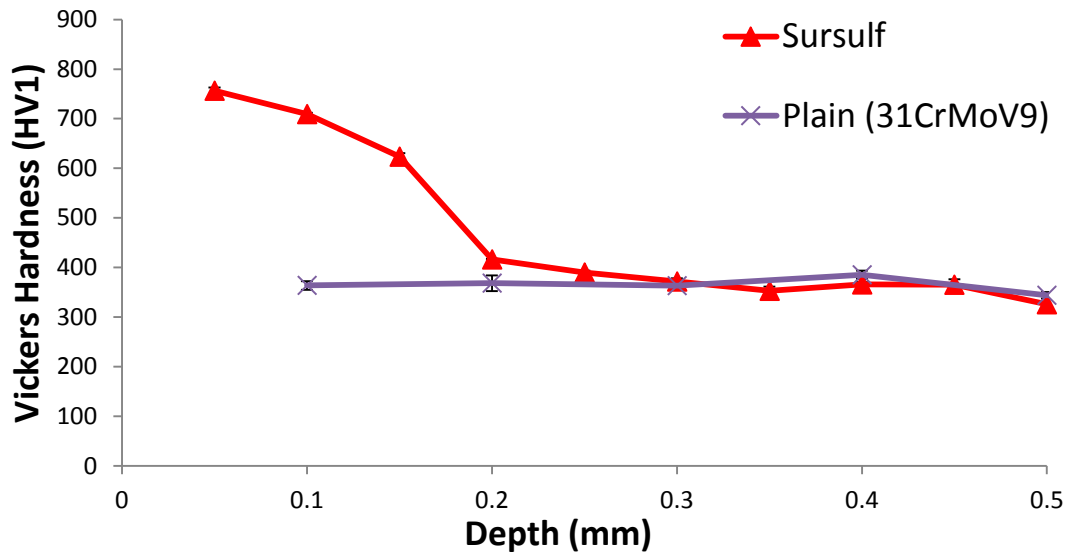
Figure 5-13. Comparison of the hardness through the treated (Sursulf) sample's cross-section compared to the untreated Plain sample.

5.2.3.3 Phase Identification

Figure 5-14 shows the X-ray diffraction diagrams of the Sursulf samples, through which the formation FeS, ε-$Fe_{2-3}N$ and γ'-Fe_4N phases were detected within the compound layer. This is due to the presence of a FeS layer above a compound layer. The sulphur activated nitrocarburising process stabilises the formation of the ε-phase within the compound layer. As stated earlier the formation of ε-carbonitride phases are preferred over γ'-Fe_4N as they are more ductile and provide higher hardness and wear resistance compared [57].
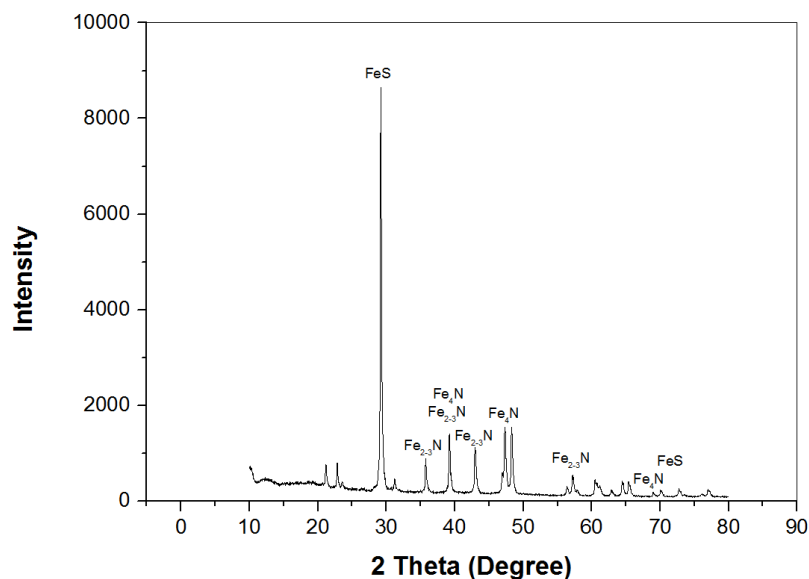
Figure 5-14. X-ray diffraction pattern of a SN sample.

5.3 Plate Substrate Material

The base material used for the plates, which were nitrided, was spheroidal graphite cast iron (FCD 600). Typical used for components where good damping is necessary such as gears, pistons, cylinders, dies and moulds [124]. The elemental composition of the material is highlighted below (Table 5-2) :

Table 5-2. Elemental composition of FCD cast iron.

%C	%Si	%Mn	%P	%S	%Ni	%Cr	%Mo	%V
3.50-4.00	2.00-2.50	0.50-0.80	≤0.06	≤0.02	-	-	-	-

5.3.1 Gas Nitriding Treatment

5.3.1.1 Microstructure and Elemental Analysis

Figure 5-15 shows the SEM microstructure of the cross-section of a gas nitrided plate sample. The process was carried out at $580 \pm 10°C$ for 10 hours within an ammonia gas atmosphere furnace. A thick compound layer (white layer) of 10 μm was formed on the top surface. Under this layer a thick diffusion zone with a fine pearlite microstructure of about 250 μm is formed.
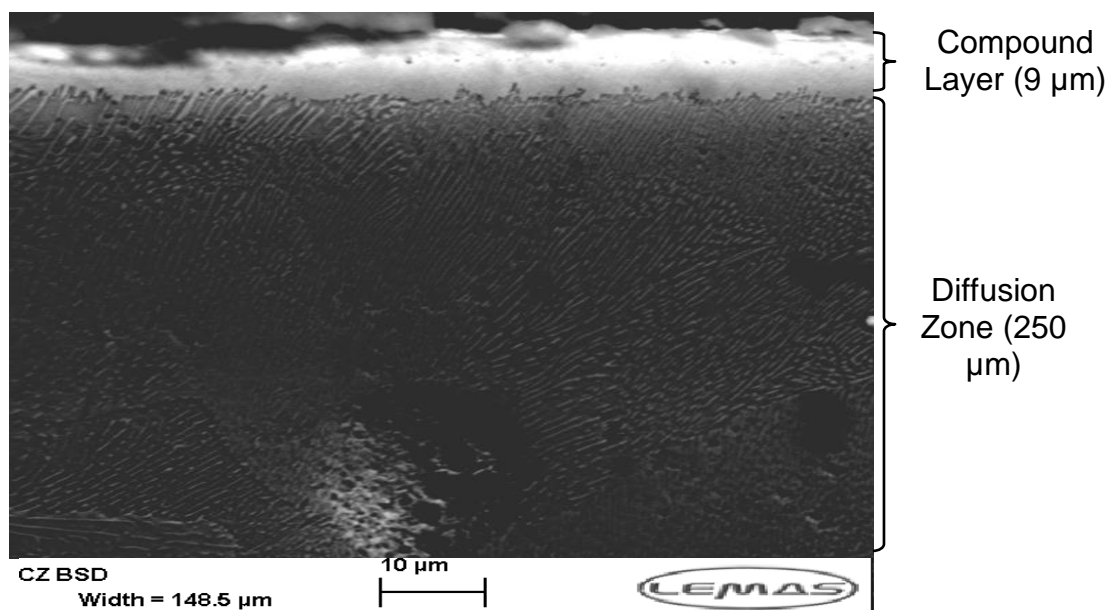
Figure 5-15. SEM image profile through the cross-section of a gas nitrided plate sample.

Using EDX the C, Fe, N, O profiles through the gas nitrided plates can be mapped from the surface to the core with a line scan (shown in Figure 5-18). The distribution of C through the cross-section shows a high content at the surface then a quick decline. Using the nitrogen profile the compound layer thickness can be verified (9 µm – highlighted with dashed line) as the nitrogen peak begins to decline through the compound layer, and then levels off when reaching the diffusion zone.

From the iron profile it is possible to see that its intensity becomes stronger after a depth of 9 µm (circled in Fe profile – Figure 5-16), where the compound layer ends and there is no real presence previous to this. This suggests that the compound layer has inert properties and the substrate has no real influence here. This changes at a greater depth where an increase in iron influence is observed.
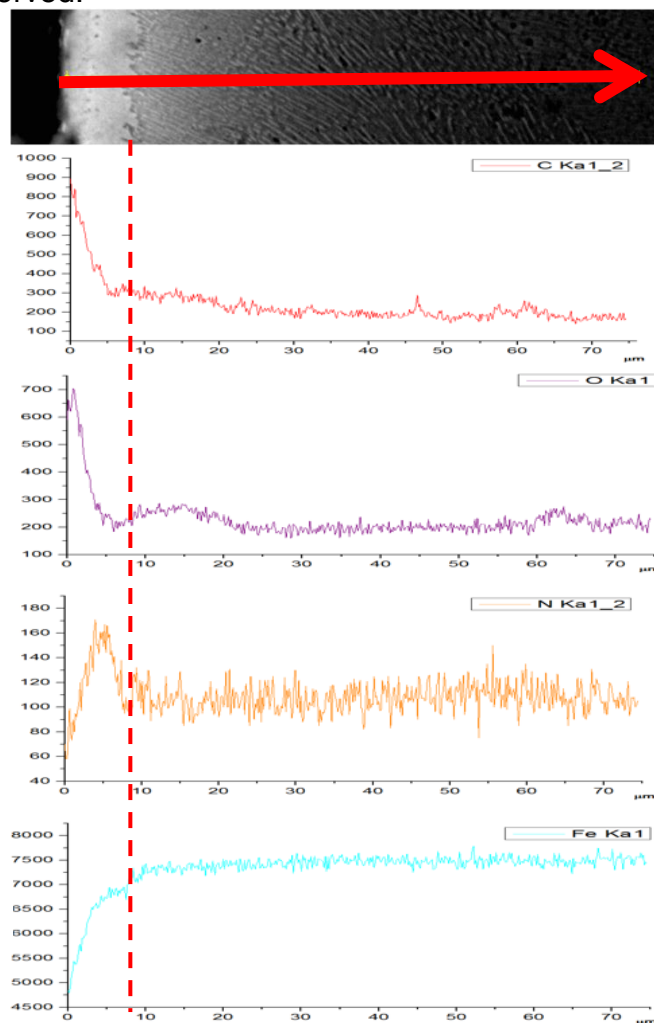
Figure 5-16. The elemental line profiles created using EDX through the cross-section of a gas nitrided plate sample: (a) C Profile (b) O Profile (c) N Profile (d) Fe Profile.

5.3.1.2 Hardness Profile

Figure 5-17 shows the microhardness curve for an applied load (9.81 N) against the distance from the surface for the oxy-nitrided samples. The peak hardness of the surface layer was 475 HV_1 at 0.05 mm from the surface, with the hardness of the diffusion layer gradually decreased with an increase in distance from the surface. The peak hardness of the gas nitrided sample is significantly lower than when gas nitriding or alternative variants are carried out on nitriding steel, this is most likely due to the absence of key elements within the FCD 600 iron needed to formed hard nitrides that help to improve the treated material's hardness.

The gradual decrease of nitrogen through the specimen would hinder the formation of iron nitrides and fine nitrides which would account for the decrease in hardness through the specimen's depth. The surface hardened layer depth at which the hardness reaches the value of the core substrate hardness (260 HV_1) was about 0.20 mm.
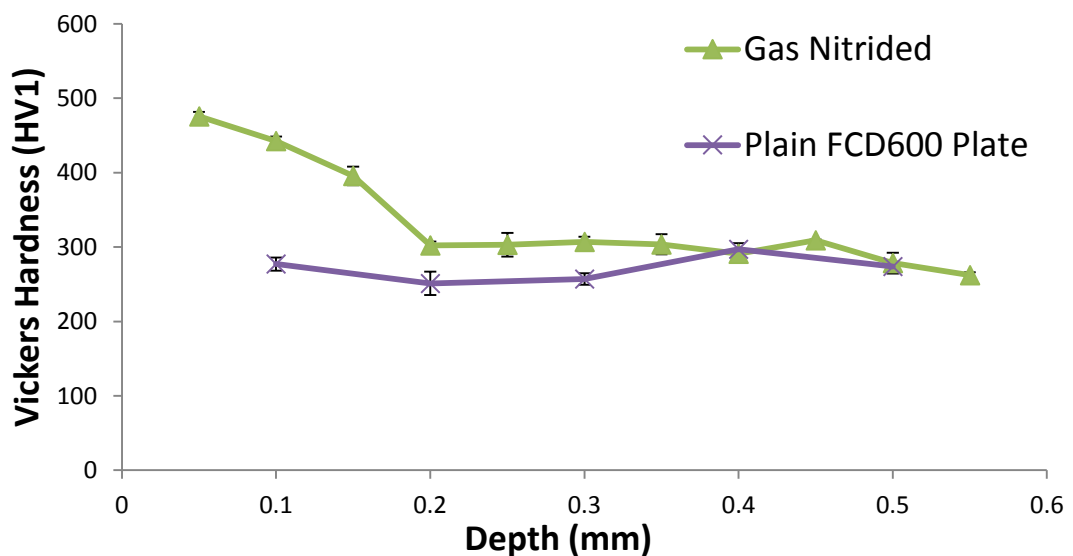
Figure 5-17. Comparison of the hardness through the treated (gas nitrided) sample's cross-section compared to the untreated Plain plate sample.

5.3.1.3   Phase Identification

Figure 5-18 shows the X-ray diffraction diagrams of the gas nitrided plate samples, with the most dominate layers being identified as ε-$Fe_{2-3}N$ and γ'-Fe_4N phases.
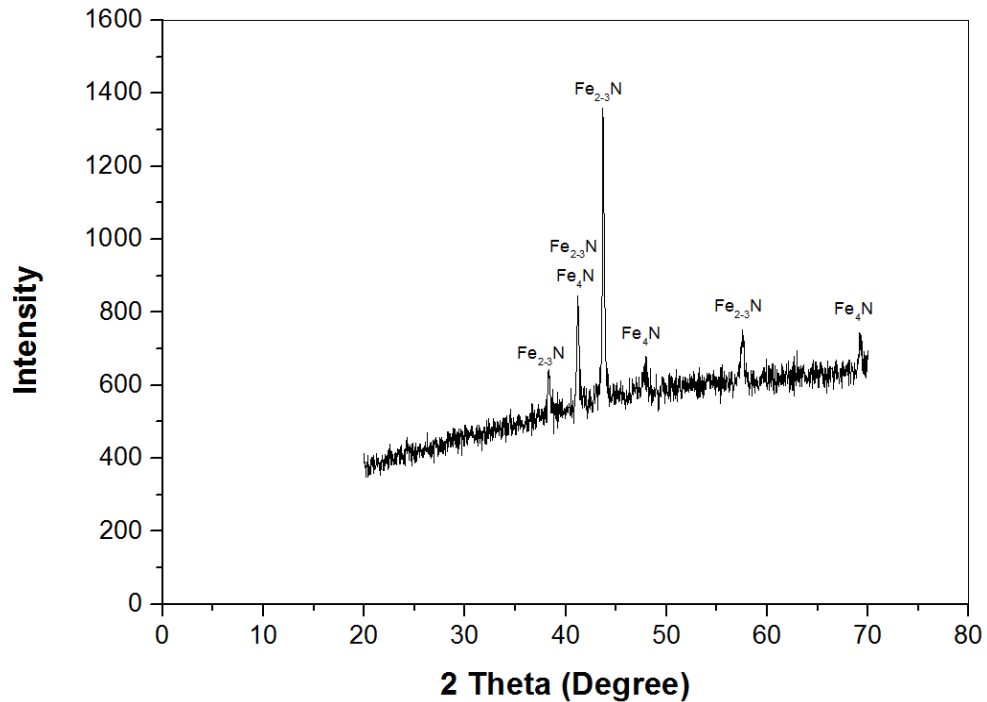
Figure 5-18. X-ray diffraction pattern of a gas nitrided plate sample.

5.4 Summary

- Salt bath nitriding (QPQ) produced three distinct layers – an oxide layer, compound and diffusion zone. The compound zone demonstrated inert properties and was composed of ε-$Fe_{2-3}N$ & γ-Fe_4N phases.
- The MoS_2 and Manganese Phosphate coating treatments apply two coatings on to a gas hardened steel surface. XRD detected the presence of MoS_2 from the soft coating and γ-Fe_4N due to the initial gas nitriding process.
- The hardness through the cross-section of QPQ treated and MoS_2 coated samples were almost identical due to the hardening of the latter samples substrate using a variant of nitriding.

- The Sursulf sample was composed of a compound and diffusion layer with a thin FeS layer at the very top. Due to the sulphur activation of the bath the compound layer is primarily composed of ε-$Fe_{2-3}N$ phases. A thinner compound layer is formed compared to the QPQ treatment and therefore a steeper decline of hardness through the depth of the sample compared to QPQ and MoS_2 coated samples is observed.

- The gas nitrided plates were also composed of a compound and diffusion zone of similar properties as the QPQ samples. However the hardness of the treated plates were significantly lower than the treated pin samples due to the application of the treatment on to non-nitriding steel.

The review of the literature highlights the lack of information of the interaction of oil additives with the modified surface. Therefore this project will focus on the tribochemistry of the different layers formed after treatment with the lubricant, which will be discussed in the following chapters. This Chapter helped to characterise the thicknesses and structure of the layers present after treatment, which will help with the identification and correlation to tribological behaviours observed.

Chapter 6 Friction and Wear Behaviour of Oxy-nitrided (QPQ) Samples in Comparison to Untreated and MoS₂ Coated Samples

6.1 Introduction

The current protective treatment applied to the piston surface of a hydraulic piston motor is the initial hardening of the surface using gas nitriding followed by the application MnP and MoS_2 layers. An alternative to this treatment is the application of the salt bath nitriding heat treatment process.

Oxy-nitriding has been found to be an effective surface treatment technique, used widely in industrial applications due to its ability to prolong the performance lifetime of components. This chapter focusses on tribological and tribochemical interactions occurring between a modified steel surface and a fully-formulated hydraulic oil (TO10). Tribology tests are supported by chemical analysis to identify the mechanisms of low friction and wear behaviour. Low friction is usually associated with high wear, due to the application of soft running-in coatings/layers which are used as a friction control measure.

This section analyses the ability to achieve and maintain low friction and wear using surface engineering techniques in the context of the oxy-nitriding and MoS_2 coating processes. By understanding the tribochemistry at the interface, avenues to optimise the lubricant formulation for that particular surface treatment are opened up.

The friction and wear properties of the alternative surface treatments were investigated with the large TE77 tribometer using contact pressures of 0.92, 1.19 & 1.90 GPa at sliding frequencies 12 & 25 Hz. Fully formulated hydraulic oil (TO10) was used at 80°C due to the closeness to the actual temperature value used within the motor. During the two hour tests, the pin samples used were plain- untreated, nitrided (QPQ) and MoS_2 coated with a 10mm sliding

radius against gas nitrided plates. The wear depths and volume loss of the plates were not analysed due to wear being negligible.

To access the tribochemical interaction between the treated samples and the lubricant FIB-SEM was used to highlight the presence of a tribofilm, followed by employing XPS and Raman Spectroscopy to characterise the chemical species present. It is important to access the impact of the chemical species formed within the tribofilms of the samples on friction and wear.

6.2 Friction Response of Sample Variants

Figure 6-1 highlights the typical change in behaviour over time observed with the three samples during the complete duration of the test with TO10 as a lubricant. Generally the friction for plain samples remains steady throughout with the surface of the sample shown to be heavily worn as shown in section 6-3. The friction values were similar to that observed in other studies using untreated steel with ZDDP [1]. When using the MoS_2 coated samples the friction curve shows that there is a running-in period at the beginning until the system reaches a steady state as the surface asperities are removed. During all testing conditions the MoS_2 coating is completely removed (section 6-4) and the diffusion layer below is exposed. The removal of the coating does not impact the friction behaviour shown by minimal changes to the friction trend (<10%) over the entirety of the testing period.

With the QPQ samples a similar friction trend compared to the MoS_2 samples is observed, with an initial running-in stage until steady state friction is achieved and maintained. The oxide layer present at the top surface of the QPQ samples is removed during testing (Figure 6-12), with no real impact on friction. Overall the friction values of the QPQ and MoS_2 coated samples were very similar; however the QPQ samples in general demonstrated better friction and wear behaviour. This chapter will show the association of friction and wear with the physical changes at the surface.
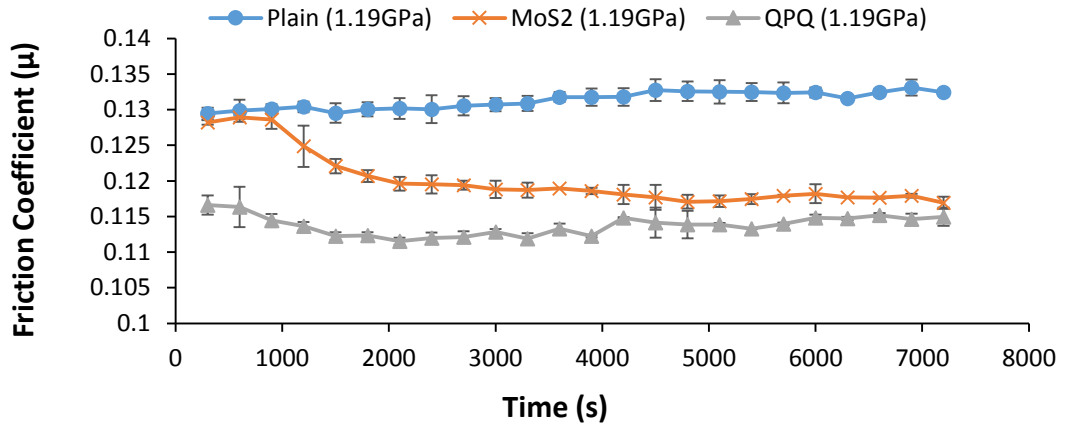
Figure 6-1. Friction coefficient vs time results over 2 hrs with the three samples at a 1.19 GPa contact pressure and sliding frequency - 12 Hz with TO10 lubricant.

The average friction coefficients for the untreated and treated samples in the stable stage (last 30 min of the test) under various contact pressures and sliding speeds are shown and compared in Figure 6-2. It is observed that the general trend is that QPQ samples produce the lowest friction results compared to the MoS_2-coated and plain samples, which confirms the role of the oxy-nitrided heat treatment in friction reduction. Similar trends have been observed in previous studies with untreated and nitrided samples [104].This general trend is observed at the different contact pressures and sliding speeds. With MoS_2-coated samples as the contact pressure is increased a drop in friction is consistently observed. For the untreated and MoS_2-coated samples the friction coefficient values are comparable across the different testing conditions. The results with the MoS_2 samples in this study are in disagreement with that observed by Demydov *et al* [125], where a significant decrease in friction was observed with MoS_2 samples and ZDDP.

A change in trend is observed at the extreme contact pressure of 1.90 GPa which was applied to simulate an environment where the compound layer of the QPQ sample is removed. At this testing condition the MoS_2 sample has a lower friction coefficient than the plain and QPQ samples. The friction value of the QPQ was also the highest observed when compared to the other contact pressures applied. This increase in friction is highlighted in Figure 6-3. The increase in friction is not substantial but is deemed to be significant in this study as in general the QPQ sample produced the lower friction trends for all previous testing conditions. With the application of the extreme contact

pressure for a shorter duration (40 minutes), Figure 6-4 highlights the return to a low friction coefficient for the QPQ sample.

Common trends were observed with the friction results (Figure 6-2) with the steady increase of contact pressure and sliding frequency. With the application of a higher contact pressure with the different types of samples at both sliding frequencies (12 & 25 Hz) it is possible to see that in general there is a slight increase in friction but the effect was not significant enough to change the behaviour of the system. However with the doubling of the tests sliding frequency to 25 Hz, a measurable reduction in friction for all treated samples is observed. This is most likely due to the impact of the change in sliding distance with the increase of frequency while keeping the sliding time constant [126]. This will be discussed in detail later in section 10.1.
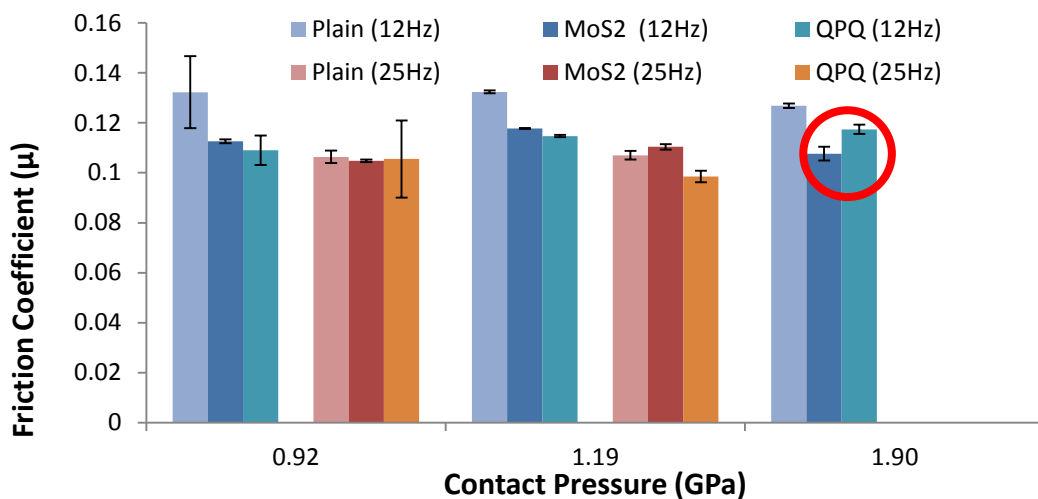
Figure 6-2. Friction coefficient results from experiments when the applied load and sliding frequency are varied using fully formulated lubricant with three types of samples at 80°C.
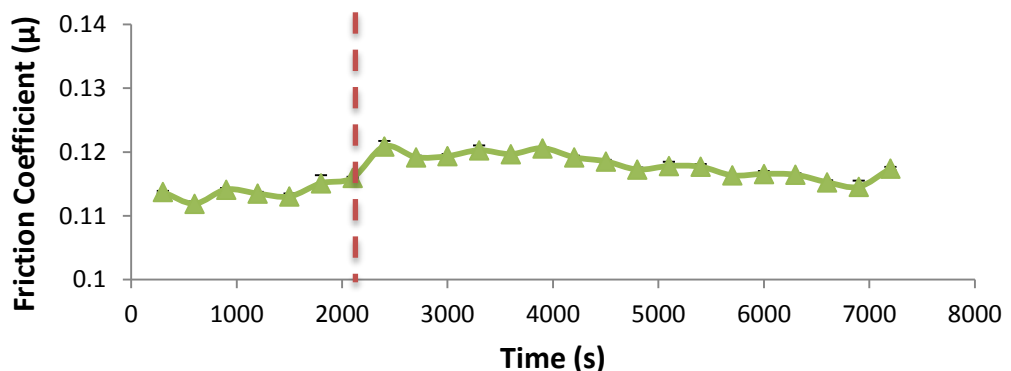
Figure 6-3. Friction coefficient result for the QPQ sample when an extreme pressure (1.90 GPa) was applied at a sliding frequency of 12Hz. The line highlights the increase in friction after a period of 2000 seconds.
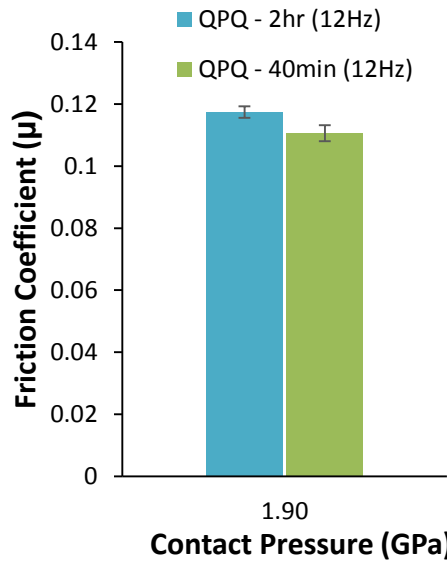
Figure 6-4. Friction coefficient result for the QPQ sample when an extreme pressure (1.90 GPa) was applied for a duration of 2 hours and 40 minutes at a sliding frequency – 12 Hz.

6.3 Wear Response of Sample Variants

Using an optical microscope the worn surfaces of the different samples (Figure 6-5) were analysed. With the QPQ pin when the compound layer was not worn away (Figure 6-5(a)), the surface showed the presence of a tribofilm formed on edges of the worn surface. In comparison to when the compound layer is removed (Figure 6-6(b)) a wider surface covering film is seen to form across the entire surface. With the MoS_2 coated samples (Figure 6-5(c)) it is possible to see a deeper penetrating wear scar, with higher magnification images showing the exposure of the substrate surface alongside the patchy remnants of the coating and the formation of a thick tribofilm. The images show the delamination of the coating and scoring of the exposed surface. The plain samples (Figure 6-5(d)) show the exposure of a rough surface with the presence of a thicker continuous tribofilm, who's composition will be confirmed using other techniques such as EDX and XPS.

a) QPQ – Compound Layer Present

b) QPQ – Compound Layer Removed
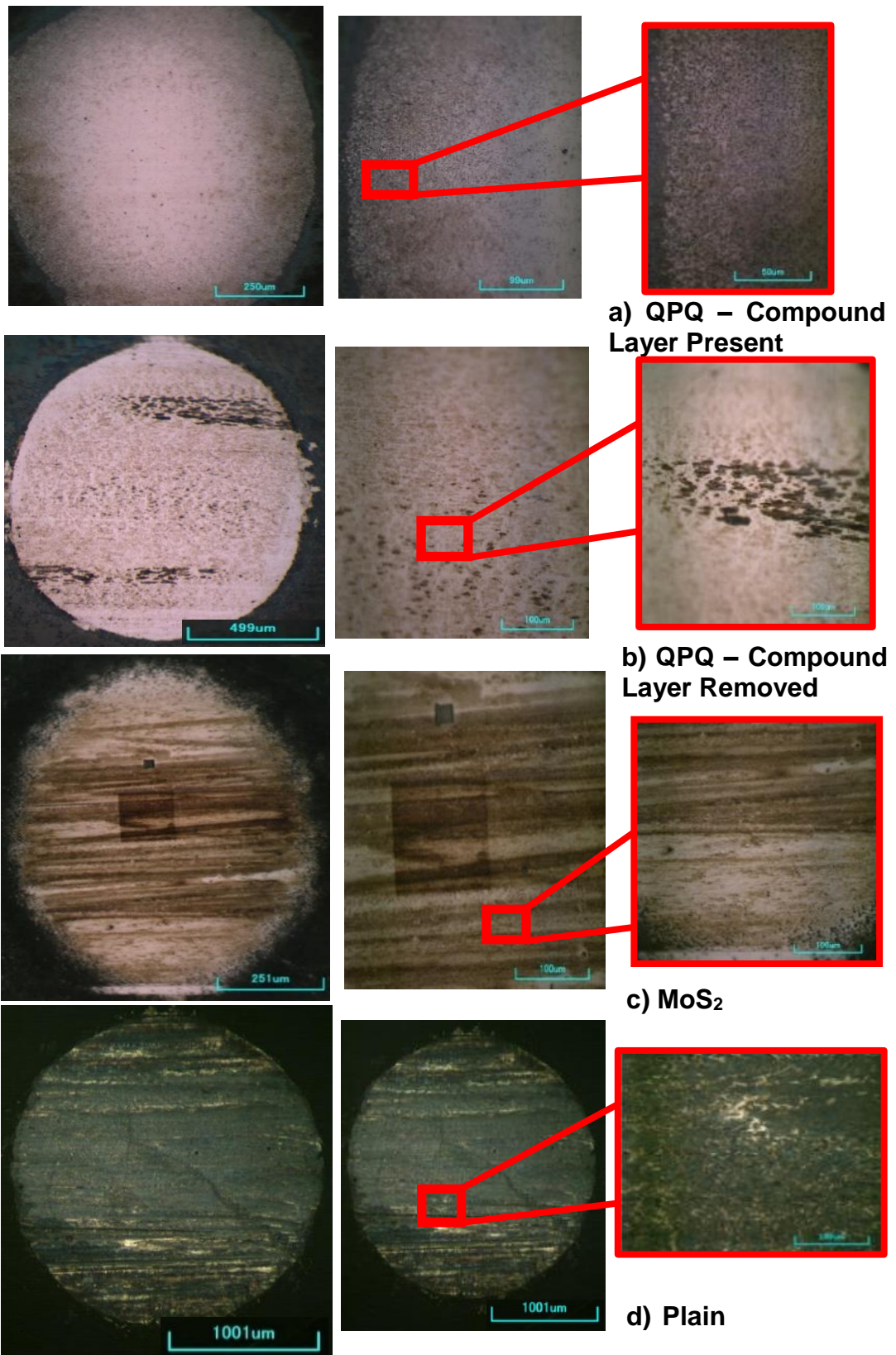
c) MoS₂

d) Plain

Figure 6-5. Optical images of the wear scar regions of the different treated pin samples when a 1.19 GPa contact pressure was applied at 12 Hz.
a) QPQ – Compound Layer b) QPQ – Compound Layer Removed c) MoS₂ Coated d) Plain

The depth profile measurements using Talysurf (Figure 6-6) showed that the QPQ pins had the lowest wear depths, compared to the other samples where the loss was significantly higher, with the plain samples showing the greatest loss. Generally, the wear depths of the pins increased with the application of higher loads and frequencies as expected. With the QPQ pins the wear depth was mainly contained within the compound layer (<13 μm), rarely reaching the diffusion zone. This is in contrast to the MoS_2 coated samples where the coating did not survive testing and in almost every case the wear depth (>28 μm) penetrated into the diffusion zone. However with the application of the extreme contact pressure of 1.90 GPa, Figure 6-7 highlights that the wear depth for the QPQ penetrates into the diffusion zone (>13 μm) and this correlates with an increase in friction observed in Figure 6-3. However when the extreme pressure test was run for a shorter duration (40 mins) wear does not penetrate through the compound layer. This indicates that the properties of the compound layer influence the samples low friction behaviour.

As with the friction results, certain trends to the wear depths of the pin samples (Figure 6-5) were observed with the increasing of applied contact pressure and sliding frequency. The wear depths of the pin samples generally increased with the application of a larger contact pressure likely relating to the removal of greater amount of material. As with increasing the applied contact pressure a general increase in wear depth is observed with increasing the sliding distance.
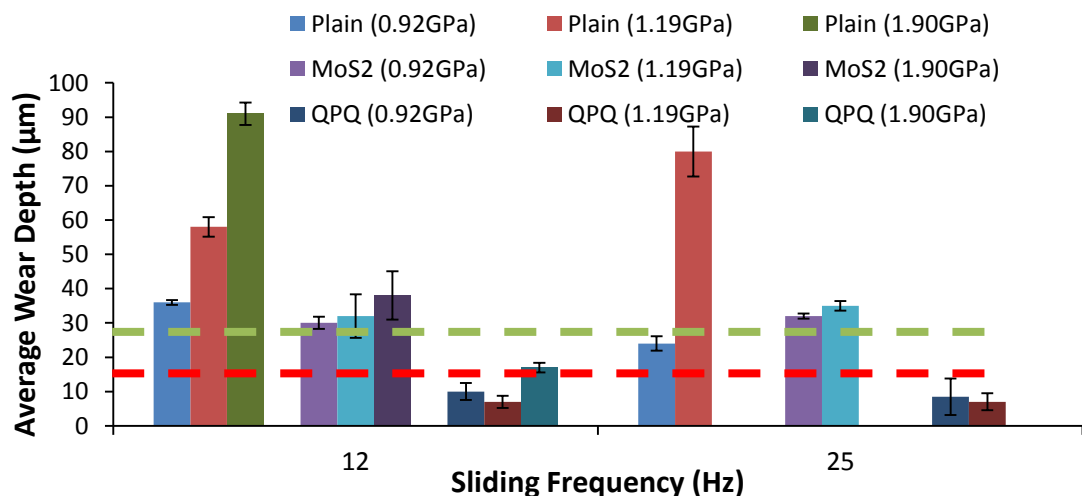
Figure 6-6. Wear depths of the three types of pins when contact pressures 0.92-1.90 GPa are applied at 12Hz & 25Hz sliding frequencies using fully formulated lubricant at 80°C. Red dashed line - thickness of the compound layer, green dashed line – MoS_2 coating thickness.
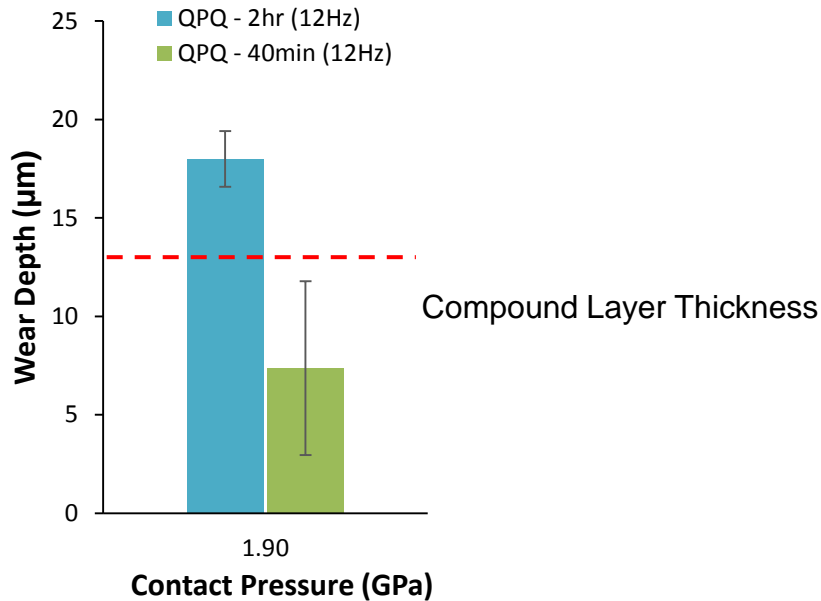
Figure 6-7. Wear depths of the QPQ pins with the application of an extreme contact pressures 1.90 GPa for a duration of 2 hours and 40 minutes at a sliding frequency – 12Hz.

The wear depth of the gas nitrided counter plates were negligible for all tests, instead there was small amounts of material transfer from pins on to the counter face.

6.4 Tribofilm Analysis

6.4.1 Tribofilm Analysis using SEM-EDX & FIB-SEM

SEM-EDX (Figures 6-8, 6-10 & 6-12) was used to analyse spots inside and outside the worn areas of the different pin samples after the tribometer tests using fully formulated lubricant (TO10). It allowed the mapping of selected elements across the surface to give an indication of the interaction of the surface with the additives within the lubricant. This process was followed by using FIB-SEM to analyse the cross-section of the samples to identify if a tribofilm was formed. Figures 6-9, 6-11 & 6-13 show the images where cross sections of the anti-wear (AW) tribofilms formed were made by FIB milling and then examined using SEM.

With the plain samples SEM-EDX (Figure 6-8) shows high concentration of Fe present on the surface of the sample as expected with an untreated steel sample. Within the worn area there is a low presence of carbon, but oxygen

is detected most likely due to natural oxidation occurring at the surface. Within the wear scar sulphur and phosphorous are clearly detected, elements which are associated with the formation of a tribofilm when using the ZDDP additive. Zinc, which is usually associated with the formation of a phosphate tribofilm, is not clearly detected. All elements are identified in the EDX spectrum.

Using FIB-SEM (Figure 6-9) the tribofilm was identified and analysed at two points on the plain samples, having thicknesses of ~104 nm and ~194 nm respectively and EDX verified the presence of a phosphate tribofilm with the detection of phosphorous and sulphur presence. XPS carried out on the worn surfaces later on (section 6.4.2) confirmed the presence of a ZDDP formed tribofilm.
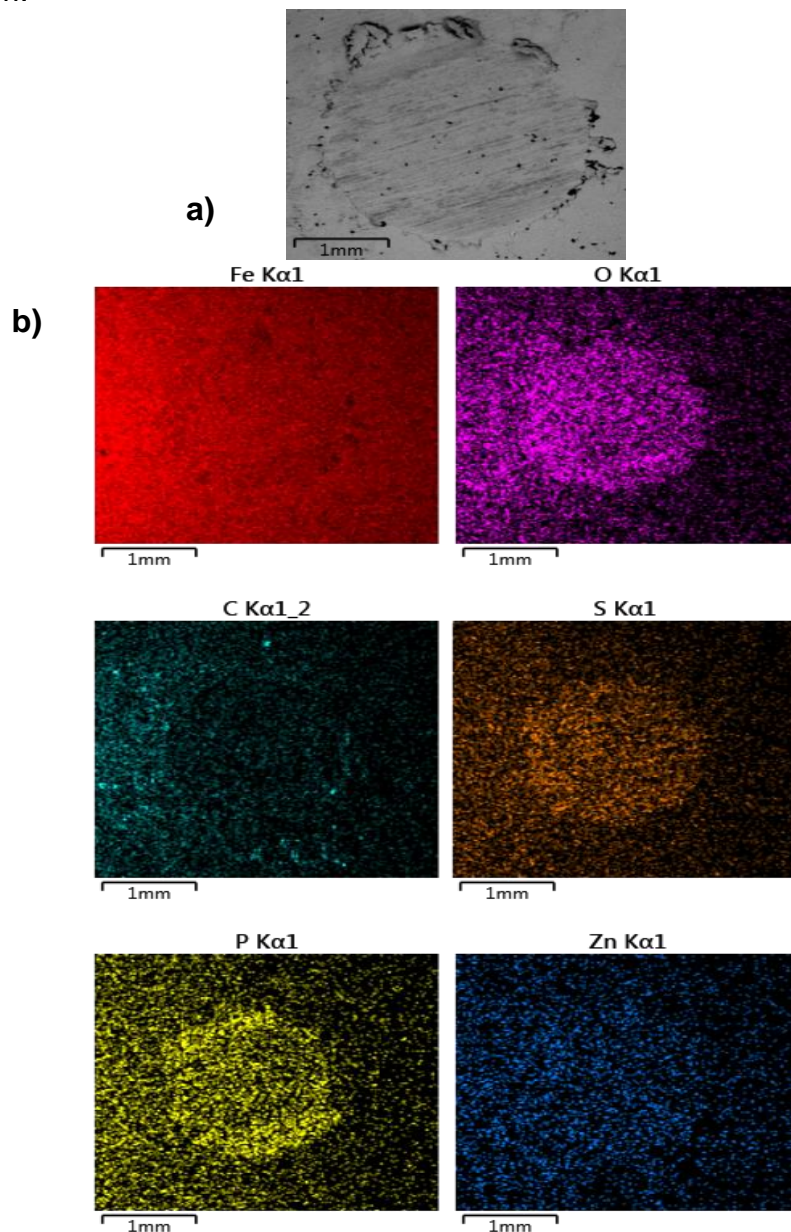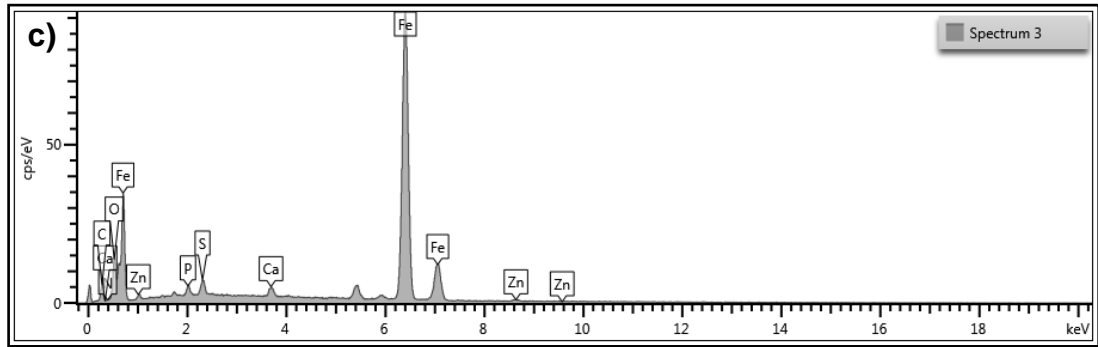
Figure 6-8. a) SEM image, b) EDX maps and c) spectrum of the unworn and worn surface of the Plain pin samples at 1.19GPa contact pressure and 12Hz sliding speed.

element: P, S, Ca, Zn, O (C, Fe, Cr, N, Si)
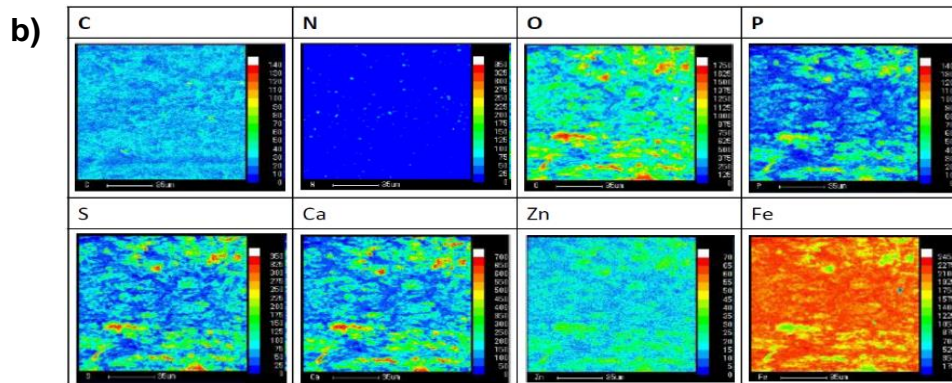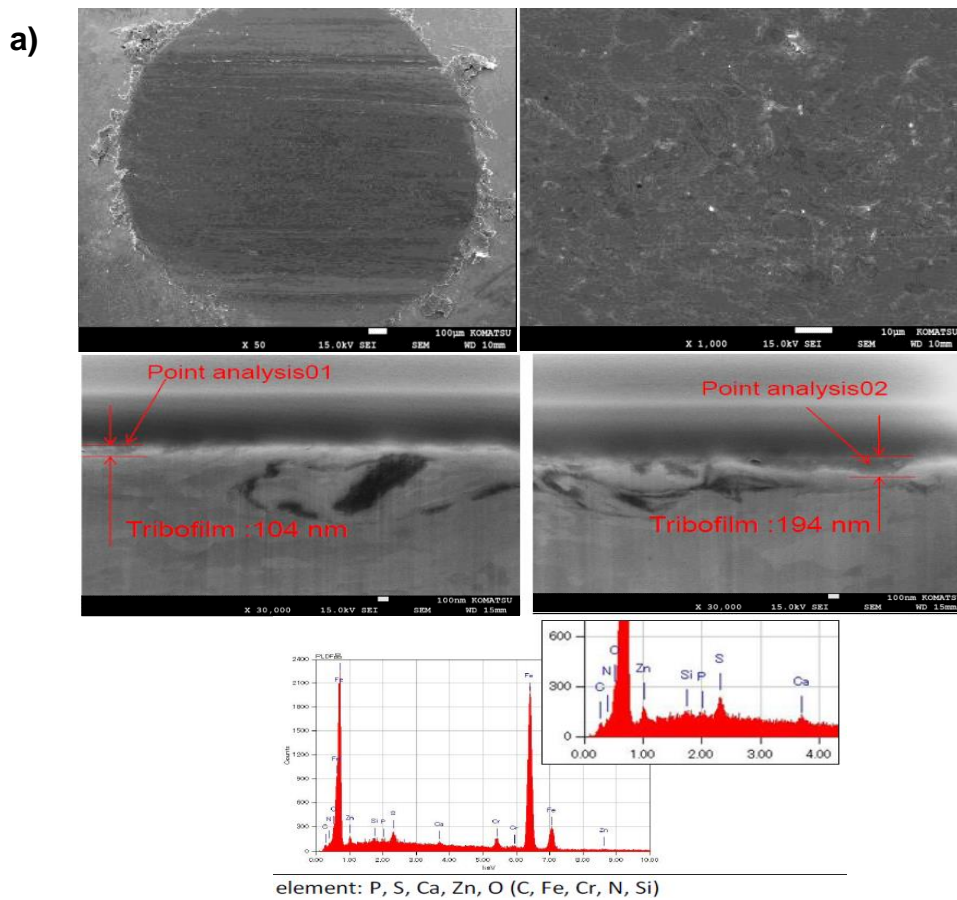
Figure 6-9. a) FIB-SEM images & b) EDX spectra of the tribofilm formed on the surface of the Plain sample at 1.19 GPa contact pressure and 12 Hz sliding speed.

With the MoS$_2$ samples high amounts of molybdenum and sulphur were detected outside the worn area when using SEM-EDX (Figure 6-10)) which relates to the presence of a MoS$_2$ coating. Within the worn area a strong presence of iron is detected, but no molybdenum or sulphur supporting the assumption the MoS$_2$ coating is completely removed during testing. Phosphorous and sulphur are not clearly detected within the worn surface with maps, however there is a clear presence of zinc detected which may indicate a tribofilm may be present. However just outside the worn area a strong presence of manganese and phosphorous is detected most likely relating to the remnants of the MnP coating which was present under the MoS$_2$ coating. No clear presence of nitrogen is detected on either the unworn or worn areas of the pin, even though the sample had initially been hardened using the gas nitriding process before the nitride layers were removed. The EDX spectrum taken within the wear scar showed the presence of Fe, P, S & Zn. When using FIB-SEM with the MoS$_2$-coated sample (Figure 6-11) a ~62 nm thick film was identified and EDX showed a strong presence of phosphorous and zinc commonly used to indicate the presence of a tribofilm. XPS (section 6.4.2) was also used confirm the presence of a tribofilm.
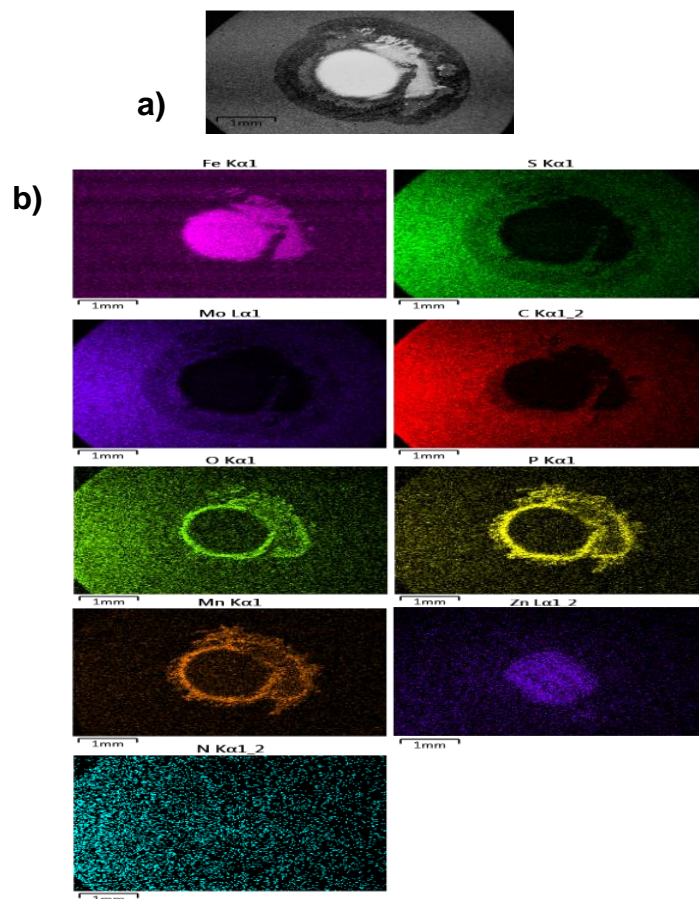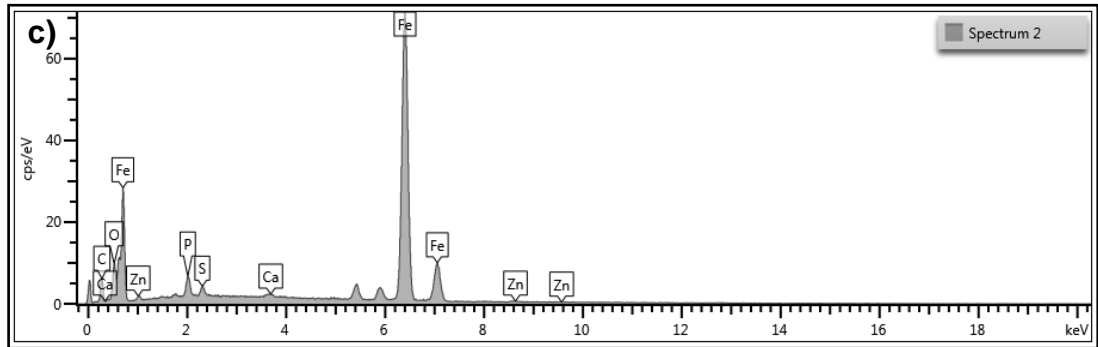
Figure 6-10. a) SEM image, b) EDX maps and c) spectrum of the unworn and worn surface of the MoS₂ pin samples at 1.19GPa contact pressure and 12Hz sliding speed.
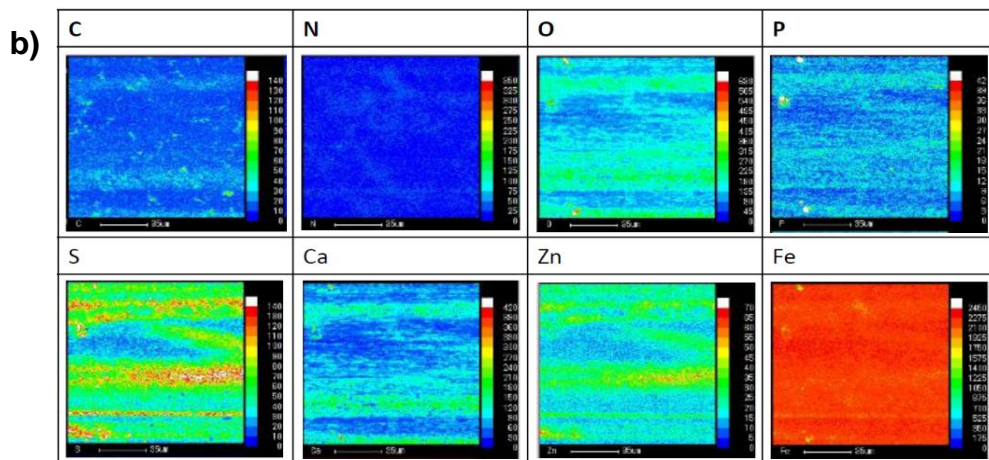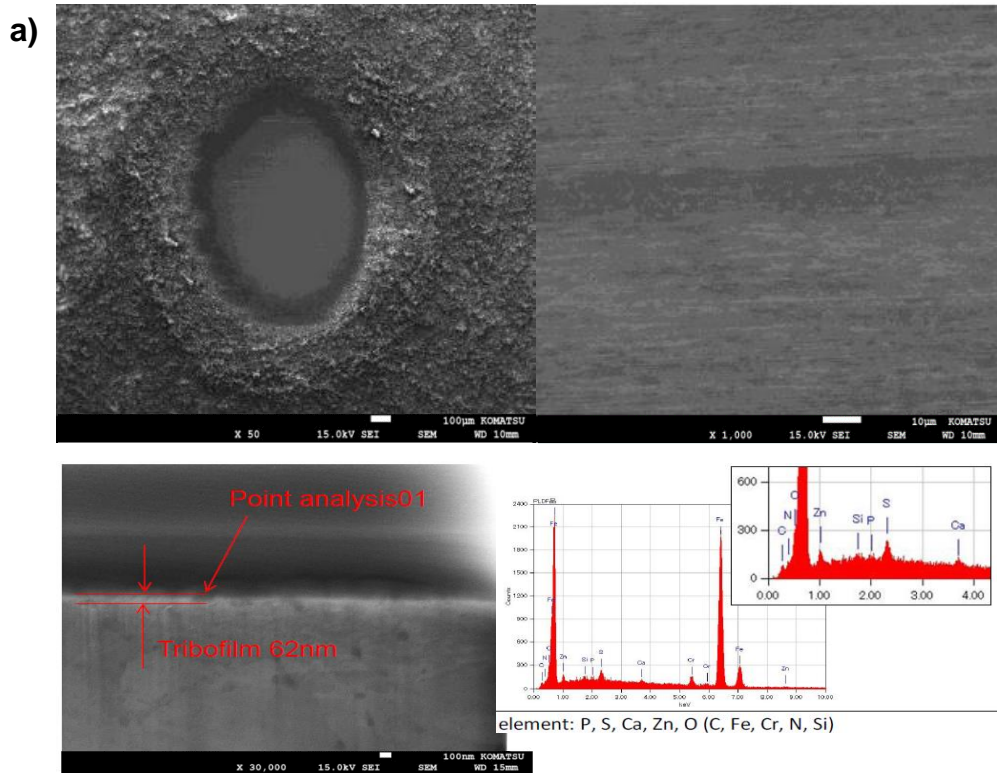
Figure 6-11. a) FIB-SEM images & b) EDX spectra of the tribofilms formed on the surface of the MoS₂ coated sample at 1.19GPa contact pressure and 12Hz sliding speed.

When analysing the QPQ samples using SEM-EDX (Figure 6-12) a high presence of oxygen is present on the unworn areas of the pin sample, which relates to the presence of a Fe_3O_4 oxide layer. However within the wear scar a significantly lower oxygen presence is detected most likely due the removal of the oxide layer during testing. Within the wear scar a high concentration of iron and nitrogen is detected relating to the nitride layer exposed under the oxide layer. A low presence of sulphur and phosphorous is detected within the wear region, however zinc is not identified. The presence of phosphorous indicates the possibility of the presence of phosphate tribofilm. The EDX spectrum shows the presence of all the expected elements including zinc within the wear scar.
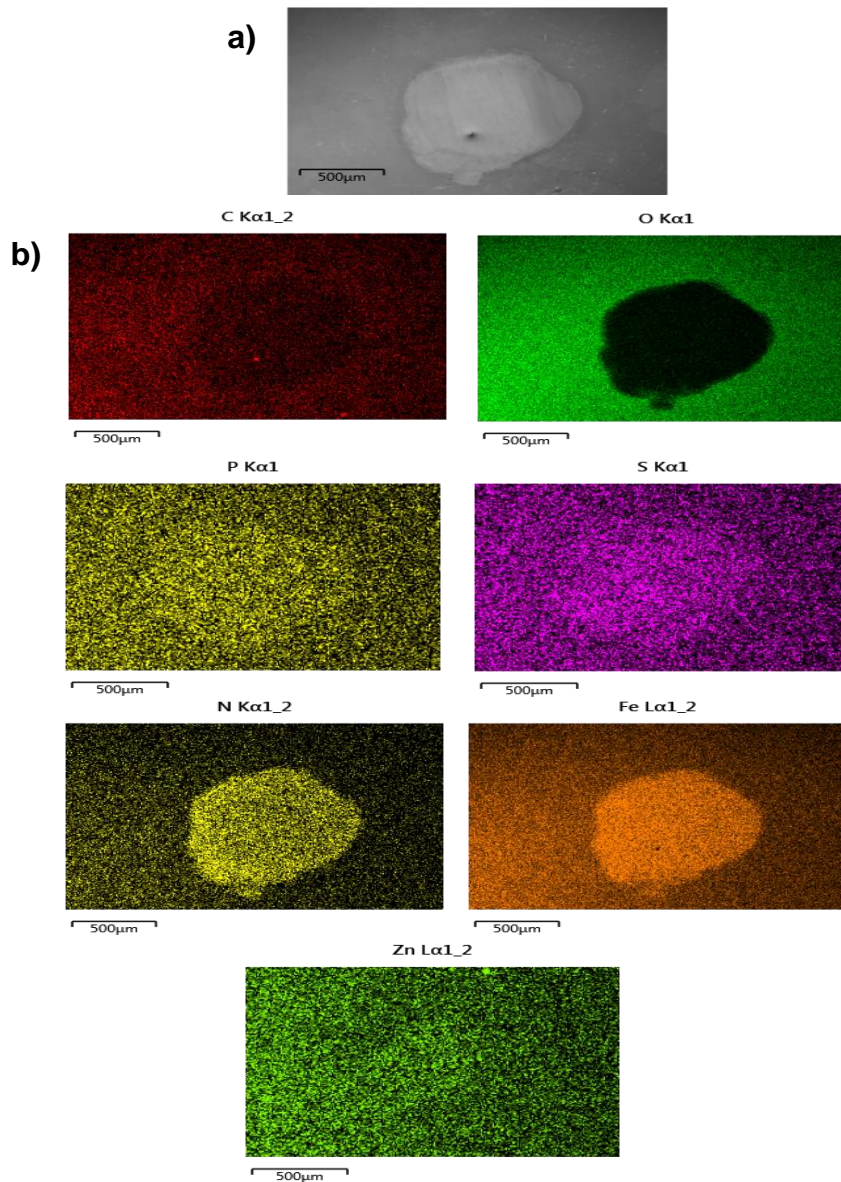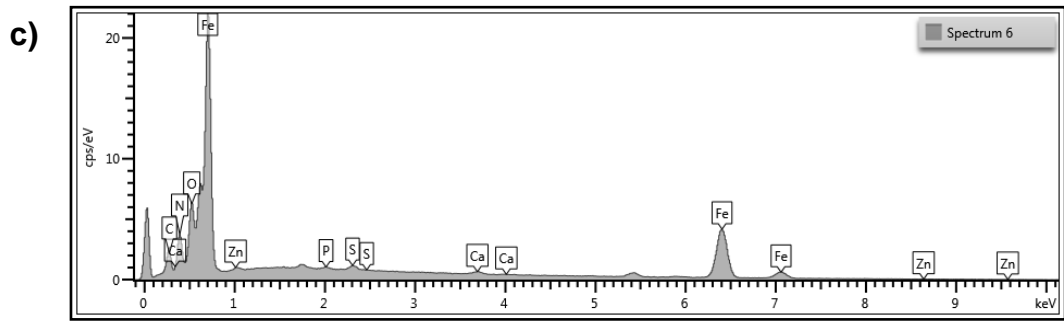
Figure 6-12. a) SEM image, b) EDX maps and c) spectrum of the unworn and worn surfaces of the QPQ pin samples at 1.19GPa contact pressure and 12Hz sliding speed.

With the QPQ samples (Figure 6-13) SEM showed the presence of a patchy tribofilm on the surface. However no significant tribofilm was visible in the areas analysed using FIB-SEM, supported by EDX measurements showed a low presence of phosphorous, sulphur and zinc which are the common elements associated with the formation of a glassy phosphate tribofilm. When using XPS to analyse the worn surface (section 6.4.2), the presence of a phosphate tribofilm was detected.
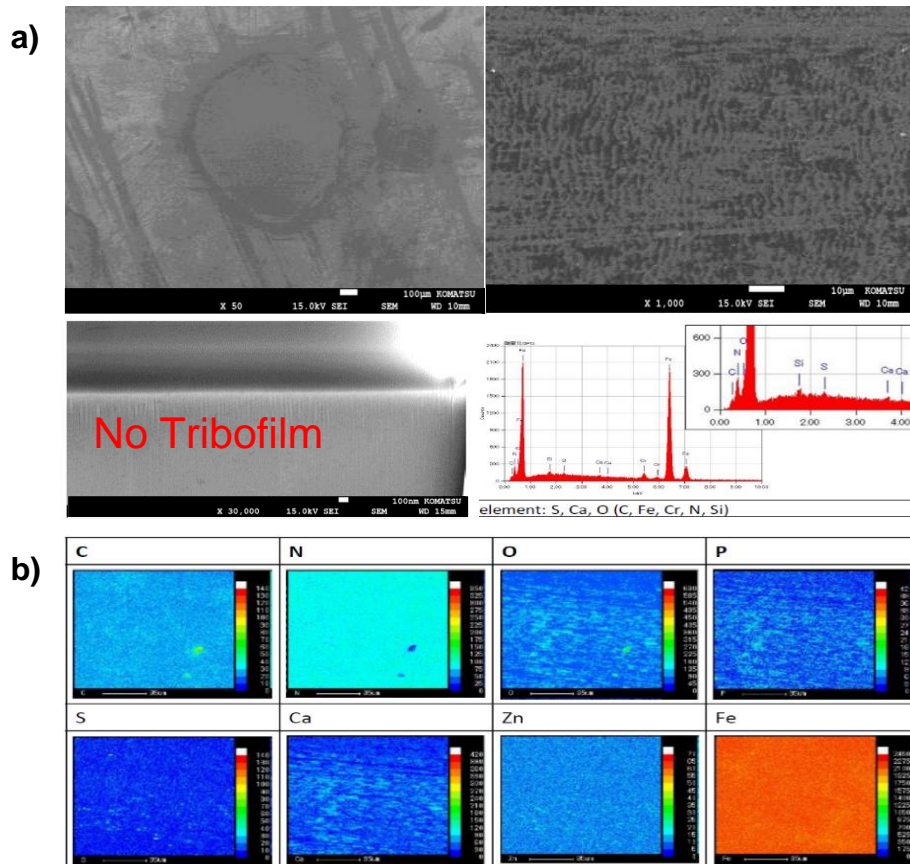
Figure 6-13. a) FIB-SEM images & b) EDX spectra of the tribofilms formed on the surface of the QPQ sample at 1.19GPa contact pressure and 12Hz sliding speed.

In the FIB-SEM images where the tribofilms were identified two dominant layers were observed. In each image the top layer is the tribofilm followed by the steel substrate underneath. A thicker non-uniform film was found to be formed on the plain sample which had the lowest surface hardness. Under boundary lubrication conditions, ZDDP reacts with the rubbing steel surface forming a tribofilm. This tribofilm is generally composed of mainly a mixed iron and zinc polyphosphate glass forming a pad-like structure. The surface is protected by the sacrificial properties of the tribofilm [127].

6.4.2 Tribofilm Characterisation using XPS

XPS was used to analyse the changes in chemical states of elements on the different treated pin sample worn surfaces. Figures 6-14 – 6-16 present the XPS data curves with fitted peaks, with Table 6-2 quantifying the elements on the different worn surfaces at a 1.34 nm etching depth. The results presented here focus on when an applied pressure of 1.19 GPa and a sliding speed of 12 Hz are applied as the tribochemical findings were representative of the findings of all contact pressures used at the lower sliding frequency. The results for an etching depth of 1.34 nm are presented and focussed on in this study as it was believed due to the relative thinness of the tribofilms formed with the QPQ samples, etching too deep may change the chemical species present within the tribofilm. Using a low etching time would allow the analysis of the tribofilm close to its top surface avoiding any possible contaminants which may be present.

Interestingly the presence of a phosphate anti-wear tribofilm was identified using XPS on the QPQ samples (Figure 6-16). This is most likely due to the larger area analysed and due to XPS being a more surface sensitive technique than EDX it was able to detect a relatively thin tribofilm. The tribofilms formed for all types of samples show the presence of ZnS/ZnO/Zn-phosphates and also the presence of sulphide and sulphate formation which are expected to appear and in agreement with EDX results (Figure 6-12). The tribofilm can mostly be classed as being composed from inorganic amorphous pyrophosphates associated with Zn and S [90].

For all samples the key elements identified were carbon, oxygen, phosphorous, sulphur, zinc, iron, calcium and nitrogen. The main chemical species identified in both samples tribofilms are listed in Table 6-1. Common compounds identified within the different sample tribofilms are $CaCO_3$ (347.0 eV) from the presence of detergents within the lubricants. As expected with the presence of ZDDP, sulphides (161.7 eV) and phosphates (133.4 eV) were detected within all the samples tribofilms which can be associated with formation of amorphous pyrophosphates alongside zinc compounds.

There are key differences between the tribofilms of the different samples. With the QPQ samples (Figure 6-16) the N 1s peaks show a tribofilm consisted of nitrides (397.8 eV) due to presence of the nitride layer and organic species attributed to absorbed nitride complex [103]. Using XPS no chemical species of Molybdenum are detected in the tribofilm of the MoS_2 coated samples after testing.

The common Fe chemical states found in the tribofilms of all types of samples were Fe_2O_3 (710.4 eV), FeO (709.4 eV) & FeS_2 (706.8 eV) (Table 6-1). The Fe chemical states found within the plain sample tribofilms were the same as the QPQ and MoS_2 samples with the additional presence of FeS (712.1 eV). The detection of FeS_2 within the plain samples (Figure 6-14) tribofilm is more common than with MoS_2-coated samples (Figure 6-15), but the at% is significantly lower than with QPQ samples (Figure 6-16) which could be due to the formation of a thin film with the latter samples. The presence of a Fe_3O_4 layer with the QPQ samples may have influenced the formation FeS_2 [102].

Due to the treatment applied to the counter plates being kept constant, the tribofilm compositions from all tests were almost identical and they were thicker than that formed on the pin samples. It was assumed that due to the varying of treatment to the pin samples that the chemical species formed on these samples would be influenced, hence only the XPS data of the pin samples is presented.

The presence of a MoS$_2$ coating and FeS$_2$ compounds may influence the improved wear and friction behaviour seen with the MoS$_2$ coated and QPQ samples.

Table 6-1. General binding energy values for compounds relevant to the tribofilms formed on the worn surfaces of all treated samples [103, 129].

Additive	Element	B.E / eV ($\pm$1eV)			Chemical State		
		Plain	MoS$_2$	QPQ	Plain	MoS$_2$	QPQ
	Fe 2p	712.1	-	-	FeS	-	-
		710.4	-	710.3	Fe$_2$O$_3$	-	Fe$_2$O$_3$
		709.4	709.4	-	FeO	Fe$_2$O$_3$	-
Fully Formulated (ZDDP)		706.8	706.8	706.8	FeS$_2$	FeS$_2$	FeS$_2$
	N 1s	-	-	397.8	-	-	Nitride
	P 2p	133.2	133.4	133.9	Phosphate	Phosphate	Phosphate
	Zn 3s	139.4	140.1	139.9	ZnS	ZnS	ZnS
	S 2p	161.8	161.7	161.7	Sulphide	Sulphide	Sulphide
	Ca 2p	347.3	347.0	347.0	CaCO$_3$	CaCO$_3$	CaCO$_3$

Figure 6-14. XPS Fe 2p, O 1s, P 2p and S 2p spectra of the tribofilms formed on the plain treated samples at an applied contact pressure 1.19 GPa and 1.34 nm etching depth.
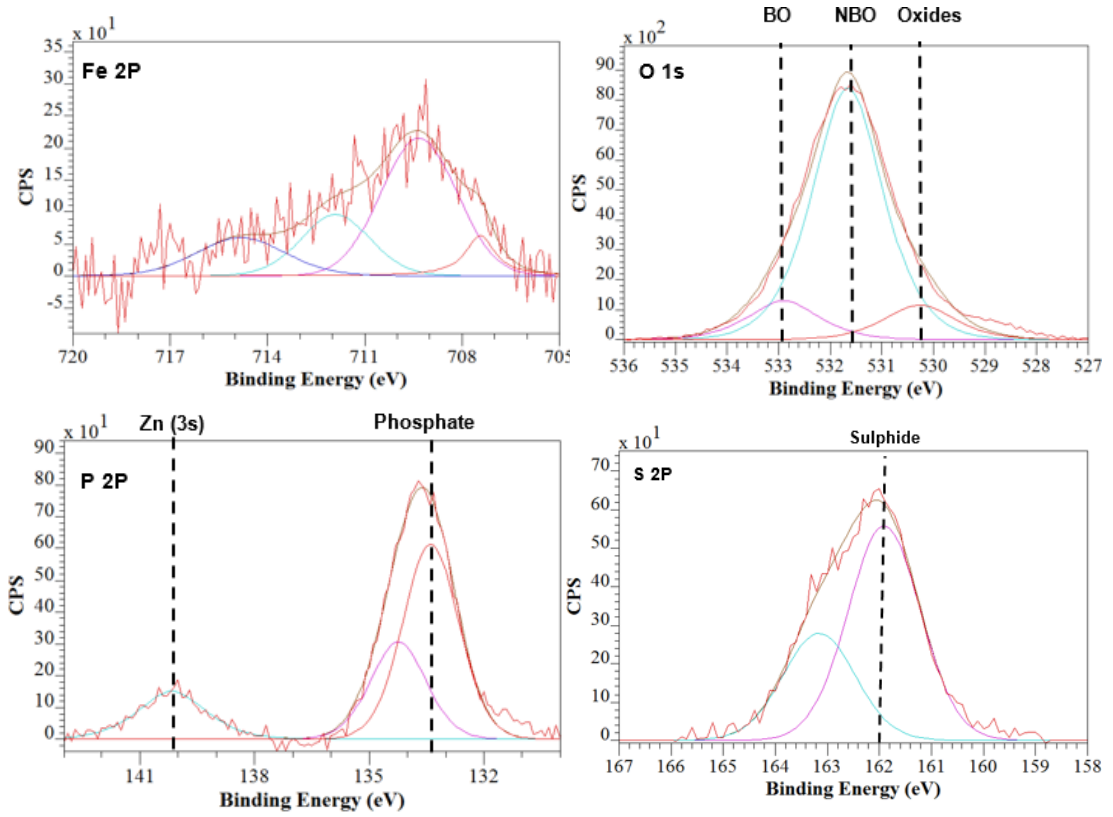
Figure 6-15. XPS Fe 2p, O 1s, S 2p and P 2p spectra of the tribofilms formed on the MoS2 treated samples at an applied contact pressure 1.19 GPa and 1.34 nm etching depth.
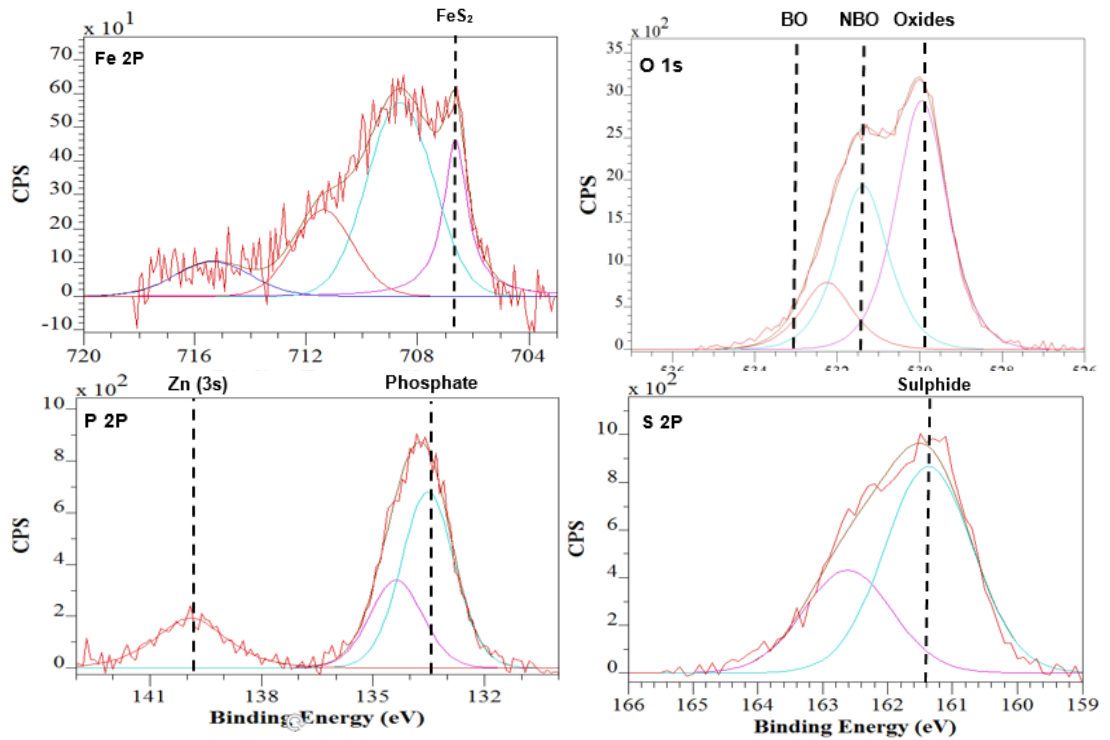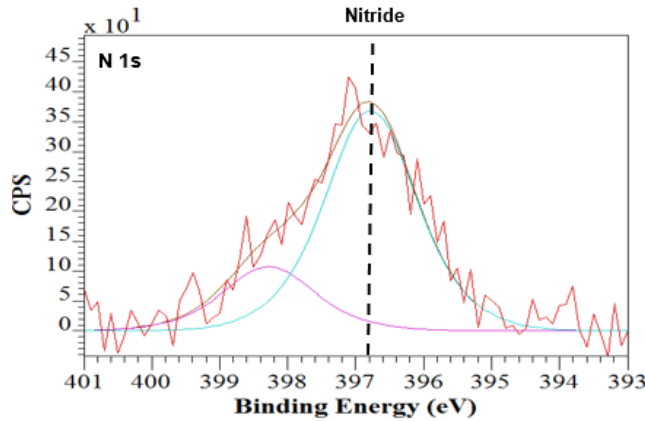
Figure 6-16. XPS Fe 2p, O 1s, P 2p, S 2p and N 1s spectra of the tribofilms formed on the QPQ treated samples at an applied contact pressure 1.19 GPa and 1.34 nm etching depth.

Table 6-2 highlights the XPS at% quantification of all elements on the worn surfaces of the three sample variants. It is shown that at a 1.34 nm etching depth the tribofilm element concentrations are very similar for all sample variants. There are slight differences in P & Zn contents between the untreated plain, MoS_2 coated and QPQ samples, most likely relating to a different tribofilm formation. As shown in Figure 6-10 (b) there is a strong presence of phosphorous within the wear scar of the MoS_2 sample due to the remnants of an MnP layer.

Table 6-2. XPS quantification (at%) of tribofilm formed on pin sample variants at 1.34 nm etching depth.

	O	N	P	S	Ca	Fe	Zn
Plain	52	-	8	8	24	5	3
QPQ	50	1	9	8	29	2	2
MoS₂	51	-	11	6	28	1	2

Interestingly when comparing the elemental composition of the tribofilm of the QPQ sample when the compound layer is present and removed, Table 6-3 shows higher Fe and P content when the compound layer is removed. This may be an indication that the removal of inert compound layer could impact the formation of a tribofilm [89, 121].

Table 6-3. XPS quantification (at%) of tribofilm formed on QPQ samples when the compound layer present and removed during testing (1.34 nm etching depth).

	O	N	P	S	Ca	Fe	Zn
QPQ (layer present)	50	1	9	8	29	1	2
QPQ (layer removed)	52	1	16	3	26	2	1

With the removal of the compound layer (Figure 6-17(b)) with the extreme contact pressure and the exposure of the nascent iron substrate, a thicker and closer packed tribofilm can be observed on the surface of the sample (Figure 6-17). This highlights the impact of the different layers on the formation of a tribofilm and potentially tribological behaviour.

Figure 6-17. SEM images of the tribofilm surface coverage of the QPQ samples a) the compound layer has not been removed b) compound layer removed.

To understand the formation of the ZDDP tribofilm, the phosphate glass can be characterized. The glass polymerisation number (n) can be calculated using the (bridging oxygen) BO (P-O-P)-to- (non-bridging oxygen) NBO (-P=O and P-O-Zn) ratio, Equation 6-1:

$$BO/NBO = (n-1)/2(n+1)$$

(6-1)

For n=1, the glass is an orthophosphate; for n=2 or higher the glass is a pyrophosphate or a metaphosphate [128, 129].

Tribological samples generally have a heterogeneous composition and the presence of overlapping species can affect the measured BO/NBO value. To unambiguously determine and distinguish between different chain length

samples the Zn 3s – P $2p_{3/2}$ binding energy (BE) difference can be used in conjunction with glass polymerisation number. Smaller BE differences indicate longer phosphate chain lengths [130].

Table 6-4. BO/NBO ratios for sample variants.

	BO (area)	NBO (area)	BO/NBO ratio	Zn 3s-P2p$_{3/2}$ BE (eV)
Plain	5000	10965	0.5	6.2
MoS$_2$	4614	15381	0.3	6.4
QPQ	2992	19384	0.2	6.8

With all types of worn samples in general pyrophosphate chains were formed, but QPQ treated samples produced shorter chain length of polyphosphate tribofilms (BO/NBO ratio and Zn 3s-P2p$_{3/2}$ BE) as shown in Table 6-4. Similar observations were made by Yue *et al* [104]. Crobu *et al* [127] showed that with higher oxide content the average chain length of the phosphates decreased. Within this study QPQ samples showed higher presence of oxides further supporting the indication of the presence of short phosphate chains (Table 6-4). The interaction of the treated surface with the lubricant could also lead to the formation of species which may influenced the shortening of chains. It has been acknowledged that non-bridging oxygen can have P-O-S bonds which would affect the BO/NBO ratio, however within this study the influence was assumed to be negligible as it was not detected. Studies have shown the phosphate chain length could influence the samples tribological behaviour [127, 131, 132].

6.4.3 Tribofilm Characterisation using Raman Spectroscopy

Raman spectroscopy was carried out to confirm the presence of key chemical compounds such as FeS$_2$, FeS & MoS$_2$ within the tribofilms formed by taking surveys of a wide coverage of the wear scars of the pins (Figure 6-18), Table 6-5 summarises the species detected. With the QPQ samples (Figure 6-18(c)) the Raman peaks of FeS$_2$ were centred at 340 cm^{-1} and 373 cm^{-1} and were clearly identified [133], with the presence of phosphates being detected with a broad peak ranging from 900-1100 cm^{-1} [134]. Uy *et al.'s* [135] study showed that Raman spectroscopy peaks centred around ~960-980 cm^{-1} and 1090 cm^{-}

[1] related to the presence of calcium and/or zinc/magnesium orthophosphates and calcium carbonate respectively. With all the samples Raman spectroscopy shows a peak at 670 cm^{-1} and broad peaks in the region 1373-1575 cm^{-1} which indicates the presence of Fe_3O_4 and amorphous carbon respectively [136, 137]. In comparison to the MoS_2 (Figure 6-18(b)) coated samples where a broad FeS_2 peak was detected (300-400 cm^{-1}), supporting the XPS and EDX findings that FeS_2 was present but at a smaller quantity than in the QPQ tribofilms. However the Raman spectroscopy peaks of MoS_2 were clearly identified at 384 cm^{-1} and 409 cm^{-1} [133] alongside the presence of phosphates (900-1100 cm^{-1}) [134]. With the plain samples (Figure 6-18(a)) no clear FeS_2 signal was identified, whereas two FeS peaks centred at 207 cm^{-1} and 283 cm^{-1} supporting the XPS findings that FeS compounds were present [138]. As observed with SEM a thick tribofilm is present on the surface, Raman spectroscopy detected the presence of a phosphate tribofilm (900-1100 cm^{-1}) [134].

Table 6-5. Summary of the species detected within the tribofilm of the sample variants using Raman.

Sample Treatment	Raman Peaks (cm^{-1})	Notes
QPQ	340, 373 (FeS$_2$) 955, 1080 (Phosphates)	Even though the peaks are noisy – FeS$_2$ is identified clearly Orthophosphates – 955 cm^{-1}, calcium carbonate – 1080 cm^{-1}
Plain	207, 283 (FeS) 955-1080 (Phosphates)	FeS Clearly identified Orthophosphates – 955 cm^{-1}, calcium carbonate – 1080 cm^{-1}
MoS$_2$	384, 409 (MoS$_2$) 955-1080 (Phosphates)	MoS$_2$ clearly identified, Noisy FeS$_2$ peaks Orthophosphates – 955 cm^{-1}, calcium carbonate – 1080 cm^{-1}
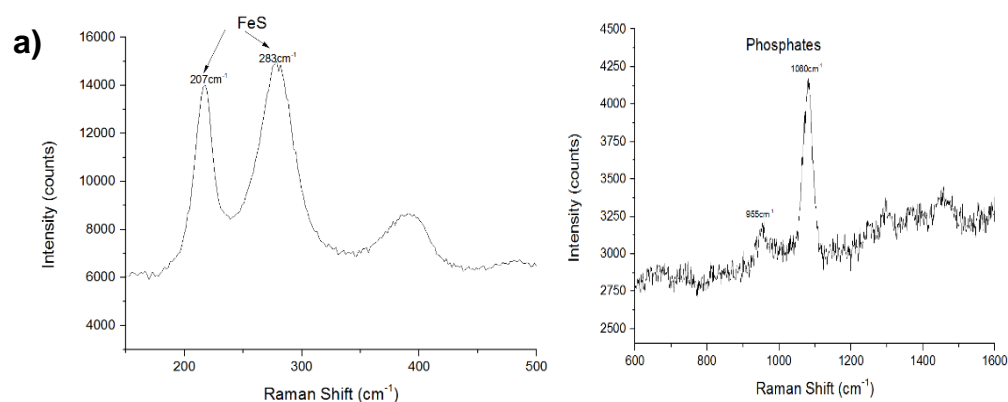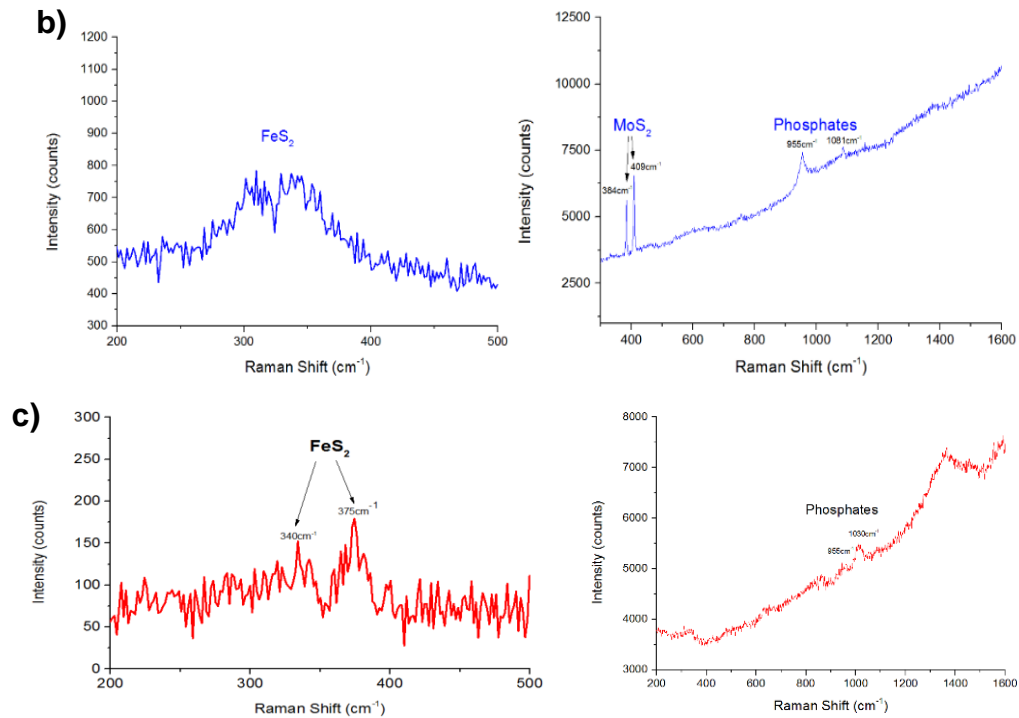
Figure 6-18. Raman spectra of different treated samples for FeS₂, FeS, MoS₂ & phosphate compounds within the formed tribofilms of the pins tested at a contact pressure 1.19 GPa and 12 Hz sliding frequency. a) Plain b) MoS₂ c) QPQ

6.5 Summary

In this chapter, the tribological performance of the untreated, MoS_2 coated and QPQ samples with a fully formulated lubricant was investigated. The following key points can be drawn from this part of the study:

- QPQ samples produce the lowest friction and wear results compared to the alternative treatments applied to the pin samples. At the application of an extreme contact pressure 1.90 GPa, an increase in friction with the QPQ samples is observed with the removal of the compound layer. This indicated the compound layer plays an important role influencing the friction behaviour of the sample.

- Doubling the sliding frequency from 12 to 25 Hz, led to a drop in friction with the increased sliding distance. A general increase in wear was also observed.

- FIB-SEM was not able to clearly identify the presence of a tribofilm with the QPQ sample. XPS and Raman were able to detect the presence of a thin tribofilm, indicating that the properties of the nitrided layer impacted its formation. The presence of higher concentration of FeS_2 within the QPQ samples tribofilm may have impacted its tribological behaviour.

- There is higher Fe and P content within the tribofilm of the QPQ samples which had their compound layer removed and the presence of a visibly thicker and greater surface covering tribofilm is observed to form.

- Using BO/NBO ratio and Zn $3s$-$P2p_{3/2}$ BE to characterise the phosphate glass present within the tribofilms, the QPQ samples were of a shorter chain length than that found in the tribofilms of the plain and MoS_2 coated samples.

With the application of coatings and surface treatment the aim is to extend the lifetime of the hydraulic motor by improving the tribological behaviour at the piston/cylinder interface. Reducing the friction and wear of the two components would help to limit the formation and trapping of abrasive particles which can eventually lead to complete system seizure. The QPQ samples demonstrated lower friction and significant lower wear than the MoS_2 treatment currently being used, which would help to improve the efficiency of the system. The Chapter shows that the layers produced by the QPQ treatment plays a significant role in the behaviour observed, however it was not possible to determine how much of an impact the Fe_3O_4 layer had on tribological and tribochemical behaviour. The next Chapter will focus on analysing the impact of an iron oxide and other layers on not only friction and wear but also their role in tribochemical interaction and formations.

Chapter 7 Tribological Impact of Varying the Layers Present on the Nitrided Surface

7.1 Introduction

The previous chapter demonstrated the effectiveness of the QPQ samples in improving tribological behaviour in comparison to the alternative treatments currently being applied. It is important to further investigate the influence of the properties of the layer which is present on top of the nitrided surface, to assess its impact on the tribological behaviour and tribofilm formation of the QPQ sample. This was achieved by using two modified QPQ samples – Isonite (Iso) & Sursulf (SN); the properties of these are highlighted in Table 7.1. Full characterisation of the different sample variants are highlighted in Chapter 5.

Table 7-1. Summary of the treatment processes applied to the sample variants.

Sample Treatment	Process
QPQ	Salt bath nitriding + Oxidising + Polishing
Isonite	Salt bath nitriding + Polishing
SN	Salt bath nitriding + FeS layer

Using the Isonite (Iso) samples allows the assessment of the impact of the oxide layer on the friction and wear behaviour of the QPQ sample. It also facilitates the investigation into the tribochemical interactions that form the tribofilm and the compounds present within it. The Sursulf (SN) samples allow the investigation of the tribological and tribochemical interactions of an alternative layer instead of an oxide layer present on the nitrided surface. This provides the analysis of the impact on friction and wear behaviour with the presence of a solid lubricant layer acting as a running-in coating.

Using the large TE77 tribometer the tribological properties of the alternatively treated samples were compared to the QPQ sample. Two contact pressures (0.92 & 1.19 GPa) whilst varying the sliding frequency between 12 & 25 Hz were applied when using the TO10 fully formulated hydraulic fluid lubricant. Post-experimental analysis using an optical microscope and surface analysis

techniques such as XPS and Raman allow the comparison of the changes in surface topography, tribofilm surface coverage and composition with the different sample variants.

7.2 Friction Response of the Nitrided Sample Variants

Figure 7-1 highlights the typical change in behaviour over time observed with the three nitriding sample variants during the complete duration of the test with TO10 as a lubricant. Similar friction trends are observed with all samples types with an initial running-in period until friction reaches a steady state value. As mentioned in Chapter 6, with the QPQ samples the oxide layer is removed in the early stages of the test and no clear impact on friction is detected. The smooth nitride layer is left exposed by the end of the test. Almost identical friction trends were observed when using the Isonite sample. As with the QPQ sample by the end of the testing period the nitride layer was left exposed. With the sulphur nitrided (SN) samples a running-in period before a steady state friction is reached is observed as with the alternative samples, however the friction values are lower. As observed with the QPQ samples the FeS layer is removed early on with testing and the nitride layer is exposed. However as shown in section 7.3 the surface shows evidence of adhesive and abrasive wear with remnants of the FeS layer remaining. The SN sample also shows the presence of a thicker film in the centre of the wear scar.
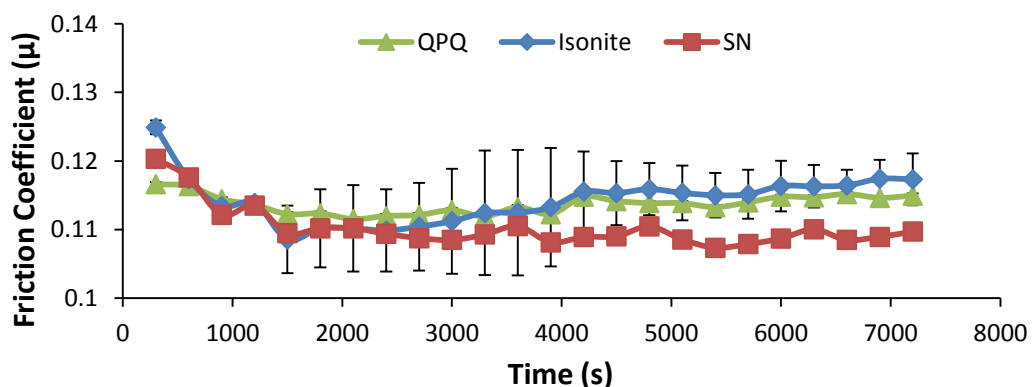
Figure 7-1. Friction coefficient vs time results over 2 hrs with the three samples at a 1.19 GPa contact pressure and sliding frequency - 12 Hz with TO10 lubricant.
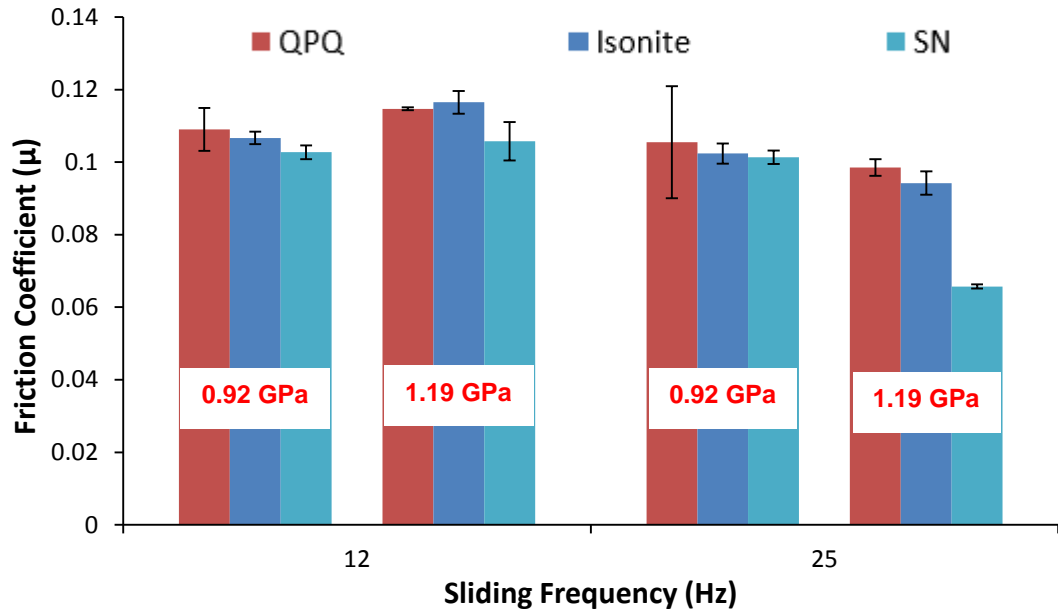
Figure 7-2. Friction coefficient results from experiments when the applied load and sliding frequency are varied with different variant pin samples when using fully formulated lubricant at 80°C.

The average friction coefficients for the QPQ samples compared to the alternatively treated samples (last 30 minutes of the test) in the steady stage when using the fully formulated (TO10) lubricant are shown and compared in Figure 7-2. The general behaviour observed was that the friction response of the QPQ and Isonite samples at the different testing conditions were almost identical and statistically overlap. The friction coefficients of the SN samples were on an average generally lower than that of the alternative samples. The frictional impact of the alternatively treated samples were not significantly different to the QPQ samples, however a clear friction behaviour pattern could be observed. The trends observed were similar to that observed in previous studies, with the lower friction behaviour of the SN samples being attributed to the presence of an FeS layer [139].

7.3 Wear Response of the Nitrided Sample Variants

Using an optical microscope the worn surfaces of the different samples (Figure 7-3) were analysed. With the QPQ and Isonite pins (Figure 7-3(a) & Figure 7-3(b)) a smooth surface is exposed. With the Sursulf (SN) samples (Figure 7-3(c)) the presence of a thick tribofilm can be observed.
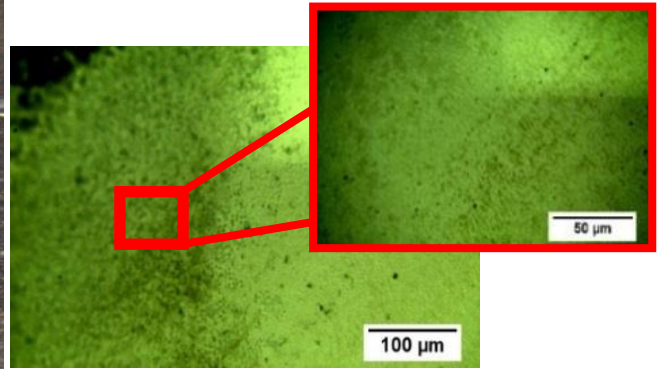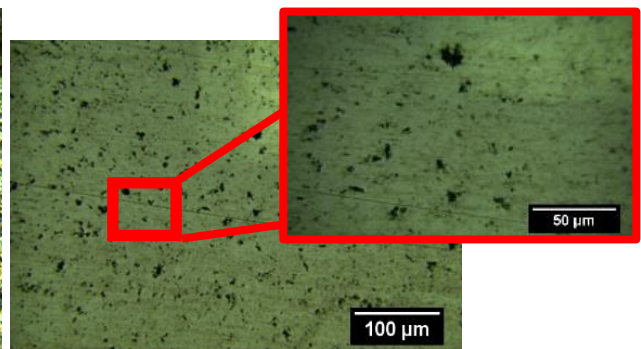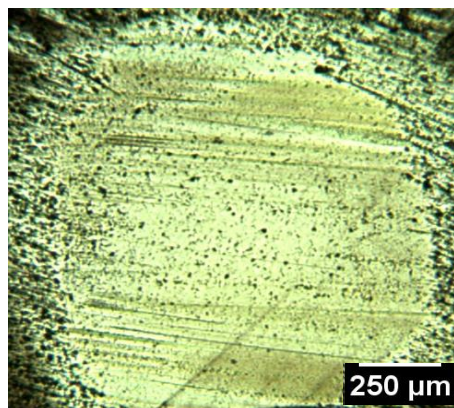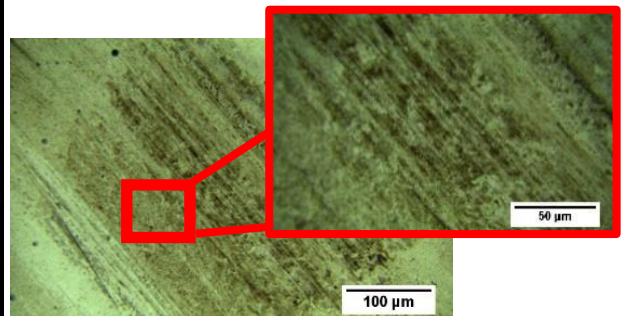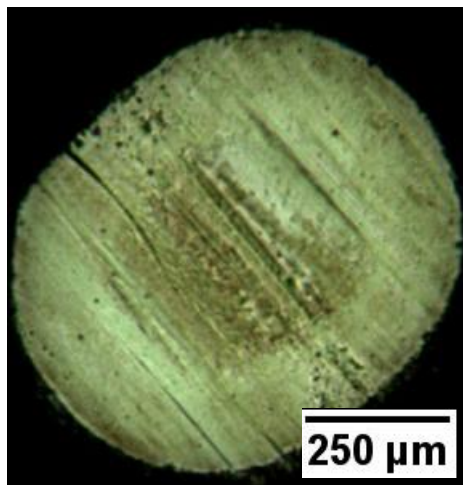
Figure 7-3. Optical images of the wear scar regions of the different treated pin samples when a 1.19 GPa contact pressure was applied at 12 Hz.
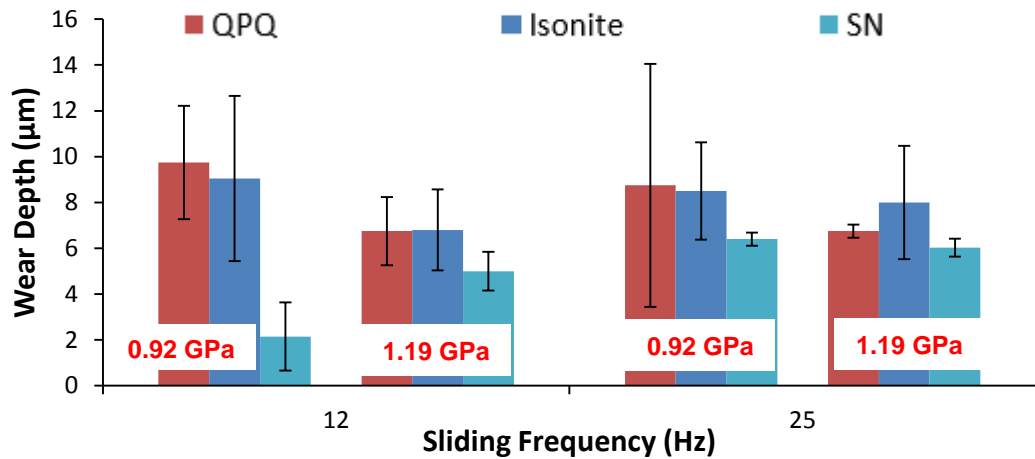
Figure 7-4. Wear depths of the three types of pins when contact pressures 0.92-1.19 GPa are applied at a 12Hz & 25Hz sliding frequencies using fully formulated lubricant at 80°C.

The depth profile measurements using Talysurf (Figure 7-4) showed that wear did not penetrate past the compound layer (QPQ & Iso = 13 µm and SN = 9 µm) for all the samples. The average wear depths for the QPQ and Isonite samples are almost identical and had statistical overlap. The SN samples on average showed lower wear depths compared to the alternative samples.

7.4 Tribofilm Characterisation

7.4.1 SEM-EDX Analysis

SEM-EDX was used to analyse the areas inside and outside the worn areas of the different nitride variant pin samples after the tribometer tests using fully formulated lubricant (TO10). The analysis gives an indication whether a tribofilm has formed on the worn surface and of its chemical composition. SEM-EDX gives a suggestion of the interaction of the surface with the additives within the lubricant.

With the QPQ samples SEM-EDX (Figure 7-5) as shown in Chapter 6, a high presence of oxygen is present on the unworn areas of the pin sample, which relates to the presence of a Fe_3O_4 oxide layer. However, within the wear scar a significantly lower oxygen presence is detected most likely due the removal of the oxide layer during testing. Within the wear scar a high concentration of iron and nitrogen is detected relating to the nitride layer exposed under the oxide layer. A low presence of sulphur and phosphorous is detected within the

wear region, however zinc is not clearly identified. The EDX spectrum showed the presence of P, S and Zn.

In comparison to the QPQ sample, with the Isonite samples SEM-EDX (Figure 7-6) showed no real presence of oxygen outside the wear scar due to the absence of an oxide layer with this sample. With the absence of an oxide layer there is a high presence of iron and nitrogen mostly likely due to the presence of the compound layer. No real presence of phosphorous, sulphur and zinc is detected within the worn area in comparison to the QPQ sample. However the EDX spectrum showed the presence of P, S and Zn within the tribofilm.

With the sulphur nitrided sample EDX (Figure 7-7) showed a strong presence of iron and sulphur outside the worn area of the pin relating to the presence of a FeS layer after treatment. Within the worn area a higher presence of iron and sulphur is detected possibly indicating the formation and presence of FeS within the contact areas, similar to that observed by Yue *et al* [139] and Liu *et al* [140]. Interestingly also present in the worn area is phosphorous and zinc indicating a protective phosphate tribofilm is also present within the wear area. The presence of nitrogen is detected on the edges of the wear scar however it is absent within it, possibly due to the high presence of iron, sulphur and phosphorous within the area. The EDX spectra shows the presence of all elements within the wear scar.

Table 7-2 highlights the P/Zn ratio of the tribofilms formed on the different sample variants. The ratios are almost identical for the Isonite and SN samples with the QPQ sample showing almost double the presence in comparison. This indicates that the presence of an oxide layer may impact the tribofilm formation of the samples. The higher presence of sulphur and greater impact of FeS with the SN samples may have impacted the P/Zn ratio.

Table 7-2. P/Zn ratio within the tribofilms of the nitrided sample variants.

Sample	P/Zn Ratio
QPQ	0.7
Isonite	0.4
SN	0.4
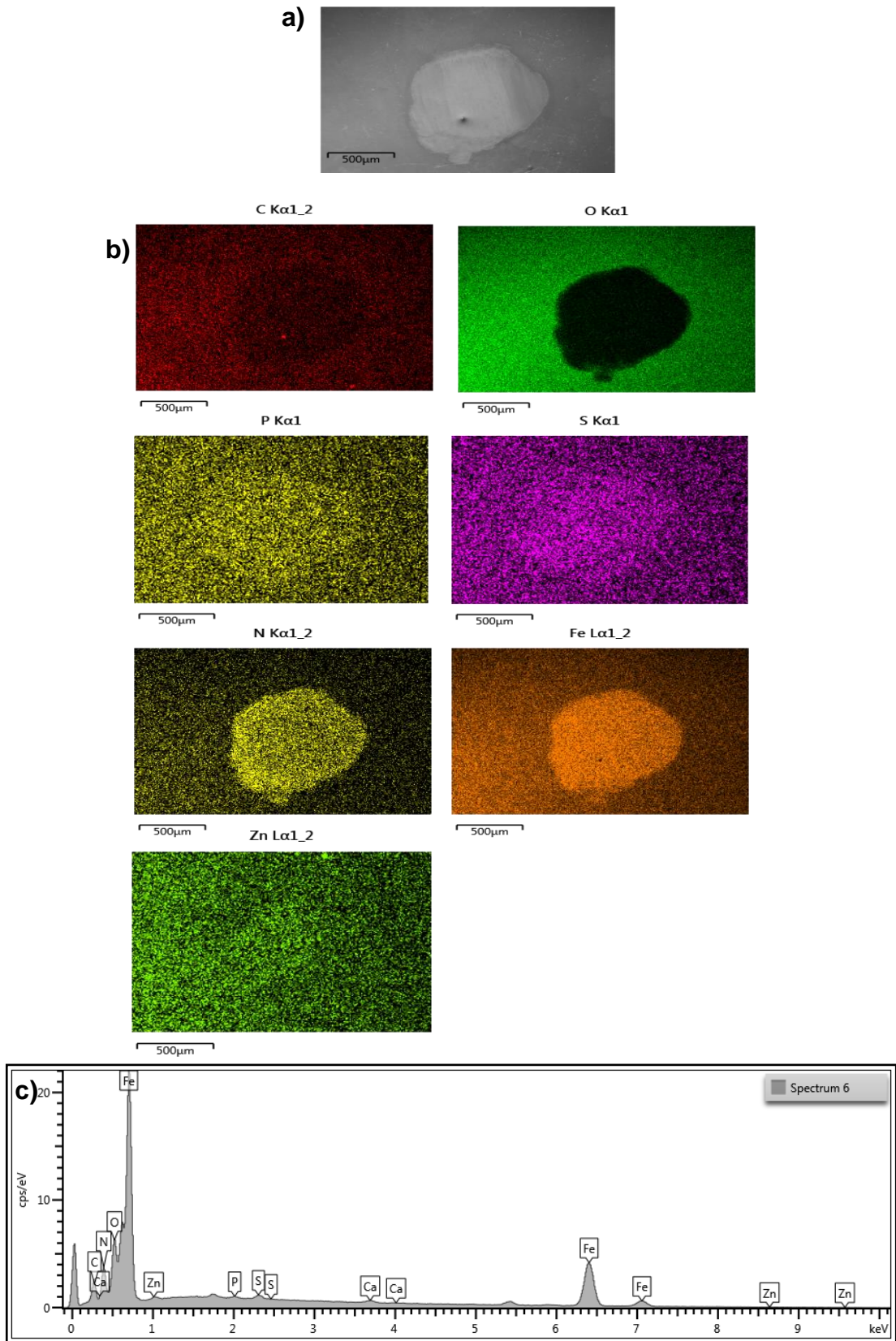
Figure 7-5. a) SEM image, b)EDX maps and c) spectra of the unworn and worn surface of the QPQ pin samples at 1.19GPa contact pressure and 12Hz sliding speed.

a)

b)

C Kα1_2

O Kα1

Fe Lα1_2

N Kα1_2

S Kα1

P Kα1

Zn Lα1_2

c)

Figure 7-6. a) SEM image, b) EDX maps and c) spectra of the unworn and worn surfaces of the Isonite pin samples at 1.19GPa contact pressure and 12Hz sliding speed.

Figure 7-7. a) SEM image, b) EDX maps and c) spectra of the unworn and worn surface of the sulphur nitrided pin samples at 1.19 GPa contact pressure and 12Hz sliding speed.
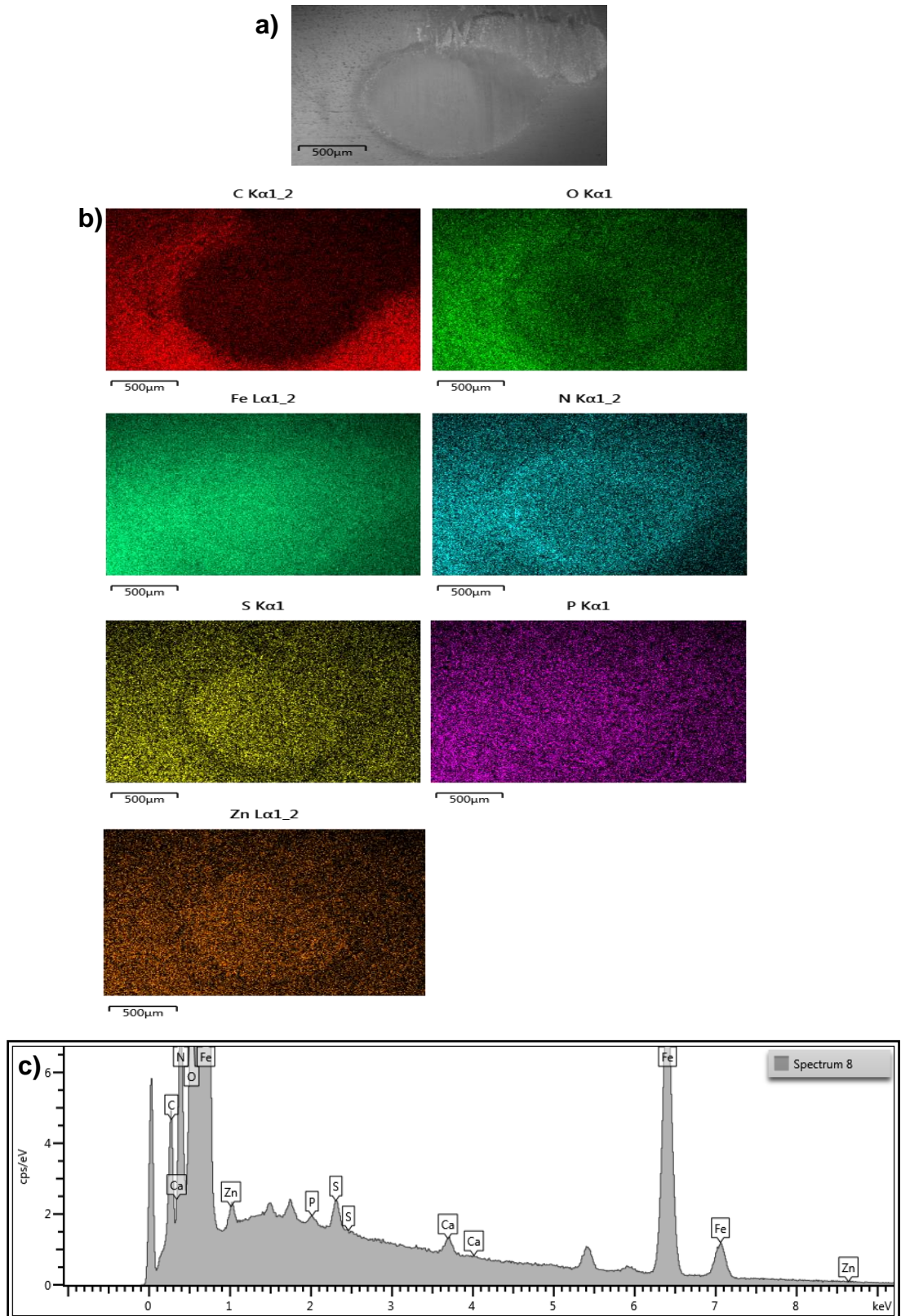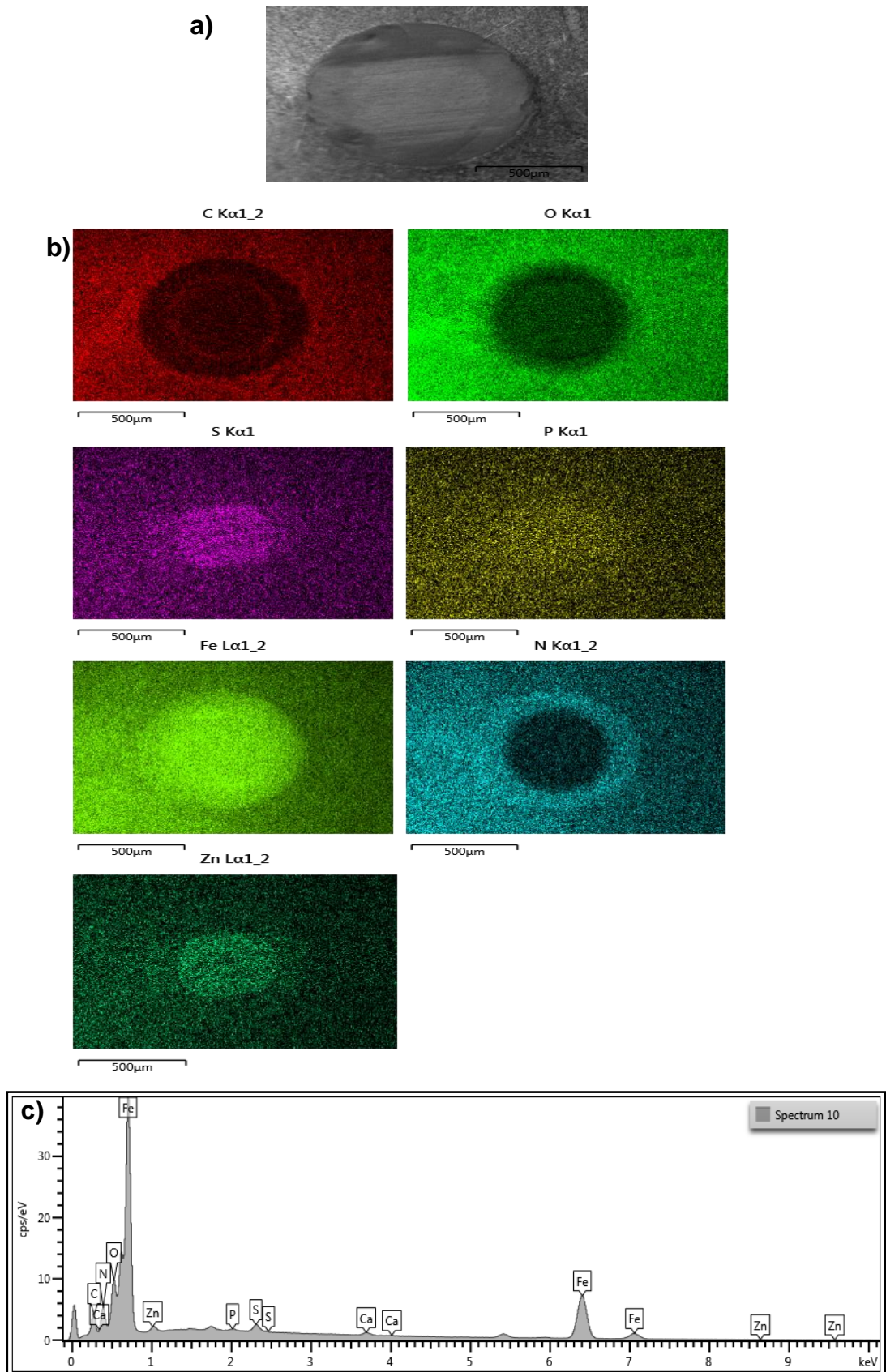
7.4.2 EPMA Analysis

EPMA was utilised to verify and support the findings from SEM-EDX. Elemental maps (Figure 7-8) were taken at the centre of the wear scars of the three nitride sample variants, allowing comparison of the concentration of elements across the samples. When comparing the QPQ (Figure 7-8(a)) and Isonite (Figure 7-8(b)) samples a higher presence of P, S and Ca were detected across the worn surface of the QPQ samples. This supported the EDX results (section 7.4.1) and indicated the formation of a patchy but thicker tribofilm on the QPQ sample surface. However higher concentrations of Zn were identified with the Isonite samples indicating the possible presence of a tribofilm.

In comparison to the other samples, the SN pins (Figure 7-8(c)) showed a higher concentration of P, S, Ca and Zn across the surface. The EPMA maps indicated the presence of a thicker tribofilm with a greater surface coverage in comparison to the QPQ samples, similar to that observed with EDX (Figure 7-7(b)).
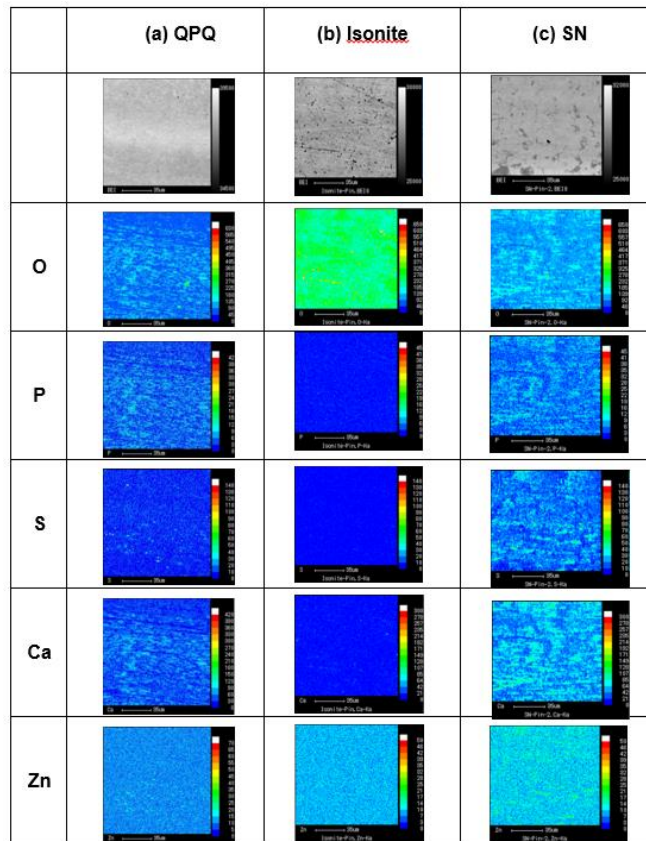
Figure 7-8. EPMA maps within the wear scars of the nitrided sample variants (a) QPQ (b) Isonite (c) SN.

7.4.3 Tribofilm Characterisation with XPS

XPS analysis was carried out to confirm the presence of a tribofilm and analyse the changes in chemical species within the tribofilm formed on the QPQ, Isonite & SN samples when using the fully formulated lubricant. Using XPS to etch 1.34 nm through the depth of the tribofilm the results generally showed the formation of a relatively thin tribofilms with QPQ and Isonite samples. The SN samples produced the thickest tribofilm. Table 7-3 highlights the species present after etching using XPS.

Table 7-3. General binding energy values for compounds relevant to the tribofilms formed on the worn surfaces of all treated samples [103, 129].

	Element	B.E / eV ($\pm$1eV)			Chemical State		
		QPQ	Isonite	SN	QPQ	Isonite	SN
Etch Depth 1.33 nm	Fe 2p	710.4	710.1	712.0	Fe_2O_3	Fe_2O_3	FeS
		706.8	-	710.1	FeS_2	-	Fe_2O_3
	N 1s	397.8	397.5	397.1	Nitride	Nitride	Nitride
	P 2p	133.9	133.1	133.2	Phosphate	Phosphate	Phosphate
	Zn 3s	139.9	139.9	139.9	ZnS	ZnS	ZnS
	S 2p	161.7	162.0	161.7	Sulphide	Sulphide	Sulphide

The tribochemical analysis using XPS (Figures 7-9 - 7-11) allowed the characterisation of the tribofilms formed, to investigate the impact the different layers applied to the top of the nitride surfaces had on chemical state of the tribofilm compared to that formed on the QPQ sample. With wear penetrating the nitride layer for all samples, nitrides (397.1 eV) were detected within each samples tribofilm (QPQ – Figure 7-9(d), Isonite – Figure 7-10(d) & SN – Figure 7-11(d)).

As seen in Chapter 6, with the QPQ samples the key species identified within the tribofilm was the presence of phosphates (133.9 eV - Figure 7-9(b)) and ZnS/ZnO (139.9 eV) as supported by the SEM-EDX analysis (Figure 7-5), further indicating the presence of a tribofilm. FeS_2 (706.8 eV) is detected within the tribofilm (Figure 7-9(a)) which in high concentrations could impact the friction behaviour of the sample.

With the Isonite samples it was possible to see that with the absence of an oxide layer the species formed within the tribofilm may have been impacted. XPS also detected the formation of a phosphate (133.1 eV - Table 7-2) containing tribofilm, which was seen when using SEM-EDX (Figure 7-5). However in comparison to the QPQ samples iron sulphides were not seen present with XPS (Figure 7-9(a)).

With the SN samples which has the presence of a FeS lubricating layer on the nitriding layer, FeS is detected with XPS (712.1 eV), Figure 7-11(a), and this is supported with EDX scans which detected the strong presence of iron and sulphur within the wear scar (Figure 7-7). The presence of phosphates (133.2 eV) are also detected within the tribofilm indicating the formation of a protective layer, supporting the SEM-EDX analysis (Figure 7-7) showing the presence of phosphorous in the wear scar.
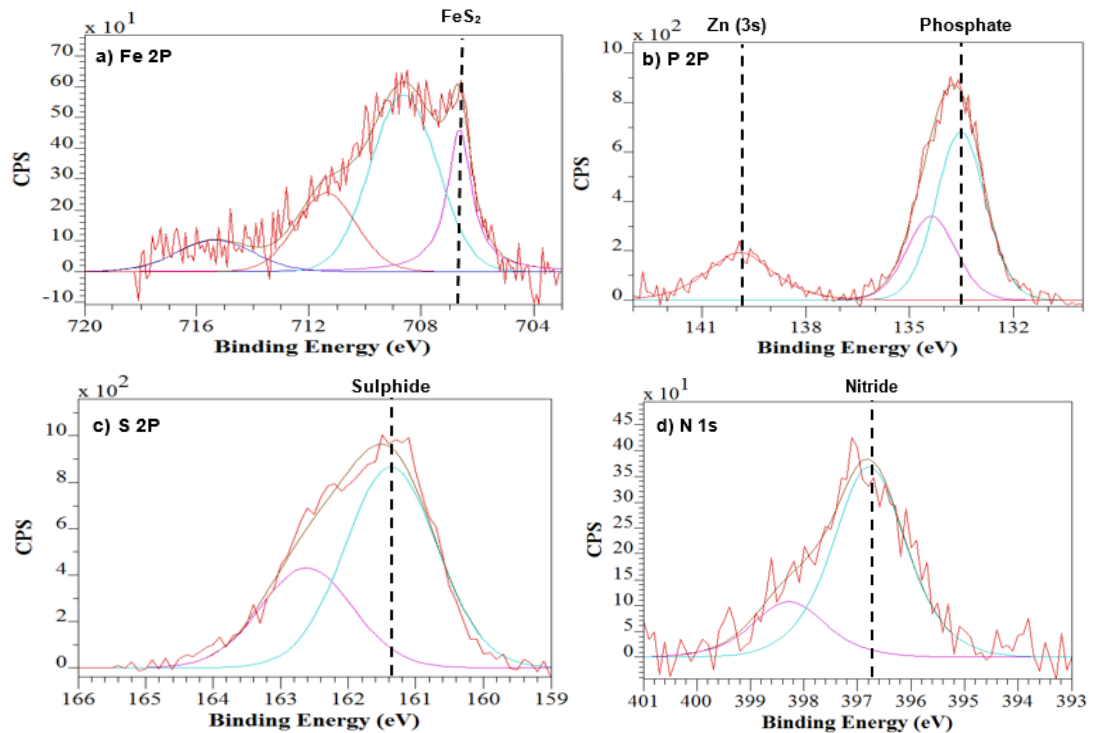
Figure 7-9. XPS Fe 2p, P 2p, S 2p and N 1s spectra of the tribofilms formed on the QPQ treated samples at an applied contact pressure 1.19 GPa and 1.34 nm etching depth.
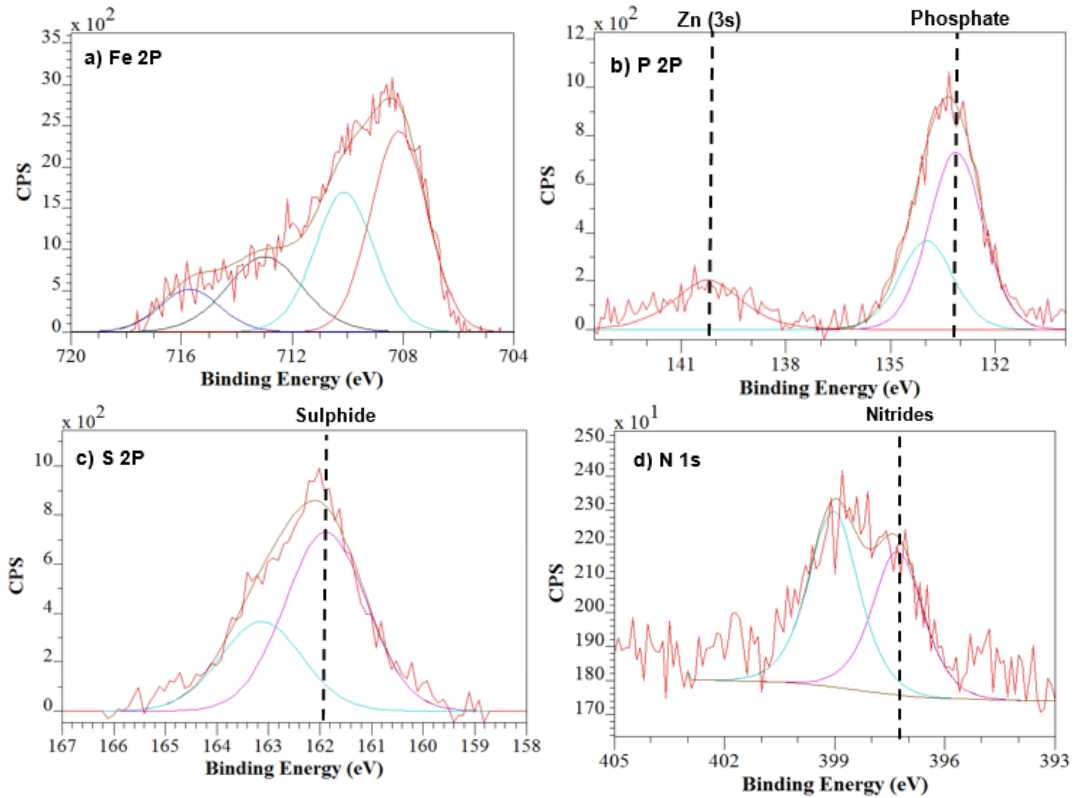
Figure 7-10. XPS Fe 2p, P 2p, S 2p and N 1s spectra of the tribofilms formed on the Isonite treated samples at an applied contact pressure 1.19 GPa and 1.34 nm etching depth.
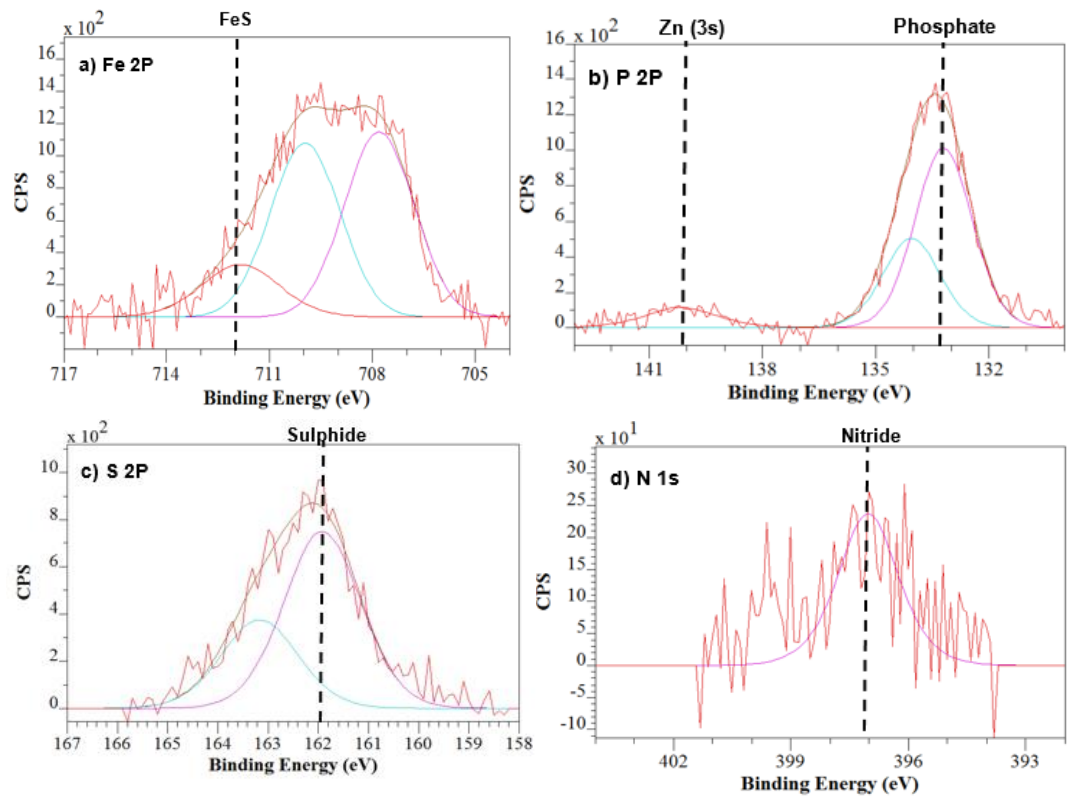
Figure 7-11. XPS Fe 2p, P 2p, S 2p and N 1s spectra of the tribofilms formed on the SN treated samples at an applied contact pressure 1.19 GPa and 1.34 nm etching depth.

7.4.4 Tribofilm Characterisation using Raman Spectroscopy

Raman spectroscopy was carried out to confirm the presence of key chemical compounds within the tribofilms formed by taking surveys of a wide coverage of the wear scars of the pins variants (Figures 7-12 – 7-14), Table 7-4 summarises the species detected.

Raman spectroscopy scans with the QPQ samples (Figure 7-12), showed the formation of FeS_2 (340 & 375 cm^{-1}) [133] alongside the presence of phosphates (900-1100 cm^{-1}) [134] which indicated the presence of orthophosphates (~960-980 cm^{-1}) and calcium carbonate (1090 cm^{-1}) [135]. This supported the findings from XPS analysis of the tribofilm formed. Raman spectroscopy shows a peak at 670 cm^{-1} and broad peaks in the region 1373-1575 cm^{-1} which indicates the presence of Fe_3O_4 and amorphous carbon respectively [136, 137].
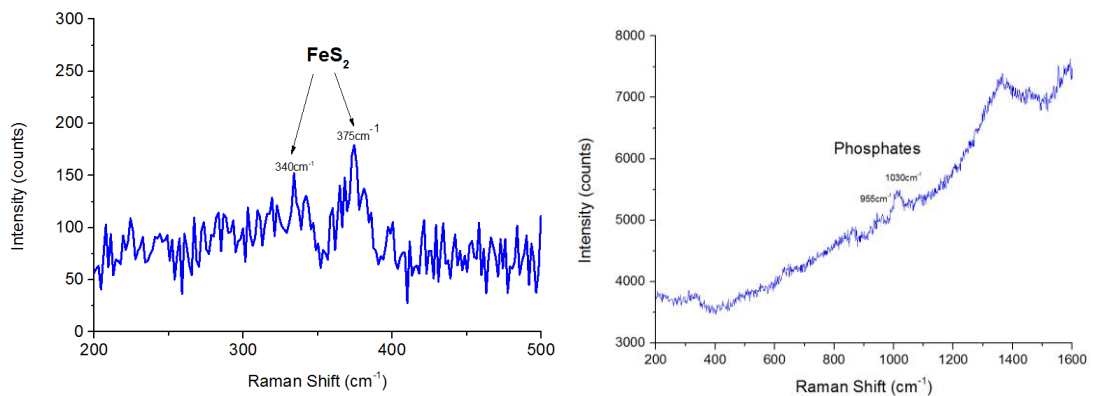
Figure 7-12. Raman spectra of the QPQ pin samples for FeS & phosphate compounds within the formed tribofilms tested at a contact pressure 1.19 GPa and 12 Hz sliding frequency with TO10 lubricant.

With the Isonite samples Raman spectroscopy was able to confirm the presence of phosphates within the tribofilm formed, with the presence of peaks from 950-1100 cm^{-1} [134]. As shown with the XPS Fe peaks, it was difficult to clearly identify the formation of iron sulphide (200-300 cm^{-1}) [138] where a broad peak is detected with Raman (Figure 7-13). Raman spectroscopy shows a peak at 670 cm^{-1} and broad peaks in the region 1373-1575 cm^{-1} which indicates the presence of Fe_3O_4 and amorphous carbon respectively [136, 137].
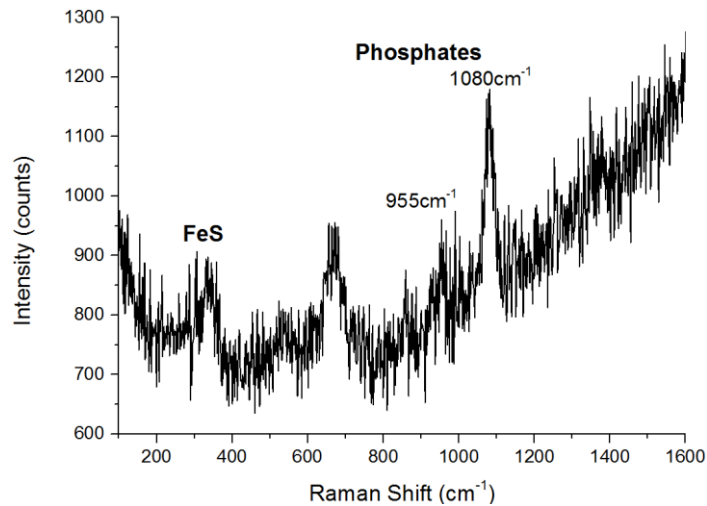
Figure 7-13. Raman spectra of the Isonite pin samples for FeS & phosphate compounds within the formed tribofilms tested at a contact pressure 1.19 GPa and 12 Hz sliding frequency with TO10 lubricant.

In comparison to the other samples, Raman spectroscopy was able to identify the strong presence of iron sulphides (200 – 300 cm^{-1}) [138] and phosphates (900 -1100 cm^{-1}) [134] within the tribofilm of the SN samples (Figure 7-14). This supported the indication from SEM-EDX (Figure 7-7) and XPS (Figure 7-11) of the formation of a thicker tribofilm.
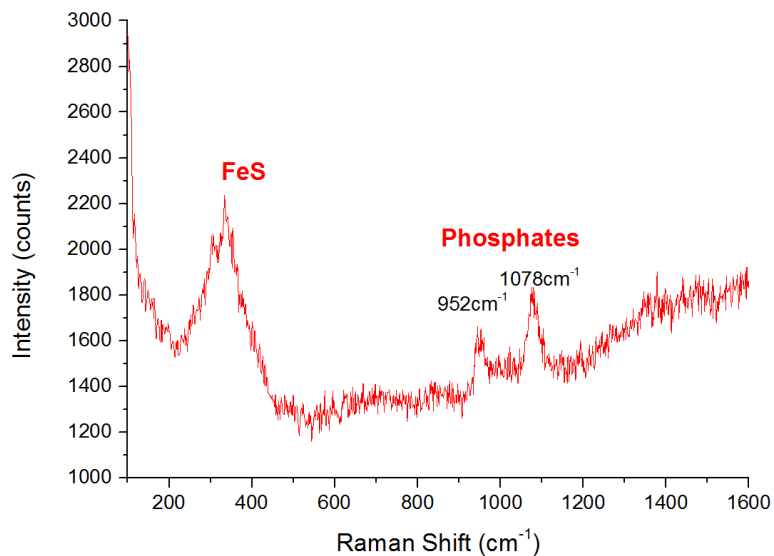
Figure 7-14. Raman spectra of the SN pin samples for FeS & phosphate compounds within the formed tribofilms tested at a contact pressure 1.19 GPa and 12 Hz sliding. frequency with TO10 lubricant.

Table 7-4. Summarises the chemical compounds detected within the different samples tribofilms using Raman Spectroscopy.

TO10 Lubricant	Sample Variant		
	QPQ	Isonite	SN
Raman Peaks (cm^{-1})	340, 375 (FeS$_2$) 955, 1090 (Orthophosphates, calcium carbonate)	955, 1080 (Orthophosphates, calcium carbonate)	280, 320 (FeS) 952, 1078 (Orthophosphates, calcium carbonate)

7.5 Summary

In this chapter, the impact of different layers formed upon a nitrided layer on friction and wear were investigated. SEM/EDX, XPS and Raman analysis were used to investigate the influence of the properties of these layers had on tribochemical interactions and tribofilm formation.

- With the Isonite samples the friction and wear response were identical to that observed with the QPQ samples. With the absence of an oxide layer XPS and Raman spectroscopy showed the absence of FeS$_2$ and a higher P/Zn ratio within the QPQ tribofilm. EPMA indicated the presence of a stronger and thicker tribofilm on the surface of the QPQ samples

- The SN samples produced better friction and wear response compared to the other nitrided variant samples. Compared to the alternative samples a thicker tribofilm is formed, EDX and EPMA showed strong presence of iron, sulphur and phosphorous within the wear scar. Using XPS and Raman spectroscopy the chemical species identified were FeS and phosphates, which would impact friction and wear behaviour.

The addition of the oxidising with nitriding process aimed to improve the corrosion resistance and cosmetic appearance of the samples. The chapter showed that the layer had minimal impact on friction and wear behaviour however the influence on FeS$_2$ formation was important and could potentially change tribological behaviour. It was also shown that the composition of the layer present played a significant role in improving the samples durability. It is also important to consider the possible role of lubricant additives in improving the performance of the applied treatments.

Chapter 8 Effects of using Alternative Extreme Pressure (EP) and Anti-Wear (AW) Additives with Sample Variants

8.1 Introduction

Friction and wear performance is influenced by a number of factors such as lubricant additives and surface modification, which can individually improve tribological properties or through a synergistic effect between the two factors. To achieve optimal tribological performance between friction pairs it is crucial to understand the mechanics of the synergistic interaction between modified surfaces and lubricant additives [104].

This chapter will focus on investigating the optimisation of the friction and wear behaviour of the plain, MoS_2 coated and QPQ samples using different fluid additives. The overall aim is to improve the tribological properties and extending the life of friction pairs within hydraulic systems.

The effect of alternative extreme pressure additives on friction and wear behaviour with the three sample variants were investigated with the large TE77 tribometer. A contact pressure of 1.19 GPa at a sliding frequency of 25 Hz was applied. During the two hour tests, the pin samples used were plain-untreated, MoS_2 coated and oxy-nitrided (QPQ) against gas nitrided plates. The wear depths and volume loss of the plates were not analysed due to wear being negligible as shown in the previous chapter. The experiments used base oil (BO) and a combination of three effective EP and AW additives (ZDDP, SO & TCP) commonly used within industry to investigate and compare the tribological responses of the samples. XPS and Raman Spectroscopy were employed to characterise the chemical species present.

8.2 Friction Response with Additive Variants

Figure 8-1 highlights the typical change in behaviour over time observed with the three sample variants during the complete duration of the tests with the different lubricant additives. Similar behaviour trends are observed with the

different samples with an initial running-in period followed by steady state friction. Key differences in behaviour observed from figure 8-1 was the general lower friction results and trends achieved with the QPQ samples with all lubricants in comparison to the alternative treatments. However a combination of the MoS_2 sample and SO additive produced the lowest friction response with a continuous reduction throughout the duration of the test. Key differences observed with the QPQ samples were friction when using base oil was higher than when using TO10 during the final duration of the test. A low friction response was also initially observed when using SO however during the final 35 minutes of the test it rose to match that observed with the TCP lubricant.

In terms of wear as shown in section 8.3 the sample surfaces when using SO showed heavy signs of wear, whereas with the TCP additive a blue tribofilm was formed on all sample variant surfaces and showed lower signs of wear. Wear trends when using the TO10 lubricant matched those observed in Chapter 6.
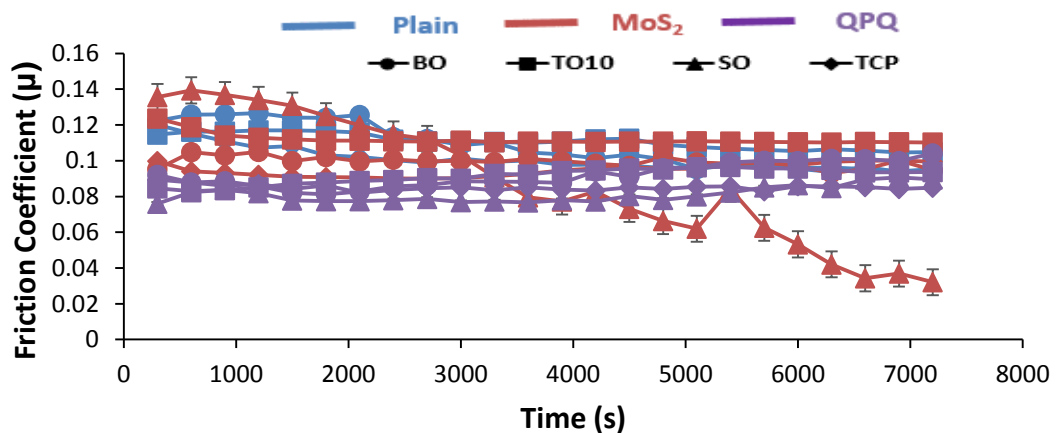
Figure 8-1. Friction coefficient vs time results over 2 hrs with the three samples at a 1.19 GPa contact pressure and sliding frequency 25 Hz with the variant lubricants.

The average friction coefficients for the sample variants in the steady stage (last 30 minutes of the test) with plain base oil and with it mixed with different EP and AW additives are shown and compared in Figure 8-2. The common trend observed was that the friction response of the QPQ samples with all the lubricant variants used were lower than that of the untreated plain and MoS_2 coated samples, with the exception of using the SO additive with the latter

treatment. This combination provided the lowest friction response from all samples types with the different additives.

The base oil and the fully formulated lubricant containing ZDDP had the highest friction compared to the other additive-containing oils, for the QPQ samples the base oil tests produced the higher friction however with the plain and MoS_2 coated samples the ZDDP containing lubricant had a clear higher friction coefficient. With the Plain samples, the SO additive produces a slightly lower friction result than when using TCP however the responses are very similar with statistical overlapping. With the QPQ samples the SO & TCP additive produced almost identical friction responses. This trend differed to that observed by Ma *et al* [105] where the oxy-nitrided samples showed lower friction behaviour with the TCP additive.

When using the SO additive with a MoS_2 coated surface a gradual continuous reduction of friction with time is observed (Figure 8-1) which differed from the other sample variants, with the overall steady state friction value being the lowest observed during this section of testing. A similar trend was observed by Wang *et al* [51] when using MoS_2/FeS multilayer samples. With the TCP additive with the MoS_2 samples a higher friction was observed than using SO but the response was almost identical to that when using base oil. The same response was observed with the plain samples, indicating that the TCP additive has no real impact on friction behaviour.

Generally the Plain and QPQ sample surfaces showed limited sensitivity to the lubricant additive variants, with friction coefficients being impacted by up to 15%. However with the MoS_2 coated surfaces the impact was significantly greater with the SO additive changing friction by over 70%, indicating the surfaces greater sensitivity.

8.3   Wear Response with Additive Variants
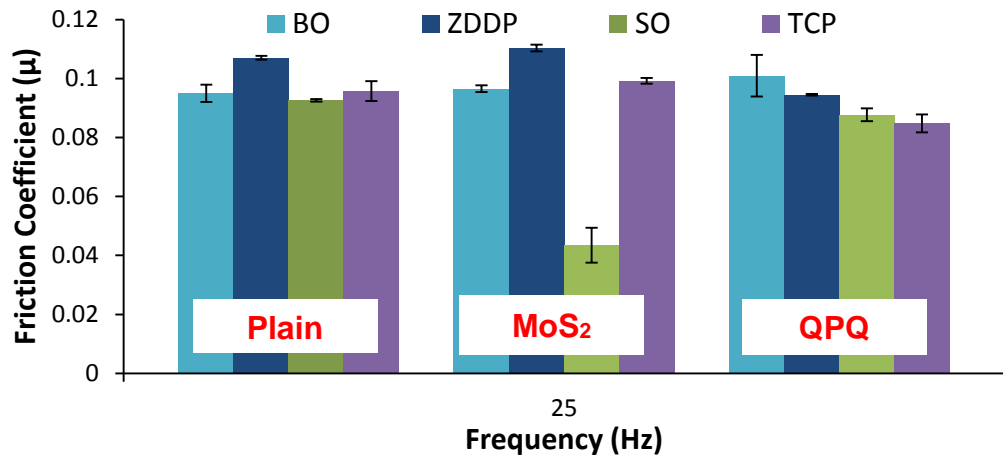
Figure 8-2. Friction coefficient results from experiments when using a contact pressure 1.19 GPa at a sliding frequency 25 Hz with four different oil additive with Plain, MoS₂ and QPQ samples.

Figures 8-(3-5) highlight the wear scars of the Plain, MoS$_2$ & QPQ samples when the different additives are used. With the plain sample when using BO (Figure 8-3(a)), wear penetrated deep in to the substrate, the scans revealed heavy scoring of the surface and abrasive wear. When using the fully formulated TO10 lubricant (Figure 8-3(b)) a thick tribofilm is seen to form on the surface. Figure 8-3(c) shows a polished surface with abrasive wear, however a tribofilm is observed covering portions of the surface. When using the TCP additive (Figure 8-3(d)) a thick blueish tribofilm is observed covering large areas of the surface.

When using BO with the MoS$_2$ samples (Figure 8-4(a)) the coating has been completely removed, with the surface showing evidence of abrasive wear. When using the TO10 fully formulated lubricant (Figure 8-4(b)) a thick tribofilm is formed on the worn surface. There are remnants of the delaminated coating still present. With the SO lubricant (Figure 8-4(c)) a tribofilm is observed to form on the surface however abrasive wear is also present. Similarly to the Plain samples when using TCP a thick blueish tribofilm is observed covering large portions of the MoS$_2$ coated surface (Figure 8-4(c)).

With the QPQ samples when using base oil (Figure 8-5(a)) the surface is heavily worn by abrasive wear and the nitride surface worn through. When using the TO10 lubricant, Figure 8-5(b), a patchy thin tribofilm is formed on the smooth nitrided surface of the sample. A different behaviour is observed when using the SO additive (Figure 8-5(c)), abrasive wear is detected on the surface alongside the delamination of the oxide layer and wearing of the nitride surface. When using the TCP additive Figure 8-5(d), the presence of a patchy tribofilm is easily identified.
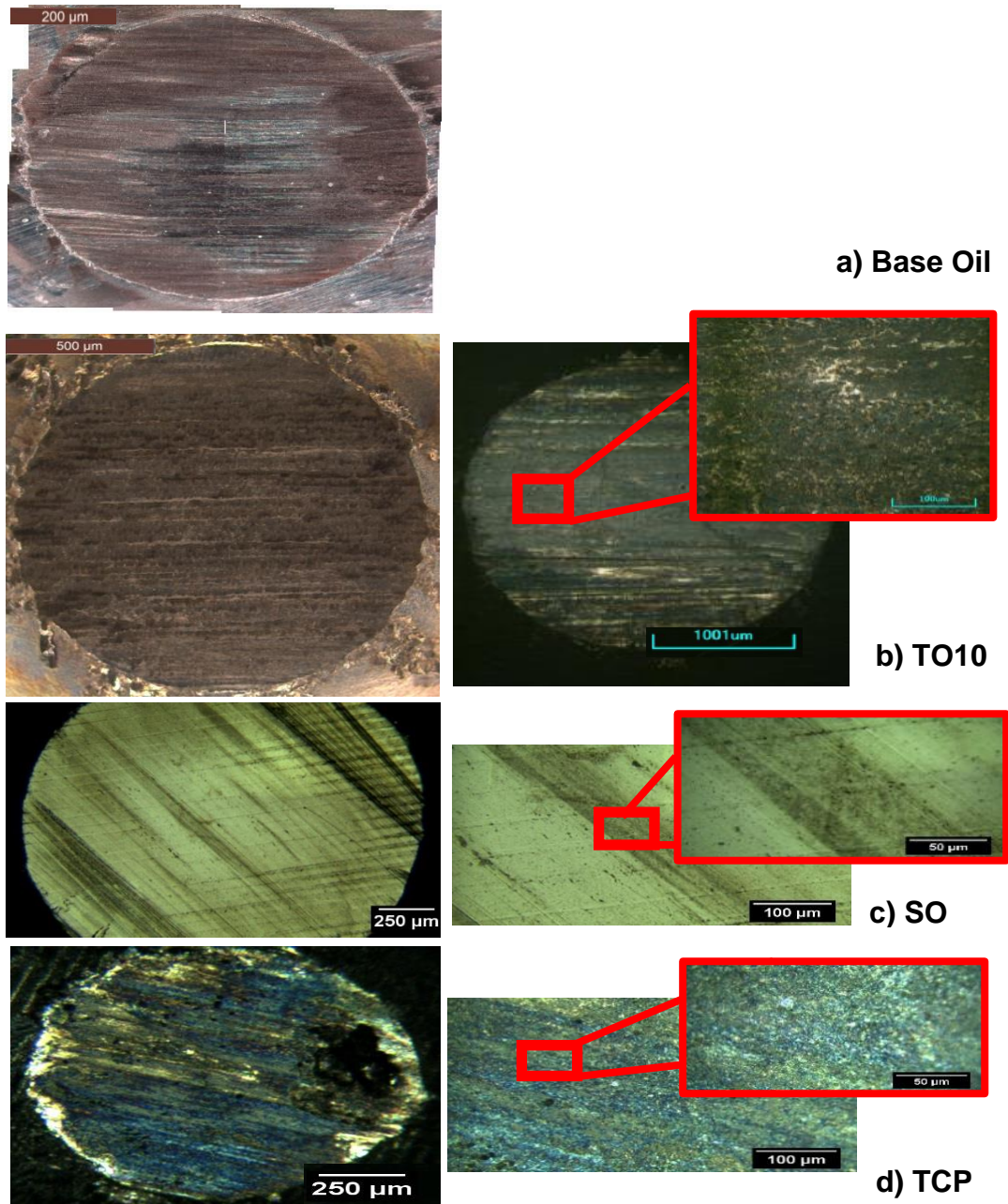
Figure 8-3. Optical images of the wear scar regions of the plain pin samples when a 1.19 GPa contact pressure was applied at 25 Hz when using various lubricants. a) Base oil b) TO10 c) SO d) TCP
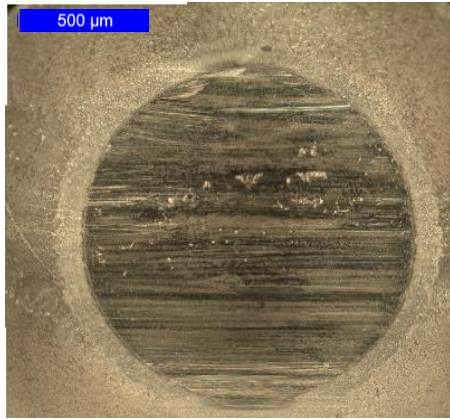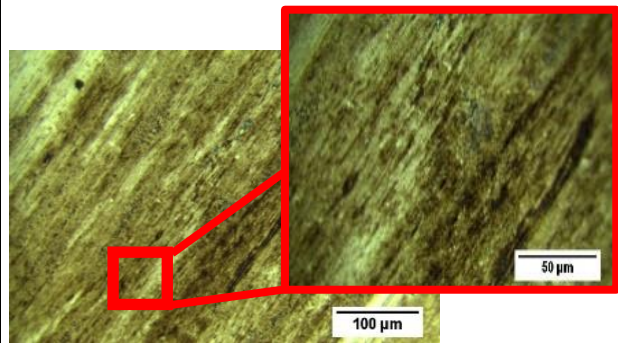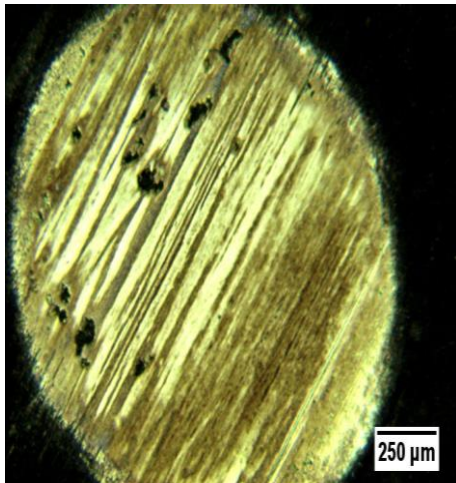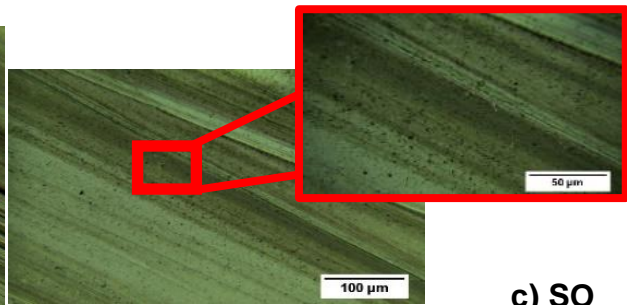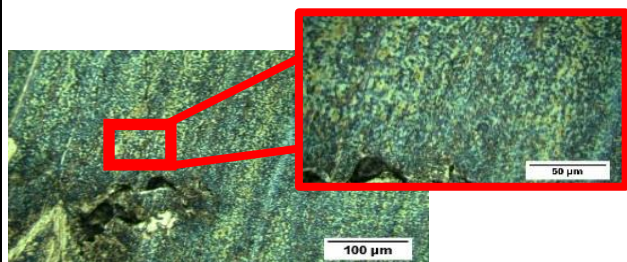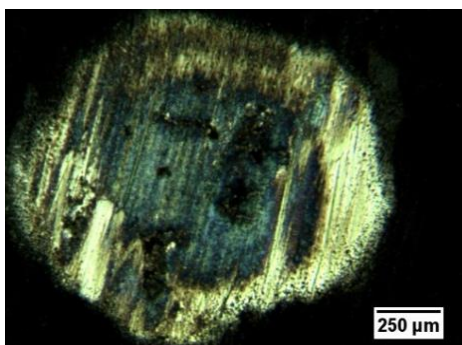
Figure 8-4. Optical images of the wear scar regions of the MoS$_2$ pin samples when a 1.19 GPa contact pressure was applied at 25 Hz when using various lubricants. a) Base oil b) TO10 c) SO d) TCP
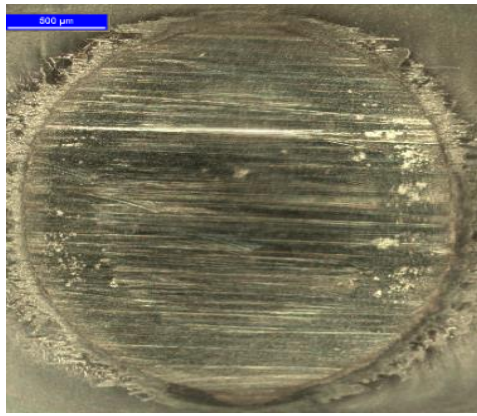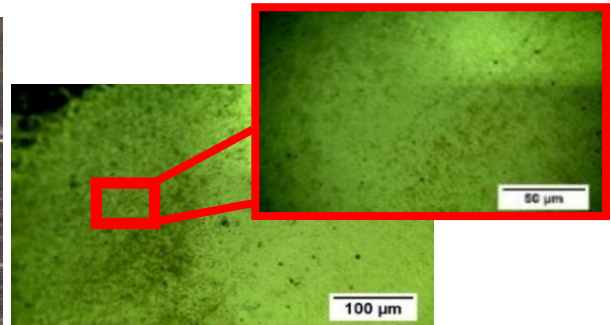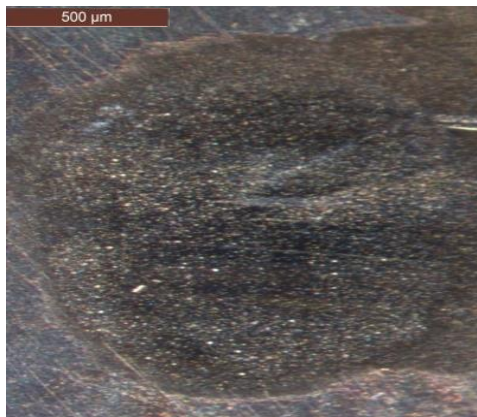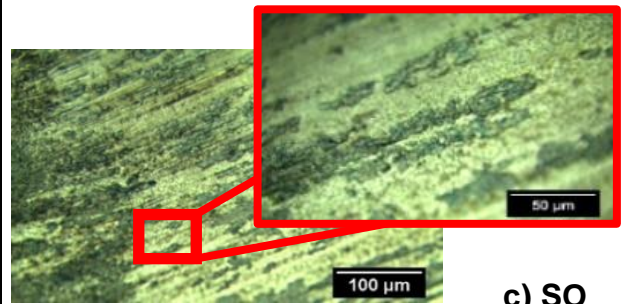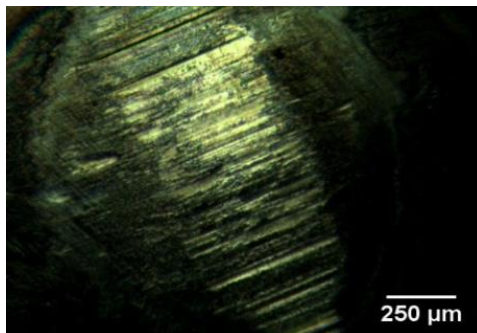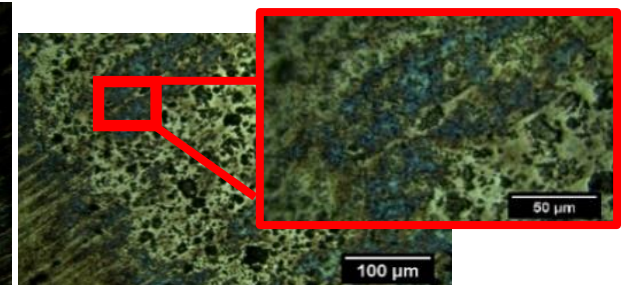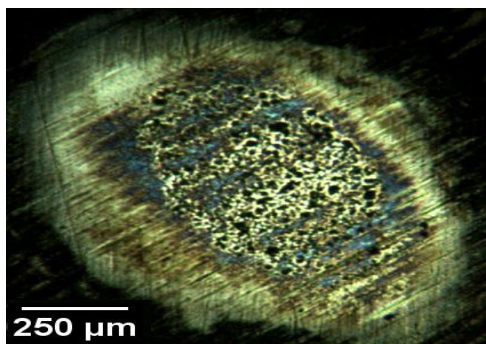
Figure 8-5. Optical images of the wear scar regions of the QPQ pin samples when a 1.19 GPa contact pressure was applied at 25 Hz when using various lubricants. a) Base oil b) TO10 c) SO d) TCP
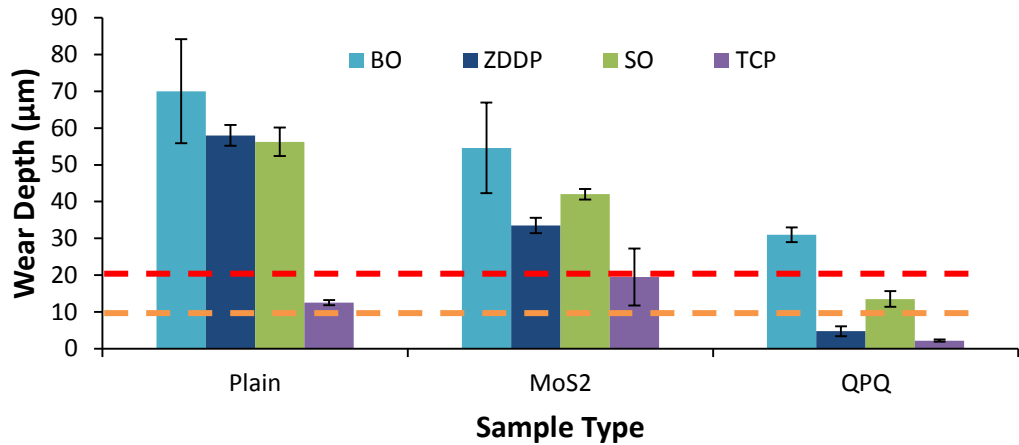
Figure 8-6. Wear depths of the Plain, MoS₂ and QPQ pins when using a contact pressure 1.19 GPa at a 25 Hz sliding frequency using base oil and four lubricant additives at 80°C. Red dashed line-MoS₂ coating thickness, Orange line – compound layer thickness.

From Figure 8-6 the plain pin samples when used with BO produced the greatest wear depths, followed by the fully formulated (ZDDP) lubricant. SO produced high wear but the depths were lower and similar to that seen with the ZDDP lubricant. The TCP additive produced significantly lower wear than the alternatives. Published work [141] showed similar wear trends with the same additives.

The wear patterns of the MoS₂ and QPQ samples were identical with the various lubricant additives. Base oil (Figure 8-6) produced the highest wear, however when additives were applied the SO additive caused the greatest wear penetration, followed by the ZDDP additive. The TCP additive had the greatest effect showing the lowest wear. With the QPQ samples when using the additives with the base oil the wear depths never penetrated past the compound layer, whereas with the BO it did (>15 µm). In all cases the MoS₂ coating was removed (>28 µm), it is also important to note that the wear depths when using BO & SO were very similar. Overall the wear of the QPQ samples were significantly lower than using the plain pins with the different additives and the trends matched those observed by Ma *et al* [105] with oxy-nitrided samples.

The surface sensitivity to wear of the plain and MoS₂ samples with different the lubricant additives were similar with depths being reduced by 20-80%. The

lubricants had a greater impact with the QPQ samples with wear being reduced by 60-90%

8.4   Tribofilm Characterisation

8.4.1 SEM-EDX Analysis

SEM-EDX was used to analyse the areas inside and outside the worn areas of the different variant pin samples when tested with the different lubricant additives. The analysis gives an indication whether a tribofilm has formed on the worn surface and the differences in chemical composition with the different surface treatments and lubricants.

The interaction of the three sample variants with the TO10 is highlighted in Chapter 6 (section 6.4.1). The plain samples SEM-EDX scans (Figure 6-8(b)) showed the clear presence of sulphur and phosphorous within the tribofilm, elements which are associated with the formation of a tribofilm when using the ZDDP additive. With the MoS_2 samples (Figure 6-10(b)) the worn area a strong presence of iron is detected, but no molybdenum or sulphur supporting the assumption the MoS_2 coating is completely removed during testing. Phosphorous, sulphur and zinc are detected within the worn area. When analysing the QPQ samples using SEM-EDX maps and spectrum (Figure 6-12(b)) there is a low presence of sulphur, phosphorous and zinc within the wear region. The presence of phosphorous indicates the possibility of the presence of phosphate tribofilm.

Different trends are observed with the different samples and the SO additive. With the plain samples (Figure 8-7) within the worn area there is a strong presence of iron and sulphur, which may indicated the formation of FeS. There is a strong presence of oxygen around the edges of the worn area most likely due to oxidation.

With the MoS_2 samples (Figure 8-8) similarly to the plain sample there is a strong presence of oxygen on the edges of the wear scar, most likely related to oxidation. Phosphorous is also detected around the edges relating to the

remnants of MnP layer which was present under the MoS_2 coating. The strong presence of iron within the wear scar indicates the complete removal of the MoS_2 and MnP coatings during testing. There is a strong overlapping detection of molybdenum and sulphur within the worn area. Combined with iron this could indicate either the formation of FeS or remnants of the MoS_2 coating are still present within the contact. With EDX it is difficult to differentiate so other analysis techniques are applied later on.

With the QPQ sample when using the SO additive (Figure 8-9) similar trends are observed to when using the TO10 lubricant. There are lower levels of oxygen detected with the worn area with the removal of the oxide layer. With the exposure of the nitride layer, a high presence of iron and nitrogen is detected. Lower of amounts of sulphur is detected in comparison to the plain and MoS_2 samples possible because of the formation of a thinner film and inertness of the nitride layer.
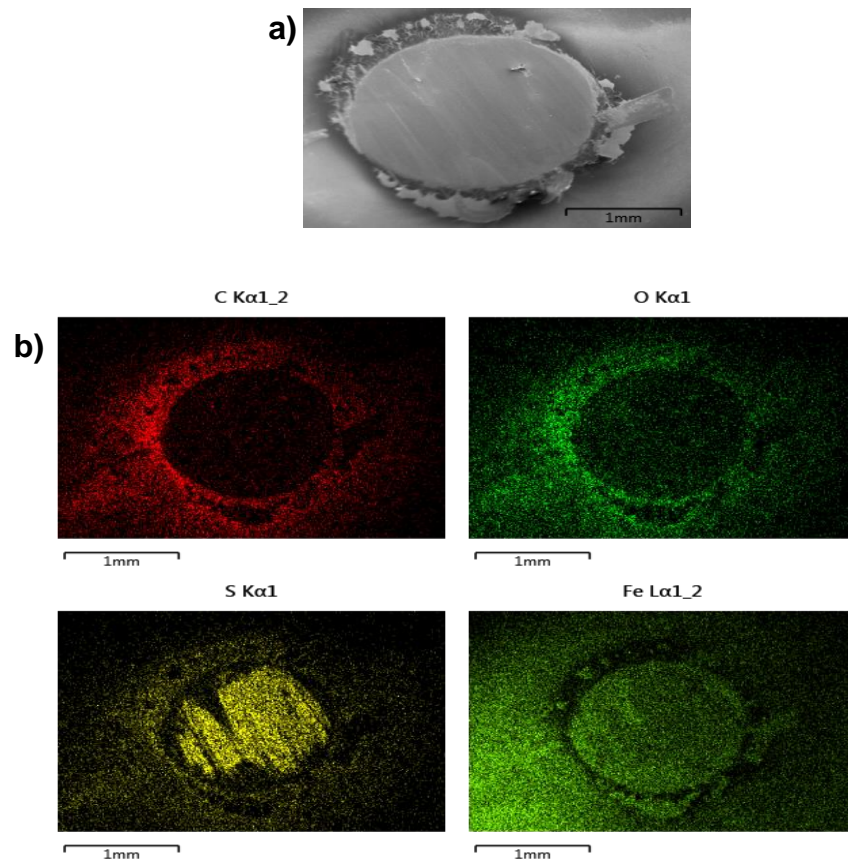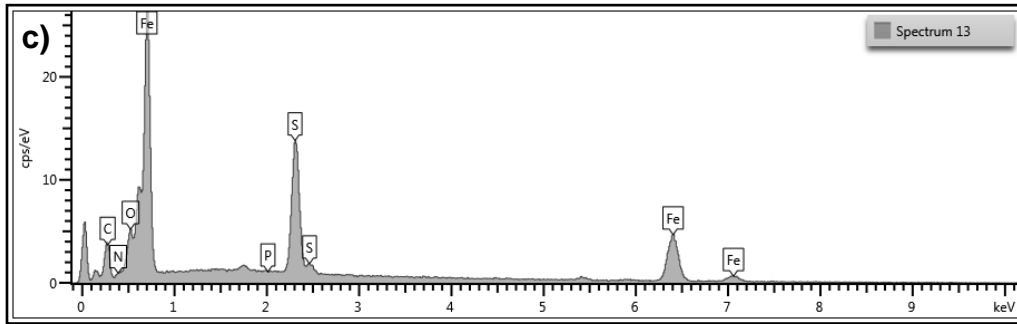
Figure 8-7. a) SEM image, b) EDX maps and c) spectrum of the unworn and worn surface of the Plain pin samples at 1.19 GPa contact pressure and 12 Hz sliding speed with SO additive.
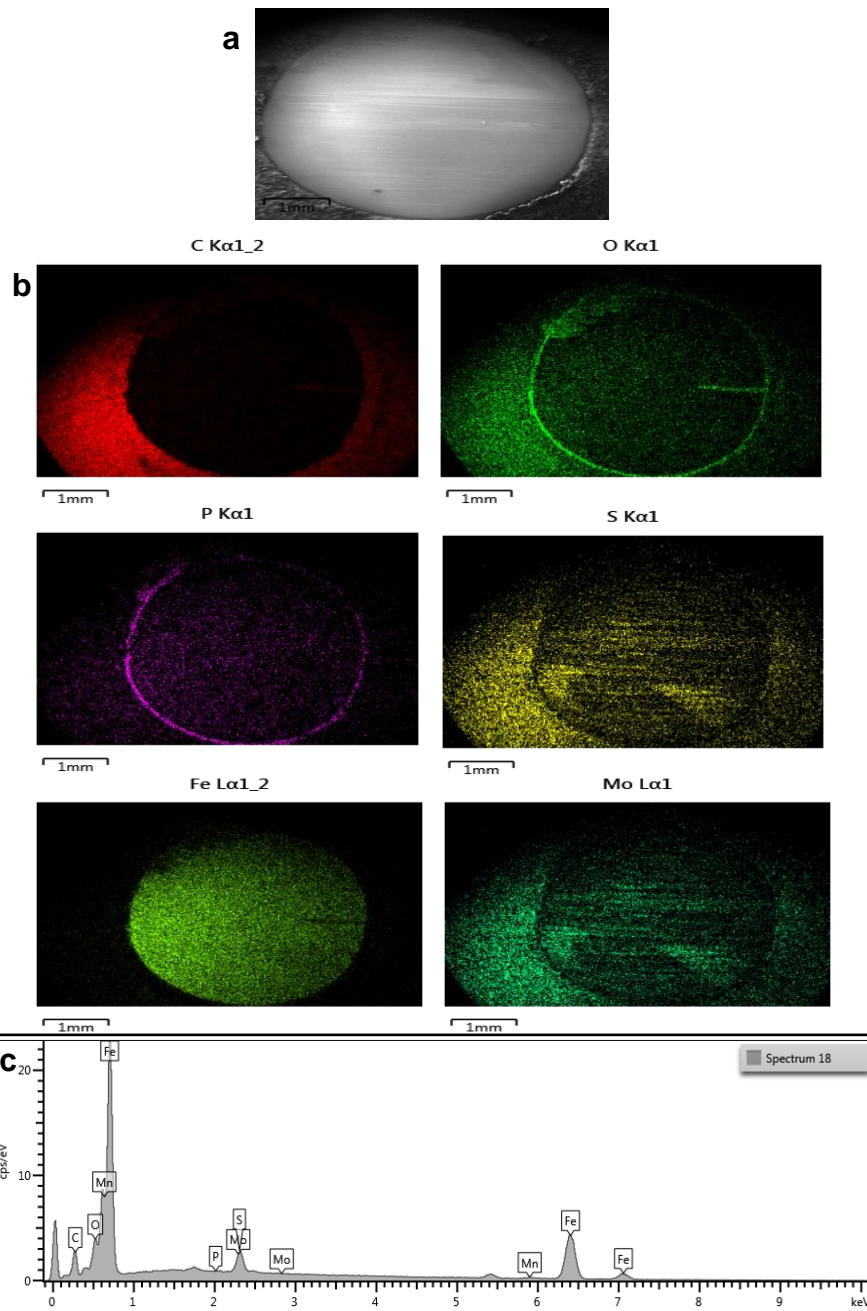
Figure 8-8. a) SEM image, b) EDX maps and c) spectrum of the unworn and worn surface of the MoS$_2$ pin samples at 1.19 GPa contact pressure and 12 Hz sliding speed with SO additive.

a)

b)

C Kα1_2

O Kα1

Fe Lα1_2

N Kα1_2

S Kα1

c)
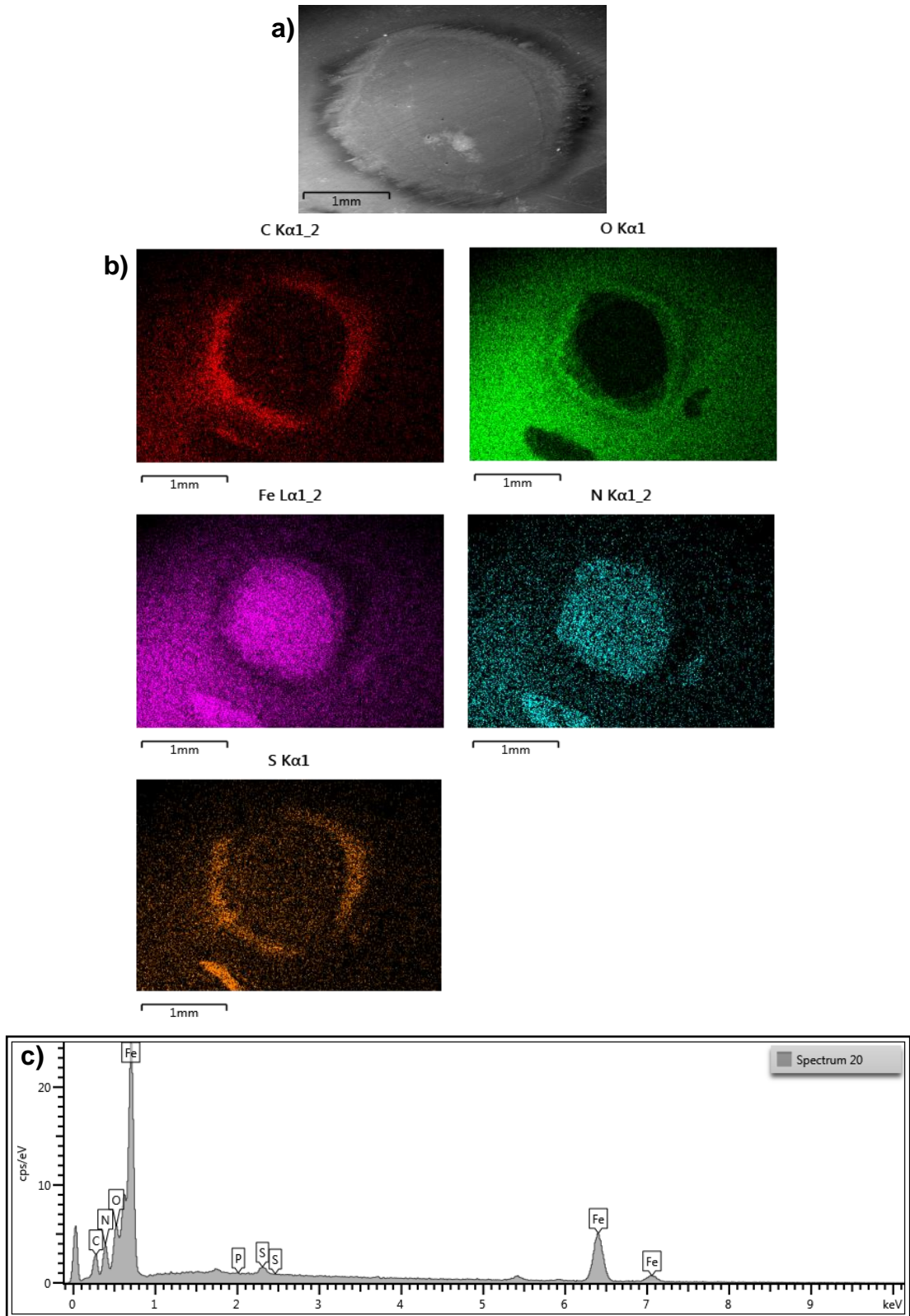
Spectrum 20

Figure 8-9. a) SEM image, b) EDX maps and c) spectrum of the unworn and worn surface of the QPQ pin samples at 1.19 GPa contact pressure and 12 Hz sliding speed with SO additive.

With the TCP additive and the plain samples (Figure 8-10), there is a strong presence of phosphorous and oxygen within the worn area. Iron is detected within the wear scar, but the darker presence indicates a lower concentration in comparison to outside the wear scar. This may be due to combination of high amounts of phosphorous and oxygen being detected within the same region. The presence of iron, phosphorous and oxygen within the wear scar may indicate the presence of phosphates and in particular the formation of $FePO_4$, which would impact the wear behaviour of the sample. Other surface analysis techniques are utilised to help identify the chemical species present within the tribofilm.

With the MoS_2 coated samples (Figure 8-11) similar elements are detected within the wear scar as with the plain samples when using TCP. There is a strong presence of phosphorous around the edges of the wear scar, this most likely due to the remnants of the MnP layer which was present under the MoS_2 coating. Both of which are removed during testing. Phosphorous is detected within the worn area indicating the formation of a tribofilm due to the interaction of the additive and surface.

With the QPQ samples (Figure 8-12), within the wear scar there is a high presence of nitrogen due to the exposure of the nitride layer. Like the other sample variants, there is a strong presence of phosphorous and iron within the worn area. However there is a low presence of oxygen within the wear scar, but this is mostly likely due to the strong signal from the oxide layer outside the scar. In comparison to when using the TO10 & SO additive it appears that there is a higher oxygen presence with the TCP additive. This indicates the possible presence of a tribofilm composed of phosphates and $FePO_4$.
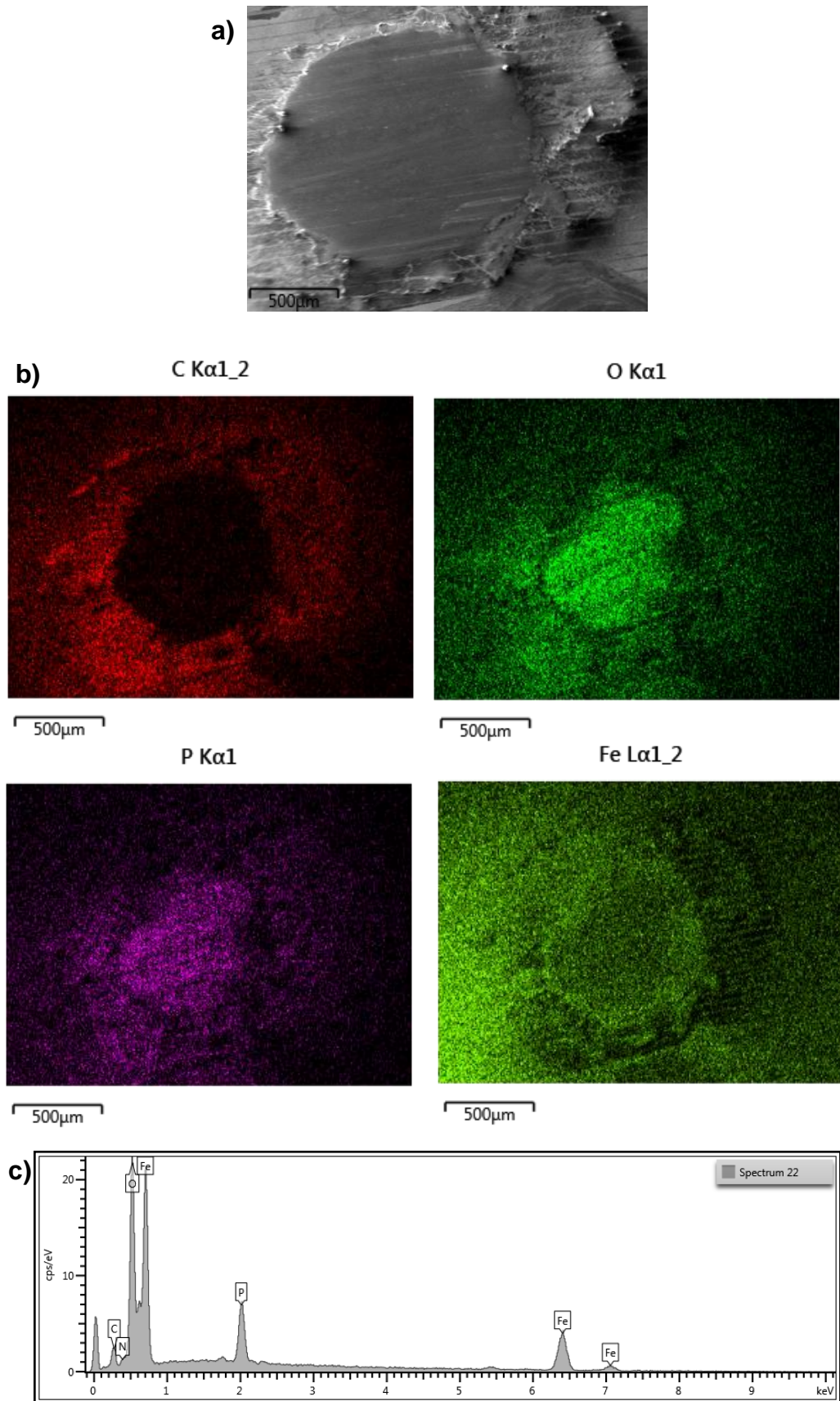
Figure 8-10. a) SEM image, b) EDX maps and c) spectrum of the unworn and worn surface of the Plain pin samples at 1.19 GPa contact pressure and 12 Hz sliding speed with TCP additive.
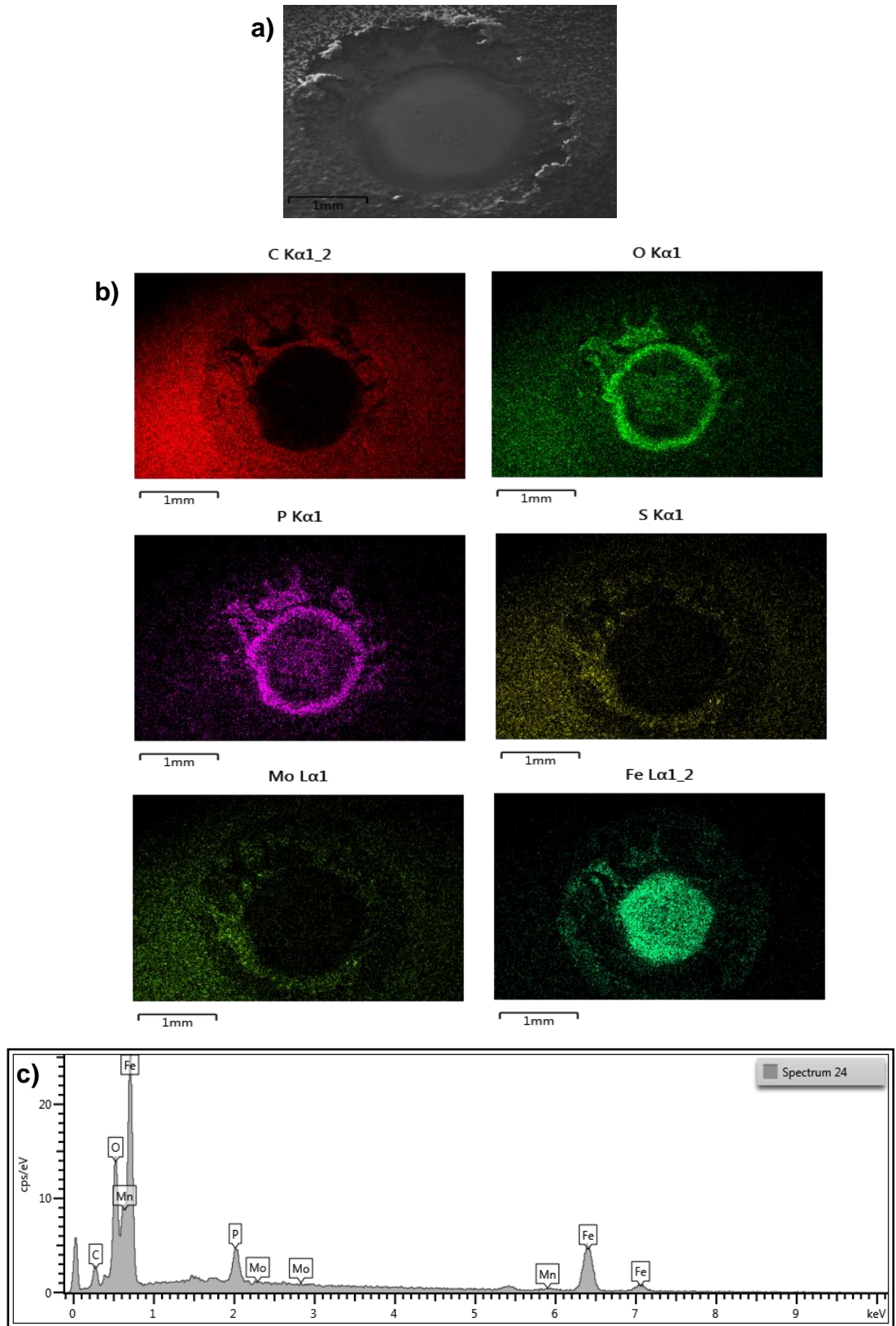
Figure 8-11. a) SEM image, b) EDX maps and c) spectrum of the unworn and worn surface of the MoS_2 pin samples at 1.19 GPa contact pressure and 12 Hz sliding speed with TCP additive.

Figure 8-12. a) SEM image, b) EDX maps and c) spectrum of the unworn and worn surface of the QPQ pin samples at 1.19 GPa contact pressure and 12 Hz sliding speed with TCP additive.
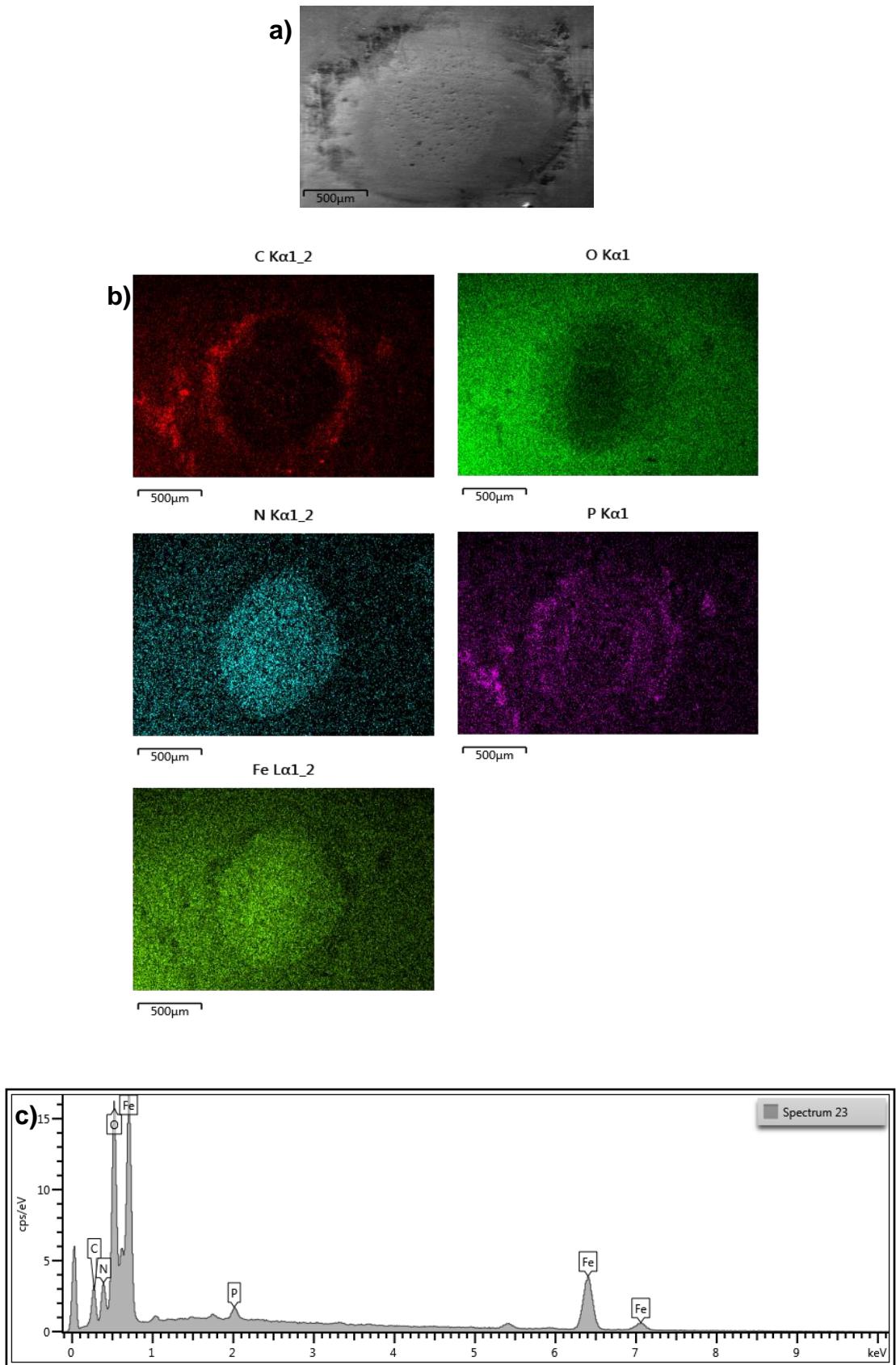
8.4.2 Tribofilm Characterisation using XPS

XPS analysis was carried out to confirm the presence of a tribofilm and analyse the changes in chemical species within the tribofilm formed on the plain, MoS_2 and oxy-nitrided samples when using the different additives. Using Ar ion etching through the depth of the tribofilm the results generally showed the formation of a relatively thin tribofilm with the QPQ samples with all additives, never exceeding more than 20 nm in thickness, however with the plain and MoS_2 samples a significantly thicker tribofilm was formed. Table 8-1 and Figures 8-(13 – 18) highlight the key species formed on the worn surface of both samples when using different additives. Table 8-1 shows the species present at an etching depth of 1.34 nm, alongside confirming the presence of a tribofilm on the sample variants with all the additives in this study.

The tribofilm composition on all sample variants with the TO10 lubricant matched that observed in Chapter 6 and are highlighted in Table 8-1. A common compound identified within the different sample tribofilms was $CaCO_3$ (347.0 eV) from the presence of detergents within the lubricants. As expected with the presence of ZDDP, sulphides (161.7 eV) and phosphates (133.2 eV) were detected within all the samples tribofilms which can be associated with formation of amorphous pyrophosphates alongside zinc compounds. Within the plain sample's tribofilm FeS (712.1 eV) and FeS_2 (706.8 eV) compounds were detected. With the MoS_2 coated samples there was no trace of the MoS_2 coating present after testing. FeS_2 (706.8 eV) was also detected within the QPQ tribofilm which in high concentrations could impact the friction behaviour of the sample. With the presence of a nitride layer, nitrides (397.8 eV) were also detected.

With the three sample variants the composition of the tribofilms formed with the various additives were of similar composition (Table 8-1). With the SO additive, the presence of sulphides (161.7 eV – Figures 8 - 13(a) – 15(a)) were detected which corresponded with the formation of FeS (712.1 eV) found within the tribofilms of all the samples (Figures 8 -13(b) – 15(b)). Similar compounds were identified within the tribofilms of other studies when using SO [142, 143]. With the MoS_2 samples XPS did not clearly detect the presence

of MoS₂. As seen when using TO10 lubricant the QPQ sample's tribofilm shows the presence of nitrides due to exposure of the nitride surface (Figure 8-15(c)) [103, 104].

Table 8-1. General binding energy values for compounds relevant to the tribofilms formed on the worn surface of the QPQ sample when using the different EP and AW additives at 1.34 nm etching depth [129].

Additive	Element	B.E / eV (±1eV)			Chemical State		
		Plain	MoS₂	QPQ	Plain	MoS₂	QPQ
Fully Formulated (ZDDP)	Fe 2p	712.1	-	-	FeS	-	-
		710.4	-	710.3	Fe₂O₃	-	Fe₂O₃
		709.4	709.4	-	FeO	Fe₂O₃	-
		706.8	706.8	706.8	FeS₂	FeS₂	FeS₂
	N 1s	-	-	397.8	-	-	Nitride
	P 2p	133.2	133.4	133.9	Phosphate	Phosphate	Phosphate
	Zn 3s	139.4	140.1	139.9	ZnS	ZnS	ZnS
	S 2p	161.8	161.7	161.7	Sulphide	Sulphide	Sulphide
	Ca 2p	347.3	347.0	347.0	CaCO₃	CaCO₃	CaCO₃
SO	Fe 2p	712.1	711.8	712.4	FeS	FeS	FeS
		710.4	709.8	710.8	Fe₂O₃	Fe₂O₃	Fe₂O₃
	N 1s	-	-	397.8	-	-	Nitride
	S 2p	161.8	161.7	161.7	Sulphide	Sulphide	Sulphide
TCP	Fe 2p	712.0	712.2	712.4	FePO₄	FePO₄	FePO₄
		710.4	710.6	710.7	Fe₂O₃	Fe₂O₃	Fe₂O₃
	N 1s	-	-	399.5	-	-	Organic Species
	P 2p	133.9	134.1	134.3	Phosphate	Phosphate	Phosphate
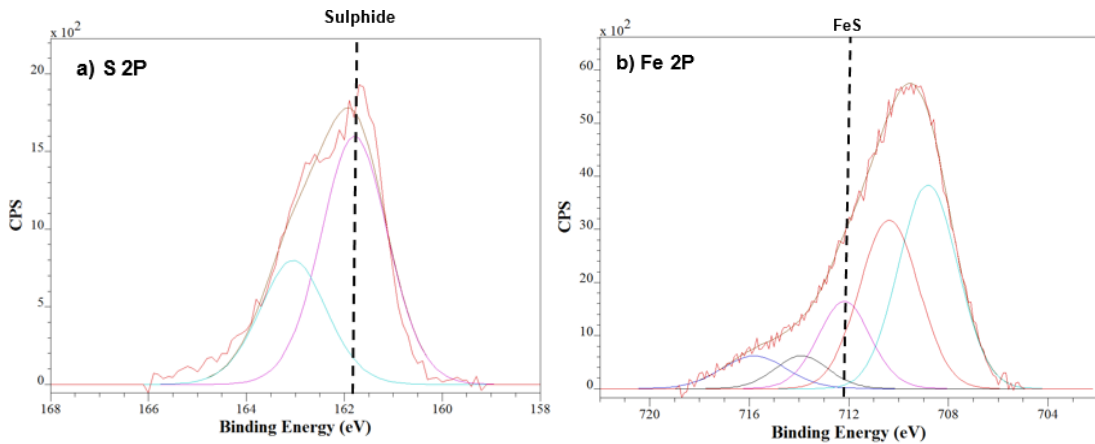
Figure 8-13. XPS S 2p and Fe 2p spectra of the tribofilms formed on the plain treated samples at an applied contact pressure 1.19 GPa and 25 Hz sliding speed at 1.34 nm etching depth with SO additive.
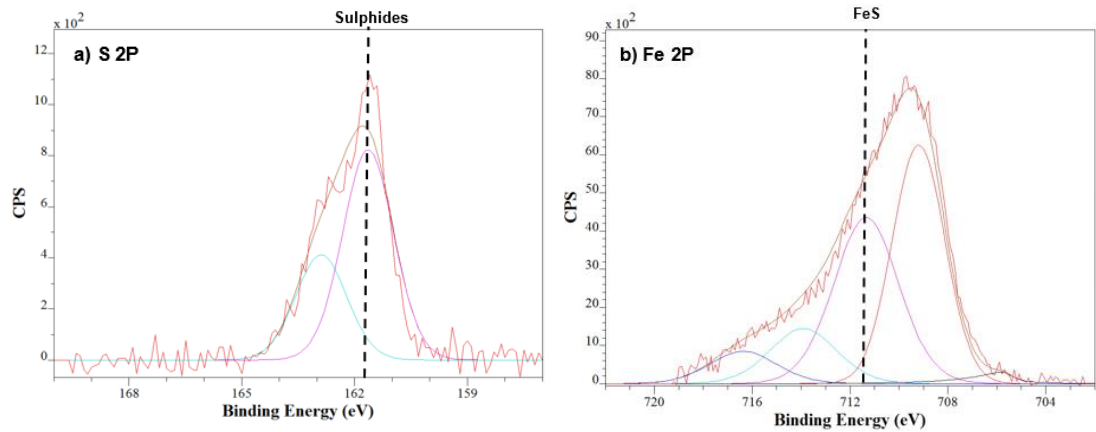
Figure 8-14. XPS S 2p and Fe 2p spectra of the tribofilms formed on the MoS₂ treated samples at an applied contact pressure 1.19 GPa and 25 Hz sliding speed at 1.34 nm etching depth with SO additive.
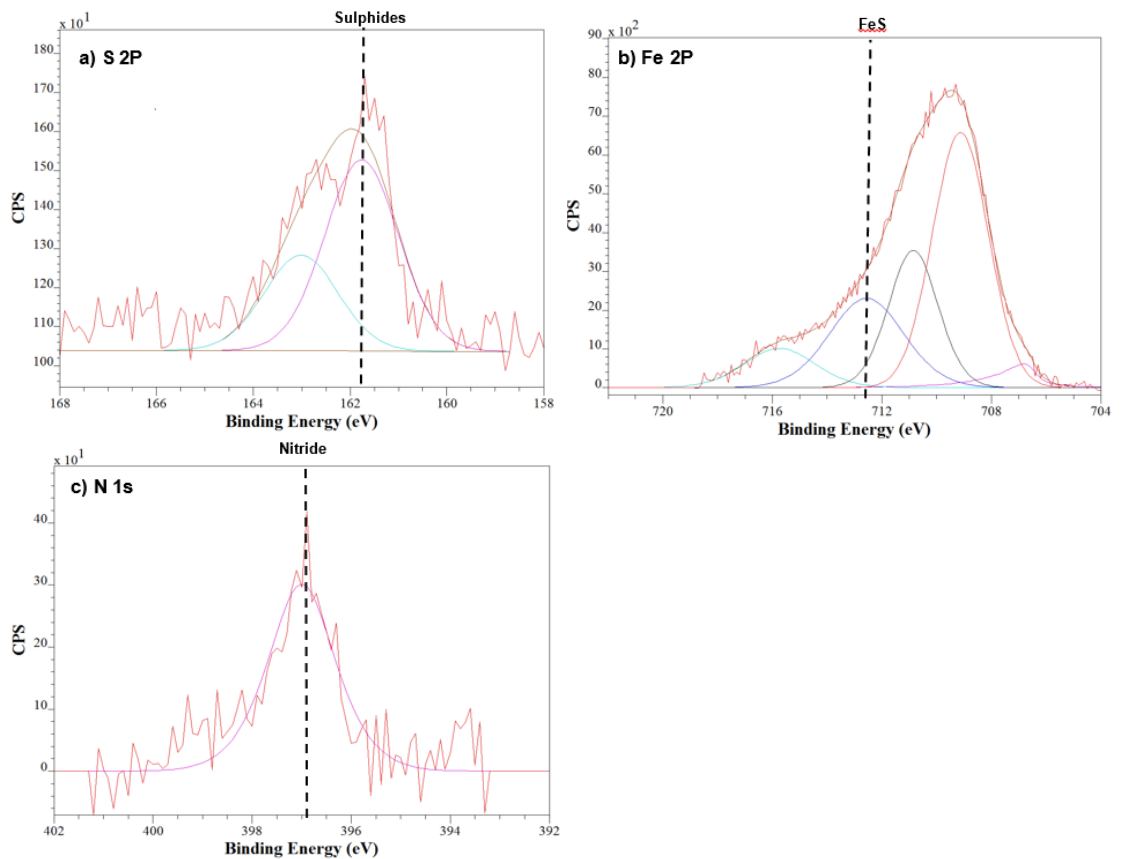
Figure 8-15. XPS S 2p, Fe 2p and N 1s spectra of the tribofilms formed on the QPQ treated samples at an applied contact pressure 1.19 GPa and 25 Hz sliding speed at 1.34 nm etching depth with SO additive.

With the TCP additive, within the tribofilm of all the sample variants phosphates (133.7 eV) were detected as shown in Table 8-1 and Figures 8-16(a) − 18(a). This indicated the formation of phosphate tribofilm which

contained $FePO_4$ compunds (712.1 eV) as shown with XPS (Figures 8- 16(b)-18(b)). Similar compounds were observed by Ma *et al* [106]. The QPQ sample's tribofilm (Figure 8-18(c)) showed the presence of organic nitrogen species (399.5 eV) due the presence of absorbed nitride complexes [103].
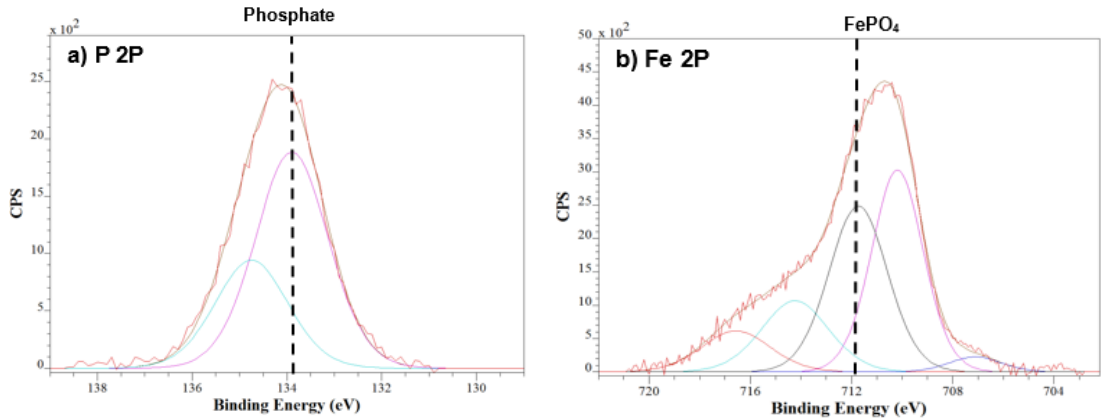
Figure 8-16. XPS P 2p and Fe 2p spectra of the tribofilms formed on the plain treated samples at an applied contact pressure 1.19 GPa and 25 Hz sliding speed at 1.34 nm etching depth with TCP additive.
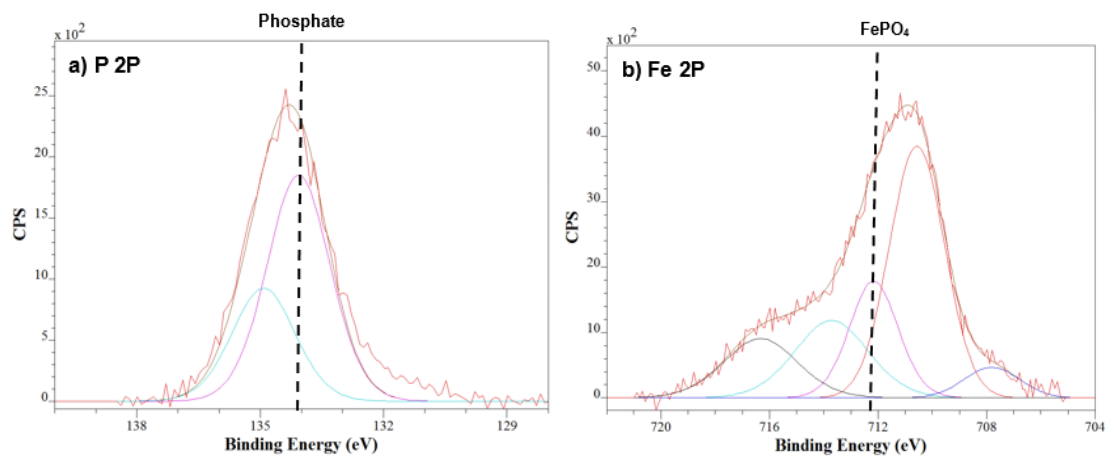
Figure 8-17. XPS P 2p and Fe 2p spectra of the tribofilms formed on the MoS₂ treated samples at an applied contact pressure 1.19 GPa and 25 Hz sliding speed at 1.34 nm etching depth with TCP additive.
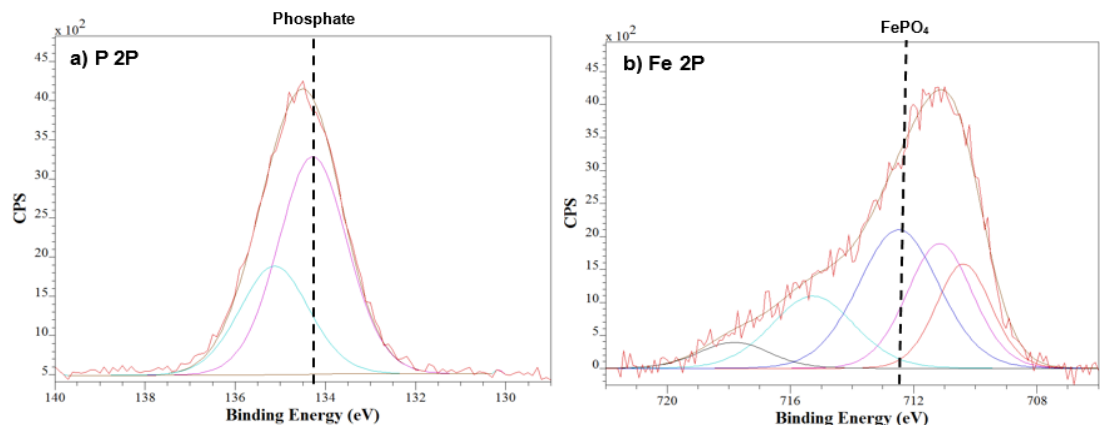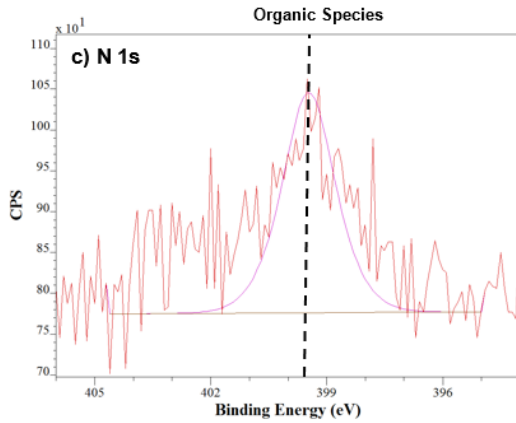
Figure 8-18. XPS P 2p, Fe 2p & N 1s spectra of the tribofilms formed on the QPQ treated samples at an applied contact pressure 1.19 GPa and 25 Hz sliding speed at 1.34 nm etching depth with TCP additive.

8.4.3 Tribofilm Characterisation with Raman Spectroscopy

To verify and support the findings of the XPS analysis, Raman spectroscopy was carried out to confirm the presence of key chemical compounds such as FeS_2, FeS, MoS_2 & $FePO_4$ within the tribofilms formed on the sample variant surfaces by taking surveys of a wide coverage of the wear scars of the pins (Table 8-2). With the SO additive on all sample variants instead of identifying FeS as seen with XPS, Raman spectroscopy detected FeS_2 with peaks clearly centred at 340 cm^{-1} and 375 cm^{-1} (Plain – Figure 8-19(a), MoS_2 coated – Figure 8-20(a) & QPQ – Figure 8-21(a)) [133]. This was most likely due to deeper depth penetration of the monocratic light from Raman spectroscopy. With the MoS_2 samples MoS_2 was detected alongside FeS_2 at 384 cm^{-1} and 409 cm^{-1} (Figure 8-20(a)) [133]. The presence of phosphates was identified with the three samples when using the TCP additive with a broad peak being detected from 900 -1100 cm^{-1} [134] supporting the results from XPS (Plain – Figure 8-19(b), MoS_2 coated – Figure 8-20(b) & QPQ – Figure 8-21(b)). Peaks centred around ~1000 cm^{-1} indicated the formation of iron phosphates [135]. The Raman spectra when using the fully formulated TO10 (ZDDP) lubricant matched that observed previously in Chapter 6 (Table 6-5) with FeS_2 & FeS being detected with the QPQ and Plain samples respectively and an MoS_2 presence with the MoS_2 coated samples. Phosphates were detected within the tribofilm of all sample variants. Due to these results being highlighted in Chapter 6 they will not be shown again here, but key species identified with the TO10 lubricant are highlighted in Table 8-2.

Table 8-2. Summarises the chemical compounds detected within the different samples tribofilms using Raman Spectroscopy.

Sample Treatment	Lubricant Additives - Raman Peaks (cm^{-1})		
	SO	TCP	TO10
Plain	340, 375 (FeS$_2$)	950 - 1100 (Phosphates)	207, 283 (FeS) 950 - 1100 (Phosphates)
MoS$_2$	340, 375 (FeS$_2$) 384, 409 (MoS$_2$)	950 - 1100 (Phosphates)	384, 409 (MoS$_2$) 950 - 1100 (Phosphates)
QPQ	340, 375 (FeS$_2$)	1045 (Iron phosphate)	340, 373 (FeS$_2$) 950 - 1100 (Phosphates)
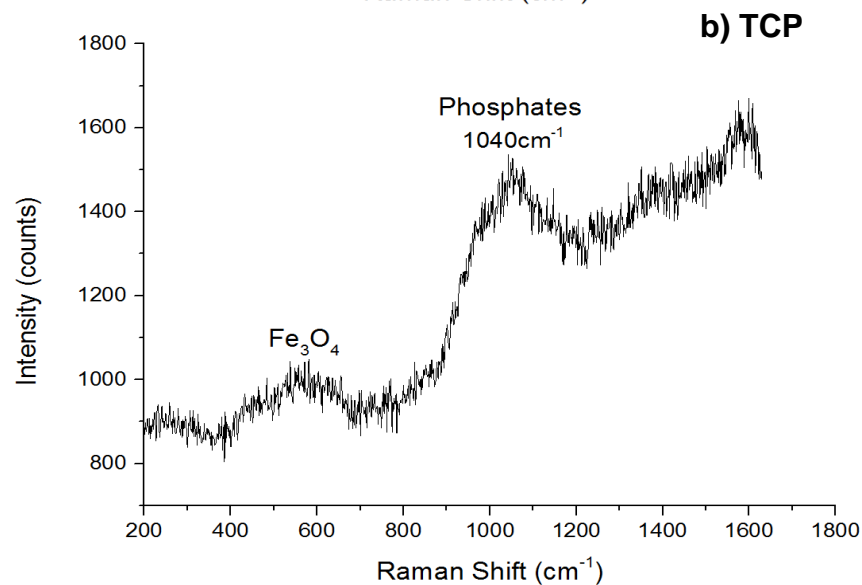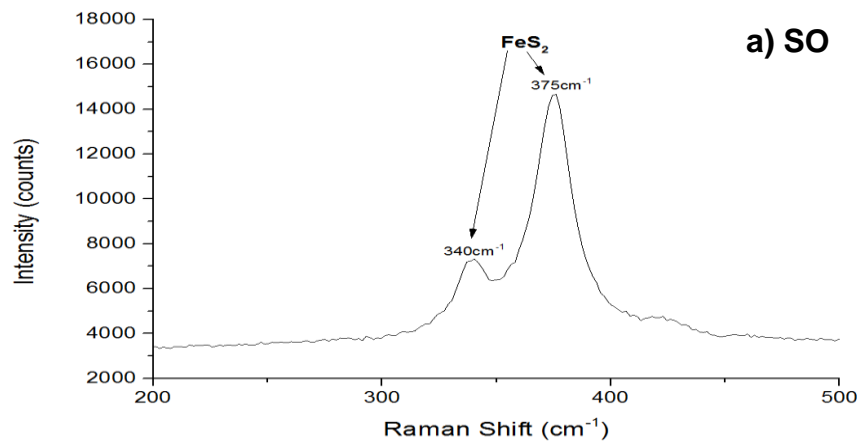
Figure 8-19. Raman spectra of the Plain samples for FeS$_2$ & phosphates compounds within the formed tribofilms tested at a contact pressure 1.19 GPa and 25 Hz sliding frequency with a) SO & b) TCP lubricants.
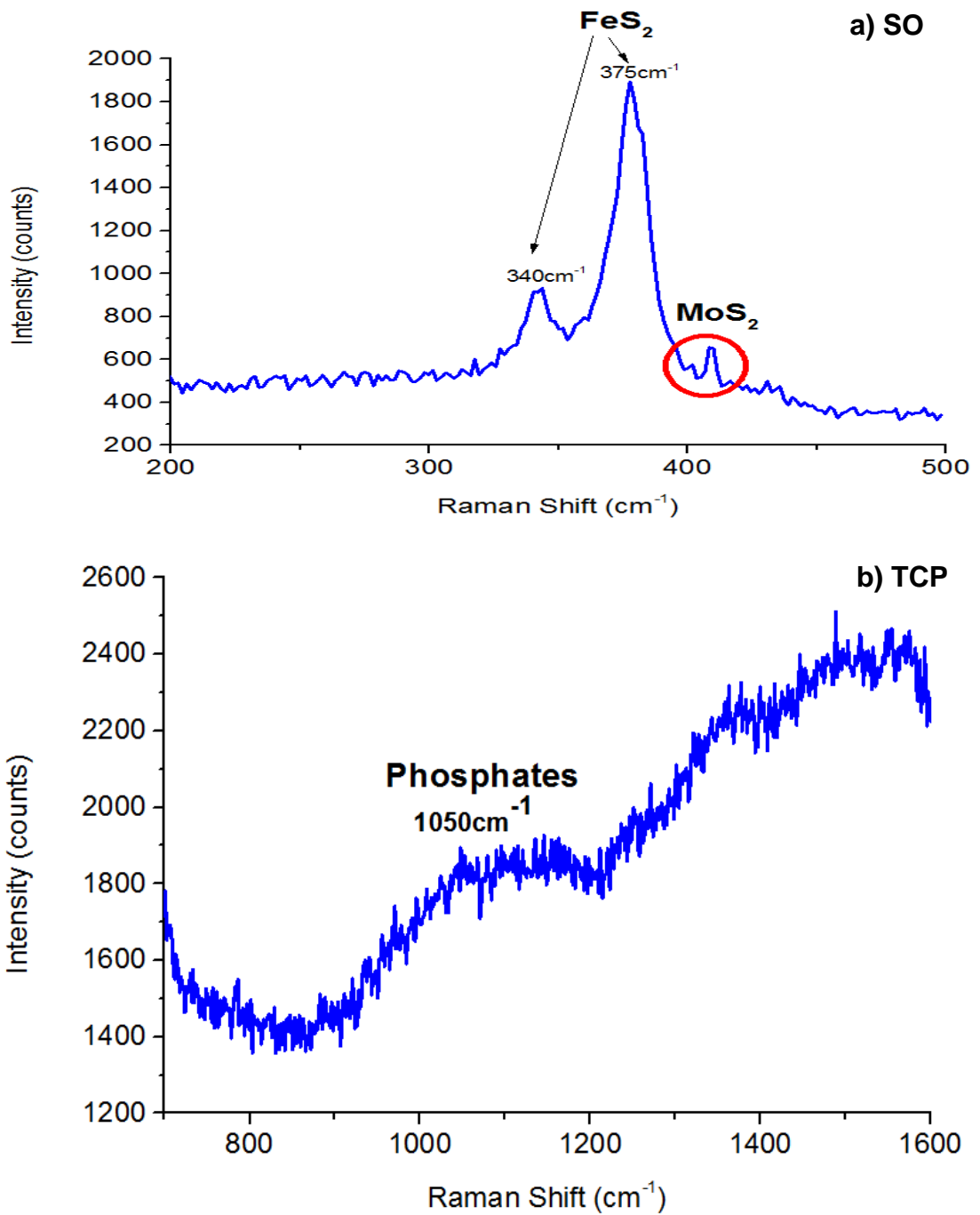
Figure 8-20. Raman spectra of the MoS_2 coated samples for FeS_2, MoS_2 & phosphates compounds within the formed tribofilms tested at a contact pressure 1.19 GPa and 25 Hz sliding frequency with a) SO & b) TCP lubricants.
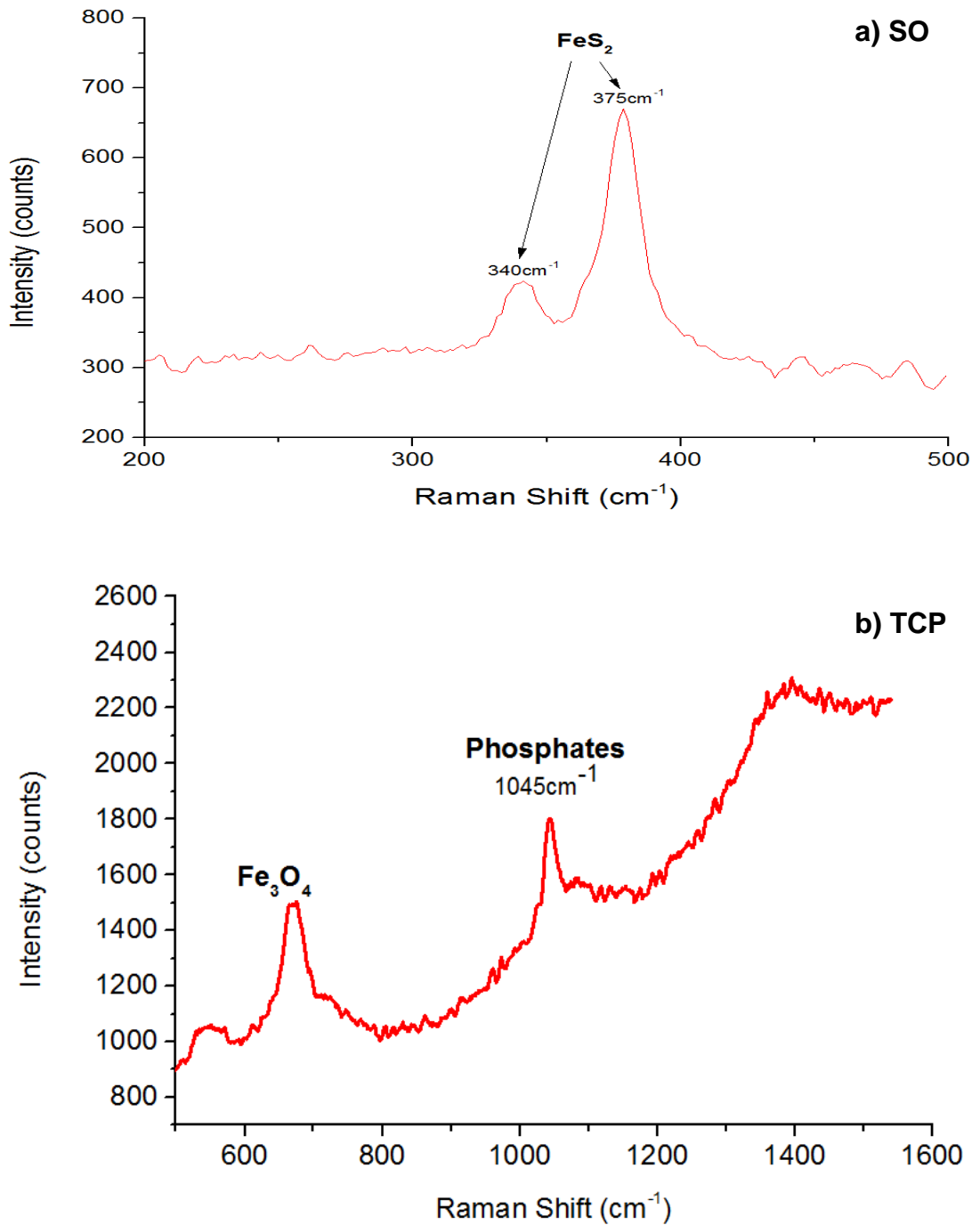
Figure 8-21. Raman spectra of the QPQ samples for FeS₂ & phosphate compounds within the formed tribofilms tested at a contact pressure 1.19 GPa and 25 Hz sliding frequency with a) SO & b) TCP lubricants.

8.5 Summary

In this phase of this research the tribological impact of various lubricant additives were investigated with the three sample variants. The results from

SEM/EDX, XPS and Raman spectroscopy analysis together aim to provide an explanation of the wear mechanism and surface chemistry. In summary, the following key points can be drawn from this part of the study:

- With the fully formulated lubricant a high friction response was observed in comparison to the other lubricants, however with the QPQ sample BO produced a higher friction response.
- A combination of an MoS_2 coating and SO additive led to a low friction response not observed with the other sample and additive variants.
- The impact of the TCP additive on friction response was minimal across all the sample variants. However with the QPQ samples both the SO and TCP additives had no impact.
- The wear behaviour of QPQ samples was shown to be affected by the different lubricant additives and showed greater sensitivity in comparison to the other samples.
- The plain sample combined with the SO additive showed similar wear levels to when using the ZDDP containing additive, whereas with the alternative samples SO lead to high wear. The plain sample showed a strong presence of FeS within the worn area in comparison to the QPQ and MoS_2 samples.
- Raman spectroscopy showed the presence of MoS_2 and FeS within the tribofilm of the MoS_2 sample with the SO additive.

The varying of lubricant additives allowed the investigation of the interaction of different surfaces with the additives. This chapter showed that additives impacted the samples friction and wear behaviour but also certain additive types had a greater impact than others. A synergistic effect between the surface and lubricant can have a significant impact of performance. It is important to verify the behaviour trends observed in this and the previous chapters using a different tribometer and conditions replicating the actual contact within a hydraulic motor.

Chapter 9 Comparison of Surface Modification Treatments with Extreme Pressure & Anti-Wear Additives Using MTM-SLIM

9.1 Introduction

To further understand and capture the interaction of the different treated samples with a range of EP and AW additives, the MTM SLIM tribometer was used. The advantage of using this technique is that it allows the replication of the contact within a piston and cylinder. Yamaguchi [41] states that the piston and cylinder component within the piston pump is a pure sliding contact, however for this study a percentage of rolling contact will be applied to replicate the rotation of the pistons within the cylinder block. The presence of a 3D Spacer Layer Imaging Method (SLIM) attachment allows in-situ capture of optical interference images of tribofilm formation during testing, which would allow the opportunity to confirm and understand the tribochemistry involved in its development. Konicek *et al* [144] states conclusions about the nature and formation of a tribofilm depend on when during a test the surface is analysed.

This chapter focuses on investigating the interaction of treated surfaces with various EP and AW additives in MTM tests, whilst allowing the in-situ capture of the formation of tribofilms. These experiments provide support and verify the results observed in Chapter 8 with the Cameron Plint tribometer alongside primarily helping to gain an understanding of the friction and wear behaviour of the modified surface with the different additives and varying lubrication regimes.

The balls were treated using the QPQ and MoS_2 coating processes which modified the surfaces as described in Chapter 5. However the thickness of the layers formed after each treatment were different in comparison to the pin samples as highlighted in Figures 9-1 & 9-2. The QPQ process forms a 19 μm thick compound layer with a 250 μm diffusion zone (Figure 9-1). Whereas the Defric process forms a 9 μm thick MoS_2 coating above a 250 μm diffusion layer on the ball samples (Figure 9-2).
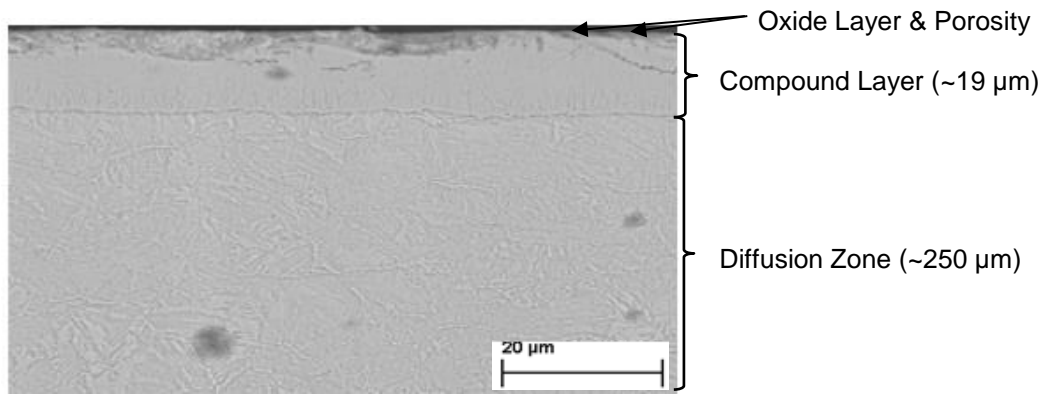
Figure 9-1. SEM image profile through the cross-section of a QPQ ball sample (R_a = 30 nm) .
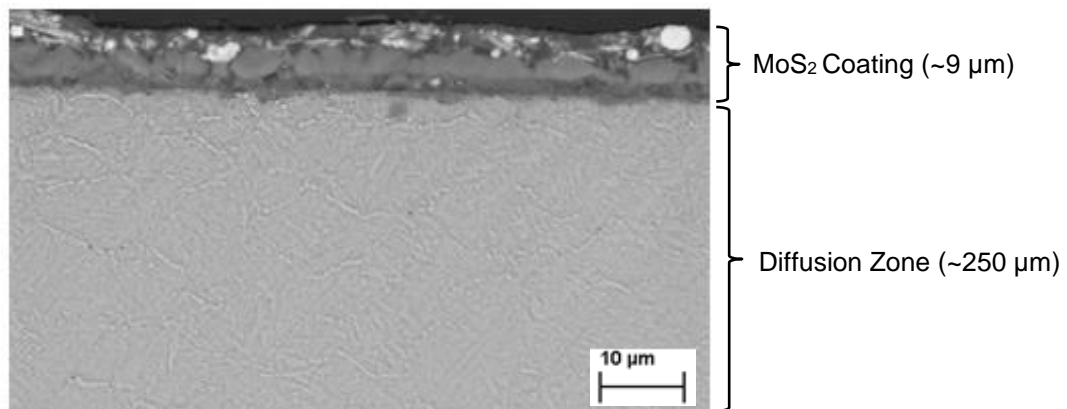
Figure 9-2. SEM image profile through the cross-section of a MoS$_2$ coated ball sample (R_a = 680 nm).

Initially all three ball sample variants (Plain, QPQ, MoS$_2$ coated) were tested using the TO10 lubricant to compare and validate the behaviour observed with TE77, however further testing with different EP and AW additives were carried out only with the two treated samples. The two alternative lubricant mixtures were composed of either sulphur or phosphorous containing additives, allowing the investigation of the effect of both elements on the tribological behaviour of the treated surfaces individually. During testing, the temperature was kept constant at 80°C and a load of 36 N was applied corresponding to an initial Hertzian contact pressure of 1 GPa. The sliding-rolling ratio (SRR) was set to 150% [5]. The tribological tests were split in to three alternative stages which were carried out at fixed time intervals. The first stage, known as the conditioning phase, included rubbing the ball and disc together at a fixed slow entrainment speed in the mixed lubrication regime to encourage the formation of tribofilm on the ball and disc wear track. This was then followed by applying the Stribeck curve parameters, starting at a high speed of 2 m/s (mixed regime) and continued towards the lowest speed value of 0.01 m/s

(boundary regime). The final stage involved halting the test and the ball sample was loaded against the spacer layer-coated window, where an image was captured which would allow the measurement of the tribofilm.

9.2 Behaviour Validation

Using similar test conditions to that of the TE77, the MTM SLIM was used to analyse the repeatability in tribological behaviour of the three samples with an alternative tribometer. The TO10 fully formulated lubricant was used as a reference oil.

9.2.1 Friction and Wear Behaviour Validation of the Three Sample Variants using the MTM-SLIM

Figure 9-3 shows the interaction of the TO10 additive with the QPQ treated sample. As the sliding speed is reduced friction steadily increases. At all entrainment speeds with an increase in time the friction coefficient is seen to reduce steadily. The optical interference images (Figure 9-4) show virtually no tribofilm was formed during the duration of the test. The optical interference images show that the wear of the sample increased with time, shown by the distortion of the wear track in the SLIM image.

However with the MoS_2 coated samples (Figure 9-5) a different friction trend was observed in the mixed lubrication regime from 100 mm/s – 2000 mm/s, it is possible to see that friction begins to reduce with time until the entrainment speed reduces below 100 mm/s (boundary regime) where friction remains constant for the 2-hr rubbing period. The change of lubrication regime is highlighted on the stribeck curves with a red dashed line. The initial decrease in friction observed with decreasing with the entrainment speed with MoS_2 coated samples in the first minute of testing relates to the initial wearing away of the MoS_2 coating. This trend is observed with all the tests using the MoS_2 samples. The optical interference images (Figure 9-6) show the formation of a thick tribofilm early on during testing, however with duration the tribofilm thickness decreases and leaving the presence of a very thin tribofilm by the end of the test.

With the Plain sample (Figure 9-7) in mixed regime the friction behaviour is similar to that observed with the previous samples, with time a reduction in friction is observed. However in boundary regime conditions with time an increase in friction is observed, which is contrary to that observed with the treated samples. SLIM (Figure 9-8) showed the formation of a thick tribofilm on the wear track with time, with wear seeming to remaining constant as the wear tracks did not seem to distort with time.

Different trends were observed by Spikes [89] and Ratoi *et al* [111], an increase in friction was observed with ZDDP containing additives over time with Stribeck curves. The friction reduction observed within this study was assumed to be due to the differences in the surface roughness's of the samples in both studies. Samples within this study were 3-20x rougher and it is believed the friction response is dominated by the asperity removal instead of the properties of the tribofilm as seen in other studies [89, 111, 145].
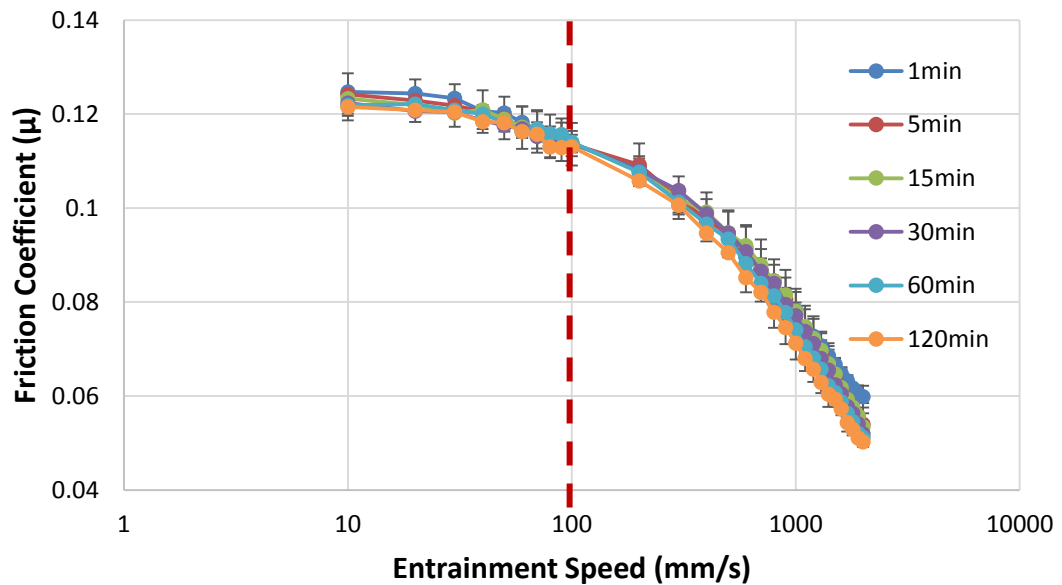
Figure 9-3. Series of Stribeck curves when using a QPQ ball and gas nitrided disc with TO10 lubricant.
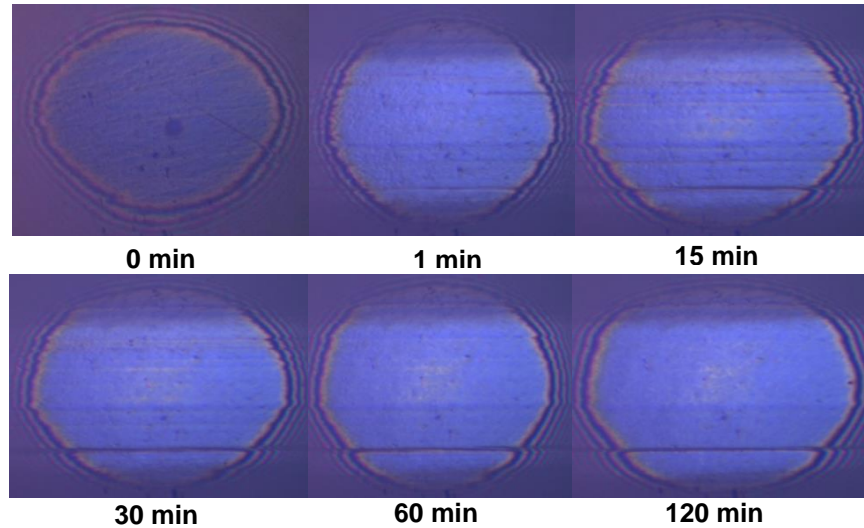
Figure 9-4. Optical interference (SLIM) images of the tribofilm formation on QPQ samples with TO10 lubricant.
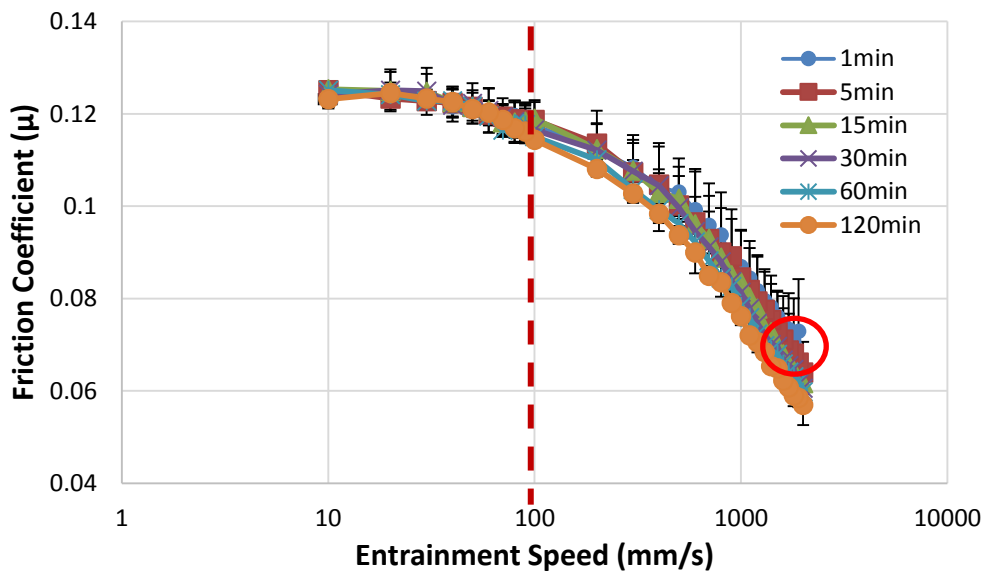
Figure 9-5. Series of Stribeck curves when using a MoS₂ coated ball and gas nitrided disc with TO10 lubricant.
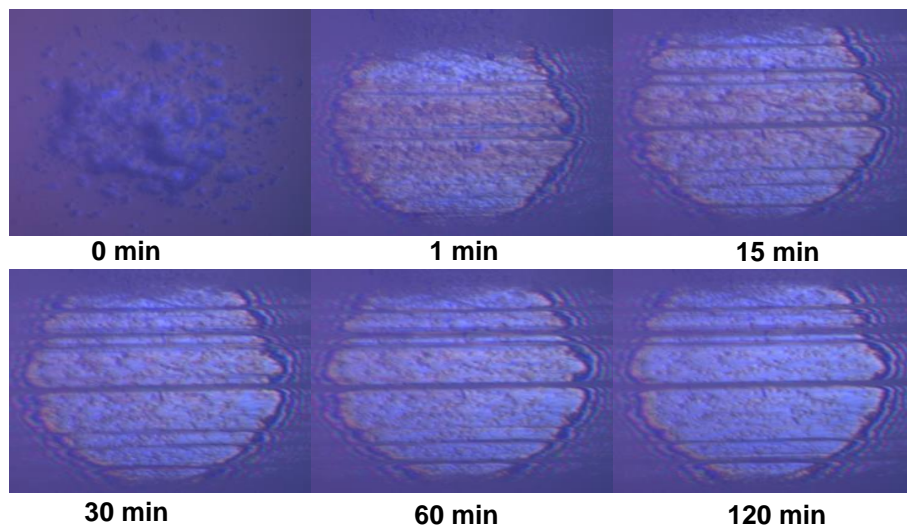
Figure 9-6. Optical interference (SLIM) images of the tribofilm formation on MoS₂ coated samples with TO10 lubricant.
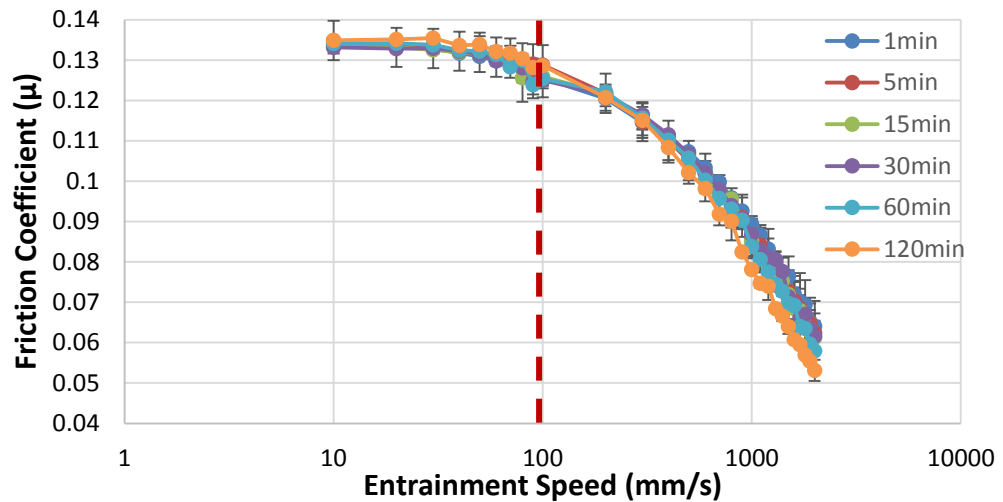
Figure 9-7. Series of Stribeck curves when using a Plain ball and gas nitrided disc with TO10 lubricant.
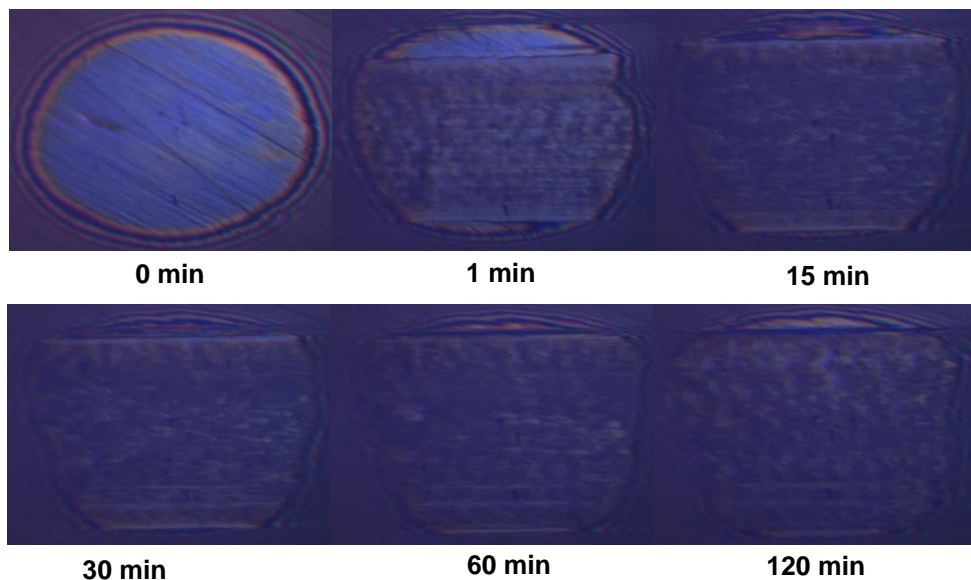
Figure 9-8. Optical interference (SLIM) images of the tribofilm formation on Plain samples with TO10 lubricant.

When comparing the friction performance of all samples after the 2hr testing period (Figure 9-9), at the starting entrainment speed (2000 mm/s) the friction responses of the sample variants are almost identical until the speed is reduced and the lubrication regime begins to move towards boundary conditions. At the lower entrainment speeds clear behaviour trends are observed for the different sample variants, the QPQ sample produced the lowest friction results in both lubrication regimes whilst the untreated sample had the highest. These trends followed that observed when testing with the Cameron Plint TE77. However in terms of wear depths (Figure 9-10), the MoS_2 coated sample produced the highest wear depths with wear penetrating

past the coating in to the substrate. Similar trends were observed by Suzuki [146], who found that the wear behaviour of MoS_2 films worsened within a rolling contact than with pure sliding. With the QPQ sample wear depths remained within the compound layer.
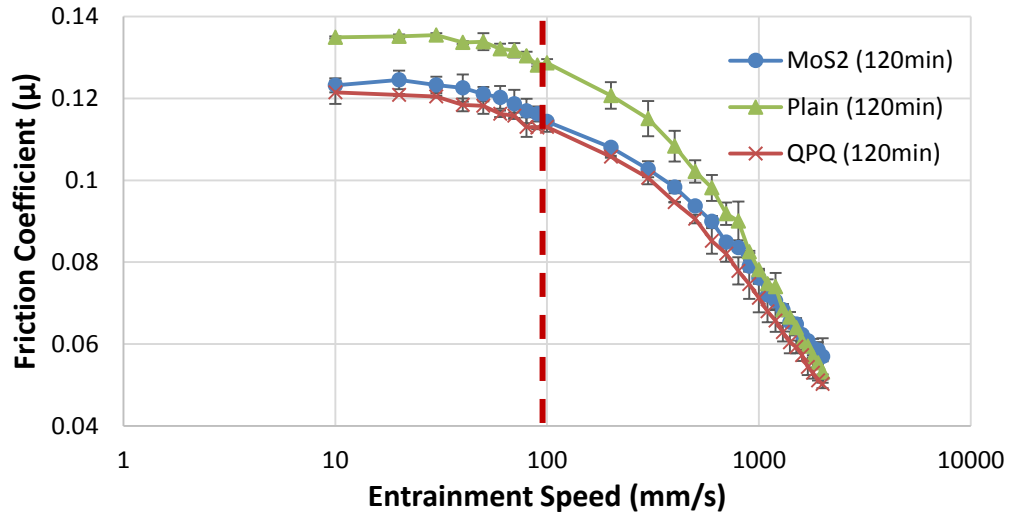
Figure 9-9. Comparison of the Stribeck curves after 2hr rubbing test for QPQ, MoS₂ coated & Plain samples and gas nitrided discs with TO10 lubricant.
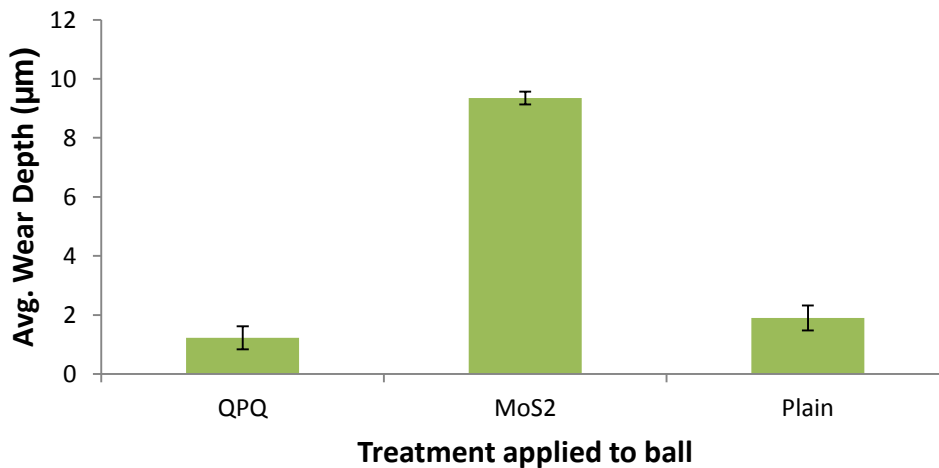
Figure 9-10. Comparison of the wear depths of QPQ, MoS₂ coated and Plain ball samples when using TO10 lubricant.

9.3   Tribological Response of Treated Balls when Lubricated with EP & AW Additives

Using the three different variants of the ball samples with the TO10 lubricant showed similar behaviour trends observed when testing with Cameron Plint

TE77 tribometer. The rest of the chapter focuses on comparing the tribological and tribochemical behaviour of the treated ball variants (QPQ & MoS_2 coated) with various EP and AW additives, to gain a better understanding of how each treated surface interacts with single element containing lubricants. The primary aim of this chapter is to investigate the tribological and tribochemical behaviour with the application of a sliding contact and different lubrication regimes representing conditions occurring with the actual piston and cylinder components. Sliding components are to operate under a mixed lubrication region, especially for the case of low speed conditions or low viscous working fluids [33].

The tests would also allow the opportunity to investigate and compare trends and gain a better understanding of the behaviours observed in Chapter 8 with the TE77 tribometer. This would be achieved by analysing the changes to surface topography and the formation of a tribofilm over the duration of the test.

9.3.1 Friction & Wear Behaviour of the Treated Samples with BO + SO Lubricant Mixture

Figure 9-11 shows the friction coefficient as a function of entrainment speed for the SO additive with the QPQ treated sample. As the entrainment speed is reduced friction steadily increases. In the mixed lubrication regime from 100 mm/s – 2000 mm/s, it is possible to see that friction begins to reduce with time until the entrainment speed reduces below 100 mm/s (boundary regime) where friction remains constant for the 2-hr rubbing period. The optical interference images (Figure 9-12) show virtually no tribofilm was formed during the duration of the test. The optical interference images show that the wear of the sample increased with time, shown by the distortion of the wear track in the SLIM image.

A different trend is observed with the MoS_2 coated sample (Figure 9-13), where at all entrainment speeds with an increase in time the friction coefficient is seen to reduce steadily. The reduction in friction after the two hour testing period at the different entrainment speeds ranged from 20-40%. The MoS_2

coated surface was significantly more sensitive to the SO additive than the QPQ samples. The SLIM images (Figure 9-14) showed the formation of a thin tribofilm and exposure of a rougher surface that that observed when using QPQ samples (Table 9-1). Once again the wear of the sample increased with the duration of the test.
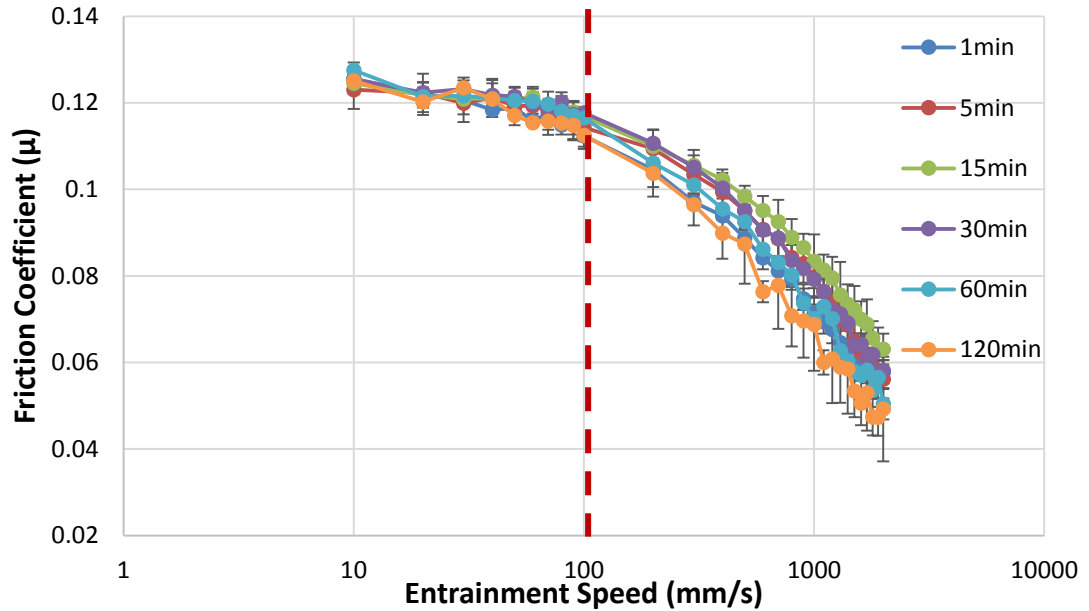
Figure 9-11. Series of Stribeck curves when using a QPQ ball and gas nitrided discs with BO+SO lubricant.
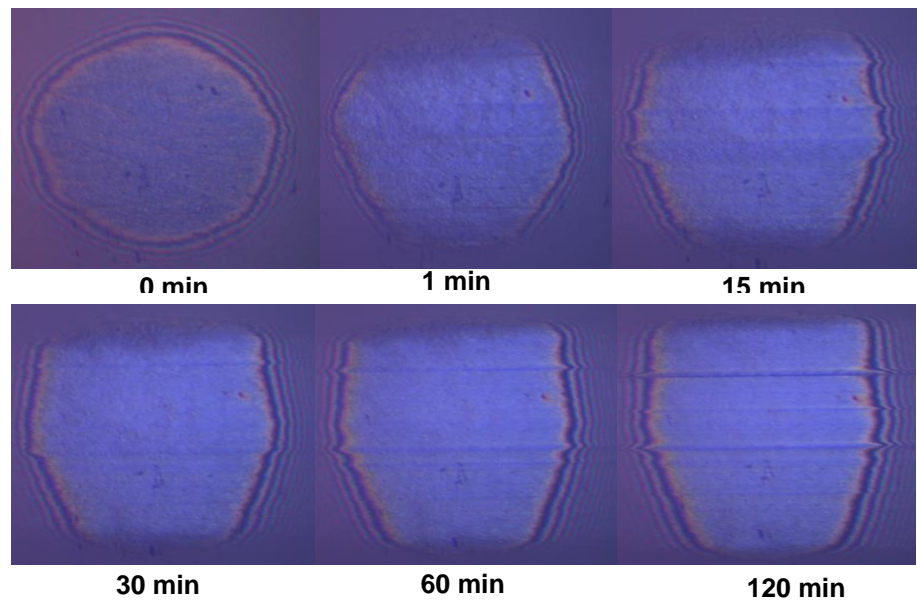
Figure 9-12. Optical interference (SLIM) images of the tribofilm formation on QPQ samples with BO+SO lubricant.
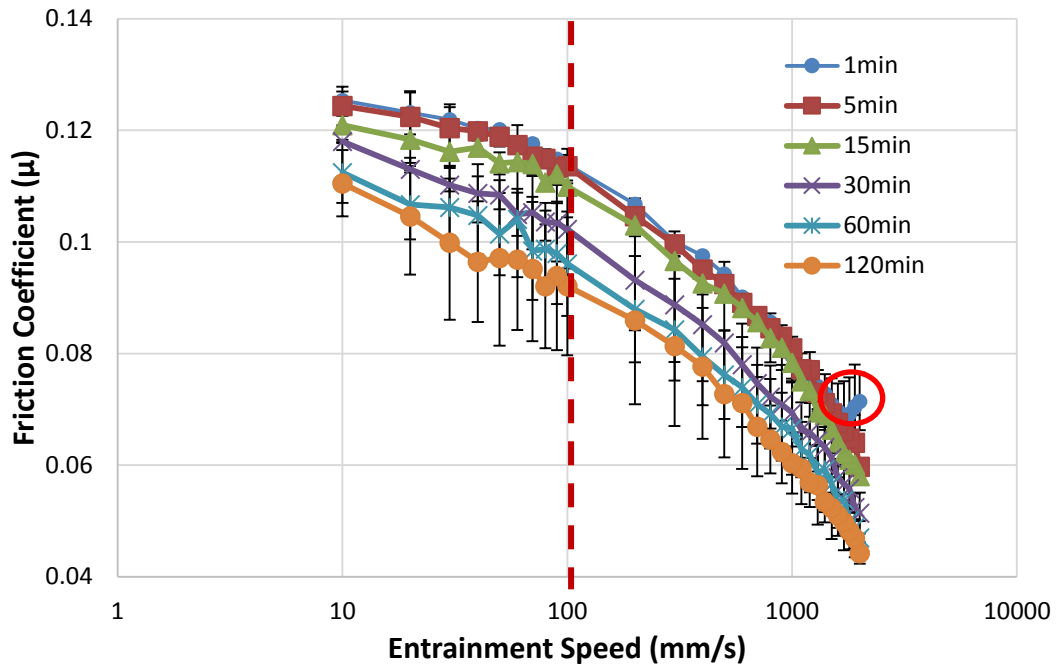
Figure 9-13. Series of Stribeck curves when using a MoS2 coated ball and gas nitrided discs with BO+SO lubricant.
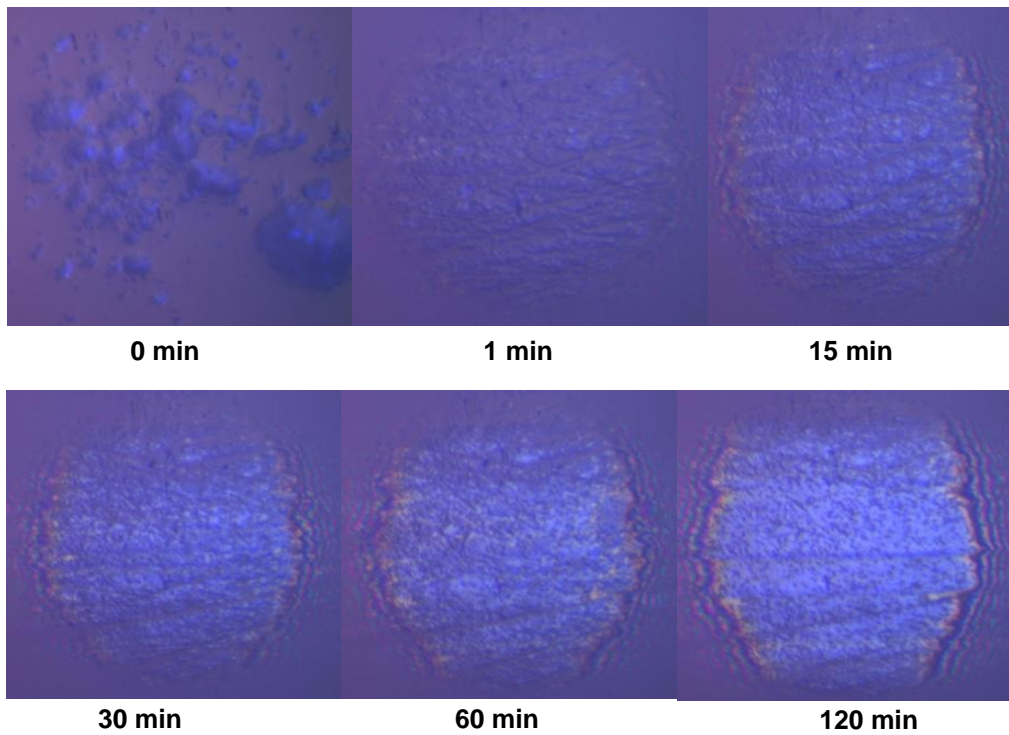
Figure 9-14. Optical interference (SLIM) images of the tribofilm formation on MoS2 coated samples with BO+SO lubricant.

	R_a (µm) Pre-test	R_a (µm) Post-test
QPQ Ball Sample	0.03	0.22
MoS$_2$ Ball sample	0.68	1.71

Table 9-1. The roughness (Ra) of the treated ball samples pre and post testing when using the SO additive.

When comparing the friction performance of the two treated samples, Figure 9-15, after 2hrs it is possible to see that the MoS$_2$ coated sample performed better in both boundary and mixed regime, producing lower friction values.

Optical images of the worn area of the QPQ MTM ball samples (Figure 9-16(a)) after testing showed the removal of the oxide layer and the exposure of a porous compound layer. There are signs of scoring across the surface.
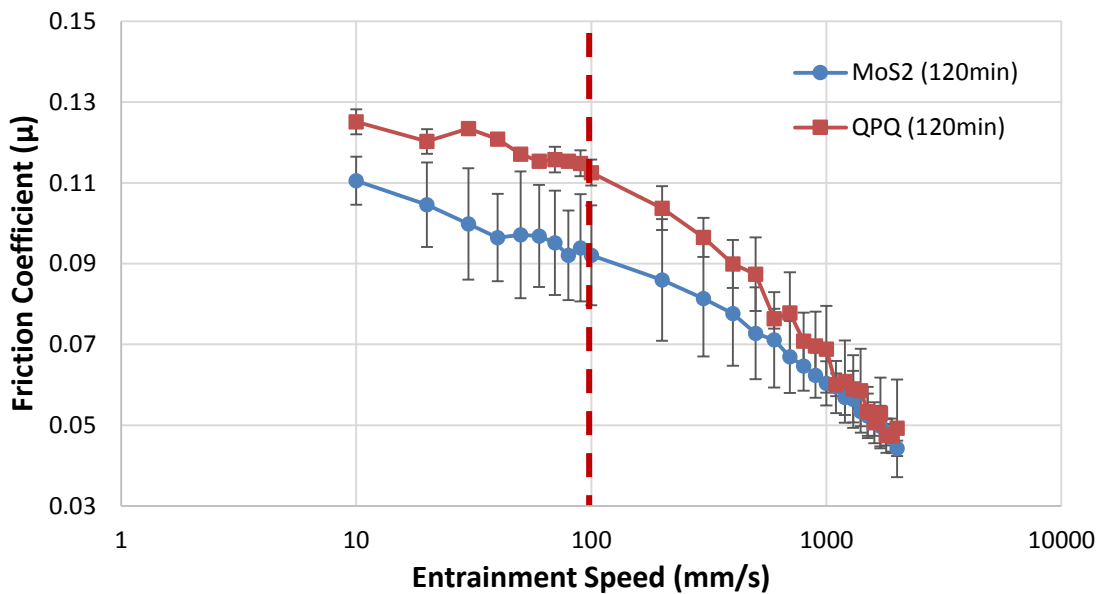
No clear tribofilm is identified on the worn surface.

Figure 9-15. Comparison of the Stribeck curves after 2hr rubbing test for QPQ and MoS$_2$ coated samples and gas nitrided discs with BO+SO lubricant.

However with the MoS$_2$ ball samples (Figure 9-16(b)) the worn surface shows the almost complete removal of the MoS$_2$ coating, with only remnants of it being observed in the wear scar. Scoring in observed across the surface alongside the presence of a uniform tribofilm covering the worn area.

In terms of wear (Figure 9-17), the MoS$_2$ coated samples had greater wear depths and penetration than the QPQ samples. The wear scar images and depth analysis indicate the MoS$_2$ coating was removed during testing.

(a)

(b)
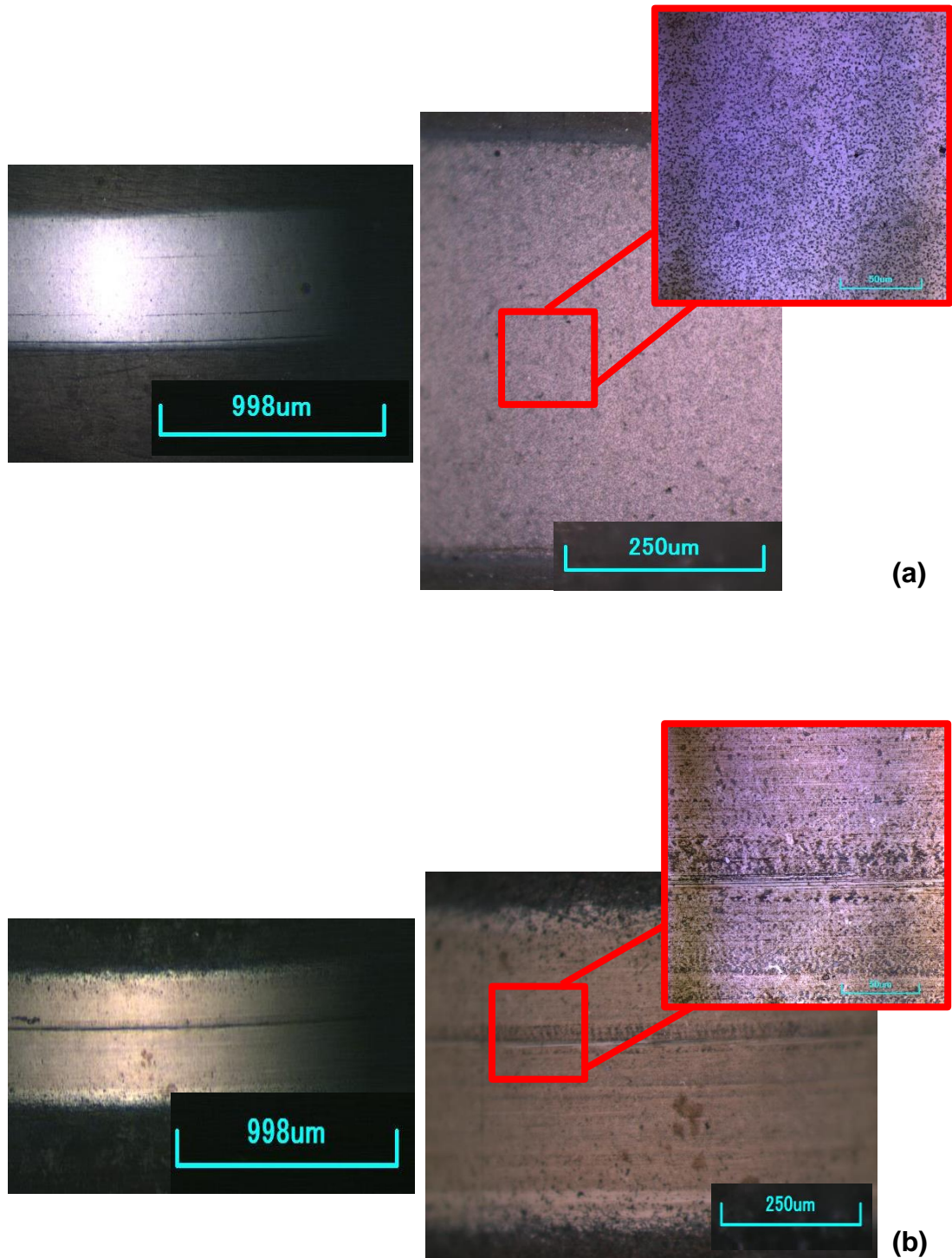
Figure 9-16. Optical images of wear scar regions of the MTM ball samples with the SO additive – (a) QPQ ball (b) MoS$_2$ ball.
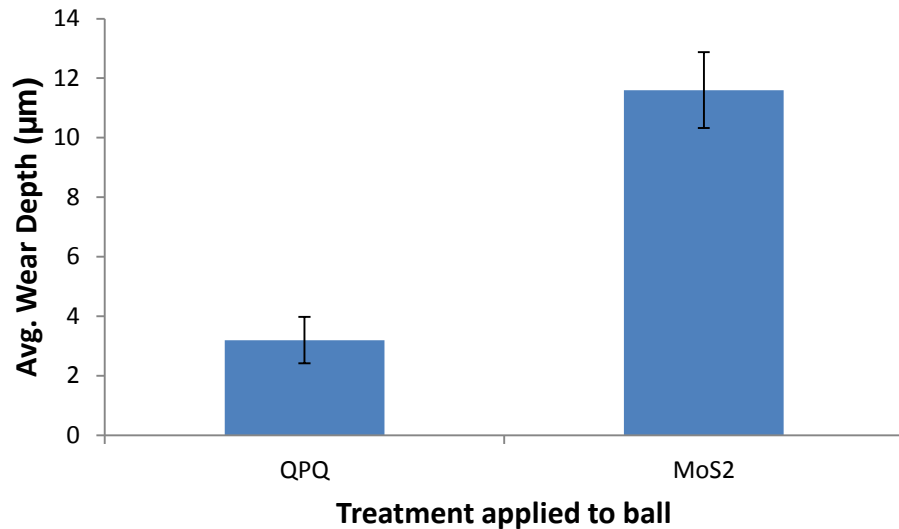
Figure 9-17. Comparison of the wear depths of QPQ & MoS$_2$ coated ball samples when using BO+SO.

9.3.2 Friction & Wear Behaviour of the Treated Samples with BO + TCP Lubricant Mixture

Figure 9-18 shows the friction coefficient of TCP additive with the QPQ treated sample. As the entrainment speed is reduced friction steadily increases. In boundary condition it is possible to see that friction is constant throughout the two hours of the test. In the mixed regime friction begins to reduce slightly with time, however taking in to consideration statistical error the change does not have a significant impact. The SLIM images are similar to those from the SO oil tests, no clear tribofilm is formed. However at 60 and 120 minutes a thin tribofilm seems to be present as highlighted in Figure 9-19. The SLIM images show less distortion of the samples wear track with time, suggesting lower wear is occurring.

With the MoS$_2$ coated sample, in boundary regime there seems to be no change in friction during the duration of the test (Figure 9-20), there is a slight reduction in friction within the mixed regime with time however the behaviour is similar to that seen with the QPQ sample and the change is not significant. The optical interference images show the formation of a tribofilm on the wear track (Figure 9-21), composed of non-uniformly distributed patches elongated along the sliding direction developing in thickness with the duration of the test.

The images also show the shape of the wear track is maintained during the test. The wear scar shows signs of adhesive wear and the surface is once again rougher than using the QPQ sample (Table 9-2). Even with the presence of a tribofilm on the QPQ and MoS_2 balls there was no real impact on friction behaviour. This indicated that the properties of the tribofilm formed when using the TCP additive were different to that observed when using the ZDDP additive which lead to an increase in friction. This behaviour was also observed when using the same treated samples and lubricant additives with the Cameron Plint TE77 tribometer (Figure 8-1), indicating TCP has no impact on frictional behaviour.
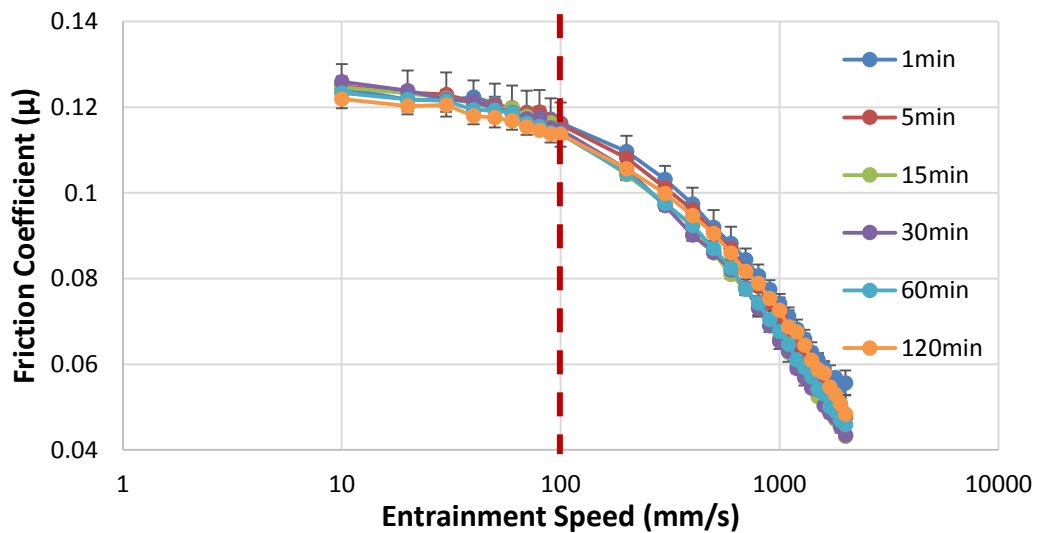
Figure 9-18. Series of Stribeck curves when using a QPQ ball and gas nitrided disc with BO+TCP lubricant.
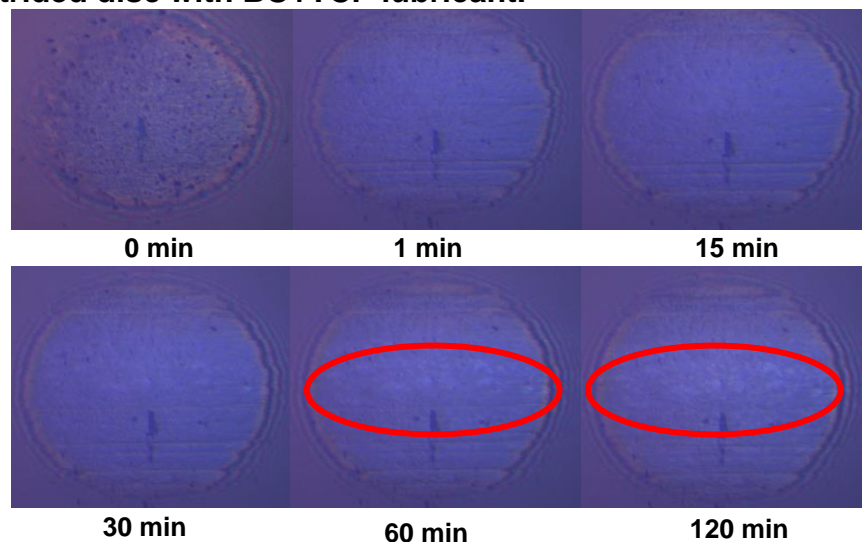
Figure 9-19. Optical interference (SLIM) images of the tribofilm formation on QPQ samples with BO+TCP lubricant. The highlighted sections show the presence of a thin tribofilm.
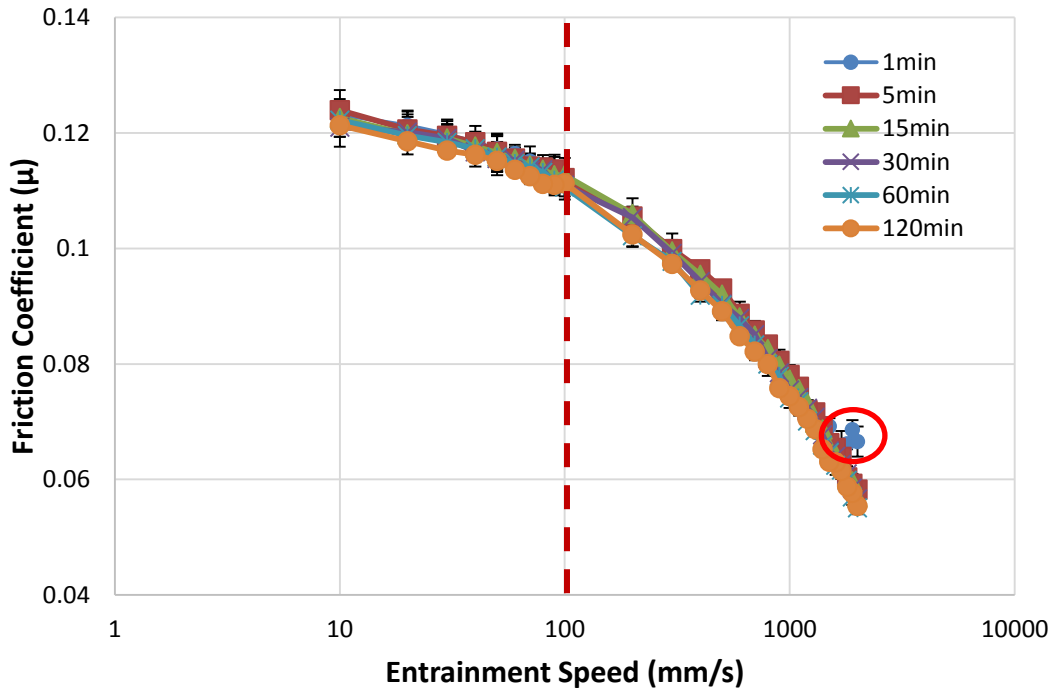
Figure 9-20. Series of Stribeck curves when using a MoS$_2$ coated ball and gas nitrided disc with BO+TCP lubricant.
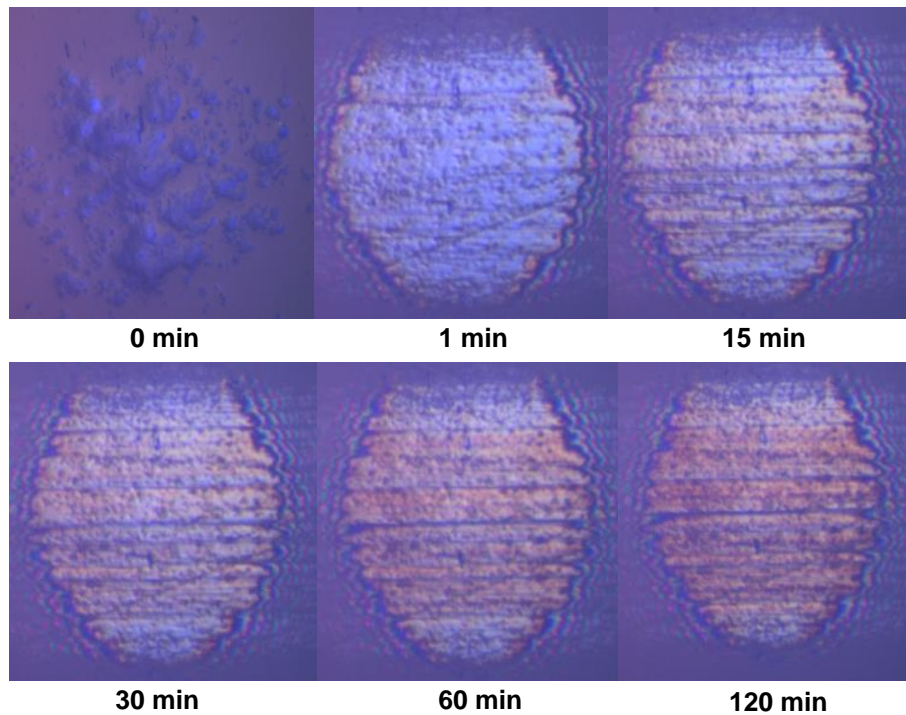
Figure 9-21. Optical interference (SLIM) images of the tribofilm formation on MoS$_2$ coated samples with BO+TCP lubricant.

Table 9-2. The roughness (Ra) of the treated ball samples pre and post testing when using the TCP additive.

	R_a (µm) Pre-test	R_a (µm) Post-test
QPQ Ball Sample	0.03	0.14
MoS$_2$ Ball sample	0.68	1.35

When comparing the friction performance of the two treated samples, Figure 9-22, after two hours it seems the friction response of the two treated samples are almost identical.
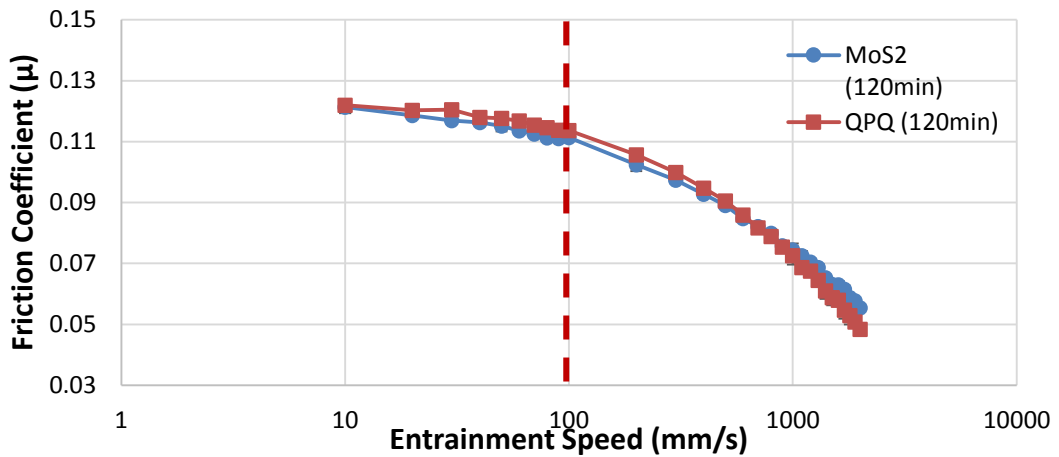
Figure 9-22. Comparison of the Stribeck curves after 2hr rubbing test for QPQ and MoS₂ coated samples gas nitrided disc with BO+TCP lubricant.

The wear track of the QPQ MTM balls (Figure 9-23(a)) with the TCP additive showed the partial wearing of the Fe$_3$O$_4$ oxide layer in contrast to using the SO additive (Figure 9-16(a)), where the layer was completely removed. Even though the Fe$_3$O$_4$ layer survived the test, sections of it were worn through. When using the TCP additive the presence of a tribofilm can be observed on the worn surface which was not the case when using the SO additive.

Similar to when using the SO additive, the MoS$_2$ coating was worn away with the TCP additive (Figure 9-23(b)) with only remnants present within the contact. A thicker tribofilm is observed to form on the surface.

However in terms of wear, once again the MoS$_2$ coated samples had greater wear depths than the QPQ samples (Figure 9-24). The wear analysis of the QPQ samples indicated wear was less than 1µm, suggesting the oxide layer survived testing as supported by the optical images (Figure 9-23(a)). With the

MoS$_2$ samples wear depths were similar to the thickness of the coating, which may explain the presence of remnants of the MoS$_2$ coating as observed by the optical images (Figure 9-23(b)).
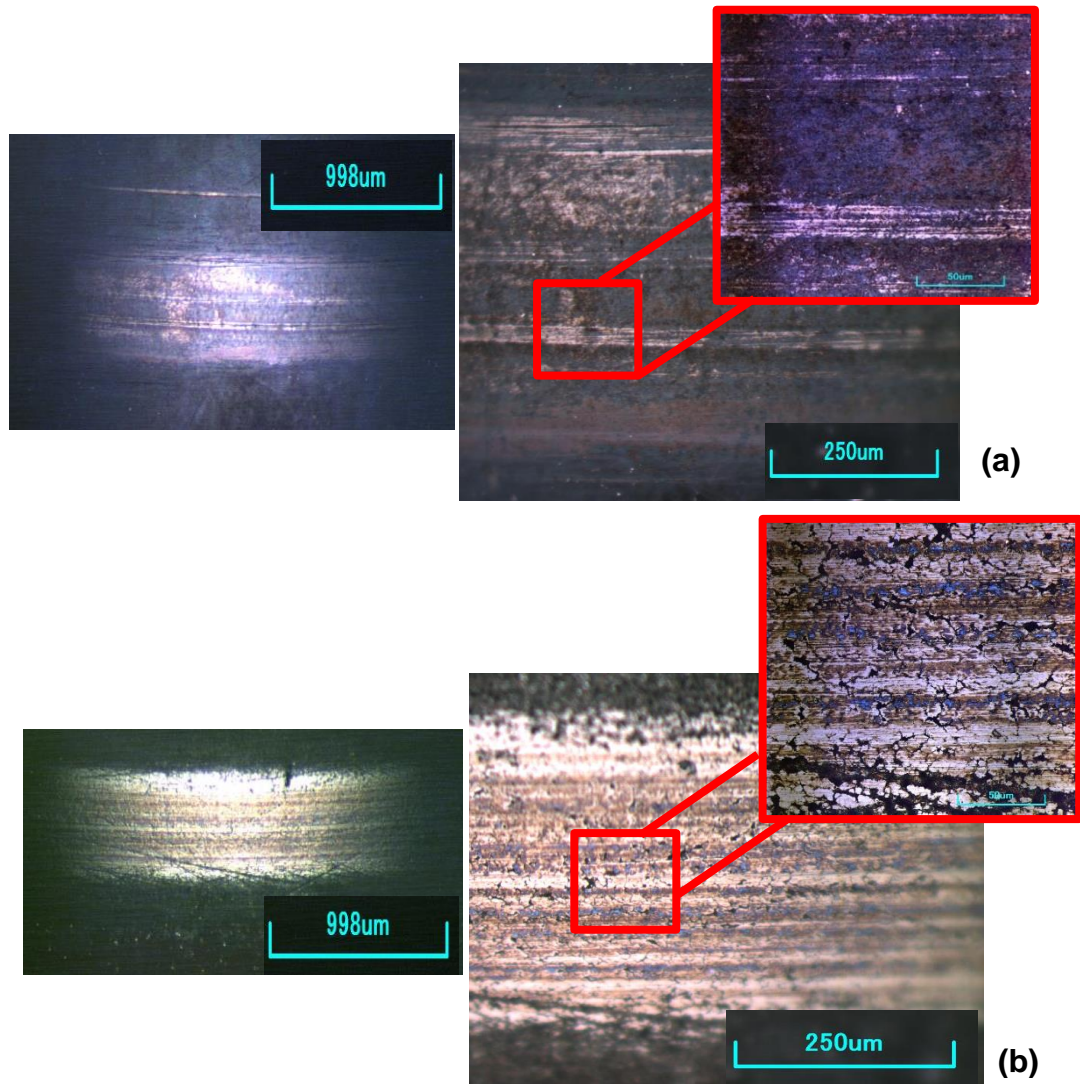
Figure 9-23. Optical images of wear scar regions of the MTM ball samples with the TCP additive – (a) QPQ ball (b) MoS$_2$ ball.
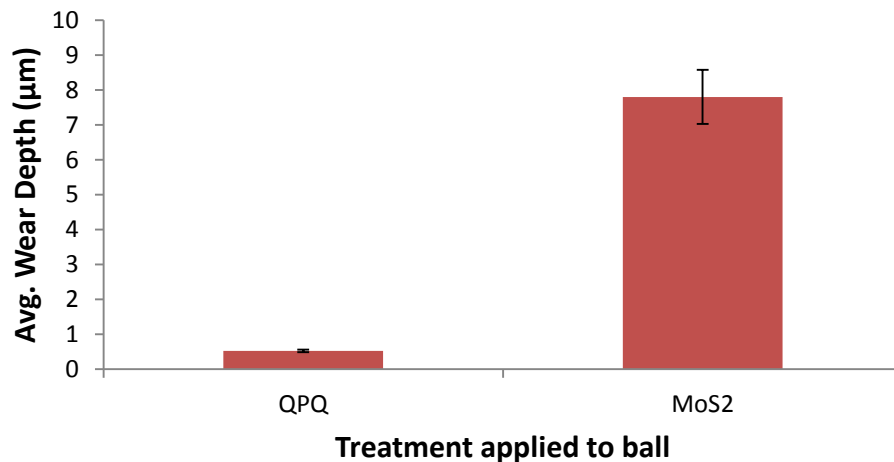
Figure 9-24. Comparison of the wear depths of QPQ & MoS$_2$ coated ball samples when using BO+TCP.

9.3.3 Tribological Response of the Each Additive on the Different Treated Surfaces

Using Figure 9-25 to compare the friction response of the two additives with the QPQ samples, it is possible to see the friction trends are almost identical and the differing additives have no real affect when compared to each other. There is a stark comparison when analysing the effect of the different additives on the wear loss of the sample (Figure 9-26), the wear depth when using the TCP additive is lower than using the alternative additive. The figure also shows that with all additives the wear never penetrated past the compound layer and in to the substrate. The SLIM also showed the formation of a thin tribofilm with the TCP additive whereas nothing was formed with the alternative oil was used.
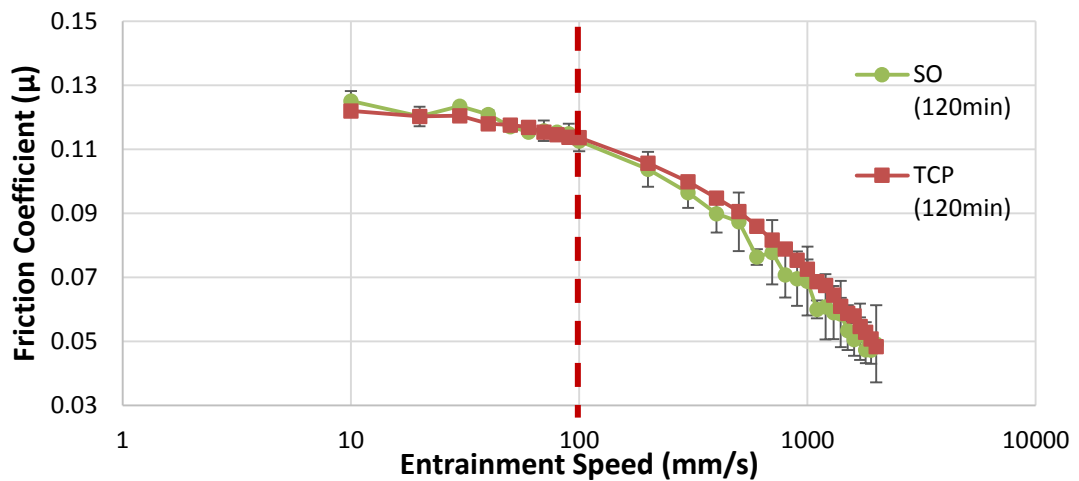
Figure 9-25. Comparison of the Stribeck curves after 2hr rubbing test for QPQ samples with gas nitridied discs when using BO+SO & BO+TCP lubricants.
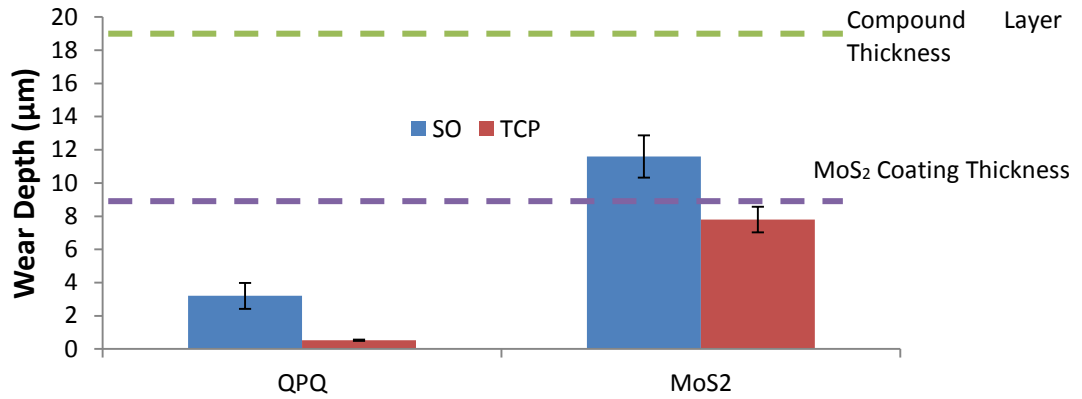
Figure 9-26. Comparison of the wear depths of QPQ & MoS₂ coated ball samples when using BO+SO & BO+TCP lubricants.
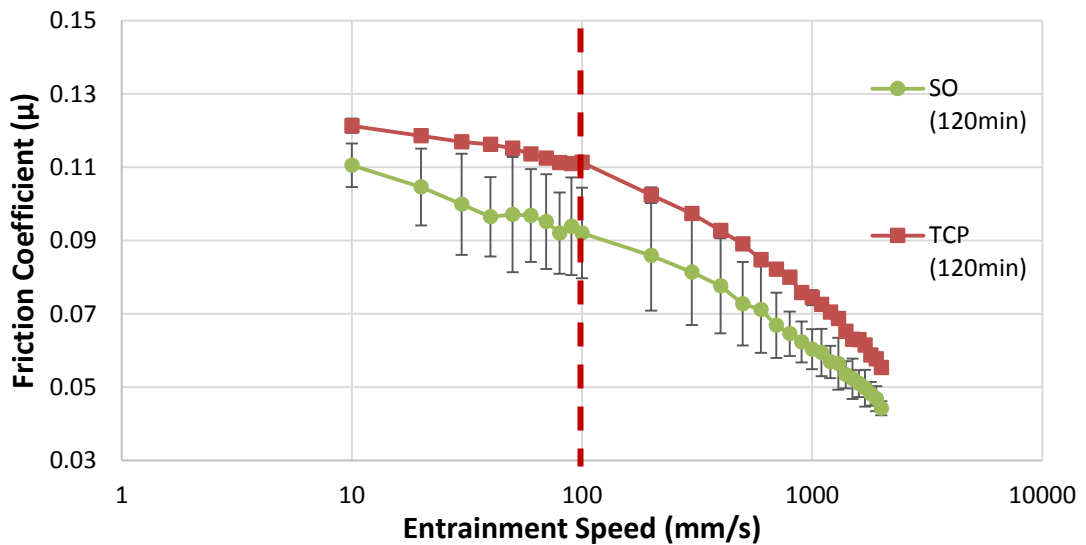
Figure 9-27. Comparison of the Stribeck curve s after 2hr rubbing test for MoS₂ coated samples and gas nitrided discs when using BO+SO & BO+TCP lubricants.

Analysing the effect of the different additives with the MoS₂ coated sample using Figure 9-27, the SO additive has a clear and effective impact on friction compared to the TCP additive. The SO additive produces significantly lower friction results in mixed and boundary conditions. These trends matched that observed when running similar tests with the TE77 tribometer.

However there is a different trend observed when comparing the depth of the wear scars on the ball, where the trend follows that seen with the QPQ sample. The samples tested with the TCP additives have the smallest wear penetration (Figure 9-26), but for both oils it seems the coating did not survive the tests

with the wear depth penetrating past the applied coating and into the substrate material. It had also been observed that a thicker tribofilm was formed when using the TCP additive, whereas it was thinner when using the SO additive.

9.4 Tribofilm Characterisation using XPS

XPS analysis was carried out to analyse the changes in chemical species formed in the tribofilms on the surface of the various samples. With the three samples tested with fully formulated TO10, the tribofilm compositions matched that found with the TE77.

The XPS results in this chapter focus on characterising the tribofilms formed on the QPQ and MoS_2 coated MTM balls when using the two different lubricant additives – SO & TCP, which vary in chemical composition. Table 9-3 and Figures 9 - (28 - 31) confirm the presence of a tribofilm and highlight the key species formed on the worn surface of the two sample types when using the different additives.

When using the SO additive with QPQ samples, sulphides (162.3 eV - Figure 9-28(a)) are detected within the MTM balls tribofilm which corresponds with the formation of FeS (712.1 eV - Figure 9-28(b)). Organic nitrogen species (399 eV - Figure 9-28(c)) are detected within the tribofilm. The species detected within the MoS_2 coated samples tribofilm were similar to that observed with the QPQ samples. Sulphides (161.9 eV - Figure 9-29(a)) and FeS (712.1 eV - Figure 9-29(b)) were identified, however there were no nitrogen species detected due to the absence of a nitride layer.

With the TCP additive, phosphates (133.4 eV - Figure 9-30(a) & Figure 9-31(a)) and $FePO_4$ (712.4 eV) alongside iron oxides (Figure 9-30(b) & Figure 9-31(b)) are detected within the tribofilms of the QPQ and MoS_2 MTM ball samples. Similarly to with the SO additive nitrides were not detected within the QPQ tribofilm, only organic nitrogen species (Figure 9-30(c)).

Table 9-3. General binding energy values for compounds relevant to the tribofilms formed on the worn surface of the QPQ and MoS2 samples when using the different EP additives at a 1.34 nm etching depth [119].

Sample Type	Additive	Element	B.E / eV (±1eV)	Chemical state
QPQ	SO	N 1s	399.0	Organic Species
		S 2p	162.3	Sulphide
		Fe 2p	712.1	FeS
			709.5	Fe_3O_4
	TCP	N 1s	398.1	Organic Species
		P 2p	133.4	Phosphate
		Fe 2p	712.4	$FePO_4$
			709.3	Fe_3O_4
MoS$_2$	SO	S 2p	161.9	Sulphide
		Fe 2p	711.9	FeS
			709.0	Fe_3O_4
	TCP	P 2p	133.7	Phosphate
		Fe 2p	712.4	$FePO_4$
			710.3	Fe_2O_3
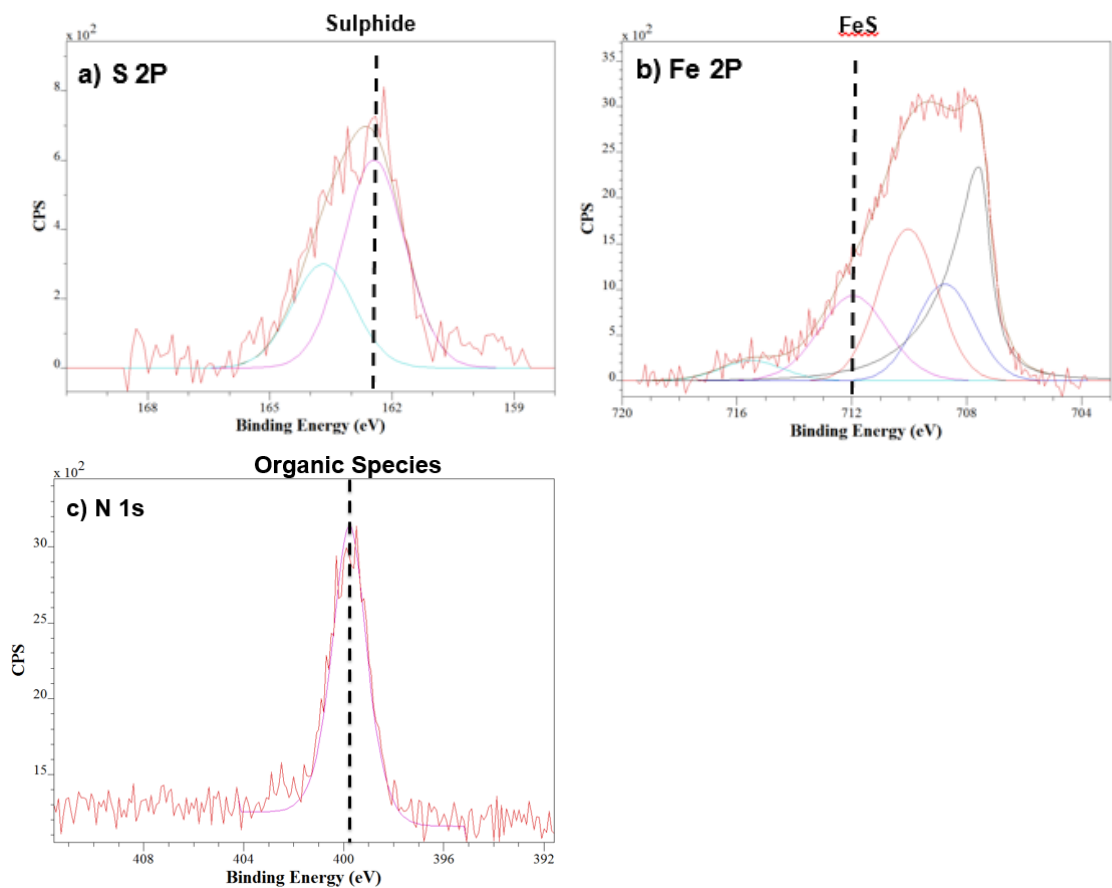
Figure 9-28. XPS spectra of S 2p, Fe 2p & N 1s on the worn surface of the QPQ MTM ball samples at 1.33 nm etching depth with SO additive.
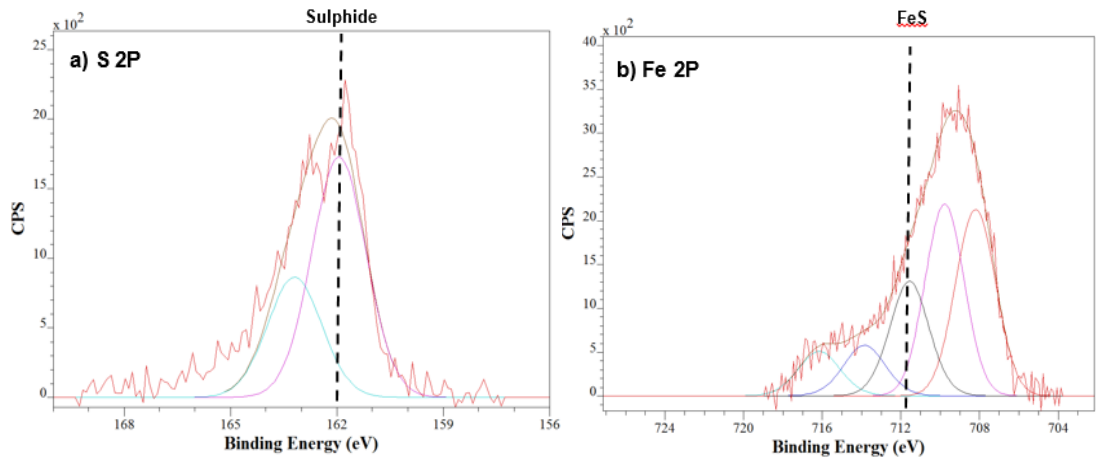
Figure 9-29. XPS spectra of S 2p & Fe 2p on the worn surface of the MoS$_2$ coated MTM ball samples at 1.33 nm etching depth with SO additive.
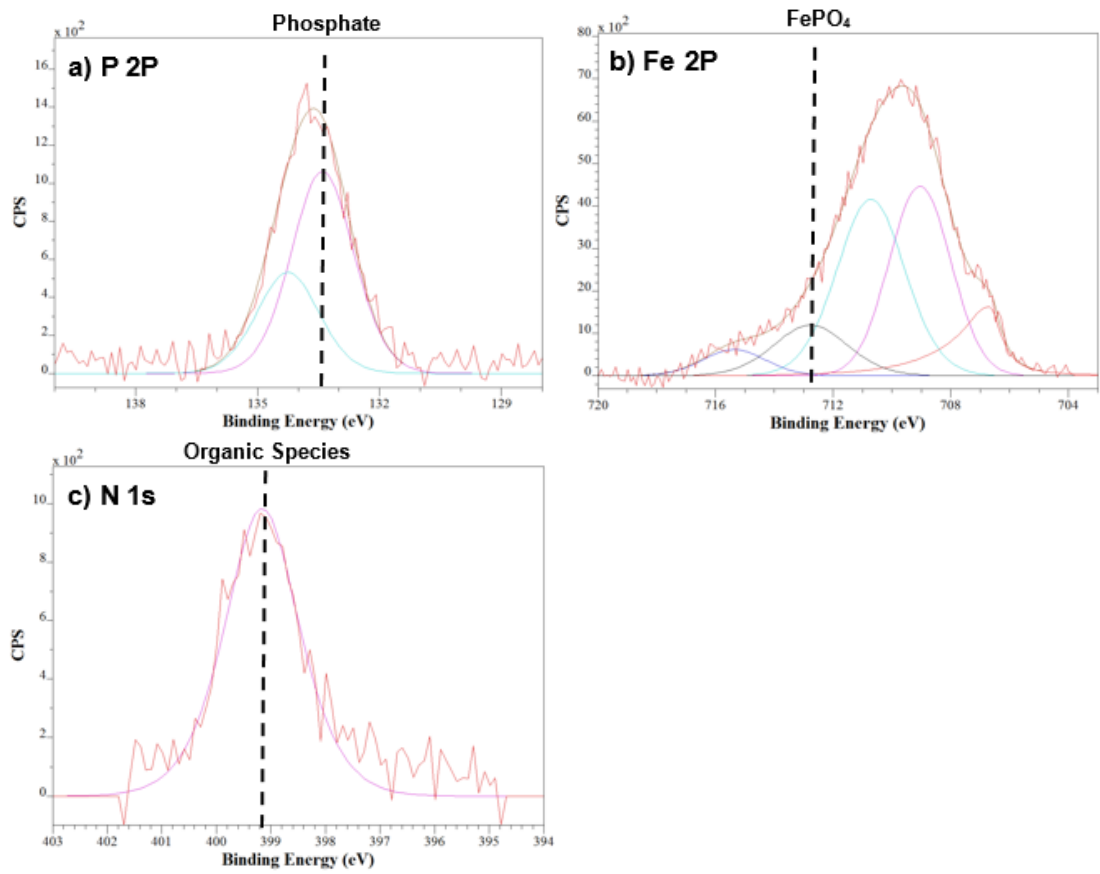
Figure 9-30. XPS spectra of P 2p, Fe 2p & N 1s on the worn surface of the QPQ MTM ball samples at 1.33 nm etching depth with TCP additive.
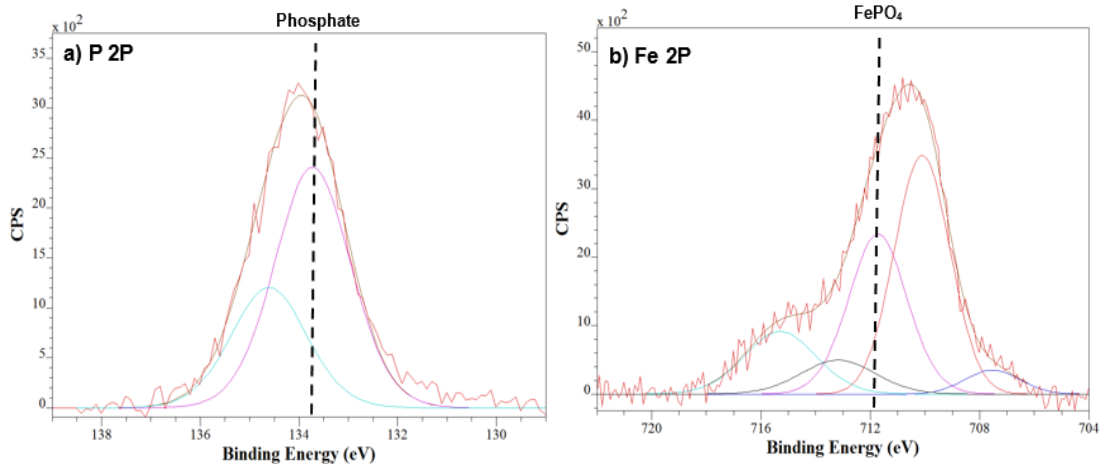
Figure 9-31. XPS spectra of P 2p & Fe 2p on the worn surface of the MoS$_2$ coated MTM ball samples at 1.33 nm etching depth with TCP additive.

9.5 Summary

This chapter aimed to investigate the tribological and tribochemical behaviour of the treated samples with the application of an almost pure sliding contact similar to that observed between the piston and cylinder component. This section also helped to verify the friction and wear trends observed with the sample and lubricants variants tested with TE77 tribometer. The results obtained in this part of the study allowed the analysis of the tribological behaviour of the surface treated MTM balls, alongside the visualisation of the formation of a tribofilm.

- In boundary lubrication there was no real change in friction behaviour which differed to the behaviour observed with the TE77. However in mixed lubrication the behaviour observed with the different samples was the reduction in friction with time.

- The different treatments applied to the MTM balls impacted the friction and wear behaviour of the samples. These behaviours could also be affected by the synergistic effect of the treated surface with the varying lubricant additive.

- With the QPQ sample all additives had no real impact on friction behaviour, however wear depths with the TCP additive were lower than

with using the alternative additives. No visible tribofilms were formed on the surface of the sample with all additives.

• With the MoS$_2$ coated sample a significantly lower friction response was achieved with using the SO additive, however with using the TCP additive a better wear response was achieved. Thin tribofilms on the sample surface were formed with the SO additive however the TCP additive a thicker tribofilm developed with time.

• On both samples the friction effect of the TCP additive was minimal, however when using SO the friction response with the MoS$_2$ samples were significantly lower than the QPQ samples in both lubrication regimes. Similar behaviour was observed when using MoS$_2$ pins with the SO additive with the Cameron Plint tribometer.

• The friction trends and behaviour observed with sample variants and the different additives matched that seen when using the TE77 tribometer. The results supported the hypothesis that the TCP made no impact on friction behaviour.

Using a tribometer which closely replicated the contact of a piston/cylinder in a hydraulic allowed verification of the behaviour trends observed when using the TE77 tribometer. The Chapter demonstrated the type of treatment applied to the samples significantly impacts the friction and wear behaviour. This is further influenced by the synergistic effect of the surface and the lubricant additive.

Chapter 10 Discussion

In the literature review, it was discussed that studies showed that one of the key causes of inefficiency and failure within hydraulic systems was due to the tribological interaction of components. In particular the contact of the piston with the cylinder wall within the hydraulic pump led to the build-up of wear particles between the components eventually leading to seizure or the breakdown of the lubricating film. The application of a wear resistant and low friction nitriding heat treatment aimed to prevent the embedding of particles in to the surfaces of interacting components and reduce clearances to minimise lubricant leakage and acting friction. This study incorporates inspiration from the findings of Yue *et al* [104, 139] who currently provides the only comprehensive work involving the interaction of lubricant additives with nitrided surfaces. This work provides a novel insight into the impact of the individual layers produced after nitriding on tribological and tribochemical behaviour. This includes investigating the influence of the presence of oxide and FeS layers produced with nitriding variants on tribological and tribochemical behaviour, which very few studies have researched.

Very few studies have investigated optimising the tribological properties of the nitride surface through lubricant additive selection. Ma *et al* [105] believed the presence of an oxide layer on the samples would enhance the friction and wear reduction properties when using TCP in comparison to SO. This research investigated the interaction of these additives with the oxy-nitrided samples however tribological parameters replicating conditions observed in the real contact of a hydraulic piston and cylinder were used. The novel aspect of this part of the study, would be employing an MTM SLIM tribometer to allow the real time in-situ analysis of tribological behaviour and tribofilm formation with heated treated and coated samples in boundary and mixed lubrication regimes.

In this chapter, the following topics will be discussed: (1) The impact of surface modification treatments on tribological and tribochemical behaviour (refer to results presented in Chapter 6 and 7); specifically:

- The link between testing parameters and tribological behaviour
- The impact of the properties of the layers produced after surface treatment on tribological behaviour
- The link between the modified layers and tribochemical interactions

(2) The effect of AW & EP additive alternatives on tribological and tribochemical performance of oxy-nitrided and MoS_2 coated samples.

10.1 Tribological Performance of the Layers Formed by the Oxy-Nitriding and MoS_2 Coating Treatments with a Fully Formulated Lubricant.

10.1.1 The Influence of the Properties of the Surface Post-Treatment on Friction

A decrease in friction is sometimes observed with the application of a higher load or sliding frequency (Figure 10-1) and may be attributed to the following: (1) a reduction in contact pressure from the enlargement of the contact area during wear and (2) the build-up of debris at the contact interface which introduces low-friction localised rolling to the otherwise high-friction two body abrasion [126]. Other studies [147] concluded the reduction in friction coefficient was due to an increase in surface temperature caused by the higher sliding speed. This would cause the flattening of surface protrusions resulting in steady state and a reduction in shear force and friction coefficient.
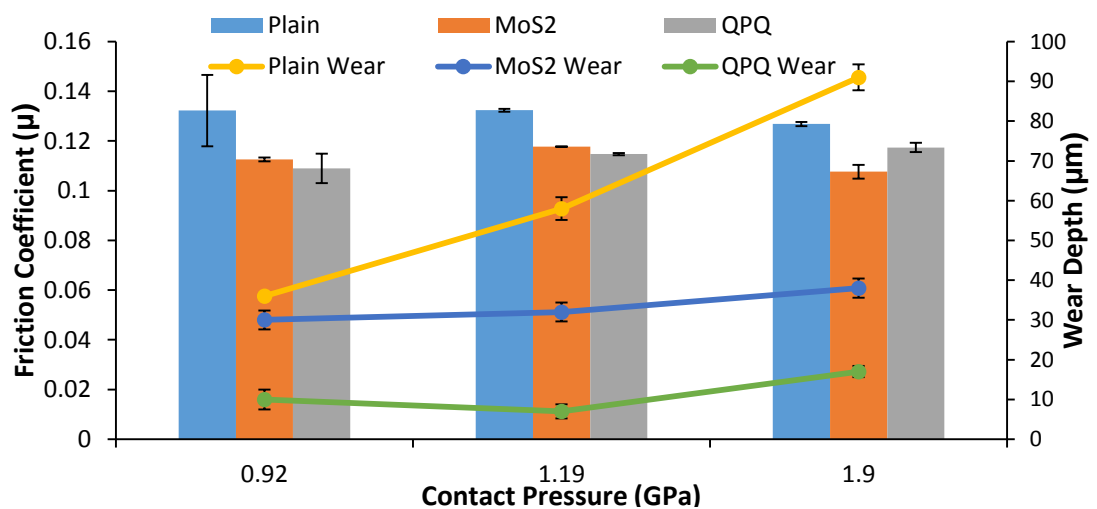
Figure 10-1. Friction and wear comparison of the three sample variants at contact pressures from 0.92 – 1.90 GPa at 12 Hz sliding frequency.

The characterisation of the MoS$_2$ coated samples in chapter 5 showed the presence of a 28 µm thick MoS$_2$ layer. The lower friction behaviour of the MoS$_2$ coated pins in comparison to the untreated samples (Figure 10-1), may be due to the presence of the MoS$_2$ layer. Martin *et al* [148] states the presence of an MoS$_2$ transfer film on the frictional counter-face can lead to low friction behaviour, due to the easy shear between lamellae within the layers [149]. The application of the soft MoS$_2$ coating on to a gas nitrided hardened surface, could have ensured that contact loads were essentially supported by the contact material instead of the formed film [150].

Demydov *et al* [125] showed that MoS$_2$ nanoparticles delivered dialkyl dithiophosphate groups to wear points between interacting surfaces, causing these groups to decompose under high pressure and temperature, forming a protective polyphosphate tribofilm integrated with MoS$_2$.They believed that the synergistic interaction between the MoS$_2$ nanoparticles and polyphosphates accounted for the decrease in friction and wear observed. Due to an MoS$_2$ coating instead of MoS$_2$ nanoparticles being used in this study, the low friction results achieved in Demydov *et al.'s* [125] work were not achieved. Even though the MoS$_2$ coating was removed there were no particles remaining within the contact area to form low friction MoS$_2$ sheets as there would be with nanoparticles.

a) QPQ Sample   b) MoS$_2$ Coated Sample
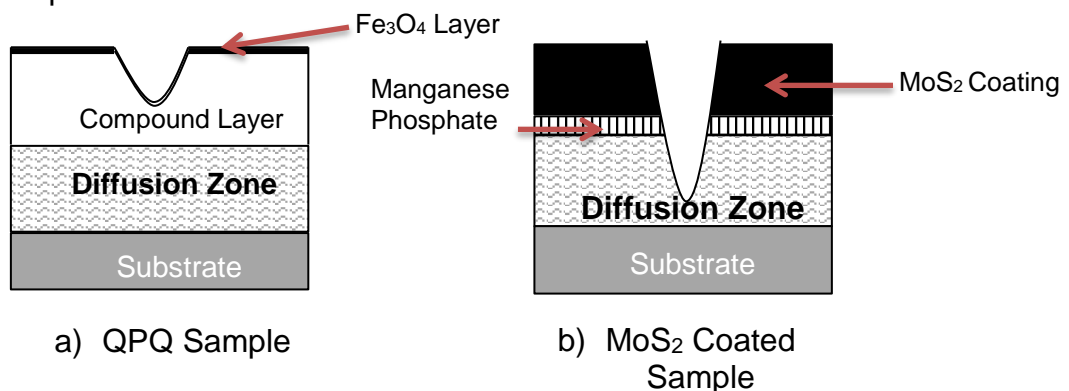
Figure 10-2. Cross-sectional scheme of treated pin sample's worn surface.

Chapter 5 showed the formation of a thin oxide layer above a ~13 µm compound/nitride layer after the QPQ process. The properties of these layers (Figure 10-2) seemed to play an influential and significant factor with wear and friction results observed. The QPQ samples produced the lowest friction

response in comparison to the alternatively treated samples (Figure 10-1). The samples wear depths after testing (Figure 10-1) showed wear remained within the compound layer (<13 µm) for all tests. Qiang *et al* [151] reported that the formation of a ε-phase containing compound layer with non-metallic properties makes it difficult for metallic counterparts to adhere with. Characterisation of the compound layer using XRD (Figure 5-5) showed a strong presence of ε-phases with samples used in this study. This combined with a lamellar close packed hexagonal microstructure, which is easy to slide and to run in along the base plane would help to reduce the heat produced by friction. These characteristics may have influenced the low friction behaviour observed.

10.1.2 The Influence of the Properties of the Surface Post-Treatment on Wear

With the application of an extreme contact pressure (1.90 GPa), wear penetrated past the compound layer (Figure 6-7) and an increase in friction was observed (Figure 10-1). This is possibly due to the non-ceramic and rougher (Table 10-1) properties of the now exposed diffusion zone. This study gives a clear indication of the influence of the compound layer and diffusion zone on friction behaviour.

Table 10-1. The roughness of different QPQ layers exposed during testing.

	Roughness, R_a (µm)
QPQ (unworn)	0.05
Compound layer present	0.11
Compound layer removed	0.23

The compound layer mainly composed of ε–$Fe_{2\text{-}3}N$, detected using XRD (Figure 5-5), is known for its high hardness and wear resistance which allows the application of large loads [57, 66]. The porosity present at the top of the compound layer is acknowledged for its ability to retain extra lubricant, combined with the presence of an oxide layer composed of magnetite (Fe_3O_4) acting as a running–in coating, would further enhance the samples friction

abilities. The oxide layer is known for its low adhesion tendency due to its ceramic features which increases its wear resistance, contributing to further friction reduction [57, 151, 152].

With the MoS$_2$ coated samples the wear depths show that by the end of the two hour testing period the entire coating is almost removed, which can be expected due to it being deemed to be a running-in coating as stated by the bonded coating manufacturer Klueber [50]. The durability of the coating is relatively short and once it has been worn through it cannot be replenished [149]. The substrate exposure is also a likely explanation why the friction results are comparable to that seen with the untreated samples and the slightly lower friction results seen may be due to the initial presence of a low friction coating and formation of low friction MoS$_2$ sheets.

The substrate exposure could explain the significantly higher wear penetration when compared to the QPQ sample due to its lower hardness compared to the compound layer, Yue *et al* [104] proposed this also contributed to the QPQ's low friction behaviour.

10.2 Tribochemical Interactions with the Modified Surfaces

FIB-SEM was used to analyse the thickness of glass phosphate tribofilm's formed the three sample variants.

10.2.1   Tribofilm Formation with Plain Samples

With the Plain sample a thick tribofilm was detected ~100-200 nm (Figure 6-9(a)) to be formed on the worn surface. Li *et al's* [153] research demonstrated that on softer substrates thicker and non-uniform films were formed, the irregularities of the film thickness were due to the deformation of the substrate, and this was common with softer surfaces. This deformation also resulted in rougher surface topographies. Within this study, plain samples had the lowest hardness (Figure 5-4), hence forming the thickest tribofilms.

10.2.2 Tribofilm Formation with MoS$_2$ Samples

A 70 nm tribofilm was detected with the MoS$_2$ samples (Figure 6-11(a)). Even with the removal of the MoS$_2$ coating and the exposure of the substrate the tribofilm formed was thinner that observed with the Plain sample. This was due to the higher hardness than the plain samples (Figure 5-9), which resulted in a thinner tribofilm being formed. Yin *et al* [90] states that the interaction against a rougher counter face would provide greater opportunity for ZDDP to become trapped between the two surfaces, which would encourage the formation of thicker tribofilms. The MoS$_2$ coated samples had the highest initial surface roughness (Table 4-3) which may led to a patchier tribofilm in comparison to the plain samples.

10.2.3 Tribofilm Formation with QPQ Samples

With the QPQ samples, the presence of a hard and smooth layer (Table 4-3) may be deemed responsible for the development of a thin tribofilm on the samples surface (Figure 6-13(a)). Spikes [89] research demonstrated that the thickness of the tribofilms formed were influenced by the elements present on the rubbing surfaces, with the absence of nascent iron in the treated layers of the QPQ samples [121, 122] it is difficult to detect a tribofilm.

The formation of a tribofilm when using ZDDP would be further hindered due to the presence of detergents and dispersants within the fully formulated oil used. Several researchers [109] have observed the deterioration of ZDDP's anti-wear properties in the presence of metallic detergents. This is due to the competition between the two additives for surface sites hence reducing the effective ZDDP surface concentration.

10.2.4 Tribofilm Composition

To investigate the role of the tribofilm and tribochemistry between the sample surfaces and lubricant in reducing friction during testing, XPS and Raman spectroscopy were used to characterise the formed protective layers. Nitrides were detected within the tribofilm of the QPQ samples. The presence of hard

nitrides detected within the tribofilm after the surface could further enhanced the wear resistance of the sample, however Yue *et al* [104] and Xia *et al* [103] believed the nitride presence was attributed to the exposure of the nitride layer. One of the key chemical species identified to be present in the QPQ tribofilms was FeS_2.

Ito *et al* [102] proposed that with the presence of an iron oxide (Fe_3O_4) layer, above 60°C ZDDP molecules present in the lubricant would decompose creating free zinc ions. These free ions would adsorb on to the iron oxide surface, forming a zinc-rich, sulphur-free absorption layer ($ZnFe_2O_4$) that can grow without modifying the crystal structure of the surface. During testing, the sliding between two surfaces causes mechanical mixing to occur allowing Zn^{2+} and Fe^{2+} ions to exchange cations. Free iron ions are able to react with sulphur from the DDP^- forming iron sulphides and FeS_2. Watanabe *et* al [154] reported that a porous FeS_2 layer was formed on Fe_3O_4, while a dense FeS layer was formed on iron. Figure 10-3 summarises schematically the chemical nature of fully formulated tribofilms formed on steel and QPQ samples.

ZDDP Tribofilm Formation			
	Plain	**QPQ**	**Notes**
Mechanically Worked Film			- ZnS indicates decomposition of ZDDP additive. - Free Fe^{2+} ions released due to mixing interact with sulphur to form FeS_2.

Figure 10-3. Schematic representation of tribofilms formed on plain and QPQ samples using fully formulated oil.

Wada *et al* [155, 156] concluded that the formation of large amounts of FeS_2 the greater the influence it would have on friction reduction, which is demonstrated in Figure 10-4. The presence of FeS_2 in the tribofilm combined with the QPQ compound layer could further enhance the samples friction reduction ability. FeS_2 had a greater presence in the QPQ sample tribofilms

than plain and MoS$_2$ -coated samples. However due to the relative thinness of the tribofilm the influence of FeS$_2$ on friction reduction could be negligible.
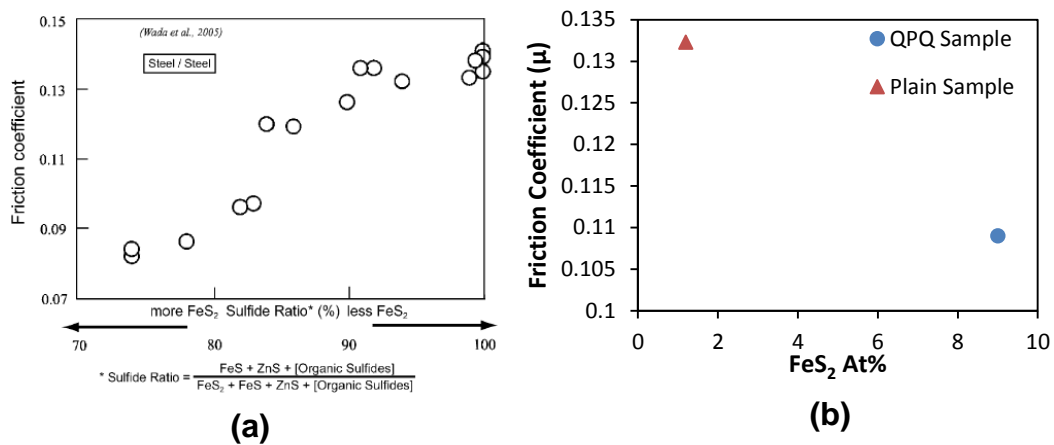
Figure 10-4. a) Effect of sulfides in tribofilm on friction coefficient [156] b) At 1.19GPa contact pressure and 1.34 nm etching depth.

With the removal of the compound layer of the QPQ sample (Figure 6-17), the tribofilm formed showed a higher content presence of Fe and P (Table 6-3). Basso *et al* [121] states that the compound layer is inert which other studies [89] indicate would impact the formation and development of a tribofilm. With the exposure of the iron rich diffusion zone a higher presence of iron is expected (Figure 5-3), however the higher presence of phosphorus may possibly be due to the formation of a thicker protective tribofilm (Figure 6-17(b)). This may be due to the removal of the inert compound layer allowing a greater rate of formation and interaction. This study shows the importance of nascent iron in the development of a tribofilm and its influence on tribological performance.

10.2.5   Tribofilm Characterisation

This study's XPS analysis showed the formation of short chain length polyphosphates within the tribofilms of the QPQ samples (Table 6-4). Shorter chained polyphosphates are regarded to enhance the mechanical and rheological properties of the surface giving it better tribological properties when compared to plain and MoS$_2$-coated samples which formed longer chained polyphosphates. Ito *et al* [102] and Yue *et al* [104] suggested that the formation of a native iron oxide layer (Fe$_2$O$_3$) and nitrides on the nitrided surface would interact with the polyphosphates forming shorter chain lengths.

5 Zn(PO$_3$)$_2$ + Fe$_2$O$_3$ → Fe$_2$Zn$_3$P$_{10}$O$_{31}$ + 2ZnO5 (ZnO, P$_2$O$_5$)(Fe$_2$O$_3$, 3 ZnO, 5 P$_2$O$_5$)   (10-1)
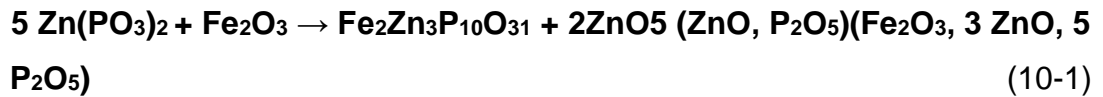
The reaction highlighted in Equation 10-1 will result in de-polymerization, resulting in the formation of shorter poly-phosphate chain [99, 128, 157, 158].

The presence of an iron oxide layer composed of Fe$_3$O$_4$ as in this study, would prevent de-polymerization occurring and the formation of longer chained poly-phosphates as seen with the formation of the QPQ samples thermal unworn film. This due to the cation exchange between the Fe^{2+} and Zn^{2+} ions in the polyphosphate layer [102]. However the exposure of the nitrided layer may have led to the formation of shorter chained polyphosphates within the worn surface tribofilm, due to the reaction of the nitrides with the polyphosphates. Similar behaviour was observed by Yue *et al* [104].

Heuberger *et al* [131] states that polyphosphates with two or three units of phosphates are possibly harder and tougher than longer chain lengths, and coupled with a hard nitride layer this would greatly reduce the wear rate, explaining the behaviour seen with the QPQ sample.

The results from this chapter showed the influence of the nitride layer on tribological and tribochemical behaviour. In the following section the implication of the presence and absence of a thin nascent iron containing layer will be discussed in detail.

10.3 Tribological and Tribochemical Influence of Modified Layers Present on a Nitrided Surface with a Fully Formulated Lubricant.

10.3.1   Isonite Samples

The friction and wear response of the Isonite samples matched that of the QPQ sample (Figure 10-5) suggesting that the impact of the Fe$_3$O$_4$ layer present with the QPQ samples has minimal impact of friction and wear behaviour.

 HEF state that the presence of the black oxide layer is primarily for cosmetic and corrosion protection purposes [59]. It was believed that the presence of the (Fe_3O_4) oxide layer led to the formation of FeS_2 (Equation 10-1) which when present in high concentrations can impact friction behaviour (Figure 10-3). XPS (Table 7-3) and Raman (Figure 7-12) showed no real presence of iron sulphides within the tribofilm of the Isonite samples, supporting the theory that the oxide layer presence was responsible for the compound's formation (section 10.2). With the FeS_2 absence within the tribofilm of the Isonite samples demonstrated that the compounds presence made minimal impact as the two samples friction behaviour were almost identical. This was most likely due to the thin tribofilm formed (Figure 6-13) which would limit the concentration of key compounds present within it.
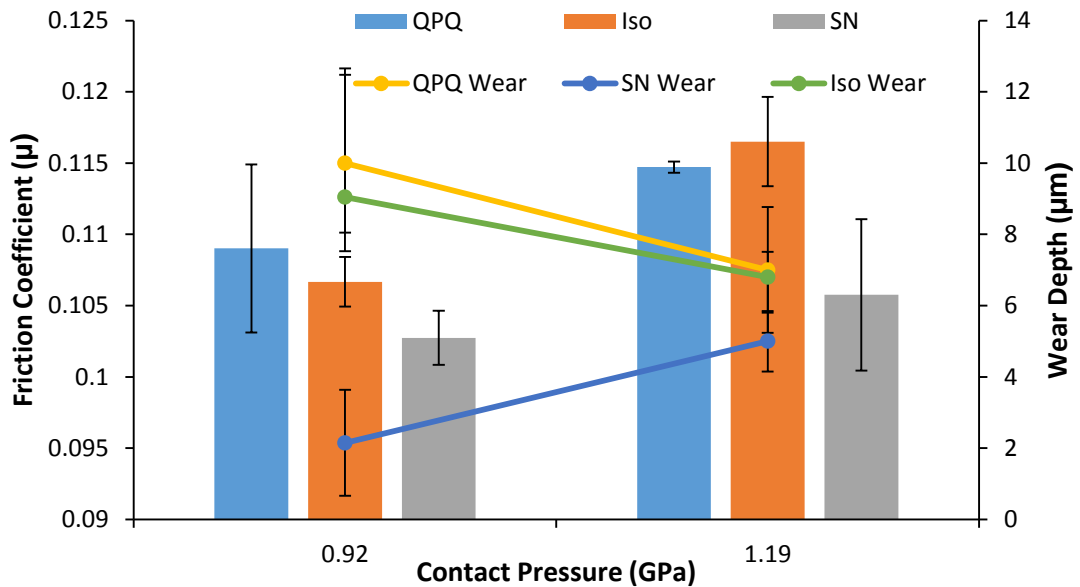
Figure 10-5. Friction and wear comparison of QPQ, Iso & SN samples at two contact pressures with a 12 Hz sliding frequency.

This study's findings demonstrated the possibility of forming a thicker tribofilm with presence of thicker oxide layer, which could have a greater FeS_2 concentration allowing a lower friction response. The Fe_3O_4 layer was shown to be a source of nascent iron which impacted the formation of a tribofilm, with the QPQ samples showing a higher P/Zn ratio (Table 7-2) than the nitride alternatives. The interaction of the nascent iron and phosphorous present within the lubricant additive would encourage the formation of a protective layer.

10.3.2   Sulphur Nitrided Samples

With the sulphur nitrided samples the friction and wear response (Figure 10-5) was lower than the QPQ and Isonite alternatives. Yue *et al* [159] and Wang *et al* [51] (Figure 10-6(a)) observed similar trends with their study. This was due to the presence of a FeS layer on the top surface of the pins as identified when the samples were characterised in chapter 5 (Figure 5-11). FeS is softer than the metal surface, acting as a solid lubricant which allows easy slip due to its layered structure and would contain wear to its thickness [141]. Even when the FeS layer was worn away to a certain extent, it could be decomposed under high friction heat and contact stress to produce S ions, which could react with Fe atoms from substrate to form FeS again, i.e. FeS could be retained continuously in a certain period [139, 159].
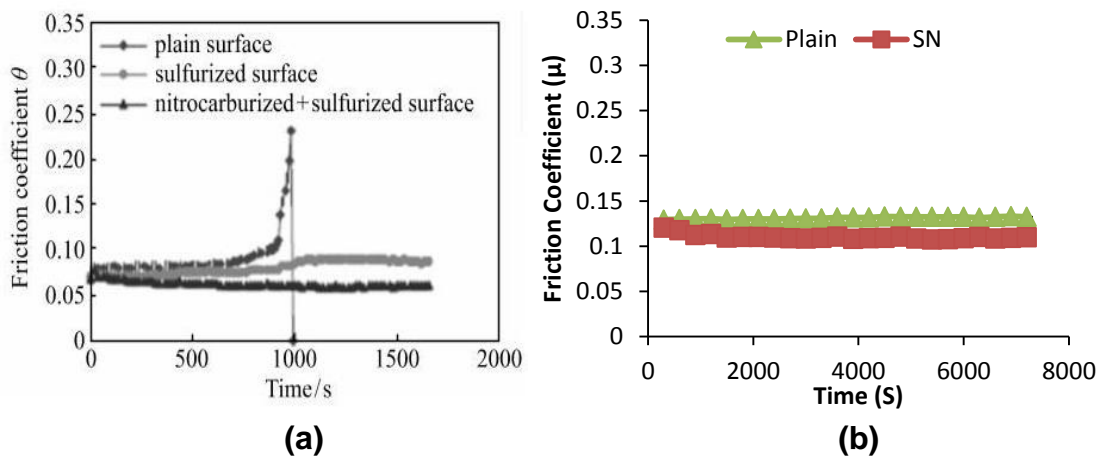
Figure 10-6. Friction response of plain and sulphur nitrided samples as shown by (a) Wang *et al* [51] and (b) this study.

The results with the sample variants from Chapter 7 support the theory that the inertness of the compound layer limits the formation of an effective tribofilm. The presence of nascent iron within the contact area could influence the formation of thicker and protective phosphate film.

10.4 Performance of Treated Samples with Extreme Pressure and Anti-Wear Additive Variants

The tribological behaviour observed in Chapter 8 is due to the tribochemical interaction of the different additives with the modified surfaces. The following sections summarises this study's findings of the role chemical interaction plays in the friction and wear behaviour observed.

10.4.1 Friction

High friction trends (Figure 8-2) were observed when using the ZDDP lubricant in comparison to using the SO and TCP additives. This is a well recorded phenomenon due to the formation of an anti-wear tribofilm which has an uneven, pad-like distribution separated by deep fissures (Figure 10-7). The roughness of these pads is usually orientated towards the direction of sliding, which is shown by the high friction coefficients in boundary condition usually ranging from 0.11 to 0.14 [160].

However, with the QPQ samples BO produced the highest friction response in contrast to behaviour observed with the alternatively treated samples. This is most likely due to the removal of the compound layer (Figure 8-6) and exposure of the diffusion zone similarly to that observed in Chapter 6 (Figure 6-4) and discussed in section 10-1.
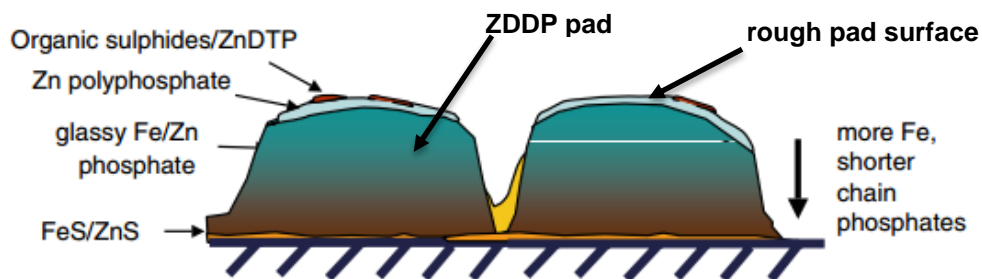
Figure 10-7. Schematic diagram of pad like structure of ZDDP tribofilms – adopted from Spikes [89].

The friction response in the last 30 minutes of testing when using BO and TCP with the non-nitrided samples were almost identical. This is in contradiction to the behaviour observed by Ma *et al* [105, 106]. However, Ma *et al* [105] believed the presence of a film formed when using a TCP additive would only

improve the samples anti-wear and load carrying properties, which was observed in this study. This study showed the properties of the tribofilm formed using TCP differed to that formed with ZDDP, with the latter increasing friction response.

When using the SO additive with the Plain samples a slightly lower friction response was recorded compared to when using the alternative lubricants. EDX (Figure 8-7(b)) and XPS (Table 8-1) showed a strong presence of FeS. The compound is softer than the metal surface and acts as solid lubricant, making it effective in friction reduction [141].

With the MoS_2 samples a significant reduction in friction with time is observed when using the SO additive (Figure 8-1). XPS showed the formation of FeS within the tribofilm formed, this combined with the remnants of the MoS_2 coating would greatly influence the friction behaviour of the sample. A similar response was observed within Wang *et al.'s* [51] (Figure 10-8(a)) work with MoS_2/FeS multilayer films under lubrication, where the friction decreased and was lower than steel with a FeS film. Wang *et al* [51] proposed this was due both compounds possessing a close packed hexagonal crystalline structure allowing easy slip along the close-packed plane. With the formation of FeS on the worn MoS_2 coated surface, this multilayer film would be subject to plastic deformation creating a plastic flow layer over the worn surface which help to reduce friction within the system. The relative softness of both compounds would have a detrimental effect on the wear rate of the sample.

(a)   (b)
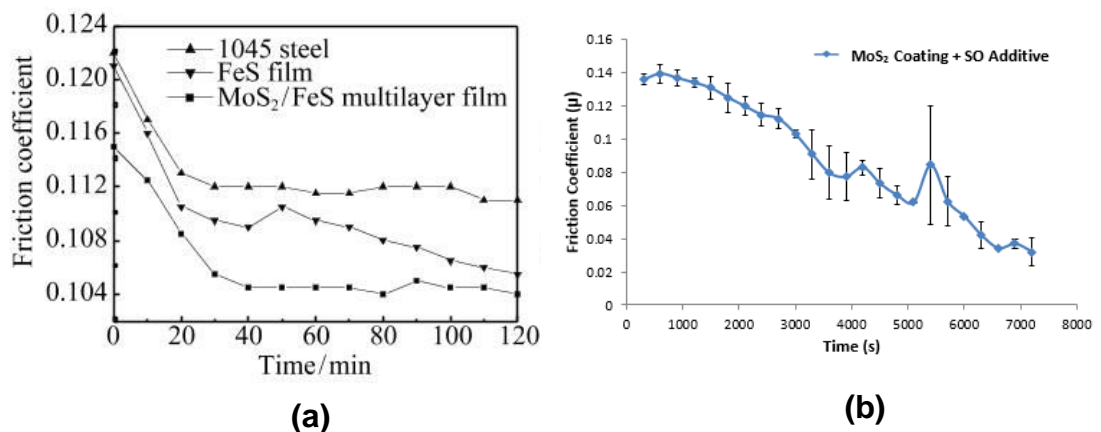
Figure 10-8. (a) Friction behaviour of MoS₂/FeS multilayer, FeS film and steel under oil lubrication as shown by Wang et al [51], (b) Change in friction coefficient with MoS₂ samples with SO additive.

With the QPQ samples when comparing the impact on friction behaviour of the SO and TCP additives the responses are almost identical. As mentioned in section 10.1 this may be due to the inertness and non-metallic properties of the compound layer, where wear was contained for all the additives used. The absence of nascent iron in the treated layers of the QPQ samples would have impacted the tribochemical behaviour of the sample. This may have caused the formation of a relatively thin tribofilm or hindered the formation of sufficient concentrations of key compounds (FeS) when using the SO additive minimalising the influence of the tribofilm on friction behaviour. As observed with Plain and MoS_2 it is also believed that the TCP additive has no impact on friction behaviour of the QPQ samples.

10.4.2   Wear

The wear trends observed with the alternative EP and AW additives were similar to Ma *et al.'s* [105] study. With the absence of additives in the lubricant to form a protective surface tribofilm, the experiments using base oil produced the highest wear results. Wear reached the diffusion zone (>15 µm) past the compound zone for the QPQ samples and deep in to the substrate for the alternative samples (Figure 8-6). The wear when solely using BO was in some cases five times higher than when an extreme pressure additive was present. Even with the formation of relatively thin tribofilms with the different additives their formation was extremely effective on the wear performance of the samples. Similar behaviour was observed by Konicek *et al* [144] where the formation of a thick tribofilm was not crucial to protect surfaces from wear.

With the MoS_2 coated samples the wear depths with BO were similar to that observed when using the SO additive, where the MoS_2 coating was removed in both cases (Figure 8-8) and similar levels of penetration in to the substrate material were achieved. However even though the wear behaviours were similar the friction responses (Figure 8-2) with the two lubricants were in stark contrast. This indicates that the low friction behaviour observed when using the SO additive was not primarily caused by mechanical or wear mechanisms occurring with the exposure and wearing of the substrate, but more likely due

to the chemical interaction of the SO additive with the worn surface similar to that observed by Wang *et al* [51].

When assessing the wear performance of the different additives, SO produced the largest wear (Figure 8-6). This is most likely due to the absence of a phosphate protective layer and the presence of soft FeS compounds within the tribofilm (Table 8-1). This behaviour is also supported by Kawamura *et al* [161] who state the crystal structure of the reaction products (FeS) when using SO would substantially affect the samples wear properties. Ma et al [105] found that TCP additives were more effective on improving the anti-wear properties and load-carrying abilities of samples whereas SO additives only tended to improve the samples load-carrying abilities.

In contrast to the other samples, with SO the Plain samples produced similar wear results to when using the ZDDP lubricant. This may be due to higher amounts of FeS being formed within the tribofilm (Figure 8-7(b)) which helps to further protect the surface as a protective layer.

The TCP additives produced the lowest wear depths in comparison to the other additives, especially with the oxy-nitrided (QPQ) surface. XPS (Table 8-1) showed the presence of $FePO_4$ within the tribofilm alongside phosphates which improved the anti-wear behaviour of the samples. Ma *et al* [106] believed due to the formation a thick and compact boundary lubrication film containing $FePO_4$ and iron oxide, oxy-nitrided samples would have better anti-wear properties and load-carrying capacity as observed within this study. It is believed that the TCP additive is activated by the presence of oxygen or oxidised surfaces, which in the case of the QPQ samples would be the presence of an Fe_3O_4 layer.

Guan *et al* [162] believed that the mechanism of decomposition of TCP involved a chemical mechanism of decomposition with an initial P=O bonding of intact TCP to the surface. This results in increased polarisation and activation of the P=O bond, followed by nucleophilic attack of residual H_2O or surface O^{2-} onto the P-atom. Ultimately this results in the formation of the

metal phosphate or polyphosphate layer. Figure 10-7 highlights the proposed model.
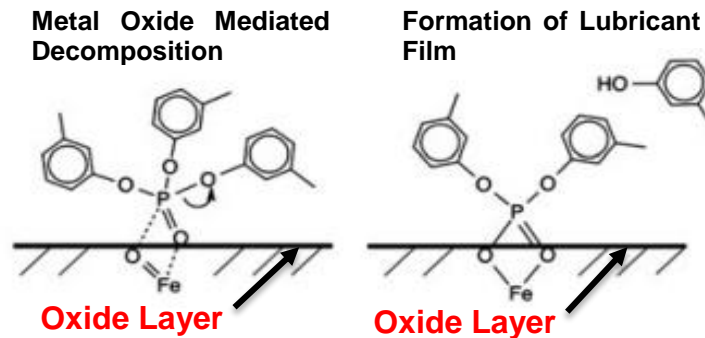
Figure 10-9. Schematic image of metal catalysed TCP decomposition mechanism – adopted from Guan [162].

The fully formulated oil had higher wear rates when compared to the TCP additive, even though ZDDP is described as the most effective anti-wear additive. This behaviour is like that observed by Khorramian *et al* [141]; this is likely due to the presence of detergents and dispersants alongside ZDDP within the fully formulated oil. Several researchers [109] have observed the deterioration of ZDDP's anti-wear properties in the presence of metallic detergents. This is due to the competition between the two additives for surface sites hence reducing the effective ZDDP surface concentration.

The presence of nitrides within the tribofilms formed when using the SO and ZDDP additives maybe due to the greater wear and exposure of the nitrided layer in comparison to using the other additives. It was important to determine whether the presence of a nitrided layer would enhance the effectiveness of the lubricant additive in reducing wear. Yue *et al* [104] found that the effect of the additive ZDDP did not greatly enhance the wear reduction properties when used with a nitrided surface compared to a plain untreated sample as shown within this study (Table 10-2).

Table 10-2. Shows the wear depth ratio's (BO/ZDDP) for untreated and nitrided samples.

	Wear Depth Ratio (BO/ZDDP)
Untreated	1.70
Nitrided	1.60

Chapter 8 showed that the tribological properties of the treated samples could be influenced by different EP and AW additives. This study further highlighted the interactions and impact of the inert compound layer on the enhancing and limiting the friction and wear performance of the QPQ sample. The results also showed an effective synergistic behaviour of the MoS_2 coating with the SO additive, which could potentially be researched to be implemented within a nitrided system to further improve tribological behaviour.

10.5 Friction and Wear behaviour of MoS$_2$ and QPQ Samples using MTM SLIM

10.5.1 Tribological Impact of a Sliding/Rolling Contact

When using almost a pure sliding contact with the MTM SLIM and the lubricant additives, no real change with friction was observed with time when in boundary lubrication however when in mixed lubrication a reduction was observed. These results are in conflict with a study by Ratoi *et al* [111]*,* who showed an increase in friction with time when using the ZDDP additive with untreated chrome steel MTM samples. The reduction in friction observed in this study may have been dominated by the removal of asperities on the ball samples surfaces, which would allow greater entrainment of lubricant between two surfaces and hence a reduction in friction is observed with time. Friction within boundary regime remained constant over time with both samples and additives; this may be due to the inability to form a tribofilm which would impact friction behaviour as observed with other studies [89, 111].

Samples used within other studies have had significantly lower surface roughness values (0.01-0.015 μm) and were untreated in comparison to the samples within this study. The QPQ samples had a surface roughness (R_a) was 0.03 μm and the MoS_2 coated samples surface roughness (R_a) was 0.68 μm. The smoothening of the contact within this study may have dominated the tribological responses and limited the chemical interaction of the surfaces with the lubricants in comparison to the behaviour observed with Ratoi's *et al.'s* [111] study. This study highlights the difficulty in using heated treated and coated sample with the MTM SLIM due to the rough surface finish.

Figure 10-10 compares the different friction behaviour trends over time in boundary lubrication with the TE77 tribometer and MTM SLIM, with the latter closely replicating contact behaviour observed with the piston and cylinder components. The friction values between the two tribometers widely differ, which is important as it highlights the impact of the application of realistic contact conditions. The MTM results may provide behaviour trends closely representative to that observed with the actual interaction of the piston and cylinder components.

(a)   (b)
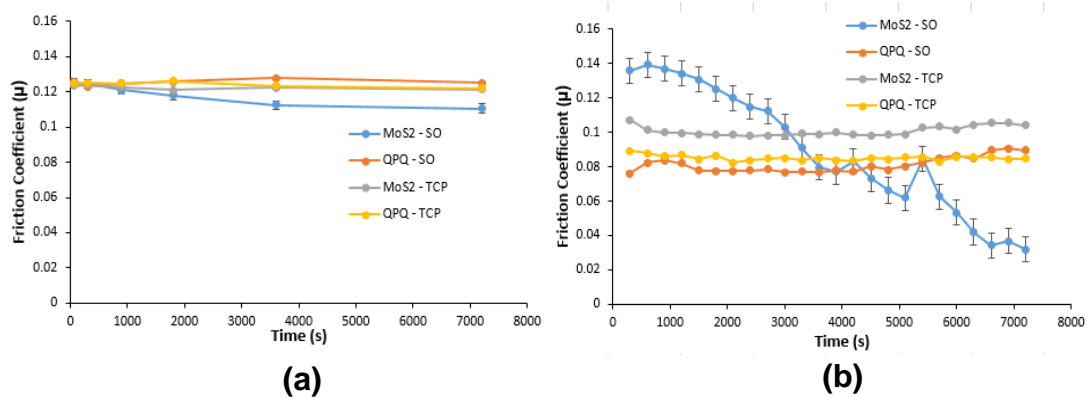
Figure 10-10. Friction response of MoS₂ and QPQ samples with SO and TCP additives in boundary lubrication (a) MTM tribometer – 10 mm/s entrainment speed (b) TE77 tribometer – 0.35 m/s sliding speed.

With the MTM samples the friction response (Figure 10-10) for all the samples and lubricants are almost identical, whereas with the TE77 tribometer different friction responses are observed with the sample and lubricant variants. The impact of the lubricants on friction may have been more effective with TE77 tribometer due to the entirety of the test being carried out in boundary lubrication where the properties of AW and EP additives are activated [49, 89, 90, 141]. The MTM SLIM tests are carried out in boundary and mixed lubrication where the surface properties of the samples as discussed earlier may have had a significant influence on tribological behaviour.

As observed when comparing the friction behaviour, the wear results observed from using the TE77 and MTM tribometers were incomparable. Figure 10-11 shows the wear depths produced with the TE77 tribometer were significantly higher than that observed with MTM for both sample and additive variants. It is believed this due to the geometry and stress distribution with the

different contact types. Bayer [163] believed with the application of a point contact as with the TE77 samples, which concentrates loading may result in the immediate wearing of a coating or layer. However with the application of a conforming or rotating contact the coating or layer may fail by gradual wear. This is due to the presence of a greater contact area alongside the distribution of contact stresses across the surface. The wear generated by the sliding rolling-contact with the MTM tribometer may give a closer representation of the expected behaviour of the surface treatments when applied to actual components within a hydraulic system.
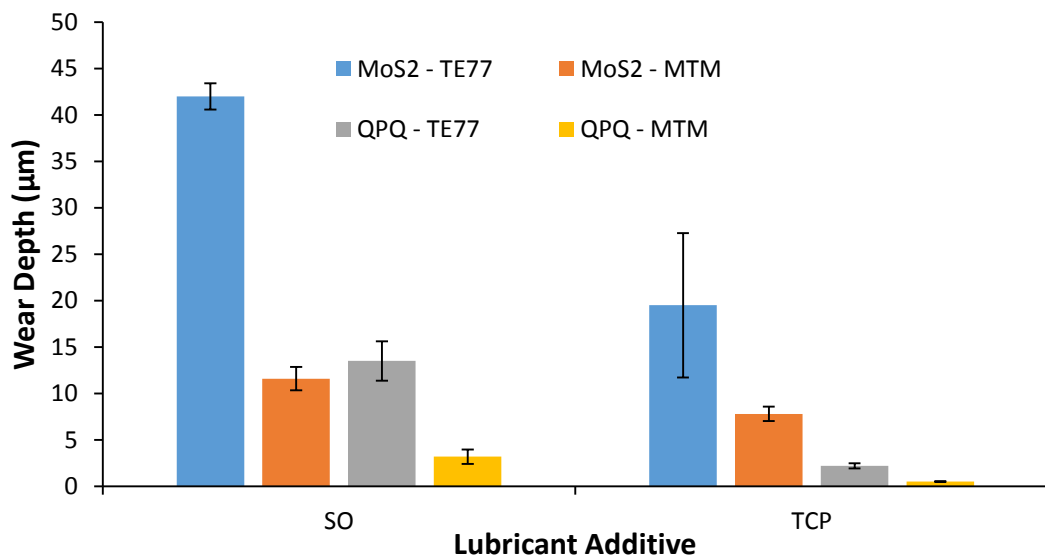
Figure 10-11. Comparison of wear results with the two sample and lubricant variants when using the TE77 and MTM tribometers.

The clear difference in friction and wear trends between the two tribometers is significant as it highlights a difference in behaviour with the application of contact parameters similar to that observed between the piston and cylinder components. Konicek *et al* [144] found that the wear and tribofilm development when comparing results from a simple tribometer and engine test differed widely. It was concluded that the ability to develop a classical adherent tribofilm or replicate traditional behaviour will depend on various experimental factors.

10.5.2   Tribological and Tribochemical Behaviour

With the application of a sliding contact and the ability to analyse the development of a tribofilm in-situ would allow further understanding of the

interaction of lubricants with nitrided surfaces. The SLIM images with all lubricant variants showed no real formation of a clear tribofilm matching the assumptions made in the previous chapters when using the TE77 tribometer, regarding the inertness of the compound layer limiting the formation of a tribofilm [89, 121]. XPS with SO and TCP additives identified the presence of organic nitrogen species within the tribofilm with the MTM samples. This indicates that the presence of nitrides observed within the tribofilm of TE77 samples was due to the greater exposure of the nitride layer [103, 104] rather than the formation of nitride species within the tribofilm, which could potential impact tribological behaviour.

The identical friction response observed after the two hour testing period when using the SO & TCP additives with the QPQ samples (Figure 9-23) matched that observed in Chapter 8 with the TE77 tribometer. These results help to further validate the assumption that the compound layers non-metallic properties limits the formation of a thick tribofilm containing a sufficient concentration of compounds which would influence tribological behaviour. SLIM images showed no real formation of a tribofilm with the two additives used (Figures 9-12 & 9-18). XPS (Table 9-3) showed the presence of FeS when using SO and $FePO_4$ with TCP. As observed in chapter 8, the TCP additive had a greater impact on reducing wear than SO (Figure 9-24).

The friction trends observed with the MoS_2 coated samples with the two additives (Figure 9-25) validated the behaviour observed in Chapter 8 with the TE77. A reduction in friction with time was also observed when using the SO additive, further supporting Wang *et al.'s* [51] findings of a synergistic effect due to the interaction of FeS formed within the tribofilm with the MoS_2 coating.

The friction response with the MoS_2 samples and TCP additive were identical to that observed with the QPQ sample (Figure 9-21). Thus adding weight to the hypothesis made in section 10.4.2 that the TCP additive and the formation of $FePO_4$ compounds (Table 9-3) had no impact on friction behaviour only on wear. Both sample variants showed a lower wear response when using the TCP additive (Figure 9-24). However the optical images (Figure 9-23(a)) of the QPQ sample wear scars showed the presence of a tribofilm of the surface,

indicating the additive was more reactive to the surface than the SO additive. This supports Quan *et al.'s* [162] assumption that the presence of an oxide layer would make the TCP additive more reactive to the surface.

10.5.3 Challenges with using the MTM SLIM

This study showed the limitations of using the MTM SLIM to analyse quantitatively the development of a tribofilm on coated or heat treated samples. The inability to estimate the thickness of the tribofilms formed on the sample surface in this work was due to the high surface roughness. The SLIM requires a conforming smooth surface to be pressed against the glass window. The contact area is illuminated by white light and any film formed by the additive reflects back part of the light which is recombined to form an interference image. However the roughness of the samples used within this study would hinder the reflection of the illuminating white light, thus limiting the ability to accurately measure the thickness of the formed tribofilm on the treated samples [164].

This study highlights the need for smoother surfaces (R_a = 0.01-0.15 µm) after the application of surface treatments to the samples, to allow the impact of tribofilms formed on tribological performance to be assessed.

However the results were able to clearly highlight the impact of the properties of the modified surfaces on tribological behaviour. The QPQ samples had greater wear resistance than the MoS_2 coated samples. The results also showed that not only can the surface impact behaviour but so can its interaction with the additives in the lubricant. The TCP additive produced lower wear when used with both samples and the synergistic interaction of the SO additive and MoS_2 surface led to low friction behaviour.

Chapter 11 Conclusions and Future Work

11.1 Conclusions

This chapter summarises the conclusions derived from the various works presented in this thesis. This study has provided an insight in to the impact of coatings and heat treatments on tribological and tribochemical behaviour with a range of lubricants. Finally, this chapter provides a series of recommendations for future works on this subject.

The key findings of this research are summarised in the following sections.

11.1.1 Tribological and Tribochemical Performance of the Layers Formed by Oxy-Nitriding and MoS$_2$ Coating.

- The characteristics and mechanical properties of the layers formed by the oxy-nitrided treatment influenced the wear resistance and friction reduction behaviour observed. Through the removal of the compound layer, an increase in friction was observed, demonstrating its influence tribological behaviour.

- The removal of the MoS$_2$ coating and the exposure of the substrate of the sample greatly reduced the samples friction and wear reduction ability.

- The presence of a Fe$_3$O$_4$ layer influenced the formation of FeS$_2$ within the QPQ sample tribofilm. However the relative thinness of the tribofilm formed may have negated the influence of the FeS$_2$ compounds.

- A thicker tribofilm was observed to form with the removal of the compound layer and the exposure of the nascent iron diffusion layer.

- The presence of the nitrided layers with the QPQ sample influenced the detection of nitrides within the tribofilm after the surface was worn and the top oxide layer was removed.

- The interaction of the nitride layer with the phosphate layer led to the presence of shorter phosphate chains within the tribofilm. The presence of short phosphate chains improves the samples mechanical and rheological behaviour.

11.1.2 Tribological and Tribochemical Influence of Modified Layers Present on a Nitrided Surface.

- The absence of Fe_3O_4 with the Isonite samples limited the presence of iron sulphide within the tribofilm formed, indicating the FeS_2 detected within the tribofilms or Fe_3O_4 layer of the QPQ samples made no impact on friction or wear behaviour.

- The presence of an FeS layer greatly improved friction and wear behaviour due it's properties as a solid lubricant and its reformation during testing.

11.1.3 Effects of using Alternative Extreme Pressure (EP) and Anti-Wear (AW) Additives with Sample Variants

- When using base oil the wear was significantly higher than with the presence of an extreme pressure additive in the lubricant. This study showed that the wear performance of nitrided surfaces can be greatly improved even with the formation of relatively thin tribofilms due to the presence of additives.

- Compared to other lubricants the fully formulated oil containing ZDDP produced high friction and wear due to the roughness of the pads forming the tribofilm. The presence of detergent within the oil reduces the effectiveness of ZDDP's anti-wear properties hence it performs worse than the TCP additive.

- The TCP additive makes no impact on friction behaviour, however with the formation of $FePO_4$ wear performance is greatly improved. The TCP additive was more effective with the presence of oxide layer as with the QPQ samples.

- A synergistic effect of the MoS_2 coating and FeS led to low friction behaviour with time.

- When using BO with the QPQ samples, the friction behaviour is similar to that observed with the application of an extreme pressure in Chapter 6. An increase in friction is observed due to the removal of the compound layer, supporting the assumption of the significant role of the layer in low friction behaviour.

- No change in friction was observed when using SO with QPQ samples compared to the alternative samples where a drop a friction is observed. This is most likely due to the relative thinness of the tribofilm formed, limiting the potential impact of FeS on friction.

11.1.4 Friction and Wear Performance under Varying Lubrication Regimes

- The friction and wear behaviour observed with MTM tribotests may have closed matched that expected within the actual contact within a hydraulic motor.

- The MTM SLIM provides different friction response in boundary lubrication in comparison to the TE77 tribometer, possibly due to the use of conditions similar to that observed within the actual application contact.

- The friction response within boundary lubrication was identical over time due to the inability to form an effective tribofilm. Friction reduction was observed within the mixed lubrication regime, however it is assumed this behaviour is dominated by the surface roughness of the samples after treatment.

- There are limitations to using heat treated or coated samples with the MTM SLIM, primarily the inability to measure the thickness of the tribofilm formed and tribological response being dominated by the surface roughness.

- The SLIM attachment highlighted the difficulty in forming a visible tribofilm with the QPQ samples in comparison to the MoS_2 samples. This gave visual support to the hypothesis presented in previous chapters regarding the influence of the nitride compound layer in the formation of a protective layer.

- The properties of the layers produced after surface treatment can impact tribological performance as seen with QPQ samples which showed lower wear penetration in comparison to the alternative sample. The interaction of the surface with various lubricant additives can further influence behaviour.

- The trends observed with the sample and lubricant additive variants matched those observed in Chapter 8, supporting the assumptions made.

11.2 Future Work

11.2.1 Influence of Friction Modifiers

This study showed interesting behaviour when using lubricants containing extreme pressure and anti-wear additives. Further tests should be carried out using lubricants containing friction modifiers such as molybdenum dialkyldithiocarbamate (MoDTC). This will allow the investigation in to the analysis of the interaction of the friction modifier with the nitrided surface in comparison to just using EP and AW additives.

Future work should focus on the interactions of using MoDTC when combined with base oil or fully formulated oil with the modified surface, with chemical analysis being carried out using XPS and Raman spectroscopy.

11.2.2 Modifying Nitriding Parameters

Variants of the nitriding process were used within this project however the treatment parameters such as treatment temperature and time were not changed. These parameters would impact the composition, thickness and properties of the layers produced. This study showed that the presence of a Fe_3O_4 layer led to the formation of FeS_2, however due to its relative thinness the impact of the formed compound was minimal. However future projects could focus on the tribological and tribochemical impact of a thicker Fe_3O_4 layer, using XPS and Raman analysis to identify any changes to the chemical species present within the tribofilm.

By influencing the phase composition of the compound layer would allow investigation in to the tribological impact of the different phases formed. Currently this study only used compound layers formed of ε-$Fe_{2-3}N$ phase or a combination ε-$Fe_{2-3}N$ & γ-Fe_4N phases, however the tribological impact of a pure γ-Fe_4N containing layer has not been analysed.

11.2.3　　Application of a Combination of Low Friction Layers

This study showed in Chapters 7 & 8 that a combination of MoS_2 and FeS layers led to a low friction response. Future work should focus on the application of a sulphur gas nitriding process to the counter plates, to form a FeS layer above the nitrided surface. For the pin/ball samples the aim would be to apply a MoS_2 layer upon the oxy-nitrided surface however due to its relative softness and high thickness this would make it unsuitable for application on a piston within a low clearance piston/cylinder arrangement. An alternative coating is a molybdenum disulphide/titanium (MoST) composite coating which is relatively thin (~2 µm) and of high hardness. The aim is to replicate the synergistic behaviour previously observed to achieve a durable low friction system.

11.2.4　　Application of surface modification and texturing techniques

This study showed the importance of the application of surface modification techniques to improve the tribological behaviour of the samples. To further improve the nitriding process the use of complex surface modification technology such as ultrasonic cold forging or texturing can help to accelerate the chemical reaction of the material surface. After cold forging the surface possesses ultrafine grains with a large number of grain boundaries which may act as fast atomic diffusion channels. It is reported that the nitride nano-particles distributed on the surface after cold-forging and then nitriding are smaller due to the increase in grain boundaries which accelerate the formation of nitride precipitates. Overall samples pre-treated using cold forging tend to form thicker and harder nitride layers with smaller nitrided nano-particles and more nitride phases. With the application of texturing/dimpling to the nitride treated surface lubricant retention maybe increased improving tribological performance in lubricant starvation conditions. A combination of the surface modifying techniques could further improve the friction and wear response of the samples compared to only the application of nitriding.

References

1. Corporation, E.M. *Hydraulic efficiency*. [Website] 2009 [cited 2014 August]; Available from: http://www.mobilindustrial.com/ind/english/files/tt-hydraulic-efficiency.pdf.

2. Murrenhoff, H., et al., *ANALYSING LOSSES IN HYDROSTATIC DRIVES.* Proceedings of the JFPS International Symposium on Fluid Power, 2008. **2008**(7-1): p. 103-108.

3. Vanwalleghem, B., et al. *Optimization of the efficiency of hydrostatic drives*. 2012.

4. Fey, C.G., et al., *Analysis of Common Failure Modes of Axial Piston Pumps*, 2000, SAE International.

5. Milestone, W.D., A. Solomon, and G. Olsen, *The kinematic analysis of axial-piston pumps.* Mechanism and Machine Theory, 1983. **18**(6): p. 475-479.

6. Manring, N.D., *Friction Forces Within the Cylinder Bores of Swash-Plate Type Axial-Piston Pumps and Motors.* Journal of Dynamic Systems, Measurement, and Control, 1999. **121**(3): p. 531-537.

7. Doddannavar, R., A. Barnard, and S. Mackay, *1 - Introduction to hydraulics*, in *Practical Hydraulic Systems*, R.D.B. Mackay, Editor. 2005, Newnes: Oxford. p. 1-15.

8. Williams, J., *Engineering Tribology*. 2005: Cambridge University Press.

9. Yazawa, S., I. Minami, and B. Prakash, *Reducing Friction and Wear of Tribological Systems through Hybrid Tribofilm Consisting of Coating and Lubricants.* Lubricants, 2014. **2**(2): p. 90.

10. Hamrock, B.J., B. Jacobson, and S.R. Schmid, *The role of tribology in the design of machine elements*, in *Tribology Series*, M.P.C.M.T.P.E.T.H.C.C.G.D.A.A.L.Y.B.L.F. D. Dowson and J.M. Georges, Editors. 2000, Elsevier. p. 217-227.

11. Desplanques, Y., *Amontons-Coulomb Friction Laws, A Review of the Original Manuscript.* SAE Int. J. Mater. Manf., 2014. **8**(1): p. 98-103.

12. Amontons, G., *De la résistance causée dans les machines, tant par les frottemens des parties qui les composent, que par la roideur des cordes qu'on y emploie, et la manière de calculer l'un et l'autre.* Mémoires de l'Académie Royale des Sciences, 1732: p. 22.

13. de Coulomb, C.A., *Théorie des machines simples: en ayant égard au frottement de leurs parties et à la roideur des cordages*. 1821: Bachelier.

14. Skytte af Sätra, U., *Wear of piston rings in hydrostatic transmissions [Elektronisk resurs]*. 2005, Stockholm: KTH.

15. Taylor, R. and Y. Wang, *Lubrication regimes and tribological properties of fire resistant hydraulic fluids.* American Society of Lubrication Engineers, 1983. **40**(1): p. 44-50.

16. Mang, T., K. Bobzin, and T. Bartels, *Industrial Tribology: Tribosystems, Wear and Surface Engineering, Lubrication*. 2011: John Wiley & Sons.

17. Anderson, W., et al. *Basics of Lubrication*. [Website] 2008 [cited 2014 January];   Available   from: http://www.stle.org/resources/lubelearn/lubrication/.

18. Nilsson, D. and B. Prakash, *Investigation into the seizure of hydraulic motors.* Tribology International, 2010. **43**(1–2): p. 92-99.

19. Stachowiak, G.W., *Wear: materials, mechanisms and practice*. 2006: John Wiley & Sons.

20. Johnson, K.L., *Contact Mechanics*. 1985: Cambridge University Press.

21. Booth, J.E., *The feasibility of using electrostatic charge condition monitoring for lubricant additive screening*, 2008, University of Southampton.

22. Francis, H., *Interfacial temperature distribution within a sliding Hertzian contact.* ASLE TRANSACTIONS, 1971. **14**(1): p. 41-54.

23. Archard, J.F., *The temperature of rubbing surfaces.* Wear, 1959. **2**(6): p. 438-455.

24. Greenwood, J.A., *An interpolation formula for flash temperatures.* Wear, 1991. **150**(1): p. 153-158.

25. Tian, X. and J.F.E. Kennedy, *Maximum and Average Flash Temperatures in Sliding Contacts.* Journal of Tribology, 1994. **116**(1): p. 167-174.

26. Stephen, M.H. and S.G. Richard, *Effect of materials on tribochemical reactions between hydrocarbons and surfaces.* Journal of Physics D: Applied Physics, 2006. **39**(15): p. 3128.

27.   Fischer, T., *Tribochemistry.* Annual Review of Materials Science, 1988. **18**(1): p. 303-323.

28.   Bulgarevich, S.B., et al., *Kinetics of mechanoactivation of tribochemical processes.* Journal of Friction and Wear, 2012. **33**(5): p. 345-353.

29.   Engineering, M. *MAXMA Hydrostatics transmission.* [Website] [cited 2014 September]; Available from: http://www.maxma.com.tw/pdf/ht/pump/hst.pdf.

30.   Cundiff, J.S., *Hydrostatic Transmissions*, in *Fluid Power Circuits and Controls.* 2001, CRC Press. p. 193-270.

31.   Vickers, I. and F.C. Wood, *Vickers Mobile Hydraulics Manual.* 1998: Vickers Incorporated Training Center.

32.   Ivantysn, J. and M. Ivantysynova, *Hydrostatic Pumps and Motors, Principles, Designs, Performance, Modelling, Analysis, Control and Testing.* 2001, New Delhi: Academia Books International.

33.   Totten, G.E., et al., *Tribology of Hydraulic Pump Testing.* 1997: ASTM.

34.   Ludema, K.C., *Tribological design: a real world approach*, in *Hydraulic Failure Analysis: Fluids, Components, and System Effects*. 2001, ASTM International.

35.   Casey, B. *Hydrostatic Balance in Hydraulic Component Design.* [Website] 2006 [cited 2016; Available from: http://www.machinerylubrication.com/Read/836/hydrostatic-balance.

36.   Ki Kim, J. and J.-Y. Jung, *Measurement of fluid film thickness on the valve plate in oil hydraulic axial piston pumps (I)-bearing pad effects.* KSME International Journal, 2003. **17**(2): p. 246-253.

37.   Sadashivappa, K., M. Singaperumal, and K. Narayanasamy, *On the efficiency of the axial piston motor considering piston form deviations.* Mechatronics, 1996. **6**(3): p. 283-301.

38.   Zhang, J. and B. Xu. *Clearance optimization of piston/cylinder pair based on virtual prototype of axial piston pump.* in *Mechatronics and Embedded Systems and Applications (MESA), 2012 IEEE/ASME International Conference on.* 2012.

39.   Pelosi, M. and M. Ivantysynova, *Heat Transfer and Thermal Elastic Deformation Analysis on the Piston/Cylinder Interface of Axial Piston Machines.* Journal of Tribology, 2012. **134**(4): p. 041101-041101.

40. Michael, P.W., et al., *Lubricant Chemistry and Rheology Effects on Hydraulic Motor Starting Efficiency.* Tribology Transactions, 2012. **55**(5): p. 549-557.

41. Totten, G.E., D.K. Wills, and D.G. Feldmann, *Hydraulic Failure Analysis: Fluids, Components, and System Effects.* 2001: ASTM.

42. Brinke, T., et al., *Plasma Assisted Surface Treatment.* 2006, Germany: SV corporate media. 36.

43. Kato, H., *SLIDING WEAR OF NITRIDED STEELS.* 1993.

44. Czichos, H., *Failure criteria in thin film lubrication— the concept of a failure surface.* Tribology, 1974. **7**(1): p. 14-20.

45. Dearnley, P.A., *Wear Resistant Surfaces in Engineering – A Guide to their Production Properties and Selection.* Surface Engineering, 1988. **4**(1): p. 28-29.

46. Bell, T., *Surface engineering: its current and future impact on tribology.* Journal of Physics D: Applied Physics, 1992. **25**(1A): p. A297.

47. Wilson, R. *Surface treatments to combat wear.* in *First European Tribology Conference, Paper.* 1973.

48. Neville, A., et al., *Compatibility between tribological surfaces and lubricant additives—How friction and wear reduction can be controlled by surface/lube synergies.* Tribology International, 2007. **40**(10–12): p. 1680-1695.

49. Rudnick, L.R., *Lubricant Additives: Chemistry and Applications, Second Edition.* 2009: CRC Press.

50. Munchen, K.L. *Bonded coatings for all metal surfaces.* [cited 2016; Available from: https://www.klueber.com/ecomaXL/files/Bonded_coatings_for_metal_surfaces.pdf.

51. Wang, H., B. Xu, and J. Liu, *Micro and nano sulfide solid lubrication.* 2013: Springer Science & Business Media.

52. Joly-Pottuz, L., et al., *Tribological properties of Mo–S–I nanowires as additive in oil.* Tribology Letters, 2005. **18**(3): p. 385-393.

53. Hivart, P., et al., *Seizure behaviour of manganese phosphate coatings according to the process conditions.* Tribology International, 1997. **30**(8): p. 561-570.

54. Ilaiyavel, S. and A. Venkatesan, *The Wear behaviour of Manganese Phosphate Coatings applied to AISI D2Steel Subject to Different Heat Treatment Processes.* Procedia Engineering, 2012. **38**(0): p. 1916-1924.

55. Prabhudev, K.H., *Handbook of Heat Treatment of Steels*. 1988: Tata McGraw-Hill.

56. *ASM Handbook: Steel Heat Treating*, ed. J. Dosset and G. Totten. Vol. 4A. 2013. 768.

57. Holm, T. and L. Sproge, *Nitriding and Nitrocarburizing*: Sweden. p. 24.

58. Binder, C., et al., *Effect of nature of nitride phases on sliding wear of plasma nitrided sintered iron.* Wear, 2015. **332–333**: p. 995-1005.

59. Boβlet, J. and M. Kreutz. *Tufftride-/QPQ-Process*. [cited 2014 March].

60. Menezes, P.L., et al., *Tribology for scientists and engineers*. 2013: Springer.

61. Yasavol, N. and F. Mahboubi, *The effect of duplex plasma nitriding-oxidizing treatment on the corrosion resistance of AISI 4130 steel.* Materials & Design, 2012. **38**: p. 59-63.

62. Solis Romero, J., et al., *Tribological evaluation of plasma nitride H13 steel.* Superficies y vacío, 2013. **26**(4): p. 131-138.

63. Bell, T. and P.A. Dearnley, *ENVIRONMENTAL ISSUES IN SURFACE ENGINEERING AND REIATED INDUSTRIAL SECTORS.* Surface Engineering, 1994. **10**(2): p. 123-128.

64. Yari, M. *Technical Information – Arcor Nitrocarborizing*. [Website] [cited 2016 July]; Available from: http://surface-heat.com/technical-information-arcor-nitrocarborizing.

65. King, P.C., et al., *Fluidized bed CrN coating formation on prenitrocarburized plain carbon steel.* Journal of materials engineering and performance, 2004. **13**(4): p. 431-438.

66. Karamboiki, C.M., et al., *Influence of microstructure on the sliding wear behavior of nitrocarburized tool steels.* Wear, 2013. **303**(1–2): p. 560-568.

67. Yeung, C.F., et al., *Advanced QPC complex salt bath heat treatment.* Journal of Materials Processing Technology, 1997. **66**(1–3): p. 249-252.

68. Cai, W., et al., *Effect of QPQ nitriding time on wear and corrosion behavior of 45 carbon steel.* Applied Surface Science, 2012. **261**(0): p. 411-414.

69. Li, X., et al., *Comparing tribological behaviors of plasma nitrided and untreated bearing steel under lubrication with phosphor and sulfur-free organotungsten additive.* Tribology International, 2012. **51**(0): p. 47-53.

70. Jacquet, P., J.B. Coudert, and P. Lourdin, *How different steel grades react to a salt bath nitrocarburizing and post-oxidation process: Influence of alloying elements.* Surface and Coatings Technology, 2011. **205**(16): p. 4064-4067.

71. Mirjani, M., et al., *Investigation of the effects of time and temperature of oxidation on corrosion behavior of plasma nitrided AISI 4140 steel.* Surface and Coatings Technology, 2012. **206**(21): p. 4389-4393.

72. Esfahani, A., et al., *Effect of treating atmosphere in plasma post-oxidation of nitrocarburized AISI 5115 steel.* Vacuum, 2007. **82**(3): p. 346-351.

73. Mahboubi, F. and M. Fattah, *Duplex treatment of plasma nitriding and plasma oxidation of plain carbon steel.* Vacuum, 2005. **79**(1–2): p. 1-6.

74. Holm, T., *Furnace Atmospheres: Gas Nitriding and Nitrocarburizing*: Germany. p. 48.

75. Ebrahimi, M., et al., *Effect of plasma nitriding temperature on the corrosion behavior of AISI 4140 steel before and after oxidation.* Surface and Coatings Technology, 2010. **205, Supplement 1**(0): p. S261-S266.

76. Bell, T., Y. Sun, and A. Suhadi, *Environmental and technical aspects of plasma nitrocarburising.* Vacuum, 2000. **59**(1): p. 14-23.

77. Pye, D., *Practical nitriding and ferritic nitrocarburizing.* 2003: ASM International.

78. Alsaran, A., et al., *Effect of post-oxidizing on tribological and corrosion behaviour of plasma nitrided AISI 5140 steel.* Surface and Coatings Technology, 2004. **176**(3): p. 344-348.

79. Pennings, B. and S. Van der Zwaag, *The Effect of Metalworking Fluids on the Gas-nitriding Behavior of 31CrMoV9 Steel.* Journal of Materials Science Letters, 1998. **17**(14): p. 1215-1217.

80. Stachowiak, G.W. and A.W. Batchelor, *Engineering Tribology*. 2005: Elsevier Butterworth-Heinemann.

81. Corporation, N. *Understanding the Differences in Base Oil Groups*. 2012 [cited 2016; Available from: http://www.machinerylubrication.com/Read/29113/base-oil-groups.

82. Hsu, S.M., *Molecular basis of lubrication.* Tribology International, 2004. **37**(7): p. 553-559.

83. Smith, E., *Mechanical Engineer's Reference Book*. 12 ed. 2013: Butterworth-Heinemann. 1190.

84. Rostro, B. and N. Nalence, *HYDRAULIC FLUIDS: The pressure to perform better*, in *Tribology & Lubrication Technology*2007.

85. Podgornik, B. and J. Vižintin, *Tribological reactions between oil additives and DLC coatings for automotive applications.* Surface and Coatings Technology, 2005. **200**(5–6): p. 1982-1989.

86. Lin, Y.C. and H. So, *Limitations on use of ZDDP as an antiwear additive in boundary lubrication.* Tribology International, 2004. **37**(1): p. 25-33.

87. So, H. and R.C. Lin, *The combined effects of ZDDP, surface texture and hardness on the running-in of ferrous metals.* Tribology International, 1999. **32**(5): p. 243-253.

88. Nicholls, M.A., et al., *Review of the lubrication of metallic surfaces by zinc dialkyl-dithiophosphates.* Tribology International, 2005. **38**(1): p. 15-39.

89. Spikes, H., *The History and Mechanisms of ZDDP.* Tribology Letters, 2004. **17**(3): p. 469-489.

90. Yin, Z., et al., *Application of soft X-ray absorption spectroscopy in chemical characterization of antiwear films generated by ZDDP Part I: the effects of physical parameters.* Wear, 1997. **202**(2): p. 172-191.

91. Williams, J.A., *The Behaviour of Sliding Contacts Between Non-Conformal Rough Surfaces Protected by 'Smart' Films.* Tribology Letters, 2004. **17**(4): p. 765-778.

92. Jahanmir, S., *Wear reduction and surface layer formation by a ZDDP additive.* 1987.

93. Taylor, L., H. Spikes, and H. Camenzind, *Film-forming properties of zinc-based and ashless antiwear additives*, 2000, SAE Technical Paper.

94. Taylor, L.J. and H.A. Spikes, *Friction-enhancing properties of ZDDP antiwear additive: part II—influence of ZDDP reaction films on EHD lubrication.* Tribology transactions, 2003. **46**(3): p. 310-314.

95. Sheasby, J., et al., *A reciprocating wear test for evaluating boundary lubrication.* Tribology International, 1990. **23**(5): p. 301-307.

96. Cann, P. and A. Cameron, *Studies of thick boundary lubrication—influence of zddp and oxidized hexadecane.* Tribology international, 1984. **17**(4): p. 205-208.

97. Zhang, Z., et al., *Tribofilms generated from ZDDP and DDP on steel surfaces:Part 1, growth, wear and morphology.* Tribology Letters, 2005. **19**(3): p. 211-220.

98. Wang, Y. and S.C. Tung, *Scuffing and wear behavior of aluminum piston skirt coatings against aluminum cylinder bore.* Wear, 1999. **225–229, Part 2**(0): p. 1100-1108.

99. Martin, J.M., et al., *The two-layer structure of Zndtp tribofilms: Part I: AES, XPS and XANES analyses.* Tribology International, 2001. **34**(8): p. 523-530.

100. Willermet, P., et al., *The composition of lubricant-derived surface layers formed in a lubricated cam/tappet contact II. Effects of adding overbased detergent and dispersant to a simple ZDTP solution.* Tribology International, 1995. **28**(3): p. 163-175.

101. Palacios, J., *Thickness and chemical composition of films formed by antimony dithiocarbamate and zinc dithiophosphate.* Tribology international, 1986. **19**(1): p. 35-39.

102. Ito, K., et al., *Formation Mechanism of a Low Friction ZDDP Tribofilm on Iron Oxide.* Tribology Transactions, 2007. **50**(2): p. 211-216.

103. Xia, Y., et al., *Remarkable friction stabilization of AISI 52100 steel by plasma nitriding under lubrication of alkyl naphthalene.* Wear, 2010. **268**(7–8): p. 917-923.

104. Yue, W., et al., *Synergistic Effects between Plasma-Nitrided AISI 52100 Steel and Zinc Dialkyldithiophosphate Additive under Boundary Lubrication.* Tribology Transactions, 2012. **55**(3): p. 278-287.

105. Ma, Y., J. Liu, and L. Zheng, *The synergistic effects of EP and AW additives with oxynitrided surface of steel.* Tribology International, 1995. **28**(5): p. 329-334.

106. Ma, Y., et al., *The effect of oxy-nitrided steel surface on improving the lubricating performance of tricresyl phosphate.* Wear, 1997. **210**(1–2): p. 287-290.

107. Papay, A., *Antiwear and extreme-pressure additives in lubricants.* Lubrication Science, 1998. **10**(3): p. 209-224.

108. Fang, Y. and M. Shirakashi, *Mixed Lubrication Characteristics Between the Piston and Cylinder in Hydraulic Piston Pump-Motor.* Journal of Tribology, 1995. **117**(1): p. 80-85.

109. Wan, Y., et al., *Effects of detergent on the chemistry of tribofilms from ZDDP: studied by X-ray absorption spectroscopy and XPS*, in *Tribology Series*, M.P.G.D. D. Dowson and A.A. Lubrecht, Editors. 2002, Elsevier. p. 155-166.

110. Delgado, Y.P., et al., *Impact of wire-EDM on dry sliding friction and wear of WC-based and ZrO 2-based composites.* Wear, 2011. **271**(9): p. 1951-1961.

111. Ratoi, M., et al., *The impact of organic friction modifiers on engine oil tribofilms.* RSC Advances, 2014. **4**(9): p. 4278-4285.

112. Kermani, M.B. and A. Morshed, *Carbon Dioxide Corrosion in Oil and Gas Production—A Compendium.* Corrosion, 2003. **59**(8): p. 659-683.

113. Bjeoumikhov, A., M. Haschke, and N. Kemf. *Electron probe micro analysis (EPMA) and x-ray fluorescence (XRF) analysis for exact results.* 2005; Available from: http://www.imaging-git.com/science/electron-and-ion-microscopy/electron-probe-micro-analysis-epma-and-x-ray-fluorescence-xrf-an.

114. Chen, T., et al., *In-situ monitoring the inhibiting effect of polyphosphinocarboxylic acid on CaCO3 scale formation by synchrotron X-ray diffraction.* Chemical Engineering Science, 2009. **64**(5): p. 912-918.

115. Zemlyanov, D., *ELECTRON SPECTROSCOPY A new window opens.* 2011.

116. Hofmann, S., *Practical surface analysis: state of the art and recent developments in AES, XPS, ISS and SIMS.* Surface and Interface Analysis, 1986. **9**(1): p. 3-20.

117. Liu, H. and T.J. Webster, *Nanomedicine for implants: a review of studies and necessary experimental tools.* Biomaterials, 2007. **28**(2): p. 354-369.

118. Wagner, C.D. and G. Muilenberg, *Handbook of X-ray photoelectron spectroscopy.* 1979: Perkin-Elmer.

119. Naumkin, A.V., A. Kraut-Vass, and C.J. Powell, *NIST X-ray photoelectron spectroscopy database.* 2008: Measurement Services Division of the National Institute of Standards and Technology (NIST) Technology Services.

120. Chusuei, C.C., et al., *Calcium phosphate phase identification using XPS and time-of-flight cluster SIMS.* Analytical chemistry, 1999. **71**(1): p. 149-153.

121. Basso, R.L., et al., *Effect of carbon on the compound layer properties of AISI H13 tool steel in pulsed plasma Nitrocarburizing.* Plasma Processes and Polymers, 2007. **4**(S1): p. S728-S731.

122. Leite, M., et al., *Wear mechanisms and microstructure of pulsed plasma nitrided AISI H13 tool steel.* Wear, 2010. **269**(5): p. 466-472.

123. Thelning, K.-E., *Steel and its heat treatment.* 2013: Butterworth-Heinemann.

124. Steel, W.Y. *Graphite Cast Iron Grades.* Available from: https://www.westyorkssteel.com/cast-iron-bar/s-g-iron/600-3/.

125. Demydov, D., et al., *Advanced Lubricant Additives of Dialkyldithiophosphate (DDP)-Functionalized Molybdenum Sulfide Nanoparticles and Their Tribological Performance for Boundary Lubrication*, in *Nanoscale Materials in Chemistry: Environmental Applications.* 2010, American Chemical Society. p. 137-163.

126. Cai, Z.-b., et al., *Comparison of the tribological behavior of steel–steel and Si3N4–steel contacts in lubricants with ZDDP or ionic liquid.* Wear, 2014. **319**(1–2): p. 172-183.

127. Crobu, M., A. Rossi, and N.D. Spencer, *Effect of Chain-Length and Countersurface on the Tribochemistry of Bulk Zinc Polyphosphate Glasses.* Tribology Letters, 2012. **48**(3): p. 393-406.

128. Martin, J.M., *Antiwear mechanisms of zinc dithiophosphate: a chemical hardness approach.* Tribology Letters, 1999. **6**(1): p. 1-8.

129. Willermet, P.A., et al., *Mechanism of formation of antiwear films from zinc dialkyldithiophosphates.* Tribology International, 1995. **28**(3): p. 177-187.

130. Crobu, M., et al., *Chain-length-identification strategy in zinc polyphosphate glasses by means of XPS and ToF-SIMS.* Analytical and Bioanalytical Chemistry, 2012. **403**(5): p. 1415-1432.

131. Heuberger, R., A. Rossi, and N.D. Spencer, *XPS study of the influence of temperature on ZnDTP tribofilm composition.* Tribology Letters, 2007. **25**(3): p. 185-196.

132. Heuberger, R., A. Rossi, and N.D. Spencer, *Pressure Dependence of ZnDTP Tribochemical Film Formation: A Combinatorial Approach.* Tribology Letters, 2007. **28**(2): p. 209-222.

133. Uy, D., et al., *Soot–additive interactions in engine oils.* Lubrication Science, 2010. **22**(1): p. 19-36.

134. Berkani, S., et al., *Structural Changes in Tribo-Stressed Zinc Polyphosphates.* Tribology Letters, 2013. **51**(3): p. 489-498.

135. Uy, D., et al., *Raman Characterization of Anti-Wear Films Formed from Fresh and Aged Engine Oils*, 2006, SAE International.

136. Zabinski, J.S. and N.T. MacDevitt, *Raman spectra of inorganic compounds related to solid state tribochemical studies*, 1996.

137. Kwon, T.Y., T. Fujishima, and Y. Imai, *FT-Raman spectroscopy of calcium hydroxide medicament in root canals.* International Endodontic Journal, 2004. **37**(7): p. 489-493.

138. El Mendili, Y., et al., *Phase transitions of iron sulphides formed by steel microbial corrosion.* Rsc Advances, 2013. **3**(48): p. 26343-26351.

139. Yue, W., et al., *A comparative study on the tribological behaviors of nitrided and sulfur-nitrided 35CrMo steel lubricated in PAO base oil with MoDTC additive.* Tribology International, 2011. **44**(12): p. 2029-2034.

140. Liu, C., et al., *The Interactions Between Sulfur-Nitrided Layer on Steel Surface and MoDTC Lubricating Additive and Their Effects on Tribological Performance.* Tribology Letters, 2012. **47**(2): p. 313-322.

141. Khorramian, B.A., et al., *Review of antiwear additives for crankcase oils.* Wear, 1993. **169**(1): p. 87-95.

142. Xia, Y.-q., W.-m. Liu, and Q.-j. Xue, *Comparative study of the tribological properties of various modified mild steels under boundary lubrication condition.* Tribology International, 2005. **38**(5): p. 508-514.

143. Ma, Y., et al., *Lubricating mechanisms of sulfurized olefin on oxynitrided steel surface under boundary lubrication condition.* Wear, 1996. **194**(1): p. 174-177.

144. Konicek, A.R., et al., *Role of tribofilms in wear protection.* Tribology International, 2016. **94**: p. 14-19.

145. Topolovec-Miklozic, K., T.R. Forbus, and H.A. Spikes, *Film thickness and roughness of ZDDP antiwear films.* Tribology Letters, 2007. **26**(2): p. 161-171.

146. Suzuki, M., *Comparison of tribological characteristics of sputtered MoS2 films coated with different apparatus.* Wear, 1998. **218**(1): p. 110-118.

147. Al-Samarai, R., et al., *Effect of Load and Sliding Speed on Wear Friction of aluminum-silicon casting alloy* International Journal of Scientific and Research Publications, 2012. **2**(3): p. 1-4.

148. Martin, J.M., et al., *Superlubricity of molybdenum disulphide.* Physical Review B, 1993. **48**(14): p. 10583-10586.

149. Roberts, E.W., *Thin solid lubricant films in space.* Tribology International, 1990. **23**(2): p. 95-104.

150. Roberts, E.W., *Ultralow friction films of MoS2 for space applications.* Thin Solid Films, 1989. **181**(1): p. 461-473.

151. Qiang, Y.H., S.R. Ge, and Q.J. Xue, *Microstructure and tribological properties of complex nitrocarburized steel.* Journal of Materials Processing Technology, 2000. **101**(1–3): p. 180-185.

152. Lee, I., *Post-oxidizing treatments of the compound layer on the AISI 4135 steel produced by plasma nitrocarburizing.* Surface and Coatings Technology, 2004. **188–189**: p. 669-674.

153. Li, Y.-R., et al., *The Effect of Steel Hardness on the Performance of ZDDP Antiwear Films: A Multi-Technique Approach.* Tribology Letters, 2008. **29**(3): p. 201.

154. Watanabe, M., et al., *Formation and oxidation of sulfides on pure iron and iron oxides.* Materials Transactions, JIM, 2000. **41**(7): p. 865-872.

155. Wada, H., Y. Iwanami, and M. Nomura, *XANES study on boundary lubrication films generated from belt-drive continuously variable transmission fluids.* Synopses of the international tribology conference, 2005.

156. Ito, K., et al., *Low-friction tribofilm formed by the reaction of ZDDP on iron oxide.* Tribology International, 2006. **39**(12): p. 1538-1544.

157. Martin, J., *Lubricant additives and the chemistry of rubbing surfaces: metal dithiophosphates triboreaction films revisited.* Japanese Journal of Tribology, 1997. **42**(9): p. 1095.

158. Minfray, C., *PhD Diss*, 2004, Ecole Centrale de Lyon.

159. Yue, W., et al., *Tribological properties of sulfurized-nitrided layer prepared by a two-step method.* Vacuum, 2011. **85**(11): p. 1011-1016.

160. Taylor, L., A. Dratva, and H.A. Spikes, *Friction and Wear Behavior of Zinc Dialkyldithiophosphate Additive.* Tribology Transactions, 2000. **43**(3): p. 469-479.

161. Kawamura, M. and K. Fujita, *Organic sulphur and phosphorus compounds as extreme pressure additives.* Wear, 1981. **72**(1): p. 45-53.

162. Guan, B., B.A. Pochopien, and D.S. Wright, *The chemistry, mechanism and function of tricresyl phosphate (TCP) as an anti-wear lubricant additive.* Lubrication Science, 2016. **28**(5): p. 257-265.

163. Bayer, R.G., *Mechanical Wear Fundamentals and Testing, revised and expanded*. 2004: CRC Press.

164. Instruments, P. *MTM 3D-SLIM Option: Film Thickness Measurement*. [cited 2016; Available from: http://pcs-instruments.com/product/mtm-3d-slim-option-film-thickness-measurement/.